M. BISMARCK-NASR

Structural Dynamics in Aeronautical Engineering

Structural Dynamics in Aeronautical Engineering

This page intentionally left blank

Structural Dynamics in Aeronautical Engineering

Maher N. Bismarck-Nasr
Instituto Tecnológico de Aeronáutica
Centro Técnico Aeroespacial
São José dos Campos, São Paulo, Brazil

AIAA

American Institute of Aeronautics and Astronautics, Inc., Reston, Virginia

5   4   3   2   1

**To my wife Maria Eunice
and daughters
Paula Christina and Elizabeth Maria**

This page intentionally left blank

Foreword

Structural Dynamics in Aeronautical Engineering by Maher N. Bismarck-Nasr from the Instituto Tecnológico de Aeronáutica at the Centro Técnico Aeroespacial in São Paulo, Brazil, is a comprehensive introduction to the modern methods of dynamic analysis of aeronautical structures. The text is particularly suitable for undergraduate students. For advanced students, the text provides numerous references on seminal work in structural dynamics that can be used for graduate-level research. The text represents carefully developed course materials used at the author's institute. It starts with an introductory chapter on matrix algebra and methods for numerical computations, followed by a series of chapters discussing specific aeronautical applications. In this way, the student can be guided from the simple concept of the single-degree-of-freedom structural system to the more complex multiple-degree-of-freedom and continuous systems, including random vibrations, nonlinear systems, and aeroelastic phenomena. Among the various examples used in the text, the chapter on aeroelasticity of flight vehicles is particularly noteworthy with its clear presentation of the phenomenon and its mathematical formulation for structural and aerodynamic loads.

The Education Series of textbooks and monographs published by the American Institute of Aeronautics and Astronautics embraces a broad spectrum of theory and application of different disciplines in aeronautics and astronautics, including aerospace design practice. The series includes also texts on defense science, engineering, and management. The complete list of textbooks published in the series (more than 60 titles) can be found at the end of this volume. The series serves as teaching texts as well as reference materials for practicing engineers, scientists, and managers.

J. S. Przemieniecki
Editor-in-Chief
AIAA Education Series

This page intentionally left blank

Table of Contents

This page intentionally left blank

Preface

This book is a textbook on the fundamental concepts of structural dynamics and aeroelasticity. It is intended to be used for senior undergraduate and first-year graduate students in aeronautical and aerospace engineering courses. The book can also be used as a reference book by practicing engineers in these related fields. The prerequisites for the material presented are the mathematical courses included in the usual engineering curriculum.

The book starts with an introductory chapter on matrix algebra and techniques, where the basic principles and the main matrix operations involved in the subsequent text are presented. Chapter 2 presents, in a detailed and organized manner, the fundamental concepts, basic properties, and methods of analysis of the single-degree-of-freedom linear mechanical system. Chapter 3 is devoted to the multidegree-of-freedom linear system. The modal transformation and numerical integration methods are treated in detail. Several case studies are given for the practical estimation of the dynamic properties of complex structural configurations in aeronautical and aerospace engineering applications. Chapter 4 deals with the dynamic behavior of continuous elastic bodies. Chapter 5 addresses the nonlinear structural dynamic system, and Chapter 6 is concerned with random vibration problems.

The second part of the book is concerned with aeroelasticity. Chapter 7 addresses in detail the typical section aeroelasticity, where the basic concepts and fundamentals of aeroelastic stability are presented. Classical extension to three-dimensional lifting surfaces using the strip theory is given for the solution of aeroelastic stability and control reversal problems. Chapter 8 addresses the problem of aeroelasticity of complex flight vehicle configurations using numerical discrete methods. The book ends with Chapter 9, which is devoted to the problem of aeroelasticity of plates and shells.

The problem of gust loads determination and gust response of flexible flight vehicles has not been addressed in the present text because a modern and excellent textbook by F. M. Hoblit, published in the AIAA Education Series, completely devoted to the subject is available. Special topics on aeroelasticity, such as ground and flight vibrations experimental techniques, whirl flutter analysis, rotary wing aeroelasticity, and stall flutter predictions, have not been treated because the present book is concerned with fundamentals and, furthermore, such topics to be covered will need more than one additional volume, and they are already available elsewhere.

This book complements, and the author is indebted to, the authors of previous textbooks on structural dynamics and aeroelasticity, among which must be cited

the books of Scalan and Rosenbaum, Fung, Bisplighoff, Ashley and Halfmann, Bisplinghoff and Ashley, Mazet, Dat, Petre, Forshing, Dowell, Librescu, Dowell, Curtis, Scalan, and Sisto.

Maher N. Bismarck-Nasr
February 1999

1
Matrix Algebra and Techniques

This chapter on matrix algebra and techniques is not intended to be an exhaustive or rigorous treatment of the subject. Instead, it is limited to the presentation of the basic principles and main matrix operations involved in applications considered in subsequent text. For more details the reader may consult available standard textbooks on the subject.[1-3]

1.1 Notations and Definitions

1.1.1 Matrix

A matrix is a rectangular array of symbols or numbers arranged in a formation of m rows and n columns, as given below

$$[a] = \begin{bmatrix} a_{11} & a_{12} & \cdots & a_{1n} \\ a_{21} & a_{22} & \cdots & a_{2n} \\ \cdot & \cdot & \cdot & \cdot \\ a_{m1} & a_{m2} & \cdots & a_{mn} \end{bmatrix} \tag{1.1}$$

The symbol $[a]$ stands for the whole array; an individual element will be denoted by a_{ij}, where i stands for the ith row and j stands for the jth column. Such an array will be defined as a matrix of order mn.

1.1.2 Row Matrix

When $m = 1$, the matrix will be defined as a row matrix, or a vector of the first kind, and will be denoted by

$$(a) = (a_1\, a_2 \cdots a_n) \tag{1.2}$$

1.1.3 Column Matrix

When $n = 1$, the matrix will be called a column matrix, or a vector of the second kind, point, or simply vector, and will be denoted by

$$\{a\} = \begin{Bmatrix} a_1 \\ a_2 \\ \cdot \\ a_n \end{Bmatrix} \tag{1.3}$$

1.1.4 Transposed Matrix

If we make a complete interchange of the rows and columns of a matrix $[a]$, we will obtain its transposed matrix, which will be denoted by $[a]^T$, or

$$[a]^T = [a_{ji}] \qquad (1.4)$$

1.1.5 Null or Zero Matrix

We define a null or zero matrix as a matrix with all its elements equal to zero, which will be denoted by $[0]$.

1.1.6 Square Matrix

When the number of the rows m is equal to the number of the columns n, the matrix is defined as a square matrix of the order n.

1.1.7 Special Types of Square Matrices

Diagonal matrix.   A diagonal matrix is a square matrix whose elements are defined as

$$\begin{aligned} a_{ij} &= 0 \quad &\text{for } i \neq j \\ a_{ij} &\neq 0 \quad &\text{for } i = j \end{aligned} \qquad (1.5)$$

and will be denoted by $\lceil a \rfloor$.

Scalar and unit matrix.   If in a square matrix, the elements are defined as

$$\begin{aligned} a_{ij} &= 0 \quad &\text{for } i \neq j \\ a_{ij} &= a \quad &\text{for } i = j \end{aligned} \qquad (1.6)$$

Where a is a scalar quantity, the matrix is called a scalar matrix, and, if the value of a is equal to one, the matrix is defined as a unit or identity matrix and will be denoted by $[I]$.

Symmetric and skew symmetric matrices.   If the elements of a square matrix are defined by

$$a_{ij} = a_{ji} \qquad \text{for all values of } i \text{ and } j \qquad (1.7)$$

the matrix is said to be symmetric, and we can write the following for a symmetric matrix:

$$[a]^T = [a] \qquad (1.8)$$

If the elements of a square matrix are defined by

$$\begin{aligned} a_{ij} &= -a_{ji} \quad &\text{for } i \neq j \\ a_{ij} &= 0 \quad &\text{for } i = j \end{aligned} \qquad (1.9)$$

the matrix will be called a skew symmetric matrix. Furthermore, if some of the elements of the main diagonal are not equal to zero, the matrix will be called a skew matrix.

Triangular matrices. A square matrix whose elements are defined by

$$a_{ij} = 0 \qquad \text{for } i > j \tag{1.10}$$

is called an upper triangular matrix, and a square matrix whose elements are defined by

$$a_{ij} = 0 \qquad \text{for } i < j \tag{1.11}$$

is called a lower triangular matrix. We notice that a diagonal matrix is both a lower and upper triangular matrix. Upper and lower triangular matrices are often denoted by $[U]$ and $[L]$, respectively.

Band matrix. A square matrix of order n, whose elements are defined by

$$a_{ij} = 0 \qquad \text{for } |i - j| > k, \quad k < n \tag{1.12}$$

is called a band matrix, and we define the bandwidth of the matrix as a $2k + 1$ and the half bandwidth as $k + 1$.

1.2   Matrix Algebra

1.2.1   Equality of Matrices

Two matrices $[a]$ and $[b]$ of the same order are said to be equal to each other if and only if

$$a_{ij} = b_{ij} \qquad \text{for all values of } i \text{ and } j \tag{1.13}$$

and we write $[a] = [b]$.

1.2.2   Matrix Addition and Subtraction

Two matrices $[a]$ and $[b]$ of the same order can be added or subtracted, and the result is a matrix $[c]$ of the same order, whose elements are given by

$$c_{ij} = a_{ij} \pm b_{ij} \tag{1.14}$$

for all values of i and j, and we write $[c] = [a] \pm [b]$.

1.2.3   Multiplication of Matrices

Scalar multiplication. We define the multiplication of a matrix $[a]$ by a scalar k as

$$k[a] = [b] \tag{1.15}$$

where $b_{ij} = k a_{ij}$ for all values of i and j.

Matrix multiplication.   Two matrices $[a]$ and $[b]$ can be multiplied if and only if the number of columns of the first one is equal to the number of rows of the second one, and we say that the matrices are conformables, and we write $[c] = [a][b]$, where

$$c_{ij} = \sum_{k=1}^{k=p} a_{ik} b_{kj} \tag{1.16}$$

$$i = 1, 2, \ldots, m \qquad j = 1, 2, \ldots, n$$

and the order of the matrices $[a]$, $[b]$, and $[c]$ are mp, pn, and mn, respectively. Now from the definition of the equality of two matrices, we know that the two matrices are equal to each other if and only if they have identical elements; hence, we conclude that, in general, if the product $[b][a]$ exists, it will be different from $[a][b]$. In the case when the two products are equal, i.e., $[a][b] = [b][a]$, we say that the matrices $[a]$ and $[b]$ commute with each other. In particular, we notice that a scalar matrix commutes with any square matrix of the same order. The operation of matrix multiplication can be extended to the product of more than two matrices, provided that the adjacent matrices of the chain are conformables.

1.2.4   Positive Power of a Square Matrix

For a square matrix $[a]$, we define the positive power of $[a]$ as

$$[a]^n = [a][a][a] \cdots [a] \qquad n \text{ factors} \tag{1.17}$$

where n is a positive integer number.

1.2.5   The Inverse of a Square Matrix

For a square matrix $[a]$, if there exists a matrix $[b]$ such that the relation

$$[a][b] = [b][a] = [I] \tag{1.18}$$

is satisfied, we say that $[b]$ is the inverse of $[a]$ and vice versa, and we write

$$[b] = [a]^{-1} \qquad \text{and} \qquad [a] = [b]^{-1} \tag{1.19}$$

We will see that not every square matrix has an inverse; however, if the inverse exists, it can be easily shown that it is unique. We call a matrix $[a]$, for which an inverse exists, a nonsingular matrix. Now, if for a square matrix $[a]$ there exists an inverse and the following relation is satisfied

$$[a][a]^{\mathrm{T}} = [I] \tag{1.20}$$

i.e., $[a]^{\mathrm{T}} = [a]^{-1}$, the matrix $[a]$ is called an orthogonal matrix. Furthermore, if for a square matrix $[a]$ the following is satisfied

$$[a][a] = [I] \tag{1.21}$$

i.e., $[a] = [a]^{-1}$, the matrix $[a]$ is called an involutory matrix. The unit matrix, for example, is an involutory matrix. Now, let $[a]$ be a square matrix, for which an

inverse exists, say $[b]$, i.e., $[a]^{-1} = [b]$; then from the definition for Eq. (1.18) we have

$$[b][a] = [I] \tag{1.22}$$

Performing the matrix multiplication $[b][a]$ and using the definition of matrix equality, we can write for the first row

$$b_{11}a_{11} + b_{12}a_{21} + \cdots + b_{1n}a_{n1} = 1$$
$$b_{11}a_{12} + b_{12}a_{22} + \cdots + b_{1n}a_{n2} = 0$$
$$\cdot \tag{1.23}$$
$$b_{11}a_{1n} + b_{12}a_{2n} + \cdots + b_{1n}a_{nm} = 0$$

where n is the order of the matrices. Making use of Cramer's rule, we obtain

$$b_{11} = D_1/D, b_{12} = D_2/D, \ldots, b_{1n} = D_n/D \tag{1.24}$$

where D is the determinant of the matrix $[a]$ (notice that, from the properties of the determinants, the following relation is satisfied, $|a_{ij}| = |a_{ji}|$) and is given by

$$D = \begin{vmatrix} a_{11} & a_{12} & \cdots & a_{1n} \\ a_{21} & a_{22} & \cdots & a_{2n} \\ \cdot & \cdot & \cdot & \cdot \\ a_{n1} & a_{n2} & \cdots & a_{nn} \end{vmatrix} \tag{1.25}$$

and D_r is the determinant obtained by replacing the row $a_{r1}a_{r2}\cdots a_{rn}$ in Eq. (1.25) by the right-hand side of Eq. (1.23), i.e., $1, 0, 0, \ldots, 0$. We notice that Eq. (1.24) exists if and only if $D \neq 0$, giving the condition for the existence of the inverse of $[a]$; furthermore, the values of D_r are the cofactors of the elements a_{r1} in the determinants in Eq. (1.25); thus we can write

$$b_{1j} = A_{j1}/|a| \qquad j = 1, 2, \ldots, n \tag{1.26}$$

where A_{j1} are the cofactors of a_{j1} of the determinant in Eq. (1.25) and $|a|$ is the determinant of the matrix $[a]$. Now if we perform the multiplication in Eq. (1.22) for the ith row and using the definition of the matrix equality, we will obtain

$$b_{ij} = A_{ji}/|a| \qquad j = 1, 2, \ldots, n \tag{1.27}$$

Thus, we can write the inverse of $[a]$ as

$$[a_{ij}]^{-1} = [b_{ij}] = [A_{ji}]/|a| \tag{1.28}$$

The matrix $[A_{ji}]$ is called the adjoint of the matrix $[a]$, and a typical element of it is equal to the cofactor of the corresponding element in the determinant of the transposed $[a]$. We notice that the adjoint matrix exists always and is independent of $[a]$ being singular.

1.2.6 Negative Power of a Matrix

If a square matrix $[a]$ is nonsingular, its inverse exists, and we define the negative power of $[a]$ as

$$[a]^{-n} = [a]^{-1} \cdots [a]^{-1} \qquad n \text{ factors} \tag{1.29}$$

or $[a]^{-n} = ([a]^{-1})^n$, where n is a positive integer.

1.2.7   The Reversal Law in Transposed and Inverse Products

Transposition.   Let $[a]$ and $[b]$ be two matrices of orders mn and np, respectively; then from the definition of the matrix multiplication, we can write

$$[c] = [a][b] \tag{1.30}$$

where $[c]$ is of the order mp, with a typical element given by

$$c_{ij} = \sum_{k=1}^{n} a_{ik}b_{kj} \tag{1.31}$$

Now, transposing $[a]$ and $[b]$, we will obtain $[a]^T$ and $[b]^T$ of orders nm and pn, respectively, and the product $[b]^T[a]^T$ exists, and we can write

$$[d] = [b]^T[a]^T \tag{1.32}$$

with a typical element of $[d]$ given by

$$d_{ij} = \sum_{k=1}^{n} b_{ki}a_{jk} \tag{1.33}$$

Comparing Eqs. (1.31) and (1.33), we conclude that $d_{ij} = c_{ji}$, or

$$[d] = [c]^T \tag{1.34}$$

and making use of Eqs. (1.32) and (1.30), we get

$$[[a][b]]^T = [b]^T[a]^T \tag{1.35}$$

Similarly, if $[a]$, $[b]$, and $[c]$ are three matrices and the product $[a][b][c]$ exists, we can write

$$[[a][b][c]]^T = [c]^T[[a][b]]^T = [c]^T[b]^T[a]^T \tag{1.36}$$

We conclude that, when a matrix chain product is transposed, the result is equal to the product of the transposed matrices in the reverse order, i.e.,

$$[[a_1][a_2]\cdots[a_n]]^T = [a_n]^T \cdots [a_2]^T[a_1]^T \tag{1.37}$$

Inverse.   Consider the matrix equation

$$[c] = [a][b] \tag{1.38}$$

where $[c]$, $[a]$, and $[b]$ are square nonsingular matrices of order n. Premultiplying both sides of Eq. (1.38) by $[b]^{-1}[a]^{-1}$, we get

$$[b]^{-1}[a]^{-1}[c] = [b]^{-1}[a]^{-1}[a][b] = [I] \tag{1.39}$$

Postmultiplying Eq. (1.39) by $[c]^{-1}$, we obtain

$$[b]^{-1}[a]^{-1}[c][c]^{-1} = [c]^{-1}$$

or $[b]^{-1}[a]^{-1} = [c]^{-1}$, and making use of Eq. (1.38) we obtain

$$[b]^{-1}[a]^{-1} = [[a][b]]^{-1} \tag{1.40}$$

$$[a] \quad = \quad [a][a][a] \qquad [a] \qquad n \text{ factors} \qquad (1.17)$$

Similarly, for a chain product of nonsingular square matrices of order n, we can write

$$[[a_1][a_2] \cdots [a_n]]^{-1} = [a_n]^{-1} \cdots [a_2]^{-1}[a_1]^{-1} \tag{1.41}$$

The relations (1.37) and (1.41) are known as the reversal laws in transposed and inverse products.

1.2.8 Partitioned Matrices

A partitioned matrix is one that is subdivided into submatrices or minor matrices. As an example, consider the matrix $[a]$ partitioned as

$$[a] = \begin{bmatrix} a_{11} & a_{12} & \cdot & a_{13} \\ a_{21} & a_{22} & \cdot & a_{23} \\ \cdot & \cdot & \cdot & \cdot \\ a_{31} & a_{32} & \cdot & a_{33} \end{bmatrix} = \begin{bmatrix} [A_{11}] & [A_{12}] \\ [A_{21}] & [A_{22}] \end{bmatrix}$$

$$[A_{11}] = \begin{bmatrix} a_{11} & a_{12} \\ a_{21} & a_{22} \end{bmatrix} \quad [A_{12}] = \begin{Bmatrix} a_{13} \\ a_{23} \end{Bmatrix} \tag{1.42}$$

$$[A_{21}] = (a_{31} \quad a_{32}) \quad \text{and} \quad [A_{22}] = [a_{33}]$$

and let $[b]$ be another matrix of the same order and partitioned in the same manner as $[a]$, i.e.,

$$[b] = \begin{bmatrix} b_{11} & b_{12} & \cdot & b_{13} \\ b_{21} & b_{22} & \cdot & b_{23} \\ \cdot & \cdot & \cdot & \cdot \\ b_{31} & b_{32} & \cdot & b_{33} \end{bmatrix} = \begin{bmatrix} [B_{11}] & [B_{12}] \\ [B_{21}] & [B_{22}] \end{bmatrix} \tag{1.43}$$

Then, by addition and multiplication, it can be shown that

$$[a] + [b] = \begin{bmatrix} [A_{11}] + [B_{11}] & [A_{12}] + [B_{12}] \\ [A_{21}] + [B_{21}] & [A_{22}] + [B_{22}] \end{bmatrix} \tag{1.44}$$

and

$$[a][b] = \begin{bmatrix} [A_{11}][B_{11}] + [A_{12}][B_{21}] & [A_{11}][B_{12}] + [A_{12}][B_{22}] \\ [A_{21}][B_{11}] + [A_{22}][B_{21}] & [A_{21}][B_{12}] + [A_{22}][B_{22}] \end{bmatrix} \tag{1.45}$$

We notice that the resulting matrices are of the same order and partitioned in the same manner as the original matrices. We have seen that matrix multiplication can be performed if and only if the matrices are conformable; thus, if $[a]$ and $[b]$ are conformable for the multiplication $[a][b]$ and, furthermore, if $[a]$ and $[b]$ are partitioned into submatrices such that the grouping of the columns of $[a]$ agrees with the grouping of the rows of $[b]$, we can easily prove that the product $[a][b]$ can be obtained by considering the submatrices as elements while applying the rule of multiplication. Indeed, in forming the product $[a][b]$, where $[a]$ is of order mn and $[b]$ of order np, we have partitioned $[a]$ into n row matrices and $[b]$ into p column matrices. The use of the matrix partitioning while performing matrix

operations can be very useful if some of the submatrices are of special types, e.g., null, scalar, or diagonal matrices.

1.2.9   Definite Positive Matrix

A quadratic form for the variables $(x_1, x_2, \ldots, x_n)$ is defined as an expression containing the sum of all the quadratic terms of $(x_1, x_2, \ldots, x_n)$, or

$$F(x_1, x_2, \ldots, x_n) = \sum_{i=1}^{n} \sum_{j=1}^{n} a_{ij} x_i x_j \qquad (1.46)$$

In matrix notation, we can write Eq. (1.46) as

$$F(x_1, x_2, \ldots, x_n) = \{x\}^{\mathrm{T}} [a] \{x\} \qquad (1.47)$$

Now, given a square matrix $[a]$ and if the relation

$$\{x\}^{\mathrm{T}} [a] \{x\} > 0 \qquad (1.48)$$

is satisfied, for any vector $\{x\}$ different from the null vector, we call the matrix $[a]$ a positive definite matrix.

1.3   Differentiation and Integration of Matrices

If the elements of a matrix $[a]$ are functions of a scalar variable t, i.e., $a_{ij} = a_{ij}(t)$, and if the derivatives

$$\frac{\mathrm{d}}{\mathrm{d}t} [a_{ij}(t)]$$

and the definite integrals

$$\int_{\alpha}^{\beta} a_{ij}(t) \, \mathrm{d}t$$

exist for all values of i and j, we define the differentiation and the integration of the matrix $[a]$ as

$$D[a(t)] = [D a_{ij}(t) \, \mathrm{d}t] \qquad (1.49)$$

where $D = \mathrm{d}/\mathrm{d}t$ and

$$\int_{\alpha}^{\beta} [a(t)] \, \mathrm{d}t = \left[\int_{\alpha}^{\beta} a(t) \, \mathrm{d}t \right] \qquad (1.50)$$

It is thus seen that the differentiation and integration of a matrix, whose elements are functions of a scalar variable, are obtained by differentiating and integrating each of its corresponding elements, provided that such operations exist. The above definitions are extended when the elements of the matrix are functions of more than one variable, provided the respective operations exist.

1.4 Transformations

1.4.1 Linear Transformation

Let $(x_1, x_2, \ldots, x_n)$ and $(y_1, y_2, \ldots, y_m)$ be two sets of independent variables (coordinates) that define uniquely the state or configuration of a system. Because of the uniqueness of the relation, every variable, say y_s, of the set $(y_1, y_2, \ldots, y_m)$ can be expressed as a unique function of the set $(x_1, x_2, \ldots, x_n)$, and we can write

$$
\begin{aligned}
y_1 &= y_1(x_1, \ x_2, \ \ldots, \ x_n) \\
y_2 &= y_2(x_1, \ x_2, \ \ldots, \ x_n) \\
&\ \ \cdot \qquad\quad \cdot \quad\ \cdot \\
y_m &= y_m(x_1, \ x_2, \ \ldots, \ x_n)
\end{aligned}
\tag{1.51}
$$

Similarly, we can write the inverse relations, or

$$
\begin{aligned}
x_1 &= x_1(y_1, \ y_2, \ \ldots, \ y_m) \\
x_2 &= x_2(y_1, \ y_2, \ \ldots, \ y_m) \\
&\ \ \cdot \qquad\quad \cdot \quad\ \cdot \\
x_n &= x_n(y_1, \ y_2, \ \ldots, \ y_m)
\end{aligned}
\tag{1.52}
$$

The differentials of Eq. (1.51) read

$$
\begin{aligned}
dy_1 &= y_{1.1}dx_1 + y_{1.2}dx_2 + \cdots + y_{1.n}\,dx_n \\
dy_2 &= y_{2.1}dx_1 + y_{2.2}dx_2 + \cdots + y_{2.n}\,dx_n \\
&\ \ \cdot \qquad\qquad\qquad\qquad\qquad\quad \cdot \\
dy_m &= y_{m.1}dx_1 + y_{m.2}dx_2 + \cdots + y_{m.n}dx_n
\end{aligned}
\tag{1.53}
$$

where $y_{1.1} = \partial y_1/\partial x_1$. Now, in matrix notation we can write Eq. (1.53) as

$$
d\{y\} = [T]d\{x\}
\tag{1.53$'$}
$$

where $\{y\} = (y_1, y_2, \ldots, y_m)^T \{x\} = (x_1, x_2, \ldots, x_n)^T$ and $[T_{ij}] = [y_{ij}]$. From Eq. (1.53$'$), we observe that the matrix $[T]$ represents the transformation of the differentials of the coordinates $\{y\}$ into the differentials of the coordinates $\{x\}$. Now, if all the partial derivatives in $[T]$ were constants, i.e., independent of the coordinates, we can integrate Eq. (1.53) to obtain

$$
y_i = \sum_{j=1}^{j=n} t_{ij}x_j + b_i \qquad i = 1, 2, \ldots, m
\tag{1.54}
$$

where $t_{ij} = \partial y_i/\partial x_j$ and b_i are the constants of the integration. Now if it is required, as is the usual case that $y_i = 0$ for $x_1 = x_2 = \cdots = x_n = 0$, the constants of the integration b_i in Eq. (1.54) drop out, and we can write

$$
\{y\} = [t]\{x\}
\tag{1.55}
$$

In this case, we define the matrix $[t]$ as a linear transformation matrix.

1.4.2   *Translation Matrix*

We consider two sets of orthogonal Cartesian unit base vectors e_{1x}, e_{2x}, e_{3x} and e_{1y}, e_{2y}, e_{3y} parallel to each other as shown in Fig. 1.1. Furthermore, let $(x_1, x_2, \ldots, x_n)$ be the set of independent variables (coordinates) related to the base x and $(y_1, y_2, \ldots, y_n)$ be the set of the independent variables (coordinates) related to the base y. For example, $y_q e_{yq}$ may represent a displacement in the e_{yq} direction of magnitude y_q and $x_p e_{xp}$ may represent a rotation in the e_{xp} direction of magnitude x_p. Now, let a small change in the coordinate y_q be given by $\mathrm{d}y_q$, while all the other coordinates of the set y are held as constants. Because of this change, small changes will correspond in all the coordinates related to the base x; in particular, in the coordinate x_p, a change will correspond given by $\mathrm{d}x_p$. Furthermore, if we consider y_p as a displacement and x_p as a rotation, then from the geometry of Fig. 1.1 we can write

$$\mathrm{d}y_q = \mathrm{d}x_p \Delta_1 \qquad (1.56)$$

where Δ_1 is as given in Fig. 1.1. Now, using Eq. (1.56), we can write

$$\frac{\mathrm{d}x_p}{\mathrm{d}y_q} = \frac{1}{\Delta_1} \qquad (1.56')$$

and because the change y_q was made while keeping all the other coordinates y_s of the set y held fixed, Eq. (1.56') reads

$$\frac{\partial x_p}{\partial y_q} = \frac{1}{\Delta_1} \qquad (1.57)$$

Similarly, we can obtain all the other elements $\partial x_i / \partial y_j$ and we can write

$$\{x\} = [t]\{y\} \qquad (1.58)$$

where $[t]$ in this case is called a translation matrix. We notice that, when $\Delta_1 = 0$ corresponding to a change $\mathrm{d}y_q$, there will be no change in x_p, i.e., $\mathrm{d}x_p$ will be zero; hence $\partial x_p / \partial y_q = 0$ for $\Delta_1 = 0$.
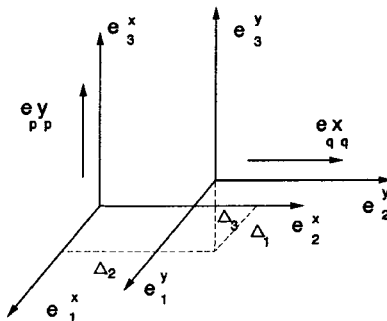
Fig. 1.1   Translation.

1.4.3   Rotation Matrix

We consider two sets of orthogonal Cartesian unit base vectors e_{1x}, e_{2x}, e_{3x} and e_{1y}, e_{2y}, e_{3y} having the same origin as shown in Fig. 1.2. Furthermore, let $(x_1, x_2, \ldots, x_n)$ be the set of independent variables (coordinates) related to the base x and let $(y_1, y_2, \ldots, y_n)$ be the set of independent variables (coordinates) related to the base y. Now, let a small change dx_s be given to the variable x_s while all the other variables of the set x are held fixed. Because of this small change in the variable x_s, small changes will correspond in all the variables of the set y, given by the components of the vectors $dx_s e_{sx}$ in the respective direction in y. And, in particular, in the e_{ry} direction we will have change given by $e_{ry} \cdot e_{sx} dx_s$ and because no change in the other variables of the set x occurred, this change will be equal to dy_r. Hence we write $dy_r = e_{ry} \cdot e_{sx} dx_s$, or

$$\frac{dy_r}{dx_s} = e_{ry} \cdot e_{sx} \tag{1.59}$$

and because the change was made while keeping all other variables of the set x fixed, Eq. (1.59) reads

$$\frac{\partial y_r}{\partial x_s} = e_{ry} \cdot e_{sx} \tag{1.60}$$

Similarly, we can obtain all the other elements and write

$$\{y\} = [R]\{x\} \tag{1.61}$$

where $[R]$ is called a rotation matrix with elements given by

$$R_{ij} = e_{iy} \cdot e_{jx}$$

and it can be shown by expansion that

$$[R][R]^{\mathrm{T}} = [R]^{\mathrm{T}}[R] = [\mathrm{I}] \tag{1.62}$$

Therefore, we conclude from Eq. (1.20) that the rotation matrix is an orthogonal matrix, i.e., $[R]^{-1} = [R]^{\mathrm{T}}$. The extension to successive transformations is
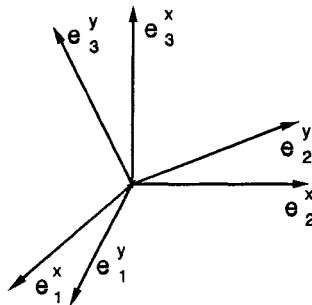
Fig. 1.2   Rotation.

straightforward. For example, if we have $\{x\} = [t_1]\{y\}$ and $\{y\} = [t_2]\{z\}$, we can write

$$\{x\} = [t]\{z\} \tag{1.63}$$

where $[t] = [t_1][t_2]$.

1.5 Solution of Large Systems of Linear Equations

In linear analysis, using numerical methods as a final step of the solution of the problem, we will be faced with the problem of solving a large system of linear simultaneous equations cast in matrix notation as

$$[A]\{x\} = \{P\} \tag{1.64}$$

The matrix $[A]$ often presents the special character of being symmetric and banded. The solution of the system of Eq. (1.64) using Cramer's rule, as given in Section 1.2, shows that we will have to perform arithmetic operations of the order of $(n+1)!$ (Refs. 2 and 4), where n is the number of the equations. Fortunately, using other methods of solutions summarized below, it can be shown that the number of arithmetic operations involved in the solution will be about $n^3/3$ for a full matrix and much less for a banded symmetric system. Furthermore, the solution of the system of Eq. (1.64) falls into two categories, known as direct methods,[2,4,5] and iterative methods.[4,6] In direct methods after a given number of operations, we will obtain the exact solution if roundoff errors in the computations are disregarded. In iterative methods, an initial start for the iteration process must be guessed, and successive iterations will be performed for obtaining better approximations for the solution. The iterations will be stopped when a desired accuracy is attained. Generally, we see that in iterative methods, the number of operations required in the solution will be a function of the initial guess and accuracy desired. Sometimes, iterative methods have been used in the solution of large systems of simultaneous equations generated in numerical analyses; however, with the improvements made in digital computer hardware, direct methods prove to be a more powerful tool for such solutions. Thus, only direct methods will be summarized below. For iterative methods, the reader can consult the available literature on the subject.[4,6] Basically, direct solutions reside on the fact that the matrix $[A]$, if it is nonsingular, can be decomposed as

$$[A] = [L][D][U] \tag{1.65}$$

where $[L]$ is a lower triangular matrix with unit values on the main diagonal, $[D]$ is a diagonal matrix, and $[U]$ is an upper triangular matrix with unit values on the main diagonal. The difference in the various methods lies in the way of incorporating $[D]$ in one or both of the triangular matrices, and thus the corresponding main diagonal elements of the affected matrix will be different from unity. We will begin this section by studying the triangularization process and the solution of triangular systems. Several methods of solving Eq. (1.64) will then be given.

1.5.1 Triangularization

If $[A]$ is nonsingular, we can write Eq. (1.65) as

$$[A] = [l][u] \tag{1.66}$$

where $[D]$ is now incorporated in $[l]$ or $[u]$ or both. Performing the multiplication and using the matrix equality property, we get

$$A_{ij} = \sum_{k=1}^{\min(i,j)} l_{ik} u_{kj} \tag{1.67}$$

Now Eq. (1.67) represents n^2 relations for determining the $(n^2 + n)$ unknowns, namely $(n^2 + n)/2$ values for l_{ij} and $(n^2 + n)/2$ values for u_{ij}. However, there will be always n values of the unknown specified; namely if $[D]$ is totally incorporated to $[u]$, all the diagonal elements of $[l]$ are unity and vice versa. Thus we will be left with n^2 relations for determining n^2 unknowns. In other methods as explained below, we will require that the corresponding diagonal elements in $[u]$ and $[l]$ be set equal and again we will have n^2 relations for determining n^2 unknowns. Explicit formulas for the elements of $[u]$ and $[l]$ are given in the following sections using various methods.

1.5.2 Solution of Triangular Systems

Upper triangular system.   Consider an upper triangular system written as

$$[U][X] = [B] \tag{1.68}$$

where, in general, $[X]$ and $[B]$ are rectangular matrices composed of a set of unknown vectors and a corresponding set of known vectors, respectively. The solution of Eq. (1.68) is given by

$$X_{nj} = B_{nj}/U_{nn} \qquad j = 1, 2, \ldots, r$$

$$X_{ij} = \left[B_{ij} - \sum_{k=i+1}^{n} U_{ik} X_{kj} \right] \Big/ U_{ii} \tag{1.69}$$

$$i = (n-1), (n-2), \ldots, 1$$

$$j = 1, 2, \ldots, r$$

where n is the order of the system and r is the number of vectors in $[X]$ and $[B]$. Now, if $[B]$ is a unit matrix of order n, we will obtain the inverse of $[U]$ or $[U]^{-1} = [X]$, with the elements of $[X]$ given by

$$X_{ii} = 1/U_{ii} \qquad i = 1, 2, \ldots, n$$

$$X_{ij} = \left[-\sum_{k=i+1}^{j} U_{ik} X_{kj} \right] \Big/ U_{ii} \tag{1.70}$$

$$i = (n-1), (n-2), \ldots, 1$$

$$j > i$$

and we observe that the inverse of an upper triangular matrix is an upper triangular matrix. Furthermore, if $[U]$ is banded, with a semibandwidth given by $(l + 1)$, the solution of (1.69) reads

$$X_{nj} = B_{nj}/U_{nn} \qquad j = 1, 2, \ldots, r$$

$$X_{ij} = \left[B_{ij} - \sum_{k=1+i}^{\lambda} U_{ik} X_{kj} \right] \Big/ U_{ii} \qquad (1.71)$$

where

$$i = (n - 1), (n - 2), \ldots, 1$$

$$j = 1, 2, \ldots, r$$

$$\lambda = l + i \qquad \text{for } l + 1 \leq n$$

$$\lambda = n \qquad \text{for } l + 1 > n$$

and n and r are as given before.

Lower triangular system.   Consider a lower triangular system written as

$$[L][X] = [B] \qquad (1.72)$$

where, in general, $[X]$ and $[B]$ are rectangular matrices composed of a set of unknown vectors and a corresponding set of known vectors, respectively. The solution of Eq. (1.72) is given by

$$X_{1j} = B_{1j}/L_{11} \qquad j = 1, 2, \ldots, r$$

$$X_{ij} = \left[B_{ij} - \sum_{k=1}^{i-1} L_{ik} X_{kj} \right] \Big/ L_{ii} \qquad (1.73)$$

$$i = 2, 3, \ldots, n$$

$$j = 1, 2, \ldots, r$$

where n is the order of the system and r is the number of vectors in $[X]$ and $[B]$. Again, for the case $[B]$ being a unit matrix, we will obtain the inverse of $[L]$ or $[L]^{-1} = [X]$, with the elements of $[X]$ given by

$$X_{ii} = 1/L_{ii} \qquad i = 1, 2, \ldots, n$$

$$X_{ij} = \left[-\sum_{k=j}^{i-1} L_{ik} X_{kj} \right] \Big/ L_{ii} \qquad (1.74)$$

$$i = 2, 3, \ldots, n \qquad j < i$$

and we conclude that the inverse of a lower triangular matrix is a lower triangular matrix. Furthermore, if $[L]$ is banded with a semibandwidth given by $(l + 1)$, the

solution to Eq. (1.73) reads

$$X_{1j} = B_{1j}/L_{11} \qquad j = 1, 2, \ldots, r$$

$$X_{ij} = \left[B_{ij} - \sum_{k=\lambda}^{i-1} L_{ik} X_{kj} \right] \Big/ L_{ii} \tag{1.75}$$

where

$$i = 2, 3, \ldots, n$$

$$j = 1, 2, \ldots, r$$

$$\lambda = 1 \qquad \text{for } i \leq l$$

$$\lambda = i - l \qquad \text{for } i > l$$

1.5.3 The Gauss Method

In the Gauss method of solution, successive eliminations are performed in such a way as to reduce the original matrix to an upper triangular form. The product of the matrices affecting the row operations is a lower triangular matrix $[L]$ with unit values on the main diagonal so that we can write $[L][A] = [U]$, or

$$[A] = [L]^{-1}[U] \tag{1.76}$$

and because, as has been explained in the last section, the inverse of a lower triangular matrix is also a lower triangular matrix, we conclude that the procedure of the Gauss elimination is equivalent to a decomposition in the form $[A] = [L][D][U]$ in which $[D]$ is totally incorporated $[U]$. Furthermore, we notice that we do not have to find to $[L]$ explicitly; only $[U]$ is calculated. The procedure of the elimination will consist of eliminating the first column of $[A]$ for $i = 2, 3, \ldots, n$; then we eliminate the second column for $i = 3, 4, \ldots, n$; and so on until getting an upper triangular matrix whose solution was given in the previous section. During the elimination, the elements of the transformed matrix will be given by

$$A_{ij}^{(k)} = A_{ij}^{(k-1)} \qquad i = 1, 2, \ldots, k \qquad j = i, \ldots, n$$

$$B_{il}^{(k)} = B_{il}^{(k-1)} \qquad i = 1, 2, \ldots, k \qquad l = 1, 2, \ldots, r$$

and

$$A_{ij}^{(k)} = A_{ij}^{(k-1)} - \left[A_{ik}^{(k-1)} \Big/ A_{kk}^{(k)} \right] A_{kj}^{(k)} \qquad i = k+1, \ldots, n \qquad j = k+1, \ldots, n$$

$$B_{il}^{(k)} = B_{il}^{(k-1)} - \left[A_{ik}^{(k-1)} \Big/ A_{kk}^{(k)} \right] B_{kl}^{(k)} \qquad i = k+1, \ldots, n \qquad l = 1, 2, \ldots, r$$

$$A_{ij}^{(k)} = 0 \qquad \text{for } j = 1, 2, \ldots, k \qquad i = j+1, \ldots, n$$

$$\tag{1.77}$$

where n is the order of the system, r is the number of vectors in the unknown set $[X]$, and $k = 0$ represents the original $[A]$ and $[B]$ matrices. The elimination

procedure will begin at the stage $k = 1$ and terminate at the stage $k = (n - 1)$. The back substitution, i.e., the solution of the upper triangular system, will furnish the values of the unknown $[X]$, and this is given by Eq. (1.69) for the case of a full matrix and Eq. (1.71) for a banded matrix. Now, for the case of a banded matrix with a semibandwidth $l + 1$, Eq. (1.77) reads

$$A_{ij}^{(k)} = A_{ij}^{(k-1)} \qquad i = 1, 2, \ldots, k \qquad j = 1, 2, \ldots, i + l$$

$$B_{il}^{(k)} = B_{il}^{(k-1)} \qquad i = 1, 2, \ldots, k \qquad l = 1, 2, \ldots, r$$

$$A_{ij}^{(k)} = A_{ij}^{(k-1)} - \left[A_{ik}^{(k-1)} \big/ A_{kk}^{(k)} \right] A_{kj}^{(k)} \qquad i = k+1, \ldots, \lambda \qquad j = k+1, \ldots, \lambda$$

$$B_{il}^{(k)} = B_{il}^{(k-1)} - \left[A_{ik}^{(k-1)} \big/ A_{kk}^{(k)} \right] B_{kl}^{(k)} \qquad i = k+1, \ldots, \lambda \qquad j = 1, 2, \ldots, r$$

$$(1.78)$$

where n and r are as defined before and

$$\lambda = k + l - 1 \qquad \text{for } k + l - 1 < n$$

$$\lambda = n \qquad \text{for } k + l - 1 \geq n$$

Furthermore, we notice that, if $[A]$ is positive definite, as is the usual case in finite element analysis, no pivoting will be necessary during the decomposition.

1.5.4   General Choleski–Crout Method

In this method of solution, the diagonal matrix $[D]$ is incorporated to one of the triangular matrices. For example, if it is incorporated to $[l]$, the decomposition will be given by

$$u_{kk} = 1 \qquad k = 1, 2, \ldots, n$$

$$l_{ik} = a_{ik} - \sum_{m=1}^{k-1} l_{im} u_{mk} \qquad i = k, \ldots, \lambda$$

and

$$u_{kj} = \left[a_{kj} - \sum_{m=1}^{k-1} l_{km} u_{mj} \right] \bigg/ l_{kk} \qquad j = k+1, \ldots, \lambda \qquad (1.79)$$

where $\lambda = n$ and $\mu = 1$ for a full matrix, or

$$\lambda = k + l - 1 \qquad \text{for } k + l - 1 < n$$

$$\lambda = n \qquad \text{for } k + l - 1 \geq n$$

$$\mu = 1 \qquad \text{for } i < l + 1$$

$$\mu = k - l + i \qquad \text{for } i \geq l + 1$$

for a banded matrix with semibandwidth $= (l + 1)$. From Eq. (1.79), we see that the order of the computation will be as follows: the first column of $[l]$ is computed,

then the first row of $[u]$ is calculated, then the second column of $[l]$, followed by the second row of $[u]$, etc. After making the decomposition, we will have to perform two triangular solutions, i.e., after obtaining $[l]$ and $[u]$ we can write $[a][X] = [B]$ as

$$[l][u][X] = [B] \qquad (1.80)$$

Now let

$$[\xi] = [u][X] \qquad (1.81)$$

Then, Eq. (1.80) reads

$$[l][\xi] = [B] \qquad (1.82)$$

The system of Eq. (1.82) represents a lower triangular system (whose solution was treated before), with $[\xi]$ regarded as the unknown vectors. When $[\xi]$ are obtained, the upper triangular system (Eq. 1.81) will be solved for the unknowns $[X]$. The first step of the solution is known as the forward substitution step and the second as the back substitution step. Furthermore, we notice that if $[A]$ is symmetric, the elements of $[u]$ will not be calculated during the decomposition because the ith row of $[u]$ will be equal to the ith column of $[l]$, with all its elements divided by the diagonal value, i.e., l_{ii}, because when $[A]$ is symmetric the decomposition of $[A]$ reads

$$[A] = [L][D][L]^{\mathrm{T}} \qquad (1.83)$$

1.5.5   The Square Root Method
(Symmetric Choleski Decomposition)

In this section, we consider the solution of the system

$$[A][X] = [B] \qquad (1.84)$$

where $[A]$ is a symmetric and a positive definite matrix, which thus can be decomposed as

$$[A] = [L][L]^{\mathrm{T}} = [U]^{\mathrm{T}}[U] \qquad (1.85)$$

where $[L]$ and $[U]$ are unique upper and lower matrices with the diagonal elements given by $l_{ii} = u_{ii}$. Working with $[U]$ and writing Eq. (1.67) as

$$A_{ij} = \sum_{k=1}^{\min(i,j)} U_{ik} U_{kj} \qquad (1.86)$$

the elements of $[U]$ can be calculated from

$$U_{11} = (A_{11})^{\frac{1}{2}}$$
$$U_{1j} = [A_{1j}/U_{11}] \qquad j = 2, 3, \ldots, \lambda$$

and

$$U_{ii} = \left[A_{ii} - \sum_{k=\alpha}^{i-1} U_{ki}^2 \right]^{\frac{1}{2}} \qquad i = 2, 3, \ldots, n$$

$$U_{ij} = \left[A_{ij} - \sum_{k=\beta}^{i-1} U_{ki} U_{kj} \right] \Big/ U_{ii} \qquad j = i+1, \ldots, \gamma$$

(1.87)

with $\lambda = \gamma = n, \alpha = \beta = 1$ in the case of a full matrix, and

$$\lambda = l + 1$$

$$\alpha = i - l \qquad \text{for } i - l > 1 \qquad \text{or} \qquad = 0 \qquad \text{for } i - l \leq 1$$

$$\beta = j - l \qquad \text{for } j - l > 1 \qquad \text{or} \qquad = 1 \qquad \text{for } j - l \leq 1$$

$$\gamma = i + l - 1 \qquad \text{for } i + l - 1 < n \qquad \text{or} \qquad = n \qquad \text{for } i + l - 1 \geq n$$

where $(l + 1)$ is the half bandwidth for the case of a banded matrix. After obtaining $[U]$, the forward and backward substitutions will be performed as given in the last section. We notice that, because $[A]$ was assumed to be a positive definite matrix, all the expressions under the square root sign will be positive real numbers. To prove it, we substitute u_{ki} in terms of a_{ij} and we notice that the resulting expression will be a quotient of the determinants of the upper left minors of $[A]$, which are positive if $[A]$ is a positive definite matrix.

1.5.6   Tridiagonal Systems

Consider the following system, $[A][X] = [B]$, with $[A]$ being a tridiagonal matrix in the form

$$[A] = \begin{bmatrix} a_{11} & a_{12} & & & & \\ a_{21} & a_{22} & a_{23} & & & \\ & a_{32} & a_{33} & a_{34} & & \\ & \cdot & \cdot & \cdot & \cdot & \cdot \\ & & & & a_{n,n-1} & a_{n,n} \end{bmatrix}$$

(1.88)

which can be decomposed as

$$[A] = \begin{bmatrix} l_{11} & & & & \\ l_{21} & l_{22} & & & \\ & l_{32} & l_{33} & & \\ & \cdot & \cdot & \cdot & \cdot \\ & & & l_{n,n-1} & l_{n,n} \end{bmatrix} \begin{bmatrix} 1 & u_{12} & & & \\ & 1 & u_{23} & & \\ & & 1 & u_{34} & \\ & \cdot & \cdot & \cdot & \cdot \\ & & & & 1 \end{bmatrix}$$

(1.89)

The elements of $[l]$ and $[u]$ are given by

$$l_{11} = a_{11}$$

$$u_{12} = a_{11}^{-1} a_{12}$$

$$l_{i+1,i} = a_{i+1,i} \qquad i = 1, 2, \ldots, n \tag{1.90}$$

$$l_{ii} = a_{ii} - a_{i,i-1} u_{i-1,i} \qquad i = 1, 2, \ldots, n$$

$$u_{i,i+1} = l_{i,i}^{-1} a_{i,i+1} \qquad i = 2, 3, \ldots, n-1$$

The forward substitution [Eq. (1.82)] reads

$$\xi_{1j} = l_{1,1}^{-1} b_{1,j} \qquad j = 1, 2, \ldots, r$$

$$\xi_{ij} = l_{i,i}^{-1} [b_{ij} - l_{i,i-1} \xi_{i-1,j}] \qquad i = 2, 3, \ldots, n \qquad j = 1, 2, \ldots, r \tag{1.91}$$

and the back substitution [Eq. (1.81)] reads

$$X_{nj} = \xi_{nj} \qquad j = 1, 2, \ldots, r$$

$$X_{ij} = \xi_{ij} - u_{i,i+1} x_{i+1,j} \qquad i = n - 1, \ldots, 1 \qquad j = 1, 2, \ldots, r \tag{1.92}$$

where n is the order of the system and r the number of columns in $[X]$ and $[B]$. The above procedure can be extended to the case of banded matrices if these are partitioned in the form of blocks of tridiagonal submatrices, and the elements in Eqs. (1.88–1.92) will thus be replaced by the corresponding submatrices, on the condition that the required inverses of l_{ii} exist. Furthermore, if $[A]$ is symmetric, fewer operations will be required during the decomposition.

1.6   The Eigenvalue Problem

If $[A]$ is a square matrix of order n and λ is a scalar parameter, we define the eigenvalue problem written in the standard form as

$$[[A] - \lambda_i [I]]\{x_i\} = \{0\} \qquad i = 1, 2, \ldots, n \tag{1.93}$$

The matrix $[[A] - \lambda_i [I]]$ is called the characteristic matrix of the matrix $[A]$, λ_i represents the eigenvalues of $[A]$, and the vectors $\{x_i\}$ are called the eigenvectors of $[A]$. Furthermore, the system of Eq. (1.93) represents a set of linear homogeneous equations in the unknowns $\{x_i\}$. Except for trivial solutions, i.e., $\{x_i\} = \{0\}$, we must have $|[A] - \lambda_i [I]| = 0$, and this is an equation of nth degree in λ, whose solution will give the n eigenvalues λ_i of the problem. We call this equation the characteristic equation of the matrix $[A]$. In this section, various methods of eigenvalue and eigenvector extraction techniques will be discussed. For a detailed study on the subject, the reader is referred to standard textbooks on the subject.[5,7–9] The solution of the eigenvalue problem in the standard form [Eq. (1.93)] can be performed using direct or iterative methods. In direct methods, all the eigenvalues will be obtained at once, while in the iterative methods we can obtain needed values of eigenvalues. Depending on the problem to be solved and its order, one of the two methods will be preferable. For instance, in elastic stability analysis, we will be interested in determining only the lowest critical load, and, in dynamic analyses, we will be interested in the determination of the lowest modes; in such cases, iterative methods will be advantageous, principally if the order of the matrices

is large. In other situations, for instance in aeroelastic analyses, we will need to determine all the eigenvalues of the problem, and, in such cases, direct methods would be advantageous.

1.6.1 Determinantal Solution

For a nontrivial solution of Eq. (1.93), we write

$$|[A] - \lambda[I]| = 0 \tag{1.94}$$

which can be written as

$$\Delta(\lambda) = |[A] - \lambda[I]| = 0$$

$$= \lambda^n + c_1\lambda^{n-1} + c_2\lambda^{n-2} + \cdots + c_{n-1}\lambda + c_n = 0 \tag{1.95}$$

Now, defining the trace of a square matrix as the sum of the elements on its main diagonal and denoting it as $T_r[A]$, i.e.,

$$T_r[A] = \sum_{i=1}^{n} A_{ii} \tag{1.96}$$

we can show by expansion of Eq. (1.94) that

$$c_1 = -T_r[A] \tag{1.97}$$

Furthermore, if we write s_i as the trace of the ith power of $[A]$, i.e.,

$$s_1 = T_r[A], \quad s_2 = T_r[A]^2, \ldots, \quad s_n = T_r[A]^n$$

it can be shown by expansion that the coefficients c_r of Eq. (1.95) are given by

$$c_1 = -T_r[A] = -s_1$$

$$c_2 = -[c_1 s_1 + s_2]/2$$

$$c_3 = -[c_2 s_1 + c_1 s_2 + s_3]/3$$

$$\cdot$$

$$c_n = -[c_{n-1}s_1 + c_{n-2}s_2 + \cdots + c_1 s_{n-1} + s_n]/n$$

or

$$c_0 = 1 \qquad c_1 = -s_1$$

$$c_r = -\frac{1}{r}\sum_{i=1}^{r} c_{r-i}s_i \qquad r = 2, 3, \ldots, n \tag{1.98}$$

This process enables us to calculate in an efficient manner the coefficients of the characteristic equation, whose solution will determine the n eigenvalues, and these, when substituted in Eq. (1.93), will determine the corresponding eigenvectors of $[A]$. We notice that this process is lengthy and can be used only for matrices of very small order.

1.6.2 Von Mises Power Method

The von Mises power method is an iterative method for determining the eigenvalues and eigenvectors of a matrix $[A]$. Consider Eq. (1.93), which can be written as

$$[D]\{x\} = \frac{1}{\lambda}\{x\} \tag{1.99}$$

where $[D] = [A]^{-1}$. Assume now any approximate value for $\{x\}$, say $\{x_0\}$, which when substituted in the left-hand side of Eq. (1.99) and through multiplication by $[D]$, a vector $\{x_1\}$ is obtained, given by

$$\{x_1\} = [D]\{x_0\} \tag{1.100}$$

If we normalize $\{x_1\}$ by dividing all its elements by the largest element of $\{x_1\}$ and denoting the result by $\{x_1^*\}$, i.e.,

$$\{x_1^*\} = \frac{1}{\max[D]\{x_0\}}[D]\{x_0\} \tag{1.101}$$

it can be shown[9] that $\{x_1^*\}$ is a better approximation for the eigenvector $\{x\}$ than the initial trial vector $\{x_0\}$. If we repeat the process of multiplication and normalization, taking now $\{x_1^*\}$ as the initial trial vector, it is clear that a closer approximation will be obtained. Continuing the iteration until the convergence to a desired accuracy, i.e.,

$$\{x_{s+1}^*\} = \frac{1}{\max[D]\{x_s^*\}}[D]\{x_s^*\} = \{x_s^*\} \tag{1.102}$$

and comparing Eqs. (1.99) and (1.102), we see that $\{x_{s+1}^*\}$ converges to an eigenvector of $[D]$, thus of $[A]$, and the scaling factor, i.e., $\max[D]\{x_s\}$, will converge to $1/\lambda$, i.e., the corresponding eigenvalue. Furthermore, it can be shown[9] that this eigenvalue corresponds to the highest of $[D]$, i.e., the lowest of $[A]$. Now, in some eigenvalue problems, e.g., in linear elastic stability analysis, we will be interested only in determining the lowest characteristic value; therefore, the solution of the problem will be obtained at this stage. However, in other applications, e.g., free vibrations, we will be interested in general in determining not only the first mode but also few other modes above the lowest. To determine the second eigenvalue using the von Mises method, we use the property of orthogonality of the eigenvectors in relation to the matrix $[A]$. If we designate the first eigenvector, already calculated by $\{x_1\}$, and the second one to be found by $\{x_2\}$, the orthogonality condition reads

$$\{x_1\}^T[D]\{x_2\} = 0 \tag{1.103}$$

Setting

$$\{B\}^T = \{x_1\}^T[D] \tag{1.104}$$

we get

$$\{B\}^T\{x_2\} = 0 \tag{1.105}$$

Now, choosing arbitrary values for $x_{(2)2}, \ldots, x_{(2)n}$, we can calculate from Eq. (1.105) the value of $x_{(2)1}$ to satisfy the condition of $\{x_2\}$ being orthogonal to $\{x_1\}$. In matrix form, this condition is written as

$$
\begin{Bmatrix} x_{(2)1} \\ x_{(2)2} \\ \cdot \\ \cdot \\ \cdot \\ x_{(2)n} \end{Bmatrix} = \begin{bmatrix} 0 & -B_2/B_1 & -B_3/B_1 & \cdots & -B_n/B_1 \\ 0 & 1 & 0 & \cdots & 0 \\ \cdot & \cdot & \cdot & \cdot & \cdot \\ \cdot & \cdot & \cdot & \cdot & \cdot \\ \cdot & \cdot & \cdot & \cdot & \cdot \\ 0 & 0 & 0 & \cdots & 1 \end{bmatrix} \begin{Bmatrix} x_{(2)1} \\ x_{(2)2} \\ \cdot \\ \cdot \\ \cdot \\ x_{(2)n} \end{Bmatrix} \qquad (1.106)
$$

We call the matrix in Eq. (1.106) a "sweeping matrix" and denote it by $[s_1]$. Now, taking $\{x_2\}$ as an initial trial vector for the iterative process, we will converge to the second eigenvector and eigenvalue of $[A]$. The process of orthogonalization must be performed during each cycle of the iteration. However, this can be avoided if we postmultiply the matrix $[D]$ by $[s_1]$ and write the result as $[D_2]$, i.e.,

$$
[D][s_1]\{x_2\} = [D_2]\{x_2\} \qquad (1.107)
$$

We notice that the first column of $[D_2]$ is composed of zero elements so that the matrix $[D_2]$ can be reduced to $[D_2']$ of order $(n-1)$ and $\{x_2\}$ to $\{x_2'\}$ of order $(n-1)$. Iterating now on $[D_2']$ we will converge to the first eigenvalue and eigenvector of $[D_2']$. Finally, using Eq. (1.106), the first element of $\{x_2\}$ is determined, and thus the second eigenvalue and eigenvector of $[D_2]$ are obtained. The above procedure is then extended to calculate higher eigenvalues by choosing initial vectors orthogonal to the already calculated ones by constructing $[s_{(n)}]$ and iterating on $[D_{n+1}']$.

1.6.3   The Inverse Iteration Method

We notice that the von Mises power iteration method described in the previous section needs the inversion of the matrix $[A]$ as a first step in the solution if the eigenvalues are required in ascending order, and this is a time-consuming process. A more efficient process will be iterating directly on the matrix $[A]$ for obtaining the eigenvalues in ascending order. Such a process is called the inverse iteration method. Consider the eigenvalue problem written in the standard form as

$$
[A]\{x\} = \lambda\{x\} \qquad (1.108)
$$

Assuming now an initial trial vector $\{x_0\}$, the first step in the inverse iteration method will be the solution of the system of equations

$$
[A]\{z_1\} = \{x_0\} \qquad (1.109)
$$

with $\{z_1\}$ regarded as the unknown vector. An improved approximation for the trial vector will be given by

$$
\{x_1^*\} = \frac{1}{\max\{z_1\}}\{z_1\} \qquad (1.110)
$$

which is then used in the solution of the system of equations

$$
[A]\{z_2\} = \{x_1^*\} \qquad (1.111)
$$

to obtain a better approximation given by

$$\{x_2^*\} = \frac{1}{\max\{z_2\}}\{z_2\} \tag{1.112}$$

The process of iteration will be continued until the desired accuracy is reached, i.e.,

$$\{x_s^*\} = \frac{1}{\max\{z_s\}}\{z_s\} = \{x_{s-1}^*\} \tag{1.113}$$

This will give the first approximate eigenvector, and the corresponding lowest eigenvalue will be

$$\lambda = \frac{1}{\max\{z_s\}} \tag{1.114}$$

To obtain subsequent eigenvectors and eigenvalues, the process of orthogonalization and sweeping described in the previous section will be used. We notice that the matrix $[A]$ will be triangularized only at the beginning of the solution, and, during each step of iteration, we will have to perform only the solution of two triangular systems.

1.6.4 Iteration Method Working Directly on the Eigenvalue Problem $[k]\{x\} = \lambda[M]\{x\}$

In many engineering problems, using numerical methods of solution, e.g., the finite element method for the solution of free vibration problems and linear elastic stability analyses, we will be faced with an eigenvalue problem cast in the form

$$[k]\{x\} = \lambda[M]\{x\} \tag{1.115}$$

where the matrices $[k]$ and $[M]$ are symmetric and banded matrices. Furthermore, in free vibration problems, the matrix $[M]$ is often a diagonal matrix if the lumped mass technique is used in the problem formulation and sometimes with many zero elements in the diagonal if the masses are concentrated only at a few nodal points and few degrees of freedom of these nodes. The iterative methods described in the last two sections work on the eigenvalue problem written in the standard form of Eq. (1.93) so that a first step in the solution would be the transformation of Eq. (1.115) to the standard form if the iteration methods are to be applied as described in the last two sections. Now, if both $[k]$ and $[M]$ are symmetric and $[M]$ is positive definite, we can decompose $[M]$ using the Choleski method to obtain

$$[M] = [L][L]^T \tag{1.116}$$

where $[L]$ is a lower triangular matrix of the same bandwidth as $[M]$. Substituting Eq. (1.116) into Eq. (1.115) and premultiplying both sides by $[L]^{-1}$, we obtain

$$[L]^{-1}[k]\{x\} = \lambda[L]^T\{x\} \tag{1.117}$$

Now, defining a vector $\{y\}$ as

$$[L]^T\{x\} = \{y\} \tag{1.118}$$

the eigenvalue problem in Eq. (1.117) transforms to

$$[A]\{y\} = \lambda\{y\} \tag{1.119}$$

where $[A] = [L]^{-1}[k][L^T]^{-1}$. We observe that Eq. (1.119) is now in the standard form; however, the matrix $[A]$ while still symmetric is no more banded. Furthermore, the process involves the inversion of the matrix $[L]$. Clough[10] proposed an iteration process working directly on Eq. (1.115) using a modified inverse iteration method. The iteration begins by postmultiplying $[M]$ by an initial trial vector $\{x_0\}$ to obtain a vector $\{w_0\}$ given by

$$\{w_0\} = [M]\{x_0\} \tag{1.120}$$

The second step in the iteration process is to solve the system of equations

$$[K]\{z_1\} = \{w_0\} \tag{1.121}$$

where $\{z_1\}$ is regarded as the unknown vector and the improved eigenvector is given by

$$\{x_1^*\} = \frac{1}{\max\{z_1\}}\{z_1\} \tag{1.122}$$

The process of iteration is then continued until reaching the desired accuracy. We observe that in each iteration cycle we will have to perform a symmetric banded matrix multiplication [Eq. (1.120)] and two triangular banded matrix solutions [Eq. (1.121)]. The multiplication step introduced here is more than compensated because the banding nature of the matrices is conserved and the matrix inversion is avoided. Now, if $[M]$ is diagonal with no zero elements on the diagonal, the system in Eq. (1.115) is easily transformed to a standard symmetric banded system. The process starts by writing $[M]$ as

$$[M] = \left[M^{\frac{1}{2}}\right]\left[M^{\frac{1}{2}}\right] \tag{1.123}$$

where $[M^{1/2}]$ stands for a diagonal matrix formed by the square roots of the respective elements of $[M]$. Substituting Eq. (1.123) into Eq. (1.115) and premultiplying both sides by $[M^{1/2}]^{-1}$, we obtain

$$\left[M^{\frac{1}{2}}\right]^{-1}[k]\{x\} = \lambda\left[M^{\frac{1}{2}}\right]\{x\} \tag{1.124}$$

Now, defining a vector $\{y\}$ as

$$\left[M^{\frac{1}{2}}\right]\{x\} = \{y\} \tag{1.125}$$

the eigenvalue problem in Eq. (1.124) transforms to

$$[A]\{y\} = \lambda\{y\} \tag{1.126}$$

where $[A] = [M^{1/2}]^{-1}[k][M^{1/2}]^{-1}$. We observe that Eq. (1.126) is now in a standard form and $[A]$ is symmetric and banded. The solution of Eq. (1.126) will give the eigenvalues λ and the eigenvectors $\{y\}$. The system eigenvectors $\{x\}$ are obtained from Eq. (1.125). When the matrix $[M]$ is diagonal with many zero

elements in the diagonal, the system of Eq. (1.115) is efficiently solved using the so-called selective inversion technique. The process starts by solving

$$[K]\{f_i\} = \{e_i\} \tag{1.127}$$

where $\{e_i\}$ are unit vectors, having zero values in all locations except for the position corresponding to the ith nonzero value on the main diagonal of $[M]$, and $\{f_i\}$ are regarded as the unknown vectors. The solution of Eq. (1.127) will produce n_r vectors $\{f_i\}$ corresponding to the n_r nonzero values on the main diagonal of the mass matrix $[M]$. Selecting for each $\{f_i\}$ the corresponding n_r values, we can form a matrix of influence coefficients of dimension n_r, say $[F']$. This matrix by definition is a reduced flexibility matrix and its inverse is a reduced stiffness matrix so that we can write for Eq. (1.115) an equivalent reduced system as

$$[F']^{-1}\{\xi\} = \lambda[M']\{\xi\} \tag{1.128}$$

where $\{\xi\}$ is of dimension n_r and $[M']$ is a diagonal matrix of order n_r, with all zero elements of $[M]$ dropped out. The system of Eq. (1.128) can now be transformed to a standard form as follows. Premultiplying Eq. (1.128) by $[F']$, we obtain

$$\{\xi\} = \lambda[F'][M']\{\xi\} \tag{1.129}$$

writing as before $[M'] = [M'^{1/2}][M'^{1/2}]$ and defining a vector $\{\eta\}$ as

$$\left[M'^{\frac{1}{2}}\right]\{\xi\} = \{\eta\} \tag{1.130}$$

the eigenvalue problem transforms to

$$[A]\{\eta\} = (1/\lambda)\{\eta\} \tag{1.131}$$

where $[A] = [M'^{1/2}][F'][M'^{1/2}]$. The von Mises method of iteration can be applied now to Eq. (1.131) to obtain the eigenvalues λ in ascending order. Again, the system eigenvectors will be obtained using Eq. (1.130). We observe that $[A]$ is a full matrix; however, it is of a smaller order compared to the original system.

References

[1] Frazer, R. A., Duncan, W. J., and Collar, A. R., *Elementary Matrices,* Macmillan, New York, 1949.

[2] Pipes, L. A., "Matrices in Engineering," *Modern Mathematics for Engineers,* edited by E. F. Bekenbach, McGraw–Hill, New York, 1956.

[3] Lancaster, P., *Theory of Matrices,* Academic, New York, 1969.

[4] Westlake, J. R., *A Handbook of Numerical Matrix Inversion and Solution of Linear Equations,* Wiley, New York, 1968.

[5] Faddeeva, V. N., *Computational Methods of Linear Algebra,* Dover, New York, 1959.

[6] Varga, R. S., *Matrix Iterative Analysis*, Prentice–Hall, Englewood Cliffs, NJ, 1962.

[7] Wilkinson, J. H., *The Algebraic Eigenvalue Problem,* Clarendon, Oxford, England, UK, 1965.

[8] Gourley, A. R., and Watson, G. A., *Computational Methods for Matrix Eigenproblems,* Wiley, New York, 1973.

[9] Jennings, A., *Matrix Computation for Engineers and Scientists,* Wiley, New York, 1977.

[10]Clough, R. W., "Vibration Analysis of Finite Element Systems," *Lectures on Finite Elements Methods in Continuum Mechanics,* edited by J. T. Oden and E. R. A. Oliveira, Univ. of Alabama, Huntsville, 1973.

Problems

1.1   The matrices $[A]$ and $[B]$ are given by

$$[A] = \begin{bmatrix} x & z \\ z & y \end{bmatrix} \quad \text{and} \quad [B] = \begin{bmatrix} \cos\theta & -\sin\theta \\ \sin\theta & \cos\theta \end{bmatrix}$$

Find the values of θ that diagonalize the product $[B]^T[A][B]$.

1.2   Find the eigenvalues of the matrix

$$\begin{bmatrix} 2 & -2 & 3 \\ 1 & 1 & 1 \\ 1 & 3 & -1 \end{bmatrix}$$

1.3   The stiffness and mass matrices of a dynamic system are given by

$$[k] = \begin{bmatrix} 2 & -1 & & \\ -1 & 2 & -1 & \\ & -1 & 2 & -1 \\ & & -1 & 1 \end{bmatrix} \quad \text{and} \quad [m] = \begin{bmatrix} 4 & 1 & & \\ 1 & 4 & 1 & \\ & 1 & 4 & 1 \\ & & 2 & 2 \end{bmatrix}$$

Find the first two natural frequencies and the corresponding mode shapes of free vibration.

1.4   Show that for an orthogonal matrix $[A]$ the determinant of $[A]$ is 1 or -1.

1.5   Let $[A]$ and $[B]$ be two square matrices of order n. Show that

$$T_r[A][B] \sum_{i=1}^{n} \sum_{k=1}^{n} A_{ik} B_{ki}$$

1.6   If $[A]$ is a square symmetric matrix and given a matrix $[T]$ of order nm, verify that the product $[T]^T[A][T]$ is a symmetric matrix.

1.7   Writing for a quadratic form

$$F(x_1, x_2, \ldots, x_n) = \tfrac{1}{2}\{x\}^T[a]\{x\}$$

where $[a]$ is a symmetric matrix, show that

$$\left\{ \frac{\partial F}{\partial x} \right\} = [a]\{x\}$$

where

$$\left\{ \frac{\partial F}{\partial x} \right\} = \left(\frac{\partial F}{\partial x_1} \cdots \frac{\partial F}{\partial x_n} \right)^T$$

2
Single-Degree-of-Freedom Linear Systems

2.1 Equation of Motion

Consider the single-degree-of-freedom mechanical system shown in Fig. 2.1. The system consists of a concentrated mass m (kg), a spring with a spring constant k (N·m), and a dashpot having a viscous damping coefficient c (N·s/m). The external applied load is $F(t)(N)$ and the displacement $x(t)(m)$ is measured from the position of equilibrium. The potential energy stored at any instance of time t, measured from the position of equilibrium, can be written as

$$U = \int_0^x kx \, dx = \frac{1}{2}kx^2 \tag{2.1}$$

The kinetic energy of the mass m reads

$$T = \tfrac{1}{2}mx'^2 \tag{2.2}$$

where $x' = dx/dt$. The system dissipation function can be expressed as

$$D = \tfrac{1}{2}cx'^2 \tag{2.3}$$

Applying Lagrange's equation of motion,

$$[dL/dx']' - dL/dx + dD/dx' = Q \tag{2.4}$$

where $L = T - U$ and Q is the generalized force corresponding to the degree of freedom x, we obtain

$$mx'' + cx' + kx = F(t) \tag{2.5}$$

2.2 Free Vibration

We consider first the response of the system because of initial conditions $x(0)$ and $x'(0)$ in free vibration, i.e., $F(t) = 0$. The equation of motion [Eq. (2.5)] reads

$$mx'' + cx' + kx = 0 \tag{2.6}$$

Equation (2.6) is a homogeneous differential equation that admits solutions in the form

$$x = x_0 e^{pt} \tag{2.7}$$

where x_0 is an arbitrary constant to be determined from the initial conditions and p is a parameter that depends on the system properties. Substituting the solution to Eq. (2.7) into the equation of motion (2.6), we obtain

$$p^2 + (c/m)p + (k/m) = 0 \tag{2.8}$$

27
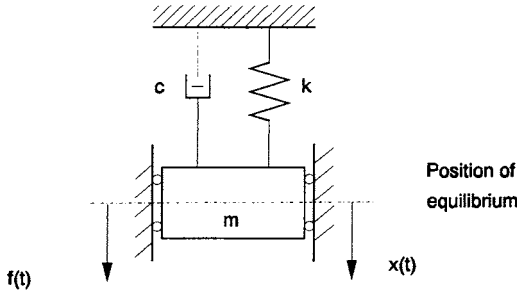
Fig. 2.1   Single-degree-of-freedom mechanical system.

Equation (2.8) is the system characteristic equation and has solutions p_1 and p_2, given by

$$p = -(c/2m) \pm [(c/2m)^2 - (k/m)]^{\frac{1}{2}} \tag{2.9}$$

Consider first the undamped system, i.e., $c = 0$. For such a case, Eq. (2.9) reads

$$p = \pm i(k/m)^{\frac{1}{2}} \qquad i = (-1)^{\frac{1}{2}} \tag{2.10}$$

The system response can be obtained using Eqs. (2.7) and (2.10) and reads

$$x = x_{01}e^{i\omega_n t} + x_{02}e^{-i\omega_n t} \tag{2.11}$$

where $\omega_n = (k/m)^{1/2}$ and will be defined as the system *undamped natural circular frequency* and has units of rad/s. Notice that because k and m are properties of the system, it follows that ω_n is also a property of the mechanical system. The values of x_{01} and x_{02} can be determined from the initial conditions of the problem. Using trigonometric relations, we can write Eq. (2.11) as

$$x = (x_{01} + x_{02})\cos \omega_n t + i(x_{01} - x_{02})\sin \omega_n t$$
$$= A_1 \cos \omega_n t + A_2 \sin \omega_n t \tag{2.12}$$

or

$$x = A \cos(\omega_n t - \phi) \tag{2.13}$$

where $A = [A_1^2 + A_2^2]^{1/2} = 2[x_{01} x_{02}]^{1/2}$ and $\phi = \tan^{-1} A_2/A_1 = \tan^{-1} i(x_{01} - x_{02})/(x_{01} + x_{02})$. The constants A and ϕ are called the amplitude and the phase of the response of the system, respectively. Substituting initial conditions at $t = 0$, we obtain

$$x = x(0)\cos \omega_n t + [x'(0)/\omega_n]\sin \omega_n t$$
$$= [x(0)^2 + \{x'(0)/\omega_n\}^2]^{\frac{1}{2}} \cos[\omega_n t - \tan^{-1}\{x'(0)/\omega_n x(0)\}] \tag{2.14}$$

A plot of the solution [Eq. (2.14)] is shown in Fig. 2.2. We observe that the system is performing a simple harmonic motion with a circular frequency ω_n.

We define the time to complete a cycle as the period and denote it by T, which is given by

$$T = 2\pi/\omega_n = 1/f_n \tag{2.15}$$
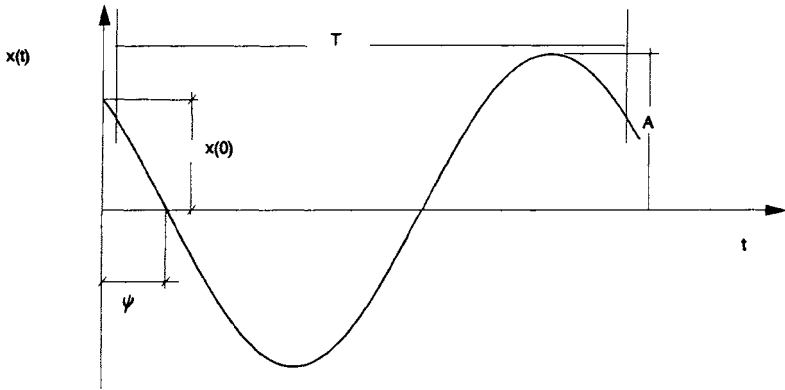
Fig. 2.2   Free vibration of an undamped single-degree-of-freedom system: $T = 2\pi/\omega_n$ $= 1/f_n$, $A = [x^2(0) + x'^2(0)/\omega_n^2]^{1/2}$, and $\psi = \phi/\omega_n = \{tg^{-1}x'(0)/[\omega_n x(0)]\}/\omega_n$.

where $f_n = \omega_n/2\pi$ and represents the number of cycles per second that the system performs in free vibration and will be called the system undamped free vibration frequency. Cycles per second is a unit commonly called hertz (Hz). Consider now the damped case, i.e., $c \neq 0$. Using the definition $\omega_n = (k/m)^{1/2}$, we can write the roots of the characteristic Eq. (2.9) as

$$p = -(c/2m) \pm \left[(c/2m)^2 - \omega_n^2\right]^{\frac{1}{2}} \qquad (2.16)$$

Examination of Eq. (2.16) reveals that we can classify the solution into three cases, depending on whether value of the expression $[(c/2m)^2 - \omega_n^2]$ assumes a positive, negative, or zero value. We consider first the case when $[(c/2m)^2 - \omega_n^2] = 0$. In such a case, we have two equal roots and the system response reads

$$x = [A + Bt]e^{-(c/2m)t} \qquad (2.17)$$

Equation (2.17) represents a damped nonoscillatory motion as shown in Fig. 2.3. The arbitrary constants A and B can be determined from the initial conditions of the problem. In this case, we will define the damping constant as the critical damping
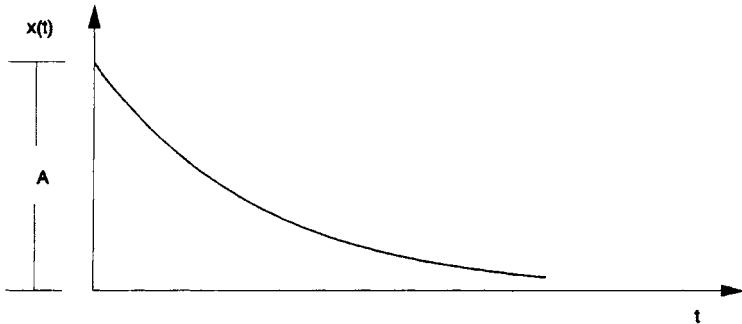
Fig. 2.3   Damped nonoscillatory motion.

coefficient c_c which is given by

$$c_c = 2m\omega_n = 2(km)^{\frac{1}{2}} \tag{2.18}$$

Now, using Eq. (2.18) and the definition of the undamped natural frequency ω_n, the equation of motion [Eq. (2.6)] can be written as

$$x'' + 2\gamma\omega_n x' + \omega_n^2 x = 0 \tag{2.19}$$

where $\gamma = c/c_c$ and will be called the viscous damping ratio or simply the damping ratio. The roots of the characteristic equation can now be written as

$$p = -\gamma\omega_n \pm i\omega_n(1 - \gamma^2)^{\frac{1}{2}} \tag{2.20}$$

and we will be left with two cases to be considered, $1 - \gamma^2 < 0$ and $1 - \gamma^2 > 0$.

For $1 - \gamma^2 < 0$, we have a nonoscillatory damped solution given by

$$x = e^{-\gamma\omega_n t}\left(A \sinh \omega_n\sqrt{\gamma^2 - 1}t - B \cosh \omega_n\sqrt{\gamma^2 - 1}t\right) \tag{2.21}$$

where A and B are arbitrary constants to be determined from the initial conditions. We notice that for this case the damping constant c must have a very high value, not common in practical applications; therefore, such cases will not be treated here. Systems with $1 - \gamma^2 < 0$ are called overdamped systems.

For $1 - \gamma^2 > 0$, we have a damped oscillatory response given by

$$x = e^{-\gamma\omega_n t}\left(x_{01}e^{i\omega_d t} + x_{02}e^{-i\omega_d t}\right) \tag{2.22}$$

where

$$\omega_d = \omega_n(1 - \gamma^2)^{\frac{1}{2}} \tag{2.23}$$

and will be called the damped circular natural frequency of the system. Notice again that ω_d depends only on the properties of the mechanical system and therefore is a property of the system. Such systems with $1 - \gamma^2 > 0$ represent the majority of practical cases and are called damped systems. The constants x_{01} and x_{02} of Eq. (2.22) are determined from the initial conditions of the problem. Using trigonometric relations, we can write Eq. (2.22) as

$$x = e^{-\gamma\omega_n t}[(x_{01} + x_{02})\cos \omega_d t + i(x_{01} - x_{02})\sin \omega_d t]$$
$$= e^{-\gamma\omega_n t}[A_1 \cos \omega_d t + A_2 \sin \omega_d t] \tag{2.24}$$

or

$$x = e^{-\gamma\omega_n t}[A \cos(\omega_d t - \phi)] \tag{2.25}$$

where $A = [A_1^2 + A_2^2]^{1/2} = 2[x_{01} x_{02}]^{1/2}$ and $\phi = \tan^{-1} A_2/A_1 = \tan^{-1} i(x_{01} - x_{02})/(x_{01} + x_{02})$. In terms of the initial conditions $x(0)$ and $x'(0)$ the system response reads

$$x = e^{-\gamma\omega_n t}\left\{x^2(0) + \left[\frac{x'(0) + x(0)\gamma\omega_n}{\omega_d}\right]^2\right\}^{\frac{1}{2}}$$

$$\times \cos\left\{\omega_d t - \tan^{-1}\left[\frac{x'(0) + x(0)\gamma\omega_n}{\omega_d x(0)}\right]\right\} \tag{2.26}$$
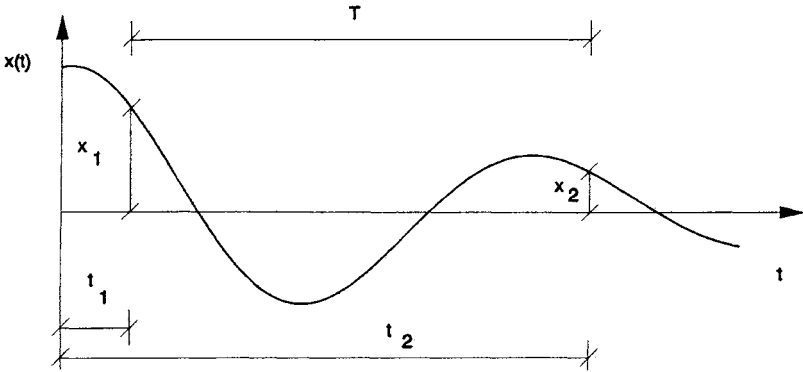
Fig. 2.4 Free vibration of a single-degree-of-freedom damped system: $T = 2\pi/\omega_d$ $= 1/f_d$ **(Curve is plotted for $\gamma = 0.15$).**

A typical response of a damped system is shown in Fig. 2.4. It is instructive to observe that the response shown in Fig. 2.4 suggests a method for determining the value of γ experimentally. Let the amplitude at a time $t = t_1$ be x_1 and at a time $t = t_2$, separated from t_1 by a Δt equal to the period of oscillation T, be x_2. Using Eq. (2.25) we can write the ratio of the amplitudes x_1/x_2 as

$$\frac{x_1}{x_2} = \frac{Ae^{-\gamma\omega_n t_1}\cos(\omega_d t_1 - \phi)}{Ae^{-\gamma\omega_n t_2}\cos(\omega_d t_2 - \phi)} = e^{\gamma\omega_n T} \tag{2.27}$$

Defining now the logarithmic decrement δ as

$$\delta = \ell n(x_1/x_2) \tag{2.28}$$

and using Eq. (2.27) we obtain

$$\delta = 2\pi\gamma/(1-\gamma^2)^{\frac{1}{2}} \tag{2.29}$$

or

$$\gamma = \delta/(\delta^2 + 4\pi^2)^{\frac{1}{2}} \tag{2.30}$$

For practical applications, the value of γ is very small compared to unity, for instance, for steel construction ($\gamma = 0.03$) and for riveted aluminum structures ($\gamma = 0.02$). Therefore, in such cases we can make the approximation $1 - \gamma^2 \cong 1$ in Eq. (2.29), and the relation [Eq. (2.30)] simplifies to

$$\gamma = \delta/2\pi \tag{2.31}$$

Now if we examine Eq. (2.25) and Fig. 2.4, we notice that the product $\gamma\omega_n$ is responsible for the exponential damping of the system. Defining $\alpha = \gamma\omega_n$ and using the relation [Eq. (2.31)], we obtain

$$\alpha \cong \delta\omega_n/2\pi \tag{2.32}$$

and because $1 - \gamma^2 \cong 1$, we can approximate ω_d by ω_n, and Eq. (2.32) reads

$$\alpha \cong \delta\omega_d/2\pi = \delta f_d \qquad (2.33)$$

Equation (2.33) represents a practical means to obtain the exponential damping α experimentally.

2.3 Response to Harmonic Excitation

In this section, the response of a single-degree-of-freedom system to an external harmonic excitation is studied. The external force $F(t)$ can be written as

$$F(t) = P_0 \cos \underline{\omega} t \qquad (2.34)$$

where P_0 is the amplitude and $\underline{\omega}$ is the frequency of the excitation force. Using Eqs. (2.5) and (2.19), we can write the equation of motion as

$$x'' + 2\gamma\omega_n x' + \omega_n^2 x = (P_0/m)\cos\underline{\omega} t \qquad (2.35)$$

The solution of Eq. (2.35) will be composed of two parts. The first part is the transient or homogeneous solution studied in the previous section and given by Eq. (2.24). The second part is the permanent solution or the particular integral solution. The solution of Eq. (2.35) can thus be written as

$$x = x_1 + x_2 \qquad (2.36)$$

where x_1 is given by Eq. (2.24) and x_2 reads

$$x_2 = A \cos(\underline{\omega} t - \phi) \qquad (2.37)$$

Applying the initial conditions at $t = t_0$, we obtain the complete solution as

$$x = e^{-\gamma\omega_n t} \left\{ [x_0 - A \cos \phi]\cos \omega_d t + \frac{1}{\omega_d}[x_0 + \gamma\omega_n(x_0 - A \cos \phi) \right.$$

$$\left. - \underline{\omega} A \sin \phi] \sin \omega_d t \right\} + A \cos(\underline{\omega} t - \phi) \qquad (2.38)$$

where A and ϕ are the amplitude and the phase of the permanent solution and can be determined by the substitution of Eq. (2.38) into Eq. (2.35). Depending on the initial conditions and the damping of the system, the influence of the transient solution will appear in limited first cycles of the response. We now concentrate our attention on the permanent solution. Differentiating Eq. (2.37) and substituting into Eq. (2.35), we obtain

$$\sin \underline{\omega} t \left[-A\underline{\omega}^2 \sin \phi - 2\omega_n\underline{\omega}\gamma A \cos \phi + \omega_n^2 A \sin \phi \right] + \cos \underline{\omega} t \left[-A\underline{\omega}^2 \cos \phi \right.$$

$$\left. + 2\omega_n\underline{\omega} A \sin \phi + \omega_n^2 A \cos \phi - (P_0/m) \right] = 0 \qquad (2.39)$$

We notice that Eq. (2.39) is valid at any instant of time t; therefore, the only condition for that equation to be satisfied is that the bracket terms vanish individually and we write

$$-A\left(\underline{\omega}^2 \sin \phi + 2\omega_n\underline{\omega}\gamma \cos \phi - \omega_n^2 \sin \phi\right) = 0 \qquad (2.40)$$

and

$$A\left(\underline{\omega}^2 \cos\phi - 2\omega_n\underline{\omega} \sin\phi - \omega_n^2 \cos\phi\right) + (P_0/m) = 0 \tag{2.41}$$

Solving Eqs. (2.40) and (2.41), we obtain

$$\tan\phi = \frac{2\gamma\Omega}{(1 - \Omega^2)} \tag{2.42}$$

and

$$A = \frac{P_0/k}{\sqrt{(1 - \Omega^2)^2 + (2\gamma\Omega)^2}} \tag{2.43}$$

where $\Omega = \underline{\omega}/\omega_n$.

The amplitude A given by Eq. (2.43) and the phase angle ϕ given by Eq. (2.42) define completely the permanent solution. The maximum response of the permanent solution can be obtained using Eqs. (2.37) and (2.43) and reads

$$x_{2_{max}} = \frac{P_0/k}{\sqrt{(1 - \Omega^2)^2 + (2\gamma\Omega)^2}}$$

Now, because $[P_0/k]$ represents a static displacement due to the application of a static load P_0, we will denote this displacement by x_{st} and write

$$\xi = \frac{x_{2_{max}}}{x_{st}} = \frac{1}{\sqrt{(1 - \Omega^2)^2 + (2\gamma\Omega)^2}} \tag{2.44}$$

The ratio ξ is called the dynamic magnification factor or the gain and is a function of γ and Ω. Figure 2.5 represents a plotting of the gain ξ vs Ω for different values of γ. From this figure, the following is observed:

1) For $\Omega = 0$, i.e., $\underline{\omega} = 0$, all the curves have a unit value, i.e., the response is equal to the static displacement.

2) For large values of $\underline{\omega}$, i.e., Ω tending to infinity, the gain ξ tends to zero for all values of γ.

3) Differentiating ξ with respect to Ω for a constant γ, we obtain

$$\frac{d\xi}{d\Omega} = -\frac{-4(1 - \Omega^2)\Omega + 8\gamma^2\Omega}{[(1 - \Omega^2)^2 + (2\gamma\Omega)^2]^{\frac{3}{2}}}$$

and the maximum value of the gain is obtained at $d\xi/d\Omega = 0$, or for

$$\Omega = \sqrt{1 - 2\gamma^2} \tag{2.45}$$

so that the maximum amplitude response will be obtained for an excitation frequency given by

$$\underline{\omega}_{Res} = \omega_n\sqrt{1 - 2\gamma^2} \tag{2.46}$$

We will define this frequency as the resonance frequency and we observe again that this is a system property.

4) Examination of Eqs. (2.23) and (2.46) shows that

$$\omega_n > \omega_d > \omega_{Res} \tag{2.47}$$
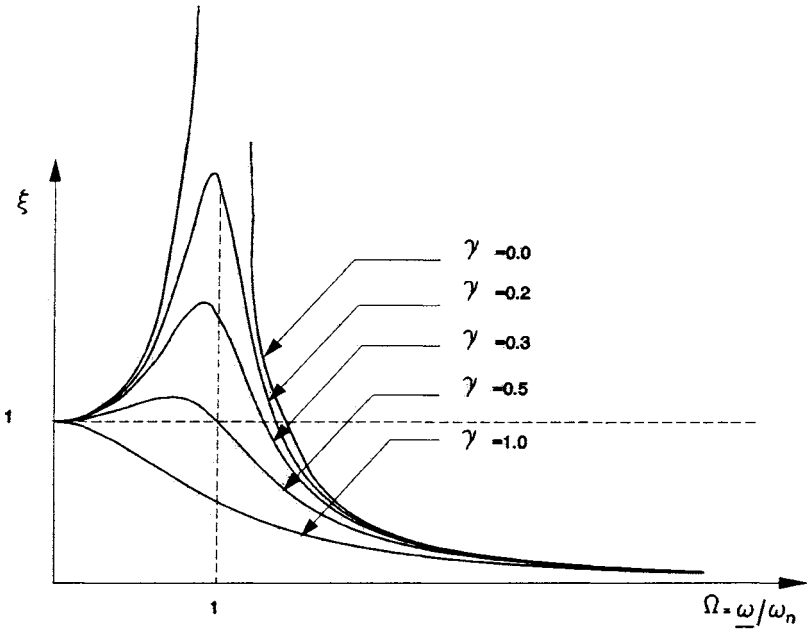
Fig. 2.5   Curves of the dynamic amplification factor $\xi = x_{max}/x_{st}$ vs Ω for different values of γ.

5) When $\gamma > (2)^{-1/2}$, the phenomenon of resonance disappears.

6) Substituting Eq. (2.45) into Eq. (2.44), we obtain the maximum value of the gain as

$$\xi_{max} = \frac{1}{2\gamma\sqrt{1 - \gamma^2}} \tag{2.48}$$

and, for very small values of γ, i.e., $\gamma^2 \ll 1$, we can write

$$\xi_{max} = 1/2\gamma \tag{2.49}$$

The ratio $1/2\gamma$ is defined as the *Q-factor* and is a measure of the system damping when $\gamma \ll 1$. Consider Fig. 2.6, which represents a typical curve of the amplitude A vs the excitation frequency in turns of the resonance frequency. Let A_R be the maximum amplitude and A_1 be an amplitude at a frequency $\underline{\omega}_1$ near the resonance phenomenon. Using Eq. (2.44), we can write

$$\frac{A_1}{x_{st}} = \frac{1}{\left\{\left[1 - (\underline{\omega}_R - \Delta\omega/2)^2/\omega_n^2\right]^2 + 4\gamma^2(\underline{\omega}_R - \Delta\omega/2)^2/\omega_n^2\right\}^{\frac{1}{2}}} \tag{2.50}$$

where $\Delta\omega/2 = \omega_R - \omega_1$ and, for $\gamma^2 \ll 1$, we have $\Delta\omega^2/\omega_n^2 \ll \Delta\omega/\omega_n \ll 1$ so
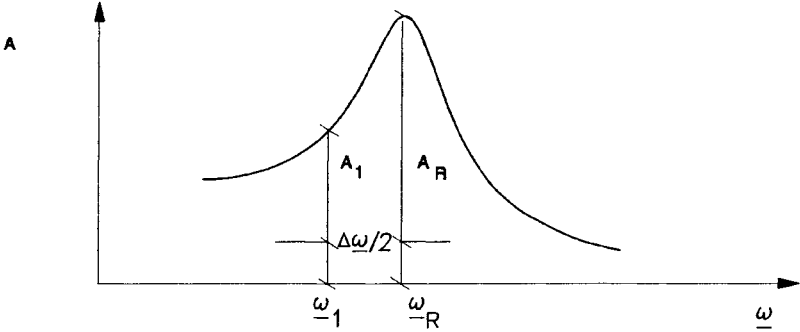
Fig. 2.6   Typical amplitude response A vs driving frequency $\underline{\omega}$ in the vicinity of resonance.

that we can write Eq. (2.50) as

$$\frac{A_1}{x_{st}} \cong \frac{1}{[(\Delta\omega/\omega_n)^2 + 4\gamma^2]^{\frac{1}{2}}} \tag{2.51}$$

Using Eqs. (2.49) and (2.51), we obtain

$$R = \frac{A_R}{A_1} \cong \frac{1}{2\gamma}[(\Delta\omega/\omega_n)^2 + 4\gamma^2]^{\frac{1}{2}} \tag{2.52}$$

or

$$\gamma = \frac{\Delta\omega}{2\omega_n}\frac{1}{\sqrt{R^2 - 1}} \tag{2.53}$$

and if we take $R^2 = 2$, i.e., $A_1 = A_R/(2)^{1/2} \cong 0.7A_R$, we have

$$\gamma = \frac{\Delta\omega}{2\omega_n} \tag{2.54}$$

Equations (2.49), (2.53), and (2.54) suggest methods for the determination of the damping ratio γ during ground vibration tests. Going back to the phase angle ϕ, we have

$$\phi = \tan^{-1}\frac{2\gamma\Omega}{1 - \Omega^2} \tag{2.55}$$

Figure 2.7 presents plots of the phase angle ϕ vs Ω for different values of the damping ratio γ.

From these curves, the following is observed:

1) For very small values of Ω and $\gamma^2 \ll 1$, we have $\tan\phi \cong 0$. Thus the response is in phase with the excitation.

2) For $\Omega = 1$, independent of the value of γ, $\tan\phi = \infty$, or $\phi = \pi/2$, i.e., the response is $\pi/2$-phased in relation to the excitation. It is instructive to observe that the passage of the response phase at $\pi/2$ is at the undamped natural frequency, while the point of the maximum amplitude of the response is at the resonance frequency.
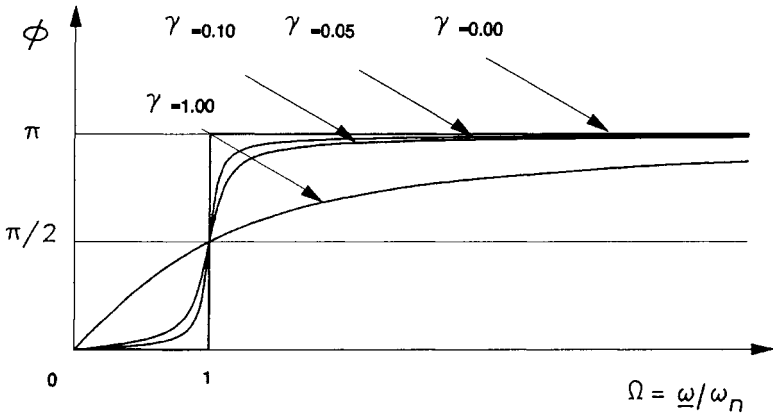
Fig. 2.7   Curves of the phase angle ϕ vs Ω for different values of γ.

Therefore, during a ground vibration test, if ξ and ϕ are plotted simultaneously, the departure of the point of maximum ξ and the passage at $\pi/2$ for the phase is an indication of how great the system damping is. Furthermore, this suggests a method for the determination of the damping ratio γ using Eq. (2.46).

3) When $\Omega \gg 1$ and $\gamma^2 \ll 1$, we have $\tan\phi \cong 1$, i.e., the response is π-phased with respect to the excitation force.

2.3.1 Transmissibility Factor

Using the equation of motion [Eq. (2.5)], we can write the force transmitted to the base as

$$F_t = cx' + kx = 2\gamma\omega_n m x' + \omega_n^2 m x \qquad (2.56)$$

Substituting the permanent solution [Eq. (2.37)] into Eq. (2.56), we obtain

$$F_t = \frac{P_0}{\sqrt{(1-\Omega^2)^2 + (2\gamma\Omega)^2}}\{-2\gamma\Omega\sin(\omega t - \phi) + \cos(\omega t - \phi)\} \qquad (2.57)$$

or

$$\frac{F_t}{P_0} = \sqrt{\frac{1+(2\gamma\Omega)^2}{(1-\Omega^2)^2 + (2\gamma\Omega)^2}}\ \cos(\omega t - \psi) \qquad (2.58)$$

where ψ is a new phase angle. We define the amplitude of F_t/P_0 as the transmissibility factor and we write

$$\eta = \left(\frac{F_t}{P_0}\right)_{max} = \sqrt{\frac{1+(2\gamma\Omega)^2}{(1-\Omega^2)^2 + (2\gamma\Omega)^2}} \qquad (2.59)$$
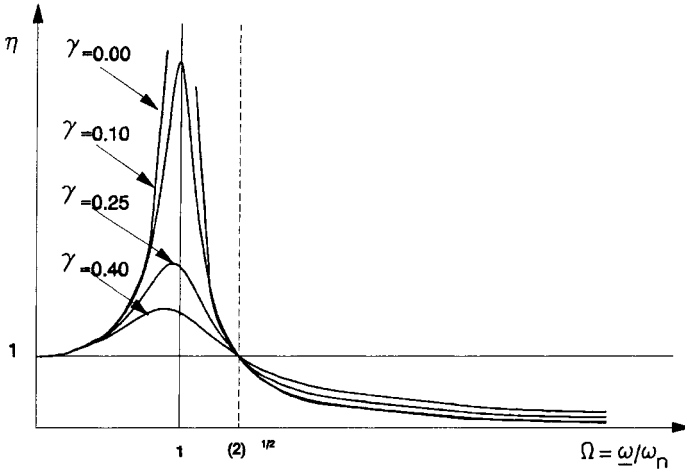
Fig. 2.8   Curves of transmissibility factor η vs Ω for different γ.

Figure 2.8 shows plots of η vs Ω for various values of γ. From these curves, the following can be observed:

1) When $\Omega^2 = 2$, we have $\eta = 1$ for any value of γ, i.e., independent of the system damping, the exciting force is totally transmitted to the base.

2) When $\Omega^2 > 2$, we have $\eta < 1$ for any value of γ, and, in this range, an increase in γ implies an increase in the force transmitted to the base.

3) Differentiating η with respect to Ω at a constant γ, we obtain

$$\Omega|_{\eta_{max}} = \left[(1 + 8\gamma^2)^{\frac{1}{2}} - 1\right]^{\frac{1}{2}} / 2\gamma$$

$$\cong \sqrt{1 - 2\gamma^2 + 8\gamma^4 - 40\gamma^6 + \cdots}$$

and

$$\eta_{max} = \left[\frac{1 + 4\gamma^2}{4\gamma^2(1 + \gamma^2)}\right]^{\frac{1}{2}} + O(\gamma^4) \tag{2.60}$$

2.3.2 Harmonic Oscillation of the Base

For the problem of accelerometer pickups, consider the dynamic system shown in Fig. 2.9. The base has a prescribed motion given by

$$x_0 = X_0 \cos \omega t \tag{2.61}$$

We will consider the motion of the mass relative to the base as the generalized coordinate x and write

$$x = x_1 - x_0 = x_1 - X_0 \cos \omega t \tag{2.62}$$

The expressions for the kinetic energy, the potential energy, and the dissipation
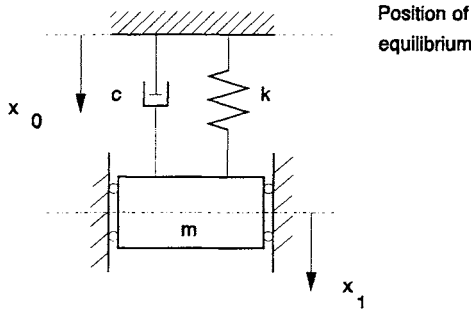
Fig. 2.9   Representation of an accelerometer pickup.

function read

$$T = (1/2)mx_1'^2 = (1/2)m(x' + x_0')^2$$

$$U = (1/2)kx^2 \tag{2.63}$$

$$D = (1/2)cx'^2$$

Applying the Lagrange equation of motion [Eq. (2.4)], we obtain

$$mx'' + cx' + kx = -mx_0'' = m\underline{\omega}^2 X_0 \cos \underline{\omega}t \tag{2.64}$$

or

$$x'' + 2\gamma\omega_n x' + \omega_n^2 x = \underline{\omega}^2 X_0 \cos \underline{\omega}t \tag{2.65}$$

Comparing Eq. (2.65) with Eq. (2.35), we conclude that the equation of motion in the present case is identical to that of an external harmonic excitation with $P_0 = m\underline{\omega}^2 X_0$; therefore, using Eq. (2.43), we can write the maximum relative amplitude A of the response as

$$A = \frac{\Omega^2 X_0}{\sqrt{(1 - \Omega^2)^2 + (2\gamma\Omega)^2}}$$

or

$$\frac{A}{X_0} = \frac{\Omega^2}{\sqrt{(1 - \Omega^2)^2 + (2\gamma\Omega)^2}} \tag{2.66}$$

Curves of A/X_0 vs Ω for different values of γ are plotted in Fig. 2.10. From these curves, the following can be observed:

1) When $\Omega = 0$, independent of the value of γ, all the curves have a zero value, i.e., $x_1 = X_0$.

2) When Ω is very large, all curves converge to $A/X_0 = 1$, i.e., $x_1 = x + x_0 = 2X_0$.

3) Near $\Omega = 1$, a resonance phenomenon exists, but now the points of maximum response are shifted to the right of $\Omega = 1$, and the maximum response values are
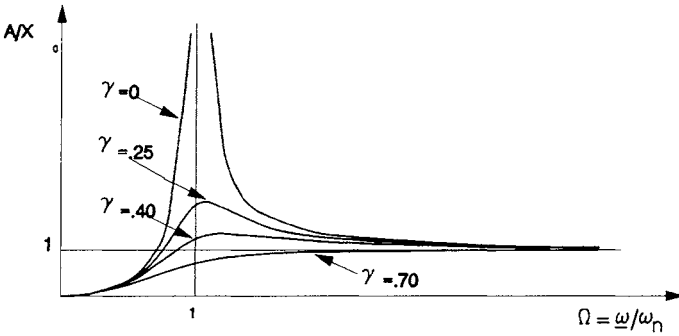
Fig. 2.10   Curves of A/X_0 vs Ω for different values of γ.

given at

$$\underline{\omega}_{\text{Res}} = \frac{\omega_n}{\sqrt{1 - 2\gamma^2}} \tag{2.67}$$

4) Again, for $\gamma > (2)^{1/2}$, the resonance phenomenon disappears, i.e., there are no peaks in the curves.

5) We define the sensitivity s as being the ratio of the product of the undamped frequency squared and the relative amplitude divided by the acceleration of the base, i.e.,

$$s = \frac{A\omega_n^2}{X_0\underline{\omega}^2} = \frac{A}{X_0\Omega^2} = \frac{1}{\sqrt{(1 - \Omega^2)^2 + (2\gamma\Omega)^2}} \tag{2.68}$$

Comparing Eq. (2.68) with Eq. (2.44), we observe that the curves of the sensibility are identical to those of the gain ξ, plotted in Fig. 2.5 and we have

$$\omega_s = \omega_n\sqrt{1 - 2\gamma^2} \tag{2.69}$$

Curves of s vs Ω for high values of γ are shown in Fig. 2.11. From these curves, we can observe that for the range $0.65 < \gamma < 0.70$ the values of s range between 1.01 and 0.99 when Ω is between 0 and 0.40. In other words, a measure of the relative displacement of the mass will be proportional to the acceleration of the base within an error less than 1% for the range of the frequency $0 < \Omega < 0.40$ and a damping range of $0.65 < \gamma < 0.70$. This fact is used in the design of acceleration pickups, i.e., if the damping ratio of the acceleration pickup is given by $0.65 < \gamma < 0.70$, accelerations measured by this pickup will have an error less than 1% if the natural frequency of the pickup is greater than 2.5 of the measured frequencies.

2.3.3   Complex Frequency Response Function

We consider in this section the response of a single-degree-of-freedom system to an external excitation force given by

$$F(t) = P_0 e^{i\underline{\omega}t} \tag{2.70}$$
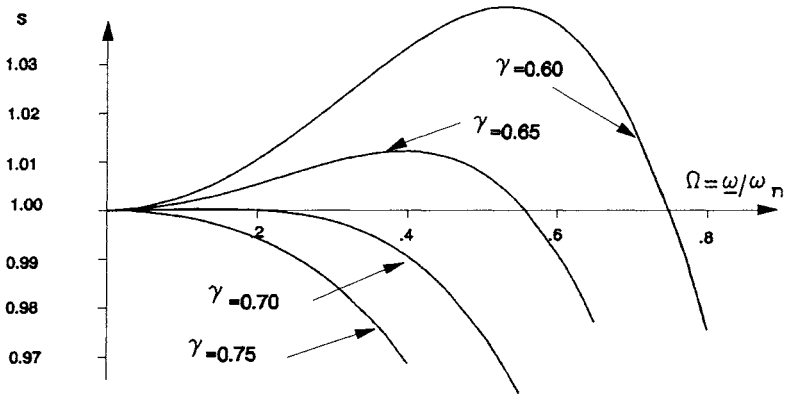
Fig. 2.11   Curves of the sensitivity s vs Ω for high values of γ.

where $\underline{\omega}$ is real. The system being linear, the permanent solution will be exponential and we can write

$$x(t) = H(\underline{\omega})P_0 e^{i\underline{\omega}t} \tag{2.71}$$

where $H(\underline{\omega})$ is a function that will be defined as the complex frequency response function. To determine $H(\underline{\omega})$, we substitute Eq. (2.71) into the equation of motion [Eq. (2.5)] to obtain

$$\left[-\underline{\omega}^2 H(\underline{\omega}) + 2i\underline{\omega}\,\omega_n\gamma\,H(\underline{\omega}) + \omega_n^2 H(\underline{\omega})\right]P_0 e^{i\underline{\omega}t} = (P_0/m)e^{i\underline{\omega}t} \tag{2.72}$$

or

$$H(\underline{\omega})[(1 - \Omega^2) + 2i\gamma\Omega] = \frac{1}{m\omega_n^2} = \frac{1}{k}$$

Thus,

$$H(\underline{\omega}) = \frac{1/k}{[(1 - \Omega^2) + 2i\gamma\Omega]} \tag{2.73}$$

and from complex algebra, the modulus of $H(\underline{\omega})$ reads

$$|H(\underline{\omega})| = \frac{1/k}{\sqrt{(1 - \Omega^2)^2 + (2\gamma\Omega)^2}} \tag{2.74}$$

Comparing Eq. (2.74) with Eq. (2.44), we conclude that

$$\xi = k|H(\underline{\omega})| \tag{2.75}$$
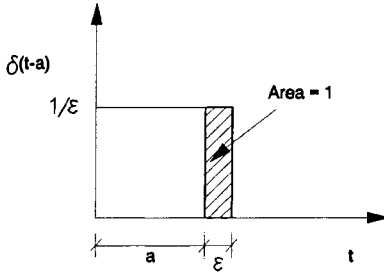
Fig. 2.12   Dirac–delta function definition.

2.4   Response to an Impulsive Excitation

A Dirac–delta function or a unit impulse function $\delta(t - a)$ (see Fig. 2.12) is defined as

$$\delta(t - a) = 0 \qquad \text{for } t \neq a$$

$$\int_{-\infty}^{\infty} \delta(t - a)\,dt = \int_{a-\varepsilon/2}^{a+\varepsilon/2} \delta(t - a)\,dt = 1 \quad _{\varepsilon \to 0} \tag{2.76}$$

Observe that $\delta(t - a)$ has dimension $[1/t]$. Consider now, a single-degree-of-freedom mechanical system excited at time $t = a$ by an impulse F. Using the above definition, we can write

$$F(t) = F\delta(t - a) \tag{2.77}$$

We observe that F has dimension N·s. We will define the response of a single degree of freedom to the application of a unit impulse at a time $(t - a)$ as the impulsive response and denote it by $h(t - a)$. If the unit impulse is applied at $t = 0$, we will have an impulsive response $h(t)$. In the following, we will study the response of a single-degree-of-freedom system due to the application of an external force $F(t) = F\delta(t)$, with initial conditions $x(0)$ and $x'(0)$ equal to zero. The equation of motion [Eq. (2.5)] can be written as

$$mx'' + cx' + kx = F\delta(t) \tag{2.78}$$

Integrating Eq. (2.78) between the time $t = 0$ and $t = \varepsilon$, where ε is the duration of the impulse, we obtain

$$\int_{0_{\varepsilon \to 0}}^{\varepsilon} (mx'' + cx' + kx)\,dt = \int_{0_{\varepsilon \to 0}}^{\varepsilon} F\delta(t)\,dt \tag{2.79}$$

Using Eq. (2.76), the right-hand side of Eq. (2.79) reads

$$\int_{0_{\varepsilon \to 0}}^{\varepsilon} F\delta(t)\,dt = F \int_0^{\varepsilon} \delta(t)\,dt = F \tag{2.80}$$

Integrating the first term of the left-hand side, we obtain

$$\int_{0_{\varepsilon \to 0}}^{\varepsilon} mx''\,dt = m[x'(\varepsilon) - x'(0)]_{\varepsilon \to 0} = mx'(0^+) \tag{2.81}$$

because at $t = 0$, $x'(0) = 0$. In Eq. (2.81), $x'(0^+)$ denotes the velocity of the system just after the application of the impulse. Considering now that there is no variation in the displacement during the application of the impulse, the second and third terms of the left-hand side of Eq. (2.79) read

$$\int_{0_{\varepsilon \to 0}}^{\varepsilon} cx' \, dt = c[x(\varepsilon) - x(0)]_{\varepsilon \to 0} = 0 \qquad (2.82)$$

and

$$\int_{0_{\varepsilon \to 0}}^{\varepsilon} kx \, dt = 0 \qquad (2.83)$$

Using Eqs. (2.80–2.83), we obtain

$$mx'(0^+) = F \qquad (2.84)$$

i.e., just after the application of the impulse, we will have a single-degree-of-freedom system in free vibration with initial condition $x(0) = 0$ and $x'(0) = F/m$. Using Eq. (2.26), the response of the system reads

$$x(t) = e^{-\gamma \omega_n t} \left[\frac{x'(0^+)}{\omega_d} \sin \omega_d t \right] = \frac{F}{m\omega_d} e^{-\gamma \omega_n t} \sin \omega_d t \qquad \text{for } t > 0$$

$$= 0 \qquad \text{for } t \leq 0 \qquad (2.85)$$

Hence, if $F = 1$, we will have the impusive response $h(t)$ given by

$$h(t) = \frac{1}{m\omega_d} e^{-\gamma \omega_n t} \sin \omega_d t \qquad \text{for } t > 0$$

$$= 0 \qquad \text{for } t \leq 0 \qquad (2.86)$$

and for a unit impulse applied at $t = \tau$, the response reads

$$h(t - \tau) = \frac{1}{m\omega_d} e^{-\gamma \omega_n (t - \tau)} \sin \omega_d (t - \tau) \qquad \text{for } t > \tau$$

$$= 0 \qquad \text{for } t \leq \tau \qquad (2.87)$$

As an application of the impulsive response, we consider in the following the response of a single degree of freedom due to the application of an arbitrary deterministic external force $F(t)$ as shown in Fig. 2.13, with null initial conditions. We consider the applied load as being composed of a series of impulses applied at $t = \tau$, and we write

$$F(\tau) = F(\tau)\Delta\tau \qquad (2.88)$$

Using Eqs. (2.85) and (2.86), we can write the increment of the response Δx due to the application of $F(\tau)$ as

$$\Delta x = F(\tau)h(t - \tau) = F(\tau)\Delta\tau h(t - \tau) \qquad \text{for } t > \tau$$

$$= 0 \qquad \text{for } t \leq \tau \qquad (2.89)$$
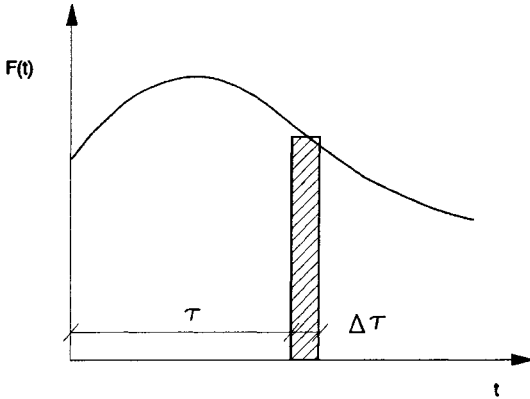
Fig. 2.13   Deterministic function.

and considering the series of impulses until $t = \tau$, we write

$$\sum \Delta x = \sum_{\Delta\tau=1,2,\ldots,n} F(\tau)\Delta\tau h(t - \tau) \qquad (2.90)$$

Changing the summation by integration, we obtain

$$x(t) = \int_0^t F(\tau)h(t - \tau)\,d\tau \qquad (2.91)$$

Equation (2.91) is called the convolution integral or Duhamel's integral. Now using Eq. (2.87), we can write the response given in Eq. (2.91) as

$$x(t) = \frac{1}{m\omega_d} \int_0^t F(\tau)e^{-\gamma\omega_n(t-\tau)} \sin \omega_d(t - \tau)\,d\tau \qquad \text{for } t > 0$$

$$= 0 \qquad \text{for } t \preceq 0 \qquad (2.92)$$

Notice that the response given by Eq. (2.92) is for initial conditions $x(0) = x'(0) = 0$. If these are different from zero, the complete solution of the system will be given by the addition of the responses [Eq. (2.26) and Eq. (2.92)] to read

$$x(t) = e^{-\gamma\omega_n t} \left\{ x^2(0) + \left[\frac{x'(0) + x(0)\gamma\omega_n}{\omega_d} \right]^2 \right\}^{\frac{1}{2}}$$

$$\times \cos\left\{ \omega_d t - \tan^{-1}\left[\frac{x'(0) + x(0)\gamma\omega_n}{\omega_d x(0)} \right] \right\}$$

$$+ \frac{1}{m\omega_d} \int_0^t F(\tau)e^{-\gamma\omega_n(t-\tau)} \sin \omega_d(t - \tau)\,d\tau \qquad (2.93)$$

Returning now to Eq. (2.91) and making the transformation,

$$t - \tau = \lambda \qquad (2.94)$$

we obtain

$$x(t) = -\int_t^0 F(t-\lambda)h(\lambda)\,d\lambda = \int_0^t F(t-\lambda)h(\lambda)\,d\lambda \qquad (2.95)$$

and because λ is the variable of the integration, we can write

$$x(t) = \int_0^t F(\tau)h(t-\tau)\,d\tau = \int_0^t F(t-\tau)h(\tau)\,d\tau$$

2.5   Response to a Step Excitation

In this section, the response of a single-degree-of-freedom system due to the application of an external force of a unit step function is studied. A unit step function (see Fig. 2.14) is defined as

$$\begin{aligned} u(t-\tau) &= 0 \qquad \text{for } t \le \tau \\ u(t-\tau) &= 1 \qquad \text{for } t > \tau \end{aligned} \qquad (2.96)$$

We observe that $u(t-\tau)$ is a nondimensional function and that the multiplication of an arbitrary function by a step function eliminates the function for $t \le \tau$ and does not affect the function for $t > \tau$. We will call the response of a single-degree-of-freedom system to the application of a unit step function the indicial response and denote it by $g(t)$. Applying Duhamel's integral for the case of a step function applied at $t = 0$ with null initial conditions, we get

$$g(t) = \int_0^t u(\tau)h(t-\tau)\,d\tau$$

$$= \frac{1}{m\omega_d} \int_0^t e^{-\gamma\omega_n(t-\tau)} \sin\omega_d(t-\tau)\,d\tau \qquad (2.97)$$
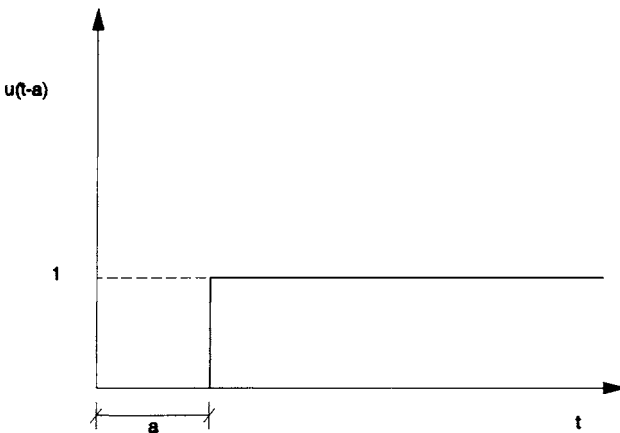
Fig. 2.14   Definition of a unit step function.

making the transformation $t - \tau = \lambda$ and integrating, we obtain

$$g(t) = \frac{1}{k}\left[1 - e^{-\gamma\omega_n t}\left(\cos\omega_d t + \frac{\gamma\omega_n}{\omega_d}\sin\omega_d t\right)\right] \tag{2.98}$$

The dimension of $g(t)$ is m/N, and, if the step function has an intensity $P_0(N)$, the response will be

$$x(t) = P_0 g(t) \tag{2.99}$$

We notice that the response given by Eq. (2.99) is for null initial conditions. If the initial conditions are different from zero, the complete solution will be obtained by the addition of the responses given in Eqs. (2.26) and (2.99). We notice further that an external arbitrary deterministic load can be represented by the summation of a series of step excitations.

2.6 Response to Periodic Excitation (Fourier Series)

Figure 2.15 represents a periodic external applied load $F(t)$ with a period T. We call $2\pi/T$ the fundamental frequency of excitation and denote it by ω_0, i.e.,

$$\omega_0 = 2\pi/T \tag{2.100}$$

Now, if the function $F(t)$ is periodic and possesses a finite number of discontinuities and if the following relation is satisfied:

$$\int_0^T |F(t)|\,dt < \infty$$

then from the theory of Fourier analysis, we can write $F(t)$ as

$$F(t) = \frac{a_0}{T} + \frac{2}{T}\left(\sum_{n=1}^{\infty} a_n \cos n\omega_0 t + b_n \sin n\omega_0 t\right) \tag{2.101}$$
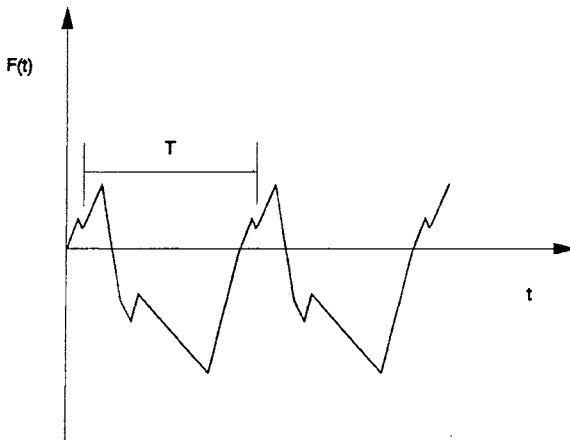
Fig. 2.15   Periodic function.

The coefficients a_i and b_i in Eq. (2.101) have the dimension N·s and can be determined by multiplying both sides of Eq. (2.101) by $\cos i\omega_0 t$ and $\sin i\omega_0 t$ and integrating both sides from 0 to T, to obtain

$$a_0 = \int_0^T F(t)\,dt \qquad a_n = \int_0^T F(t)\cos n\omega_0 t\,dt \qquad b_n = \int_0^T F(t)\sin n\omega_0 t\,dt$$

(2.102)

Now, because the system is linear, the response will be obtained by the summation of the individual responses of the series. Applying the results obtained in Section 2.3, we can write the permanent solution response as

$$x(t) = \frac{1}{kT}\left(a_0 + 2\sum_{n=1}^{\infty}\left[(1-\Omega_n^2)^2 + (2\gamma\Omega_n)^2\right]^{-1}\left\{\left[2\gamma\Omega_n a_n + (1-\Omega_n^2)b_n\right]\right.\right.$$

$$\left.\left. \times \sin n\omega_0 t + \left[(1-\Omega_n^2)a_n - 2\gamma\Omega_n b_n\right]\cos n\omega_0 t\right\}\right)$$

(2.103)

where

$$\Omega_n = n\omega_0/\omega_n$$

(2.104)

Now, returning to the trigonometric expansion [Eq. (2.101)] and omitting the constant term a_0, which can be analyzed alone, we can write the function $F(t)$ as

$$F(t) = \sum_{-\infty}^{\infty} c_n e^{in\omega_0 t} \qquad n = \pm1, \pm2, \pm3, \ldots$$

(2.105)

where c_n is in general complex and is given by

$$c_n = \frac{1}{T}\int_0^T F(t)e^{-in\omega_0 t}\,dt \qquad n = \pm1, \pm2, \pm3, \ldots$$

(2.106)

The system being linear, the response will be given by the summation of the individual exponential excitations; hence, using Eqs. (2.71) and (2.73), we obtain

$$x(t) = \sum_{-\infty}^{\infty} H_n(n\omega_0)c_n e^{in\omega_0 t} \qquad n = \pm1, \pm2, \pm3, \ldots$$

(2.107)

where

$$H_n(n\omega_0) = \frac{1/k}{(1-\Omega_n^2) + 2i\gamma\Omega_n}$$

(2.108)

where $\Omega_n = n\omega_0/\omega_n$. Notice that Eqs. (2.103) and (2.107) are only the permanent solutions. To obtain the complete solutions, we have to add to Eq. (2.103) or Eq. (2.107) the transient solutions given in Eq. (2.24) and apply the initial conditions of the problem in consideration.

2.7 Response to Aperiodic Excitation (Fourier Transform)

Consider again the exponential expansion:

$$F(t) = \sum_{-\infty}^{\infty} c_n e^{in\omega_0 t} \qquad n = \pm 1, \pm 2, \pm 3, \ldots \qquad \omega_0 = 2\pi/T \quad (2.109)$$

and the series coefficient given by

$$c_n = \frac{1}{T} \int_0^T F(t) e^{-in\omega_0 t} \, dt \qquad n = \pm 1, \pm 2, \pm 3, \ldots \quad (2.110)$$

If we extend the period T from $-\infty$ to ∞, the external applied force $F(t)$ can be considered as an aperiodic force. The discrete frequencies $n\omega_0$ are now transformed to a continuous function, and the exponential series is transformed to an infinite integral that we call the Fourier integral. Writing now at the limit,

$$n\omega_0 = \omega \quad (2.111)$$

and

$$(n+1)\omega_0 - n\omega_0 = \Delta\omega = \omega_0 = 2\pi/T \quad (2.112)$$

we can write Eqs. (2.109) and (2.110) as

$$F(t) = \sum_{-\infty}^{\infty} \frac{1}{T}(T c_n) e^{i\omega t} = \frac{1}{2\pi} \sum_{-\infty}^{\infty} (T c_n) e^{i\omega t} \Delta\omega \quad (2.113)$$

and

$$(T c_n) = \int_0^T F(t) e^{-i\omega t} \, dt \quad (2.114)$$

Extending T from $-\infty$ to ∞ and tending $\Delta\omega$ to zero, we obtain

$$F(t) = \frac{1}{2\pi} \int_{-\infty}^{\infty} F(\omega) e^{i\omega t} \, d\omega \quad (2.115)$$

and

$$F(\omega) = (T c_n)_{T \to \infty} = \int_{-\infty}^{\infty} F(t) e^{-i\omega t} \, dt \quad (2.116)$$

The transformation in Eq. (2.116) will be called the Fourier transform of $F(t)$, while the transformation in Eq. (2.115) will be called the inverse Fourier transform. In a similar manner, we can write for the response $x(t)$ the Fourier transform and the inverse transform as

$$x(\omega) = \int_{-\infty}^{\infty} x(t) e^{-i\omega t} \, dt \quad (2.117)$$

$$x(t) = \frac{1}{2\pi} \int_{-\infty}^{\infty} x(\omega) e^{i\omega t} \, d\omega \quad (2.118)$$

but from Eq. (2.71), we have

$$x(t) = H(\omega)F(t) \tag{2.119}$$

Hence we can write

$$x(\omega) = H(\omega)F(\omega) \tag{2.120}$$

and substituting into Eq. (2.118), we obtain

$$x(t) = \frac{1}{2\pi} \int_{-\infty}^{\infty} H(\omega)F(\omega)e^{i\omega t}\, d\omega \tag{2.121}$$

Notice that if the Fourier transform of the external force is known or has been calculated, Eq. (2.121) can be used to obtain the system response in the time domain and integrations can be performed analytically or numerically. Furthermore, Eq. (2.120) represents an algebraic relation between the three functions, $x(\omega)$, $F(\omega)$, and $H(\omega)$, i.e., if two functions are known, the third one can be determined using this relation. This property is extensively used in Fourier analysis experimental work. Finally, notice that ω is a real quantity.

2.8   Laplace Transform (Transfer Function)

The Laplace transform of a function $x(t)$ is defined as

$$x(s) = L[x(t)] = \int_{0}^{\infty} e^{-st} x(t)\, dt \tag{2.122}$$

where s is in general complex. Using Eq. (2.122), we can obtain the Laplace transform of the velocity and the acceleration as

$$x'(s) = L[x'(t)] = \int_{0}^{\infty} e^{-st} \frac{dx(t)}{dt}\, dt$$

$$= [e^{-st} x(t)]_0^{\infty} + s \int_{0}^{\infty} e^{-st} x(t)\, dt$$

$$= sx(s) - x(0) \tag{2.123}$$

and

$$x''(s) = L[x''(t)] = \int_{0}^{\infty} e^{-st} \frac{d^2 x(t)}{dt^2}\, dt$$

$$= \left[e^{-st} \frac{dx(t)}{dt} \right]_0^{\infty} + s \int_{0}^{\infty} e^{-st} \frac{dx(t)}{dt}\, dt$$

$$= s^2 x(s) - sx(0) - x'(0) \tag{2.124}$$

Now, consider the equation of motion,

$$mx'' + cx' + kx = F(t) \tag{2.125}$$

Applying the Laplace transform to both sides, we obtain

$$[ms^2 + cs + k]x(s) - mx'(0) - (ms + s)x(0) = F(s) \qquad (2.126)$$

Ignoring for the moment the initial conditions, we can write

$$x(s) = \frac{1}{(ms^2 + cs + k)}F(s) \qquad (2.127)$$

or

$$x(s) = G(s)F(s) \qquad (2.128)$$

where

$$G(s) = \frac{1}{(ms^2 + cs + k)} \qquad (2.129)$$

We call $G(s)$ the transfer function. We notice that Eq. (2.128) represents an algebraic relation between $x(s)$ and $F(s)$. To obtain the response as a function of time, we perform the inverse Laplace transform, i.e.,

$$x(t) = L^{-1}x(s) = L^{-1}G(s)F(s) \qquad (2.130)$$

and, for initial conditions different from zero, we write

$$x(t) = L^{-1}[G(s)F(s) + mG(s)(s + 2\gamma\omega_n)x(0) + mG(s)x'(0)] \quad (2.131)$$

Finally, notice that if s is purely imaginary, i.e., if $s = i\omega$, where ω is real, we have

$$G(i\omega) = \frac{1}{[-m\omega^2 + ic\omega + k]} = \frac{1/k}{[(1 - \Omega^2) + i\gamma\Omega]} = H(\omega) \quad (2.132)$$

i.e., when s is purely imaginary, the transfer function is equal to the complex frequency response function.

Problems

2.1   The determination of the elasticomechanical properties of the control surfaces of airplanes with precision is a requirement for aeroelastic analysis. Mathematical models used to obtain such data with the precision required are very complex and expensive. Such data can, however, be obtained using relatively simple ground vibration tests. To this end, the following ground vibration tests have been performed:

(a) Determination of the moment of inertia I_0 of a statically balanced rudder about its rotation axis. The test has been performed according to the drawing shown in Fig. P2.1a. A variation of the external excitation frequency f was made and a record of the amplitude at the point of excitation was obtained as given

L=0.2 m

k=125N/m
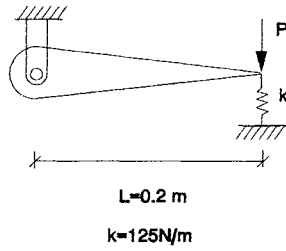
Fig. P2.1a

below

f_{Hz}	9.00	29.20	29.40	29.60	29.80	30.00	30.20
	30.40	30.60	30.80	31.00			
x/x_0	13.14	15.28	17.95	21.04	23.87	25.00	23.50
	20.57	17.42	14.73	12.60			

From these data, obtain the value of I_0.

(b) Determination of the constant torsional stiffness K_θ about the rotation axis, the undamped natural frequency, the damped natural frequency, and the modal damping ratio of the first rotational rudder mode. To obtain these data, the rudder has been connected to its system in the airplane and the ground vibration test has been repeated and executed as shown in Fig. P2.1b. The following data have been recorded:

f_{Hz}	29.5	29.6	29.7	29.8	29.9	30.0	30.1
x/x_{st}	5.01441	5.02252	5.02519	5.02233	5.01393	5.00000	4.98063
f_{Hz}	30.2	30.3	30.4	30.5	30.6	30.7	
x/x_{st}	4.95596	4.92617	4.89149	4.85219	4.80857	4.76097	

From these measurements, determine K_θ, ω_n, ω_d, and γ.
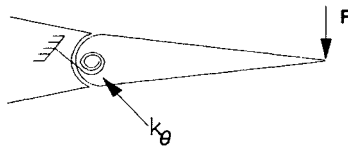
Fig. P2.1b

2.2 To decrease vibrations transmitted to instruments in aircrafts, the board panel is mounted on slightly damped springs. In an aircraft, the board panel is mounted on a spring that deflects 0.005 m in the vertical direction as a static deflection. The aircraft has an external harmonic excitation of 1800 rpm in the vertical direction. What is the percent of vibration transmitted to the panel?

2.3   In an aircraft, a gas turbine of mass 450 kg is mounted on an elastic support that deflects 0.002 m as static deflection. The turbine is running at 6200 rpm and has an unbalance of 0.003 kg·m. What is the maximum amplitude of the force transmitted to the aircraft if the suspension damping is neglected? Repeat the calculation for a damping ratio of $\gamma = 0.10$.

2.4   During a ground vibration test of a single-degree-of-freedom mechanical system under a harmonic excitation of an amplitude of 200 N, the following has been measured:
  (a) $\omega_1 = 16$ rad/s, $A_1 = 0.20$ mm, and $\phi = 15$ deg
  (b) $\omega_2 = 25$ rad/s, $A_2 = 0.20$ mm, and $\phi = 55$ deg
where ω is the excitation frequency, A is the amplitude of the displacement response, and ϕ is the response phase angle. From these results, calculate the damped and undamped natural frequencies, the damping ratio γ, the spring constant k, and the mass m of the mechanical system.

2.5   Figure P2.5 is a simple mathematical model of a car running on a road idealized as a single-degree-of-freedom mechanical system. Use the following values: $\lambda = 12$ m, $m = 1800$ kg, $k = 200,000$ N/m, and $\gamma = 0.4$. Find the value of the amplitude of the permanent solution. Repeat the solution if the system is undamped, i.e., $c = 0$.
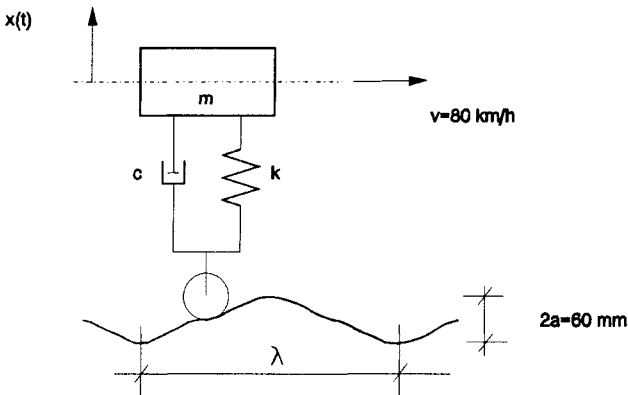
Fig. P2.5

This page intentionally left blank

3
Multidegree-of-Freedom Linear Systems

3.1 Equations of Motion

3.1.1 Position Vector

Let P_0 be the space coordinates of a point of an elastic mechanical system at a time t_0. Because of the application of an external force at $t = t_0$, the point in consideration will occupy a new position P at a time t. The vector PP_0 will thus represent the displacement of the point with initial position P_0. If we now consider a discrete system, or a continuum that has been approximated as a discrete system using a set of generalized coordinates q, we can write

$$P = F(q) \tag{3.1}$$

where q is the set of the generalized coordinates that define completely the mechanical system and F is the transformation operator. For a linear system, the transformation operator F does not depend on the generalized coordinates q, and thus we can write for any point j of the mechanical system

$$P_j = \left[\frac{\partial P_j}{\partial q_1} \ \frac{\partial P_j}{\partial q_2} \ \cdots \ \frac{\partial P_j}{\partial q_n} \right] \begin{Bmatrix} q_1 \\ q_2 \\ \cdot \\ \cdot \\ q_n \end{Bmatrix} \tag{3.2}$$

where $\partial P_j / \partial q_i$ are constants that do not depend on the generalized coordinates for a linear system and that represent the variation in the displacement at the point in consideration due to a unit variation in the generalized coordinate q_i. In this section, to simplify the notation, we will use Einstein's summation notation for repeated indices, and we write Eq. (3.2) as

$$P_j = \sum_{i=1}^{n} \left[\frac{\partial P_j}{\partial q_i} \right] q_i = \frac{\partial P_j}{\partial q_i} q_i \tag{3.3}$$

3.1.2 Velocity Vector

The velocity at any point j of the mechanical elastic system at a time t can be written as

$$V_j = dP_j/dt \tag{3.4}$$

Using Eq. (3.2), we can write the velocity vector as

$$V_j = \frac{dP_j}{dt} = \frac{\partial P_j}{\partial q_i} \frac{dq_i}{dt} = \frac{\partial P_j}{\partial q_i} q_i' \tag{3.5}$$

where $q_i' = dq_i/dt$.

3.1.3   Kinetic Energy Functional

The kinetic energy functional of the elastic mechanical system reads

$$T = \frac{1}{2} \int_v \rho(\boldsymbol{P}) V(\boldsymbol{P}) \cdot V(\boldsymbol{P}) \, \mathrm{d}v \qquad (3.6)$$

where $\rho(\boldsymbol{P})$ is the material density at point $\boldsymbol{P}$, $V(\boldsymbol{P})$ is the velocity vector at point $\boldsymbol{P}$, and v is the volume of the elastic mechanical system. For a discrete system we can use Eqs. (3.5) and (3.6) and write the kinetic energy functional as

$$T = \frac{1}{2} q'_j \left[\int_v \rho \frac{\partial \boldsymbol{P}}{\partial q_j} \cdot \frac{\partial \boldsymbol{P}}{\partial q_i} \mathrm{d}v \right] q'_i \qquad (3.7)$$

or, in matrix notation, we can write

$$T = \tfrac{1}{2} \{q'\}^T [M] \{q'\} \qquad (3.8)$$

We call $[M]$ the mass matrix of the mechanical system. The elements of the mass matrix are given by

$$M_{ij} = \int_v \rho \frac{\partial \boldsymbol{P}}{\partial q_i} \frac{\partial \boldsymbol{P}}{\partial q_j} \mathrm{d}v \qquad (3.9)$$

We conclude from Eq. (3.9) that the mass matrix is a symmetrical real matrix and because the expression $\{q'\}^T [M] \{q'\}$ represents an energy expression for any vector $\{q'\}$ different from the null vector, we further conclude that

$$\{x\}^T [M] \{x\} > 0 \qquad \forall \{x\} \neq \{0\} \qquad (3.10)$$

Therefore, $[M]$ is a positive definite matrix.

3.1.4   Strain Energy Functional

The stress–strain relationship for an elastic linear continuum can be written as

$$\{\sigma\} = [C] \{\varepsilon\} \qquad (3.11)$$

where $[C]$ is the material constitutive matrix and is a symmetric matrix because the stress and strain tensors are symmetric tensors. Writing now the strain–displacement relationship as

$$\{\varepsilon\} = [d] \{\boldsymbol{P}\} \qquad (3.12)$$

where $[d]$ is the differential operator relating the strains to the displacements, and substituting Eq. (3.3) into Eq. (3.12), we obtain

$$\{\varepsilon\} = [d][N] \{q\} \qquad (3.13)$$

where $[N]$ has been used to denote the transformation matrix of the displacements to the generalized coordinates. The strain energy functional of the elastic mechanical system reads

$$U = \frac{1}{2} \int_v \{\sigma\}^T \{\varepsilon\} \, \mathrm{d}v \qquad (3.14)$$

Using now the relation of Eqs. (3.11) and (3.13) and Eq. (3.14), we can write the strain energy functional as

$$U = \frac{1}{2}\{q\}^T \int_v [N]^T [d]^T [C][d][N] \, dv \{q\} \tag{3.15}$$

or

$$U = \frac{1}{2}\{q\}^T [K]\{q\} \tag{3.16}$$

where

$$[K] = \int_v [N]^T [d]^T [C][d][N] \, dv \tag{3.17}$$

We call $[K]$ the stiffness matrix of the elastic mechanical system. Again, we observe that $[K]$ is a real symmetrical matrix because the constitutive material matrix is a symmetric matrix and is real. Furthermore, from energy consideration concepts, we conclude from Eq. (3.16) that $[K]$ is a positive definite matrix for a constrained mechanical elastic system or a semipositive definite matrix for an elastic mechanical free body.

3.1.5 Expression of the Dissipation Function

We consider in this section that the damping forces of the elastic mechanical system are of viscous nature and are linearly related to the velocity vector, and we write

$$F_D(P) = \frac{\partial F_D(P)}{\partial q_i'} q_i' \tag{3.18}$$

where $F_D(P)$ is the damping force of the elastic mechanical system at point P. The variation in the virtual work of the damping forces in a virtual displacement δP reads

$$\delta W_D = \int_v F_D(P)\delta P \, dv = q_j' \int_v \frac{\partial F_D(P)}{\partial q_j'} \delta P \, dv$$

$$= q_j' \int_v \frac{\partial F_D(P)}{\partial q_j'} \cdot \frac{\partial P}{\partial q_i} \, dv \, \delta q_i \tag{3.19}$$

Now,

$$q_i = q_i' \Delta t \tag{3.20}$$

Thus

$$\delta q_i = \delta q_i' \Delta t \tag{3.21}$$

and substituting Eq. (3.20) into Eq. (3.19), we obtain

$$\delta W_D = q_j' \int_v \frac{\partial F_D}{\partial q_j'} \cdot \frac{\partial P}{\partial q_i} \, dv \, \delta q_i' \Delta t \tag{3.22}$$

or

$$\frac{\delta W_D}{\Delta t} = q'_j \int_v \frac{\partial F_D}{\partial q'_j} \cdot \frac{\partial P}{\partial q_i} \mathrm{d}v \, \delta q'_i \tag{3.23}$$

Defining now a dissipation or a viscous damping function D as

$$D = \tfrac{1}{2} q'_j B_{ij} q'_i = W_D / \Delta t \tag{3.24}$$

which in matrix notation can be written as

$$D = \tfrac{1}{2} \{q'\}^T [B]\{q'\} \tag{3.25}$$

we can write the variation in the dissipation function D caused by the variation in the velocities q'_i as

$$\delta D = q'_j B_{ij} \delta q'_i \tag{3.26}$$

where the elements of the matrix $[B]$ are given by

$$B_{ij} = \int_v \frac{\partial F_D}{\partial q'_j} \cdot \frac{\partial P}{\partial q_i} \mathrm{d}v \tag{3.27}$$

We call the matrix $[B]$ the dissipation, or the viscous damping matrix.

3.1.6 Equations of Motion

Applying Lagrange equations,

$$\frac{\mathrm{d}}{\mathrm{d}t}\left(\frac{\partial L}{\partial q'_i}\right) - \frac{\partial L}{\partial q_i} + \frac{\partial D}{\partial q'_i} = Q_i \tag{3.28}$$

where $L = T - U$, and using the kinetic energy functional [Eq. (3.8)], the strain energy functional equation [Eq. (3.16)], and the dissipation function [Eq. (3.22)], we obtain the equations of motion of a discrete elastic mechanical system of n degrees of freedom written in matrix form as

$$[M]\{q''\} + [B]\{q'\} + [K]\{q\} = \{Q\} \tag{3.29}$$

where $\{Q\}$ is the column of the generalized external forces. The solution of the equations of motion [Eq. (3.29)] will be studied in detail in the sequence.

3.2 Free Vibration: The Eigenvalue Problem

3.2.1 Undamped Systems

Equations of motion [Eq. (3.29)] for undamped free vibration read

$$[M]\{q''\} + [K]\{q\} = \{0\} \tag{3.30}$$

The system of equations [Eq. (3.30)] is a system of second-order differential equations with constant coefficients, whose solution can be written as

$$\{q\} = \{q_0\} e_i^{Pt} \tag{3.31}$$

Substitution of Eq. (3.31) into Eq. (3.30) gives

$$P_i^2[M]\{q_0\} + [K]\{q_0\} = \{0\} \tag{3.32}$$

Defining

$$\lambda_i = -P_i^2 \tag{3.33}$$

we get

$$[[K] - \lambda_i[M]]\{q_0\} = \{0\} \tag{3.34}$$

This represents an eigenvalue problem, whose solution was treated in Chapter 1. The solution of the eigenvalue problem will furnish the eigenvalues λ_i and the eigenvectors Q_i. In the following section, some properties of the eigenvalues and eigenvectors of undamped systems will be derived.

1) The eigenvalues $\lambda_i(\lambda_i = -P_i^2)$ are positive real numbers. Writing Eq. (3.34) for the ith eigenvalue as

$$\lambda_i[M]\{Q_i\} = [K]\{Q_i\} \tag{3.35}$$

and premultiplying by $\{Q_i\}^T$ we get

$$\lambda_i\{Q_i\}^T[M]\{Q_i\} = \{Q_i\}^T[K]\{Q_i\} \tag{3.36}$$

or

$$\lambda_i = \frac{\{Q_i\}^T[K]\{Q_i\}}{\{Q_i\}^T[M]\{Q_i\}} \tag{3.37}$$

But because $\{Q_i\} \neq \{0\}$ and both $\{Q_i\}^T[M]\{Q_i\}$ and $\{Q_i\}^T[K]\{Q_i\}$ are positive real numbers from physical considerations (since they represent energy expressions), we conclude that λ_i are positive real numbers, and therefore P_i represents pure imaginary numbers.

2) The eigenvectors are real vectors. Let us conclude that an eigenvector, say $\{Q_i\}$, is a complex vector and we write it as

$$\{Q_i\} = \{Q_i'\} + i\{Q_i''\} \tag{3.38}$$

where both $\{Q_i'\}$ and $\{Q_i''\}$ are real vectors. Substituting Eq. (3.38) into Eq. (3.36), we get

$$\lambda_i[M][\{Q_i'\} + i\{Q_i''\}] = [K][\{Q_i'\} + i\{Q_i''\}] \tag{3.39}$$

Now, because $[M]$, $[K]$, and λ_i are real, we can separate the real and the imaginary parts of Eq. (3.39) to read

$$\lambda_i[M]\{Q_i'\} = [K]\{Q_i'\}$$
$$\lambda_i[M]\{Q_i''\} = [K]\{Q_i''\} \tag{3.40}$$

Thus, we have as eigenvectors $\{Q_i'\}$ and $\{Q_i''\}$, which are both real and proportional because they correspond to the same eigenvalue λ_i. We thus conclude that the system of equations [Eq. (3.35)] admits only real eigenvectors.

3) The eigenvectors are orthogonal vectors in relation to the mass and the stiffness matrices. Writing for two different eigenvalues λ_i and λ_j

$$\lambda_i[M]\{Q_i\} = [K]\{Q_i\}$$
$$\lambda_j[M]\{Q_j\} = [K]\{Q_j\}$$

and premultiplying the first equation by $\{Q_j\}^T$ and the second by $\{Q_i\}^T$, we get

$$\lambda_i\{Q_j\}^T[M]\{Q_i\} = \{Q_j\}^T[K]\{Q_i\}$$
$$\lambda_j\{Q_i\}^T[M]\{Q_j\} = \{Q_i\}^T[K]\{Q_j\}$$

(3.41)

Transposing the second equation and noting that $[M]$ and $[K]$ are both symmetrical, we get

$$\lambda_i\{Q_j\}^T[M]\{Q_i\} = \{Q_j\}^T[K]\{Q_i\}$$
$$\lambda_j\{Q_j\}^T[M]\{Q_i\} = \{Q_j\}^T[K]\{Q_i\}$$

(3.42)

Subtracting the second equation from the first one, we obtain

$$(\lambda_i - \lambda_j)\left[\{Q_j\}^T[M]\{Q_i\}\right] = 0$$

(3.43)

We thus conclude that

$$\{Q_j\}^T[M]\{Q_i\} = 0 \qquad \text{for } \lambda_i \neq \lambda_j$$
$$\{Q_j\}^T[M]\{Q_i\} \neq 0 \qquad \text{for } \lambda_i = \lambda_j$$

(3.44)

Furthermore, using Eqs. (3.42) and (3.44), we also conclude that

$$\{Q_j\}^T[K]\{Q_i\} = 0 \qquad \text{for } \lambda_i \neq \lambda_j$$
$$\{Q_j\}^T[K]\{Q_i\} \neq 0 \qquad \text{for } \lambda_i = \lambda_j$$

(3.45)

Equations (3.44) and (3.45) represent the orthogonality relationships between the eigenvectors of the modes of free vibration of an undamped system with respect to the mass and stiffness matrices. Furthermore, we conclude that

$$[Q]^T[M][Q] = \lceil \mu \rfloor$$
$$[Q]^T[K][Q] = \lceil \gamma \rfloor$$

(3.46)

where both $\lceil \gamma \rfloor$ and $\lceil \mu \rfloor$ are diagonal matrices, and we call them the generalized stiffness and generalized mass matrices, respectively. We notice that the numerical values of μ_{ii} and γ_{ii} will depend on the way the corresponding eigenvector $\{Q_i\}$ has been normalized. In the case when the eigenvectors are normalized in such a way that the generalized mass matrix is an identity matrix, the eigenvectors are called the normal vectors. To determine the scaling factor in such a case, we write the following for a normal vector $\{N_i\}$:

$$\{N_i\} = c_i\{Q_i\}$$

(3.47)

where c_i is the scaling factor. Using Eq. (3.46), we get

$$c_i^2\{Q_i\}^T[M]\{Q_i\} = 1$$

Thus,

$$c_i = \pm \frac{1}{\left[\{Q_i\}^T [M]\{Q_i\}\right]^{\frac{1}{2}}} = \pm \frac{1}{|\mu|^{\frac{1}{2}}} \tag{3.48}$$

or

$$\{N_i\} = \pm \frac{1}{|\mu|^{\frac{1}{2}}} \{Q_i\} \tag{3.49}$$

Furthermore, we conclude that in such a case, i.e., normalization for unit generalized mass, the corresponding generalized stiffness will be equal to λ_i.

3.2.2 Damped Systems

For free vibration of a damped system, the equations of motion [Eq. (3.29)] read

$$[M]\{q''\} + [C]\{q'\} + [K]\{q\} = \{0\} \tag{3.50}$$

Again the system of equations [Eq. (3.50)] admits solutions in the form

$$\{q\} = e^{st}\{q_0\} \tag{3.51}$$

where s and $\{q_0\}$ are in general complex. Substituting Eq. (3.51) into Eq. (3.50), we obtain

$$s^2[M]\{q_0\} + s[C]\{q_0\} + [K]\{q_0\} = \{0\} \tag{3.52}$$

This represents an eigenvalue problem of the second order. However, we can easily transform it to a first-order eigenvalue problem by writing the identity

$$[M]\{q'\} = [M]\{q'\} \tag{3.53}$$

and combining Eqs. (3.50) and (3.53) to obtain

$$\begin{bmatrix} [0] & [M] \\ [M] & [C] \end{bmatrix} \begin{Bmatrix} q'' \\ q' \end{Bmatrix} + \begin{bmatrix} -[M] & [0] \\ [0] & [K] \end{bmatrix} \begin{Bmatrix} q' \\ q \end{Bmatrix} = \begin{Bmatrix} 0 \\ 0 \end{Bmatrix} \tag{3.54}$$

Now,

$$[A] = \begin{bmatrix} [0] & [M] \\ [M] & [C] \end{bmatrix} \qquad [B] = \begin{bmatrix} -[M] & [0] \\ [0] & [K] \end{bmatrix} \qquad \{y\} = \begin{Bmatrix} q' \\ q \end{Bmatrix} \tag{3.55}$$

The system of equations [Eq. (3.54)] reads

$$[A]\{y'\} + [B]\{y\} = \{0\} \tag{3.56}$$

Again the system of equations [Eq. (3.56)] admits solutions in the form

$$\{y\} = e^{st}\{y_0\} \tag{3.57}$$

Substituting Eq. (3.57) into Eq. (3.56), we get

$$[s[A] + [B]]\{y_0\} = \{0\} \tag{3.58}$$

Again this is an eigenvalue problem whose solution was treated in Chapter 1. The eigenvalues of Eq. (3.58) s are, in general, complex. Examining Eq. (3.57), we

conclude that, in the case of an eigenvalue being real and negative, we will have an overdamped motion. If s_i is a complex number with a negative real part, we will have an oscillatory stable motion. Furthermore, it can be shown that complex roots will occur in conjugate pairs for this kind of eigenvalue treated here since both $[A]$ and $[B]$ are real symmetric matrices. The imaginary part will give the modal frequency, and the real part will give the corresponding damping.

3.3   Response to an External Applied Load

For an externally applied load, the equations of motion read

$$[M]\{q''\} + [C]\{q'\} + [K]\{q\} = \{F(t)\} \tag{3.59}$$

The solution of Eqs. (3.59) falls into two categories, the modal superposition technique and numerical methods. Both categories will be discussed in the following sections.

3.3.1   The Modal Superposition Technique

The modal superposition technique consists of transforming the equations of motion [Eqs. (3.59)] into the modal base of the associated conservative system. The associated conservative system is obtained by the elimination of the damping from the equations of motion. For free vibration, the equations of motion of the associated conservative system read

$$[M]\{q''\} + [K]\{q\} = \{0\} \tag{3.60}$$

The solution of Eq. (3.60) will give the eigenvalue matrix $[\lambda]$ and the eigenvector matrix $[Q]$ as described in the last section. Making the transformation

$$\{q\} = [Q]\{\eta\} \tag{3.61}$$

where $\{\eta\}$ is the vector of the modal amplitude, the equations of motion [Eqs. (3.59)] read

$$[M][Q]\{\eta''\} + [C][Q]\{\eta'\} + [K][Q]\{\eta\} = \{F\} \tag{3.62}$$

Premultiplying Eq. (3.62) by $[Q]^T$, we obtain

$$\lceil \mu \rfloor \{\eta''\} + \lceil \beta \rfloor \{\eta'\} + \lceil \gamma \rfloor \{\eta\} = \{\phi\} \tag{3.63}$$

where

$$\lceil \mu \rfloor = [Q]^T[M][Q]$$

$$\lceil \beta \rfloor = [Q]^T[C][Q]$$

$$\lceil \gamma \rfloor = [Q]^T[K][Q]$$

$$\{\phi\} = [Q]^T\{F\}$$

The matrices $\lceil \mu \rfloor$ and $\lceil \gamma \rfloor$ are diagonal matrices due to the orthogonality properties of the eigenvectors of the associated conservative system and are called the generalized mass and the generalized stiffness matrices. The modal formulation is very attractive in the study of dynamic response of structures with small damping, e.g., aeronautical structures where the damping effect $\lceil \beta \rfloor \{\eta\}$ is small in comparison with the stiffness and inertia terms. Thus, we can make the simplification of

assuming $\lceil \beta \rfloor$ to be diagonal, i.e., we neglect the damping coupling between the modes. Doing so, Eq. (3.63) transforms to a system of uncoupled equations of a single degree of freedom in the form

$$\mu_{ii}\eta_i'' + \beta_{ii}\eta_i' + \gamma_{ii}\eta_i = \phi_i(t) \qquad i = 1, 2, \ldots, n \qquad (3.64)$$

Each equation of the system of equations given in Eq. (3.64) can be integrated using Duhamel's integral, and the result reads

$$\eta_i(t) = e^{-\omega_i \xi_i t} \left[\frac{1}{\omega_{d_i}} \{\eta_i'(0) + \omega_i \xi_i \eta_i(0)\} \sin \omega_{d_i} t + \eta_i(0)\cos \omega_{d_i} t \right]$$

$$+ \frac{1}{\omega_{d_i}\mu_i} \int_0^t e^{-\omega_i \xi_i(t-\sigma)} \phi_i(\sigma)\sin \omega_{d_i}(t - \sigma)\, d\sigma \qquad i = 1, 2, \ldots, n \qquad (3.65)$$

where ω_i is the undamped natural frequency of the mode, ξ_i is the damping ratio and is equal to $\beta_{ii}/2\mu_{ii}\omega_i$, ω_{d_i} is the modal damped frequency, and $\eta_i'(0)$ and $\eta_i(0)$ are the initial modal values and can be obtained from the initial conditions $q'(0)$ and $q(0)$ using Eq. (3.61). The integration in Eq. (3.65) can be evaluated analytically or numerically depending on the input generalized forcing function. When the modal amplitude functions $\eta_i(t)$ have been obtained, Eq. (3.61) will be used to obtain the physical displacement vector $q(t)$. Subsequently, the strains and stresses can be determined as functions of time. In practice, generally we will not incorporate all the modes in the transformation [Eq. (3.61)]; normally only the first few modes will be used, and thus $[Q]$ will be a rectangular matrix of dimension (n, n_r).

3.3.2 Numerical Methods

The modal superposition technique described in the previous section needs the determination of the modal values of the associated conservative system as a first step in the solution procedure, which is a time-consuming process, especially if such information will not be used in further analyses. Numerical methods, on the other hand, work directly on the coupled equations of motion [Eqs. (3.59)] and can be basically described as a step-by-step successive extrapolation procedure, i.e., starting with the known initial values $\{q\}$ and $\{q'\}$ at $t = t_0$, we proceed to calculate $\{q\}$ and $\{q'\}$ at $t = t_0 + h$, where $h = \Delta t$ and is a suitably selected interval of time. Using these calculated values, we proceed to calculate $\{q\}$ and $\{q'\}$ at $t = t_0 + 2h$ and so on. The numerical methods are classified into two categories, the finite difference and numerical integration methods. In the first category, the acceleration vector $\{q''\}$ is written in terms of several successive displacement values, while in the numerical integration procedure the velocity $\{q'\}$ and the displacement $\{q\}$ vectors are obtained by integrating numerically the acceleration in the interval of time h, which is approximated by a suitable polynomial within the interval. Furthermore, both methods can be divided into two groups; the first group is an explicit one in which the unknown values are explicitly written as functions of the previous known values, and the second group is an implicit one in which the unknown values are written as functions of the previous known values and the new values, thus necessitating an iterative process. In the following section, some of the numerical methods will be described.
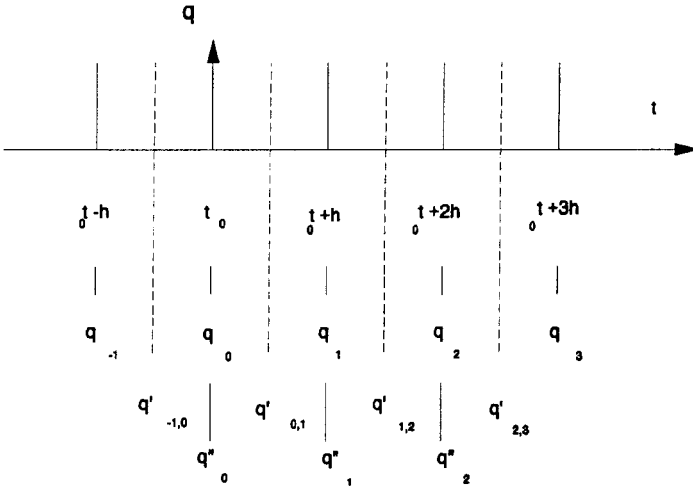
Fig. 3.1a   Central difference scheme.

Finite difference methods.   If the values of $\{q_0\}$ and $\{q_0'\}$ are given at $t = t_0$, the equations of motion [Eqs. (3.59)] can be solved for $\{q_0''\}$, and we write

$$\{q''(0)\} = [M]^{-1}[\{F(0)\} - [C]\{q'(0)\} - [K]\{q(0)\}] \qquad (3.66)$$

Writing the finite difference scheme for $\{q_{0,1}\}$ and $\{q_{0,1}'\}$, as shown in Fig. 3.1a, as

$$\{q_{0,1}'\} = (1/h)[\{q_1\} - \{q_0\}]$$

$$\{q_{-1,0}'\} = (1/h)[\{q_0\} - \{q_{-1}\}] \qquad (3.67)$$

and the accelaration $\{q_0''\}$ as

$$\{q_0''\} = (1/h)[\{q_{0,1}'\} - \{q_{-1,0}'\}] \qquad (3.68)$$

and using Eq. (3.67), we obtain

$$\{q_0''\} = (1/h^2)[\{q_1\} - 2\{q_0\} + \{q_{-1}\}] \qquad (3.69)$$

Solving for $\{q_1\}$, we get

$$\{q_1\} = 2\{q_0\} - \{q_{-1}\} + h^2\{q_0''\} \qquad (3.70)$$

and using Eq. (3.66), we obtain

$$\{q_1\} = 2\{q_0\} - \{q_{-1}\} + h^2[M]^{-1}\{\{F_0\} - [C]\{q_0'\} - [K]\{q_0\}\} \qquad (3.71)$$

Equation (3.71) is a very simple recurrence relation to proceed to step i, once steps $i - 2$ and $i - 1$ have been calculated. For the first step, we must calculate $\{q_{-1}\}$, and this can be obtained using the finite difference scheme of Fig. 3.1b, given by

$$\{q_0'\} = (1/2h)\{\{q_1\} - \{q_{-1}\}\}$$

$$\{q_{-1}\} = \{q_1\} - 2h\{q_0'\} \qquad (3.72)$$
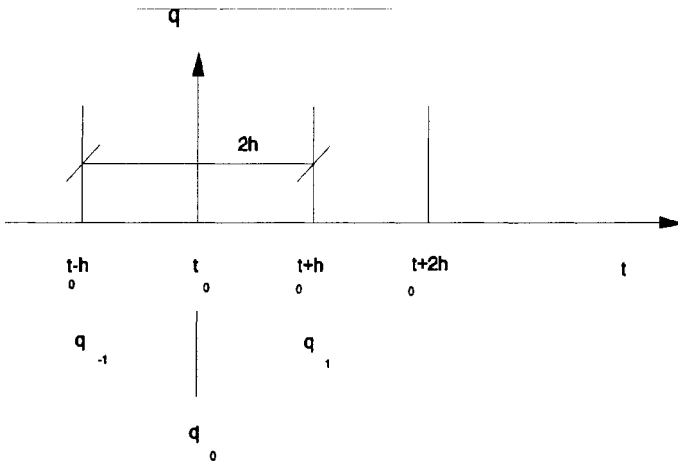
Fig. 3.1b   Central difference scheme for the first step.

Thus, for the first step, we can write

$$\{q_1\} = \{q_0\} + h\{q_0'\} + (h^2/2)[M]^{-1}\{\{F_0\} - [C]\{q_0\} - [K]\{q_0\}\} \quad (3.73)$$

and, for successive steps, we write

$$\{q_i\} = 2\{q_{i-1}\} - \{q_{i-2}\} + (h^2/2)[M]^{-1}\{\{F_{i-1}\} - [C]\{q_{i-1}\} - [K]\{q_{i-1}\}\}$$

$$(3.74)$$

This method, despite being very simple, has the disadvantage of being potentially unstable if the time interval h is greater than the minimum period of the system free vibration frequency. Higher order finite difference schemes have been proposed; however, they have the same deficiency for the limitation on the time interval and need more computational requirements.

Numerical integration methods.   For all the numerical integration variants, perform the following two integrations for each step:

$$\{q_i'\} = \{q_{i-1}'\} + \int_0^h \{q''\}\,dt \quad (3.75)$$

$$\{q_i\} = \{q_{i-1}\} + \int_0^h \{q'\}\,dt \quad (3.76)$$

The different variants of the numerical integration methods reside in the way of approximating the acceleration in the integral [Eq. (3.75)]. Assuming the integrals

in Eqs. (3.75) and (3.76) are a constant value given by the initial value through the interval of the time, we obtain Euler expressions, which can be written as

$$\{q_i'\} = \{q_{i-1}'\} + h\{q_{i-1}''\} \tag{3.77}$$

$$\{q_i\} = \{q_{i-1}\} + h\{q_{i-1}'\} \tag{3.78}$$

with the initial value of the acceleration given by

$$\{q_{i-1}''\} = [M]^{-1}[\{F_{i-1}\} - [C]\{q_{i-1}'\} - [K]\{q_{i-1}\}] \tag{3.79}$$

Equations (3.77–3.79) represent a very simple recurrence relation; however, the errors are of the order $O(h^2)$ in the interval of time h. An improvement to this method is to use the Gauss scheme for the numerical integration process by assuming the average integrand to be given by the mean value in the interval, or

$$\{q_i'\} = \{q_{i-1}'\} + (h/2)\{\{q_{i-1}''\} + \{q_i''\}\}$$

$$\{q_i\} = \{q_{i-1}\} + (h/2)\{\{q_{i-1}'\} + \{q_i'\}\}$$

and substituting $\{q_i'\}$ in the second equation from the first one, we obtain

$$\{q_i\} = \{q_{i-1}\} + (h/2)[\{q_{i-1}'\} + \{q_{i-1}'\} + (h/2)\{q_{i-1}''\} + (h/2)\{q_i''\}]$$

or

$$\{q_i\} = \{q_{i-1}\} + h\{q_{i-1}'\} + (h^2/4)[\{q_{i-1}''\} + \{q_i''\}] \tag{3.80}$$

and $\{q_{i-1}''\}$ is obtained from Eq. (3.79). We notice now that the errors are of the order $O(h^3)$ and the process is an implicit one. Hence, we will have to use an iterative algorithm for the solution. The iterations can be started by assuming initially $\{q_i''\} = \{q_{i-1}''\}$, solving for $\{q_i\}$ and $\{q_i'\}$, and then calculating $\{q_i''\}$. This new value is now used in Eq. (3.80), and the process is repeated until a required accuracy is achieved. A further formula was proposed by Newmark[1] for Eq. (3.80), which is modified to read

$$\{q_i'\} = \{q_{i-1}'\} + (1 - \lambda)h\{q_{i-1}''\} + \lambda h\{q_i''\}$$
$$\{q_i\} = \{q_{i-1}\} + h\{q_{i-1}'\} + \left(\tfrac{1}{2} - \beta\right)h^2\{q_{i-1}''\} + \beta h^2\{q_i''\} \tag{3.81}$$

where λ and β are constants. We notice that the first equation reduces to that of Euler when $\lambda = 1$ and to that of Gauss when $\lambda = 1/2$, and the second equation reduces to that of Gauss for $\beta = 1/4$. It has been shown that values of $\lambda \neq 1/2$ lead to spurious damping effects in the response. Now if we take $\beta = 1/6$, i.e., we assume a linear variation for the acceleration into the interval of time, the relations in Eq. (3.81) read

$$\{q_i'\} = \{q_{i-1}'\} + (h/2)\{q_{i-1}''\} + (h/2)\{q_i''\}$$
$$\{q_i\} = \{q_{i-1}\} + h\{q_{i-1}'\} + (h^2/3)\{q_{i-1}''\} + (h^2/6)\{q_i''\} \tag{3.82}$$

Wilson[2] transformed Eq. (3.82) into an explicit relation using the system's equation of motion by writing the second equation as

$$\{q_i''\} = (6/h^2)\{q_i\} - \{A_{i-1}\} \tag{3.83}$$

where

$$\{A_{i-1}\} = (6/h^2)\{q_{i-1}\} + (6/h)\{q'_{i-1}\} + 2\{q''_{i-1}\}$$

and by using Eq. (3.83) to write the first equation as

$$\{q'_i\} = (3/h)\{q_i\} - \{B_{i-1}\} \tag{3.84}$$

where

$$\{B_{i-1}\} = (3/h)\{q_{i-1}\} + 2\{q'_{i-1}\} + (h/2)\{q''_{i-1}\}$$

Now, substituting Eqs. (3.83) and (3.84) into the equations of motion [Eqs. (3.59)], we obtain

$$[\underline{K}]\{q_i\} = \{\underline{F}_i\} \tag{3.85}$$

where

$$[\underline{K}] = (6/h^2)[M] + (3/h)[C] + [K] \tag{3.86}$$

and

$$\{\underline{F}_i\} = \{F_i\} + [C]\{B_{i-1}\} + [M]\{A_{i-1}\} \tag{3.87}$$

The solution procedure will be as follows: $\{q_i\}$ is obtained by solving Eq. (3.85) knowing the values at $i-1$; these are used in Eqs. (3.83) and (3.84) to obtain $\{q''_i\}$ and $\{q'_i\}$, which are then used to calculate $\{A_i\}$ and $\{B_i\}$, and the process is repeated using Eq. (3.85) to get $\{q_{i+1}\}$, and so on. Furthermore, we notice that in linear analysis the matrix $[\underline{K}]$ in Eq. (3.85) is constant; hence, the triangular decomposition in the solution will be done only once at the beginning of the solution. In nonlinear analysis we will have to perform the triangular decomposition in each step of the solution.

Enhancement of the accuracy of numerical methods in dynamic response problems. In this section, a method that has been shown to improve the accuracy in response calculations when using numerical methods and at the same time achieves a reduction in the computational cost in the problem solution is presented. Refer elsewhere for details of the method.[3] The method is an application of Richardson's extrapolation technique used in numerical analysis. Consider a numerical solution of the displacement vector $\{q_1\}$ of the second-order differential equations of motion obtained using a time step Δt_1 with an error in the solution $O(\Delta t_1^m)$ and a solution of the displacement vector $\{q_2\}$ for a time step increment Δt_2 with an error in the solution $O(\Delta t_2^m)$. The Richardson extrapolation technique consists in writing a better solution as

$$q_{\text{ext}} = \left(q_2 \Delta t_1^m - q_1 \Delta t_2^m\right) / \left(\Delta t_1^m - \Delta t_2^m\right) \tag{3.88}$$

Thus, using Eq. (3.88), we expect to have a better value for the problem solution than $\{q_1\}$ and $\{q_2\}$. Furthermore, it can be shown that if the error in the solution can be written as

$$\varepsilon = C_1 \Delta t_1^m + C_2 \Delta t_2^m + \cdots \tag{3.89}$$

where C_i are constant, and having obtained the sets of solution $\{q_1\}$, $\{q_2\}$, and $\{q_3\}$ for time step increments Δt_1, Δt_2, and Δt_3, respectively, we can write a better solution for the displacement vector $\{q\}$ as

$$q_{\text{ext}} =$$

$$\frac{q_1 \Delta t_2^m \Delta t_3^m \left(\Delta t_2^m - \Delta t_3^m\right) + q_2 \Delta t_1^m \Delta t_3^m \left(\Delta t_1^m - \Delta t_3^m\right) + q_3 \Delta t_2^m \Delta t_1^m \left(\Delta t_2^m - \Delta t_1^m\right)}{\Delta t_2^m \Delta t_3^m \left(\Delta t_2^m - \Delta t_3^m\right) + \Delta t_1^m \Delta t_3^m \left(\Delta t_1^m - \Delta t_3^m\right) + \Delta t_2^m \Delta t_1^m \left(\Delta t_2^m - \Delta t_1^m\right)}$$

$$(3.90)$$

Equations (3.89) and (3.90) can be used efficiently in direct numerical integration methods to enhance the accuracy of results and, at the same time, reduce the cost of the solution. This has been demonstrated[3] where solutions for coarse steps were used to obtain more accurate results than the next finer time step size, and, at the same time, these better accuracy solutions result in fewer solution steps. The cost of the computation is thus directly reduced.

3.4 Damping Effect

To include a damping effect in the dynamic formulation, we need to consider the work done by the damping forces and include it in Hamilton's principle. Damping forces are difficult, if not impossible, to calculate. However, two types of damping forces have been extensively used and will be treated here, namely viscous damping and structural damping.

3.4.1 Viscous Damping

A viscous damping arises when a body is moving in a fluid (e.g., a dashpot); in such a case, we can assume that the damping force is proportional to the velocity, and we write

$$F_D = \gamma q' \qquad (3.91)$$

where F_D is the damping force, q' is the velocity, and γ is a constant determined from experiments. The work done by the viscous damping force reads

$$W_D = \int_V \{q\}^T \{F_D\} \, dv \qquad (3.92)$$

and its variation is given by

$$\delta W_D = \int_V \{\delta q\}^T \{F_D\} \, dv \qquad (3.93)$$

The equations of motion of the whole structure read

$$[M]\{q''\} + [C]\{q'\} + [K]\{q\} = \{F\} \qquad (3.94)$$

We notice that the matrix $[C]$ is symmetric. However, such formulation is very difficult to achieve in practice because it is difficult to determine the constant γ for

the structure. A formulation adapted to discrete formulation of a structural dynamics problem for the incorporation of a constant viscous damping in the analysis was proposed.[2] The various methods proposed reconstruct a viscous damping matrix $[C]$, knowing the modal damping ξ_i (measured or assumed) of a number of natural modes of vibration. A similar method was proposed[4] to reconstruct the viscous damping matrix $[C]$ from knowledge or assumption of the modal damping ξ_i of a number of natural modes, with $[C]$ written as

$$[C] = \left[[\phi] \lceil 1/\beta_{ii} \rfloor [\phi]^T \right]^{-1} \qquad (3.95)$$

where $[\phi]$ of dimension nm is the mode shape matrix of the m modes considered with damping, n is the total number of degrees of freedom of the system, and $\lceil 1/\beta_{ii} \rfloor$ is a diagonal matrix with $\beta_{ii} = 2\xi_{ii}\omega_{ii}\mu_{ii}$ and ω_{ii} and μ_{ii} being the natural frequency and the generalized mass of the mode in consideration. This formulation, despite leading to a full matrix $[C]$, has the advantage of attributing different modal damping ratio values to an individual number of modes and can be used in parametric studies with variation of the damping.

3.4.2 Structural Damping

Structural damping, also known as hysteretic or solid damping, is due to internal friction or friction among components of the system and is proportional to elastic internal forces and acts in the velocity direction. In such cases, if a harmonic motion was assumed for the solution of the problem, we can write the damping force as

$$F_D = igF_E \qquad (3.96)$$

where $i = (-1)^{1/2}$ and g is a constant, which again can be determined from experiments. Through calculation of the work done by the damping forces and variation, as was made in the previous section, we obtain a damping matrix written as

$$[C] = ig[K] \qquad (3.97)$$

where $[K]$ is the system stiffness matrix.

3.5 Applications

3.5.1 The Two-Degree-of-Freedom Mechanical System

In this section, we study the two-degree-of-freedom mechanical system. This is a special case of the general multidegree-of-freedom mechanical system. However, as will be seen in this section, this system presents a special application that has an important role to play in practice, namely the mechanical vibration absorption problem. This is the main reason for its study in mechanical vibration systems. Consider the two-degree-of-freedom mechanical system shown in Fig. 3.2. The kinetic energy functional, the strain energy functional, and the dissipation function
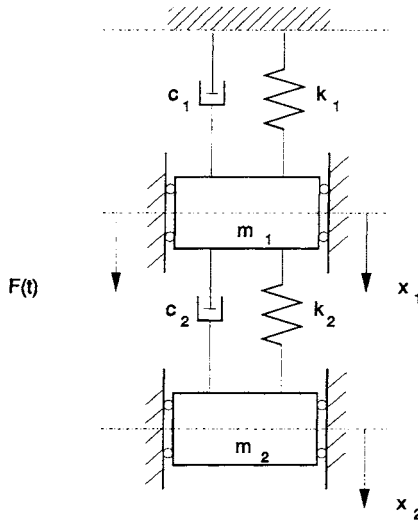
Fig. 3.2   Two-degree-of-freedom mechanical system.

of the mechanical system read

$$T = \tfrac{1}{2}m_1 x_1'^2 + \tfrac{1}{2}m_2 x_2'$$

$$U = \tfrac{1}{2}k_1 x_1^2 + \tfrac{1}{2}k_2 (x_2 - x_1)^2 \tag{3.98}$$

$$D = \tfrac{1}{2}c_1 x_1'^2 + \tfrac{1}{2}c_2 (x_2' - x_1')^2$$

Applying Lagrange's equations, we obtain the system equations of motion as

$$m_1 x_1'' + (c_1 + c_2)x_1' + (k_1 + k_2)x_1 - c_2 x_2' - k_2 x_2 = F(t)$$
$$-c_2 x_1' - k_2 x_1 + m_2 x_2'' + c_2 x_2' + k_2 x_2 = 0 \tag{3.99}$$

We consider first the free vibration problem, i.e., $F(t) = 0$. The system of equations [Eqs. (3.99)] admits solutions in the form

$$x_1 = x_{10}e^{\lambda t} \qquad \text{and} \qquad x_2 = x_{20}e^{\lambda t} \tag{3.100}$$

Substituting these solutions [Eqs. (3.100)] into Eqs. (3.99), we obtain

$$\begin{bmatrix} m_1\lambda^2 + (c_1 + c_2)\lambda + (k_1 + k_2) & -c_2\lambda - k_2 \\ -c_2\lambda - k_2 & m_2\lambda^2 + c_2\lambda + k_2 \end{bmatrix} \begin{Bmatrix} x_{10} \\ x_{20} \end{Bmatrix} = \begin{Bmatrix} 0 \\ 0 \end{Bmatrix} \tag{3.101}$$

and for a nontrivial solution of Eq. (3.101) we get

$$\begin{vmatrix} m_1\lambda^2 + (c_1 + c_2)\lambda + (k_1 + k_2) & -c_2\lambda - k_2 \\ -c_2\lambda - k_2 & m_2\lambda^2 + c_2\lambda + k_2 \end{vmatrix} = 0 \tag{3.102}$$

Expanding the determinant given in Eq. (3.102) and arranging terms, we obtain

$$\lambda^4 + [2\gamma_1\omega_1 + 2\gamma_2\omega_2(1+\mu)]\lambda^3 + \left[\omega_1^2 + \omega_2^2(1+\mu) + 4\gamma_1\omega_1\gamma_2\omega_2\right]\lambda^2$$

$$+ \left[2\gamma_1\omega_1\omega_2^2 + 2\gamma_2\omega_2\omega_1^2\right]\lambda + \omega_1^2\omega_2^2 = 0 \qquad (3.103)$$

where

$$\omega_1 = \sqrt{\frac{k_1}{m_1}} \qquad \omega_2 = \sqrt{\frac{k_2}{m_2}}$$

$$\gamma_1 = \frac{c_1}{2\sqrt{k_1 m_1}} \qquad \gamma_2 = \frac{c_2}{2\sqrt{k_2 m_2}} \qquad \mu = \frac{m_2}{m_1} \qquad (3.104)$$

We consider now the free vibration undamped case, i.e., $c_1 = c_2 = \gamma_1 = \gamma_2 = 0$. In this case, Eq. (3.103) reads

$$\lambda^4 + \left[\omega_1^2 + \omega_2^2(1+\mu)\right]\lambda^2 + \omega_1^2\omega_2^2 = 0 \qquad (3.105)$$

and the natural frequencies of free vibration read

$$\lambda_{1,2}^2 = -\tfrac{1}{2}\left[\omega_1^2 + \omega_2^2(1+\mu)\right] \pm \tfrac{1}{2}\sqrt{\left[\omega_1^2 + \omega_2^2(1+\mu)\right]^2 - 4\omega_1^2\omega_2^2} \quad (3.106)$$

We further consider the special case where the isolated single-degree-of-freedom systems have equal free vibration natural frequencies, i.e., we consider the special case when $\omega_1 = \omega_2 = \omega_a$. In this case, the system undamped free vibration natural frequencies are given by

$$\Omega^2 = \left(\frac{\lambda}{\omega_a}\right)^2 = -\left[1 + \frac{\mu}{2} \pm \sqrt{\mu + \frac{\mu^2}{4}}\right] \qquad (3.107)$$

or

$$|\Omega_1| = \frac{\sqrt{\mu}}{2} + \sqrt{1 + \frac{\mu}{4}}$$

$$|\Omega_2| = -\frac{\sqrt{\mu}}{2} + \sqrt{1 + \frac{\mu}{4}} \qquad (3.108)$$

and we observe that

$$\Omega_1\Omega_2 = 1$$

$$|\Omega_1 - \Omega_2| = \sqrt{\mu} \qquad (3.109)$$

A plot of the system mass ratio μ vs the nondimensional natural frequencies Ω is shown in Fig. 3.3. From this figure, we observe that the system natural frequencies are one lower than the isolated single-degree-of-freedom frequency ω_a and the other is higher than ω_a. This is a general property of isolated mechanical systems when coupled in a single dynamic system.

Consider now the forced vibration system with an external force applied to the mass m_1. Let the external force be a harmonic excitation with $F(t) = F_0\cos\omega t$.
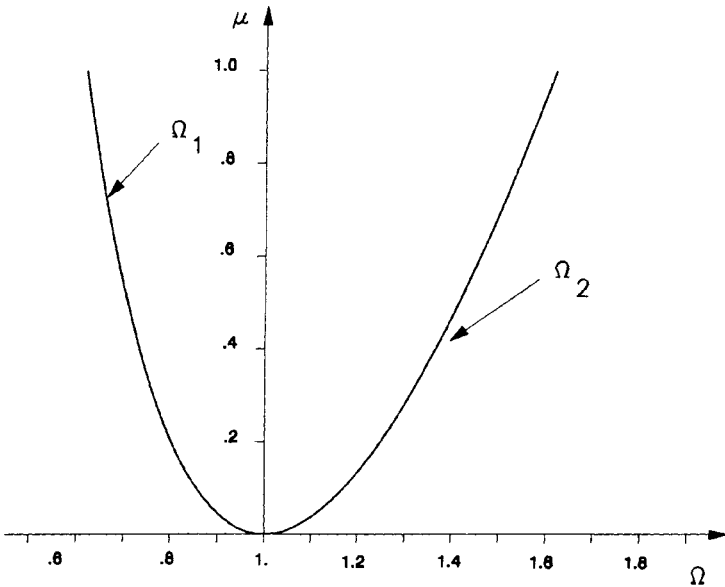
Fig. 3.3   Variation of the two-degree-of-freedom undamped natural frequencies vs the mass ratio μ.

The equations of motion of the undamped system read

$$m_1 x_1'' + (k_1 + k_2)x_1 - k_2 x_2 = F_0 \cos \omega t$$
$$-k_2 x_1 + m_2 x_2'' + k_2 x_2 = 0 \tag{3.110}$$

For the steady-state response, we can write solutions in the form

$$x_1 = x_{10} \cos(\omega t + \phi)$$
$$x_2 = x_{20} \cos(\omega t + \phi) \tag{3.111}$$

Substituting these solutions [Eqs. (3.111)] into Eqs. (3.110), we obtain

$$\left[-m_1 \omega^2 x_{10} + (k_1 + k_2)x_{10} - k_2 x_{20}\right]\cos(\omega t + \phi) = F_0 \cos \omega t$$
$$\left[-k_2 x_{10} - m_2 \omega^2 x_{20} + k_2 x_{20}\right]\cos(\omega t + \phi) = 0 \tag{3.112}$$

Solving the second equation of the system of equations [Eqs. (3.112)], we obtain

$$x_{10} = x_{20}\left[1 - \omega^2 / \omega_2^2\right] \tag{3.113}$$

We observe that, if the isolated undamped natural frequency of the auxiliary system, i.e., $\omega_2 = k_2/m_2$, is chosen to be equal to the external excitation frequency ω, the amplitude of the main mass m_1 will be zero for all values of x_{20}. This is the property of vibration absorption in a mechanical system. We now substitute x_{10}

from Eq. (3.113) into the first equation of the system [Eqs. (3.112)] to obtain

$$\left[\left[-m_1\omega^2 + (k_1 + k_2) \right] \left[1 - \frac{\omega^2}{\omega_2^2} \right] - k_2 \right] x_{20} \cos(\omega t + \phi) = F_0 \cos \omega t \quad (3.114)$$

and we conclude that $\sin \phi = 0$ or $\phi = 0$ or π, i.e., the responses are phased or π-phased with the excitation force. This was expected since we have assumed that the damping in the mechanical system is zero. Now using Eqs. (3.113) and (3.114), we obtain the amplitudes x_{10} and x_{20} as

$$\frac{x_{10}}{F_0} = \frac{\frac{1}{m_1}\left[1 - \frac{\omega^2}{\omega_2^2} \right]}{\left\{ \left[1 - \frac{\omega^2}{\omega_2^2} \right] \left[\omega_1^2 + \omega_2^2 \mu - \omega^2 \right] - \omega_2^2 \mu \right\}} \quad (3.115)$$

and

$$\frac{x_{20}}{F_0} = \frac{\frac{1}{m_1}}{\left\{ \left[1 - \frac{\omega^2}{\omega_2^2} \right] \left[\omega_1^2 + \omega_2^2 \mu - \omega^2 \right] - \omega_2^2 \mu \right\}} \quad (3.116)$$

and, at the absorption condition, we have $\omega_1 = \omega_2 = \omega$ and thus

$$x_{10} = 0 \qquad \text{and} \qquad x_{20} = -F_0/k_2 \quad (3.117)$$

The second equation permits us to size the stiffness of the mechanical absorber. Finally, if $\omega_1 = \omega_2 = \omega_a$, we can write for amplitudes x_{10} and x_{20}

$$\frac{x_{20}}{x_{2st}} = \frac{x_{20}}{F_0/k_2} = \frac{\mu}{\left\{ \left[1 - \frac{\omega^2}{\omega_a^2} \right] \left[1 + \mu - \frac{\omega^2}{\omega_a^2} \right] - \mu \right\}} \quad (3.118)$$

and

$$\frac{x_{10}}{x_{1st}} = \frac{x_{10}}{F_0/k_1} = \frac{\left[1 - \frac{\omega^2}{\omega_a^2} \right]}{\left\{ \left[1 - \frac{\omega^2}{\omega_a^2} \right] \left[1 + \mu - \frac{\omega^2}{\omega_a^2} \right] - \mu \right\}} \quad (3.119)$$

Figure 3.4 shows a plotting of the amplitude of the main mass x_{10}/x_{st} vs the frequency ratio $\Omega = \omega/\omega_a$ for a mass ratio $\mu = m_2/m_1 = 0.1$. As an example, we consider that the original system was operating with an external frequency excitation of 30 Hz, which is equal to its natural frequency and therefore is operating at resonance. From the curves of Fig. 3.4, we observe that, if a mechanical absorber has been designed for a mass ratio of $\mu = 0.1$, we see that the coupled system will have two natural frequencies of 25.5 and 35.1 Hz, respectively. At the external excitation of 30 Hz, the main system will be completely attenuated and will have an amplitude of the order of the static deflection for a variation of the external excitation frequency between 28.5 and 31.5 Hz. Notice that damping effect has not been considered in the above analysis. The system with damping can be analyzed following the same paths as given above.
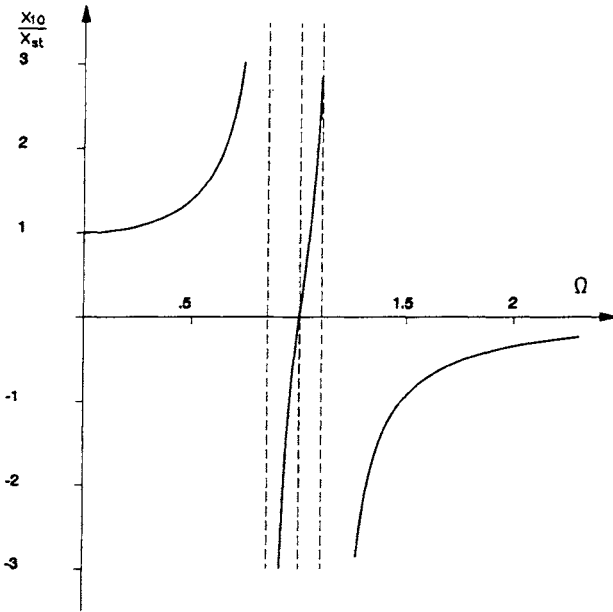
Fig. 3.4   Curves of the amplitude x_{10}/x_{st} of the main mass m_1 for a dynamic absorber vs $\Omega = \omega/\omega_a$ for a value of mass ratio $\mu = m_2/m_1 = 0.1$.

3.5.2   Determination of the Dynamic Properties of a Winglike Structure

In this section, a practical application of the calculation of the dynamic charac- teristics of a winglike structure, i.e., the calculation of the natural frequencies and mode shapes, is presented. Nowadays, almost all practical applications of such calculations are made using the finite element method. This section thus begins with a brief description of the finite element method and its application to struc- tural dynamic problems. The example in consideration is then presented, and the results of the analysis are given.

The finite element method is a numerical analysis technique for obtaining ap- proximate solutions of boundary value problems. In engineering applications, the method was presented for the first time as an intuitive idea for extending the method of matrix analysis of structures to the problems of elastic continuum in the pioneer work of Turner et al.[5] These authors considered the continuum as composed of finite regions (called latter finite elements by Clough[6]) and described the properties of each region in terms of a finite number of parameters, namely the displacements at a prescribed number of points on the boundary of the region (called nodal points or nodes); then applying the conditions of compatibility of the displacements at these points, the elements were joined together, forming then a system of lin- ear simultaneous equations with the displacements as unknowns. The solution of these equations gave the nodal displacement values, which were subsequently used to determine the stresses within each region. Nearly at the same period,

Argyris[7-11] began to publish a series of papers, covering the problem of two- and three-dimensional linear structural analysis, with suitable techniques adapted to automatic digital computations. Furthermore, early in 1943, the applied mathematic literature[12] formulated the mathematical bases of the method, describing it as an application of the Rayleigh–Ritz method for subregions of the domain. In the 1960s, numerous publications on the application of the finite element method in structural mechanics appeared and began an iteration between the intuitive engineering idea and the applied mathematic point of view to place the method on rigorous mathematical bases. The application of the method was then extremely rapid, passing from the simple linear structural analysis to nonlinear problems, dynamic problems, flow problems, coupled problems, etc. Currently, more than 500 textbooks and conference proceedings devoted to the finite element method exist in the scientific literature. To mention only a few examples, Refs. 13–25 are cited.

Boundary value problems as encountered in engineering applications are, in general, formulated in one of the following two ways. In the first way, differential equations governing the problem are written based on the behavior of an infinitesimal region of the domain and certain boundary relations are imposed. In the second way, a variational stationary principle valid for the whole domain is formulated and the exact solution of the dependent variables of the problem is that which maximizes the principle's functional. Furthermore, from the mathematical point of view, the two ways of the problem formulation are equivalent, i.e., the exact solution of an approach is the exact solution of the other. Once the problem has been formulated in one of these two ways, the finite element method can be invoked to obtain an approximate solution of the problem in a piecewise manner. The domain of interest is divided into smaller but finite subdomains called finite elements by imaginary points, lines, or surfaces in one-, two-, or three-dimensional problems. Approximate admissible solutions are then thought in each element and on its boundary. Consider, for instance, the domain of Fig. 3.5, which is divided into finite elements as shown. Let the dependent variables of the problem be represented by the vector $\{u(x)\}$ where x represents the space coordinates. Within the element (e) and on its boundary, we can assume a set of admissible solutions $\{u^e(x)\}$, and, for each component (i) of the vector $\{u^e(x)\}$, we can write

$$u_i^e(x) = \sum_{k=1}^{S_i} \left[\phi_k^e(x)C_k\right]_i, \qquad i = 1, 2, \ldots, n \qquad (3.120)$$

where n is the number of components of the vector $\{u^e(x)\}$, $\phi_k^e(x)$ is an admissible function for $u_i^e(x)$, C_k are constants, and S_i is the number of the admissible solutions taken for $u_i^e(x)$. In matrix notation, Eq. (3.120) for the complete vector $\{u^e(x)\}$ can be written as

$$\{u^e(x)\} = \lceil \phi^e(x) \rfloor \{C\} \qquad (3.121)$$

where $\lceil \phi^e(x) \rfloor$ is a partitioned diagonal matrix, with the diagonals composed of row matrices of dimension S_i, and $\{C\}$ is a vector composed of all the coefficients C_i of Eq. (3.120). In principle, $\phi^e(x)$ can be any admissible solution, but usually they are taken as polynomials, because these are easier to manipulate in subsequent integration and differentiation operations. In finite element terminology, $\{C\}$ is
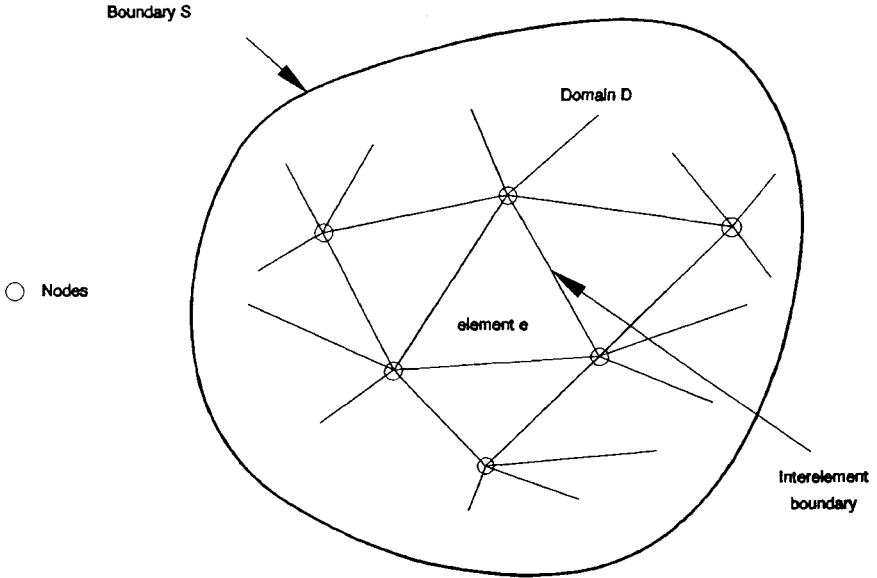
Fig. 3.5   Domain divided into finite elements.

called the vector of the generalized coordinates. Now, if we choose a set of points on the element (normally at its vertices and at specified ratios of its edges and sometimes within the element), which we define as nodal points or simply nodes in the finite element method, we can write a vector $u_i^{\prime e}(x_j)$ as

$$u_i^{e\prime}(x_j) = \sum_{k=1}^{S_i} \left(\phi_k^e(x_j)C_k\right)_i \tag{3.122}$$

where the subscript j stands for the node in consideration. Furthermore, if the nodal values in consideration are taken equal to S_i, Eq. (3.122) can be written in matrix notation as

$$\left\{u_i^{\prime e}\right\}_{S_i \times 1} = [a_i]_{S_i \times S_i}\{C_i\}_{S_i \times 1} \tag{3.123}$$

Now, if the inverse of $[a_i]$ exists (in some cases $[a_i]$ is singular, and other techniques will be used), we can write

$$\{C_i\} = [a_i]^{-1}\left\{u_i^{\prime e}\right\} \tag{3.124}$$

and for all the components, we write

$$\{C\} = \lceil A \rfloor^{-1}\{u^{\prime e}\} \tag{3.125}$$

where $\lceil A \rfloor$ is a diagonal supermatrix, with diagonal matrices given by $[a_i]$. Substitution of Eq. (3.125) into Eq. (3.121) gives

$$\{u^e(x)\} = \lceil \phi^e(x) \rfloor \lceil A \rfloor^{-1}\{u^{\prime e}\} \tag{3.126}$$

or, if we define a matrix $[N]$ as

$$[N] = \lceil \phi^e(x) \rfloor \lceil A \rfloor^{-1} \tag{3.127}$$

Eq. (3.126) reads

$$\{u^e(x)\} = [N]\{u'^e\} \tag{3.128}$$

In finite element terminology, the dimension of $\{u'^e\}$ is called the number of degrees of freedom of the element. Using Eq. (3.128), we can write for each component (i) the following expression:

$$u_i^e(x) = \sum_{j=1}^{S_i} \eta_{ij}(x) u_j'^e \tag{3.129}$$

and we conclude that, at $x = x_j$, the value of $\eta_{ij}(x)$ assumes unit value for the node in consideration j and zero value for the other nodes. The functions $\eta_{ij}(x)$ are defined as the interpolation functions; shape functions; mode functions; trial functions; or, if dependent variables are the displacements, they are called displacement functions. Hereafter, we will call $\eta_{ij}(x)$ the trial functions. As has been stated before, the inverse of $[a]$ does not always exist. Furthermore, the inversion operation is a time-consuming process; thus it will be preferable to use Eq. (3.129) to obtain $u_i^e(x)$ in terms of the nodal values. This can be done, either by inspection in simple cases or using adequate interpolation functions as is extensively described in the finite element literature, for instance Ref. 24.

Consider now a boundary value problem for which a variational principle exists and is written as

$$\delta I = 0 \tag{3.130}$$

where the functional I is written as

$$I = \int_R f_1(u_i, x_j)\, dR + \int_S f_2(u_i, x_j)\, dS \tag{3.131}$$

and u_i are the field variables and x_j are the space coordinates. The problem is defined in the domain R enclosed by the boundary S. Now, let the domain be divided into finite elements and the field variables be approximated within each element and on its boundary as

$$\{u_i^e\} = [N_i^e]\{\underline{u}_i^e\} \tag{3.132}$$

where N_i^e are the trial functions and $\underline{u}_i^e$ are the nodal values and the superscript e stands for the element in consideration. If the total number of the elements was n, then for the whole domain we can write Eq. (3.131) as

$$I = \sum_{e=1}^{n} I^e = \sum_{e=1}^{n} \left[\int_{R_e} f_1(u_i, x_j)\, dR + \int_{S_e} f_2(u_i, x_j)\, dS \right] \tag{3.133}$$

Substituting for the approximate solution Eq. (3.132) into Eq. (3.133) and performing integrations, we obtain

$$I = \sum_{e=1}^{n} I^e = I\left(\underline{u}_{i_1}, \underline{u}_{i_2}, \ldots, \underline{u}_{i_m} \right) \tag{3.134}$$

where m is the total number of the nodal points. Now the functional I has been approximated by the function $I(\underline{u}_{i_1}, \underline{u}_{i_2}, \ldots, \underline{u}_{i_m})$ given in Eq. (3.134), and, for the stationary condition of the principle, we write

$$\frac{\partial I}{\partial \underline{u}_{ij}} = 0 \qquad j = 1, 2, \ldots, m \tag{3.135}$$

Furthermore, for a typical nodal point (say j), the Eq. (3.135) reads

$$\frac{\partial I}{\partial \underline{u}_{ij}} = \sum_{e=1}^{\lambda} \frac{\partial I^e}{\partial \underline{u}_{ij}} = 0 \tag{3.136}$$

where λ is the total number of the elements connected to the nodal point in consideration. Equation (3.136) represents a global formulation for each nodal point of the domain. Examining Eqs. (3.132), (3.134), and (3.136), we conclude that only nodal values of $\lambda x s$, where s is the total number of the field variables of the problem, will be present in each equation of the system of equations [Eq. (3.136)], characterizing the banding nature of the finite element equations. Furthermore, Eq. (3.136) suggests an element formulation first, and then the contribution of all the elements will be made by the simple addition of the contribution of each element at the respective nodal points, a property well adapted to automatic digital computations.

Thus, on an element level we can write Eq. (3.136) as

$$\left\{ \frac{\partial I^e}{\partial \underline{u}_{ij}} \right\}_{j=1,2,\ldots,n} = [k^e]\{\underline{u}_i^e\} - \{f_i^e\} \tag{3.137}$$

where n is the total number of the nodal points of the element in consideration. The matrix $[k^e]$ is defined as the characteristic matrix of the element e and $\{f_i^e\}$ is defined as the characteristic vector of the element e. In static elasticity problems, using the principle of minimum total potential energy, the characteristic matrix is called the stiffness matrix, the characteristic vector is called the consistent load vector, and the field nodal values vector is called the generalized displacement vector. Now using Eqs. (3.136) and (3.137), we can write for the whole domain

$$[K]\{u\} + \{F\} = 0 \tag{3.138}$$

where $[K]$ and $\{F\}$ are defined as the characteristic matrix and the characteristic vector of the whole domain, respectively. The matrix equation [Eq. (3.138)] represents a set of simultaneous algebraic equations. These, with the application of the appropriate boundary conditions of the problem, are solved to produce the unknown nodal values of the field variable vector $\{u\}$.

Example 3.1

As an example, we consider the simple structural problem shown in Fig. 3.6. It is composed of a rod clamped at one extremity and is subjected to a concentrated axial load $2P$ at the other extremity, together with an axial load P at the middle of the rod. It is required to find the axial displacements at the middle and the free end of the rod. The problem can be solved using a finite element formulation based
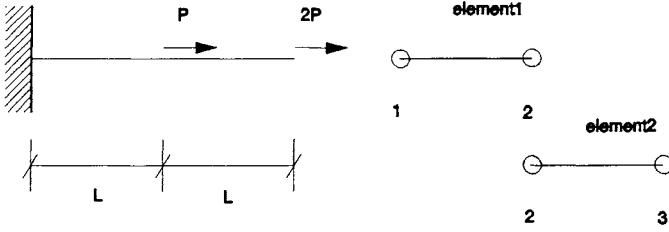
Fig. 3.6   Simple structural problem.

on the principle of miminum total potential energy. The related functional for the case at hand[24] can be written as

$$\pi_p = \frac{1}{2} \int_V \sigma \varepsilon \, dV - \int_{S_o} u \underline{p} \, ds \tag{3.139}$$

Dividing the structure into two finite elements, as shown in Fig. 3.6, we write Eq. (3.139) as

$$\pi_p = \pi_p^1 + \pi_p^2 \tag{3.140}$$

Now using the stress–strain and the strain–displacement relationships and assuming a constant cross-sectional area, we get

$$\pi_p^1 = \frac{EA}{2} \int_0^L \left(\frac{du}{dx}\right)^2 dx - u_2 P$$

$$\pi_p^2 = \frac{EA}{2} \int_0^L \left(\frac{du}{dx}\right)^2 dx - 2u_3 P \tag{3.141}$$

Because only derivatives of the first order appear under the integral sign and to have convergence in the finite element formulation, we must have C^0 continuity at the interelement boundary,[24] i.e., only the displacements must be continuous at the interelements. Trial functions achieving such requirements for the line element can be written as[24]

$$u^1(x) \cong [\xi_1 \quad \xi_2] \begin{Bmatrix} u_1 \\ u_2 \end{Bmatrix} \qquad u^2(x) \cong [\xi_1 \quad \xi_2] \begin{Bmatrix} u_2 \\ u_3 \end{Bmatrix} \tag{3.142}$$

where $\xi_1 = 1 - x/L$ and $\xi_2 = x/L$.

Substituting Eq. (3.142) into Eq. (3.141) and performing the integrations, we get

$$\pi_p^1 = \frac{EA}{2L} \left[u_1^2 + u_2^2 - 2u_1 u_2 \right] - u_2 P$$

$$\pi_p^2 = \frac{EA}{2L} \left[u_2^2 + u_3^2 - 2u_2 u_3 \right] - 2u_3 P \tag{3.143}$$

Using Eq. (3.137) for stationary conditions, we get

$$\begin{Bmatrix} \dfrac{\partial \pi_p^1}{\partial u_1} \\ \dfrac{\partial \pi_p^1}{\partial u_2} \end{Bmatrix} = \frac{EA}{L} \begin{bmatrix} 1 & -1 \\ -1 & 1 \end{bmatrix} \begin{Bmatrix} u_1 \\ u_2 \end{Bmatrix} - \begin{Bmatrix} 0 \\ P \end{Bmatrix} \qquad (3.144)$$

$$\begin{Bmatrix} \dfrac{\partial \pi_p^2}{\partial u_2} \\ \dfrac{\partial \pi_p^2}{\partial u_3} \end{Bmatrix} = \frac{EA}{L} \begin{bmatrix} 1 & -1 \\ -1 & 1 \end{bmatrix} \begin{Bmatrix} u_2 \\ u_3 \end{Bmatrix} - \begin{Bmatrix} 0 \\ 2P \end{Bmatrix} \qquad (3.145)$$

Using Eq. (3.138) for the whole structure, we get

$$\frac{EA}{L} \begin{bmatrix} 1 & -1 & \\ -1 & 2 & -1 \\ & -1 & 1 \end{bmatrix} \begin{Bmatrix} u_1 \\ u_2 \\ u_3 \end{Bmatrix} - \begin{Bmatrix} 0 \\ P \\ 2P \end{Bmatrix} = \begin{Bmatrix} 0 \\ 0 \\ 0 \end{Bmatrix} \qquad (3.146)$$

Applying the forced boundary conditions, i.e., forcing $u_1 = 0$, the system of equations [Eq. (3.146)] reduces to

$$\frac{EA}{L} \begin{bmatrix} 2 & -1 \\ -1 & 1 \end{bmatrix} \begin{Bmatrix} u_2 \\ u_3 \end{Bmatrix} = \begin{Bmatrix} P \\ 2P \end{Bmatrix} \qquad (3.147)$$

Solving for u_2 and u_3, we get

$$u_2 = 3PL/EA \qquad \text{and} \qquad u_3 = 5PL/EA \qquad (3.148)$$

In structural dynamics problems using the finite element method, Hamilton's principle is used for the problem formulation, and the same procedure as described above is applied. Following this procedure, a matrix equation is obtained for each element in the form

$$\left\{ \frac{\partial I^e}{\partial \underline{u}_{ij}} \right\}_{j=1,2,\dots,n} = [k^e]\{\underline{u}_i^e\} + [m^e]\{\underline{u}_i''^e\} - \{f_i^e\} \qquad (3.149)$$

where $[m^e]$ is called the consistent mass matrix and is given by

$$[m^e] = \int_v \rho [N]^T [N] \, dv \qquad (3.150)$$

where ρ is the material mass density. The assembly technique for the whole structure is made in exactly the same manner as described above to obtain the system equation of motion as

$$[M]\{u''\} + [K]\{u\} - \{F\} = 0 \qquad (3.151)$$

As an example for the simple structure of Fig. 3.6, the mass matrix of the element

reads

$$[m^e] = \frac{\rho A L}{6} \begin{bmatrix} 2 & 1 \\ 1 & 2 \end{bmatrix} \tag{3.152}$$

Applying the assembly technique and forcing the boundary conditions, we obtain for free vibration of the simple problem of Fig. 3.6 the following system of equations

$$\frac{\rho A L}{6} \begin{bmatrix} 4 & 1 \\ 1 & 2 \end{bmatrix} \begin{Bmatrix} u_2'' \\ u_3'' \end{Bmatrix} + \frac{E A}{L} \begin{bmatrix} 2 & -1 \\ -1 & 1 \end{bmatrix} \begin{Bmatrix} u_2 \\ u_3 \end{Bmatrix} = \begin{Bmatrix} 0 \\ 0 \end{Bmatrix} \tag{3.153}$$

from which we can calculate the free vibration undamped natural frequencies and the corresponding mode shapes.

In the following section, the calculations of the dynamic properties of a wing-like structure using the finite element method are presented. The structure studied presents certain regularity and simplicity in the input data so that it can be easily reproduced or modified for further developments. At the same time, the structure considered possesses the main properties of winglike structures so that the conclusions drawn can be generalized. This same model was studied previously using the finite element method[26] and experimentally[27] and was analyzed in detail using various finite element models to study the adequacy of the elements used and the convergence of the finite element method in Ref. 24. All these studies were performed for static linear analysis. We now extend these calculations to the dynamic properties determination of the related structure.

Figures 3.7a and 3.7b show the wing model studied. The structure is a model of a swept-back wing of 24S-T aluminum construction. All dimensions used in the analysis are in inches. The wing has 30-deg sweepback and is untapered throughout.
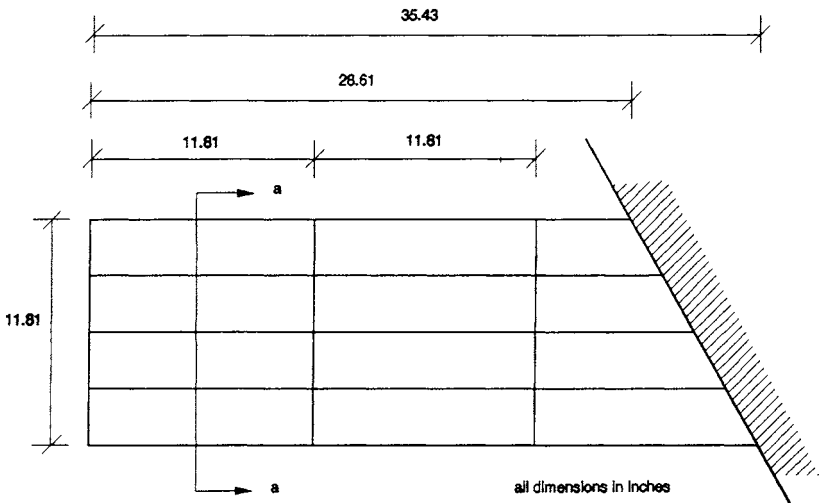
Fig. 3.7a   Configuration and general dimensions of the wing model.
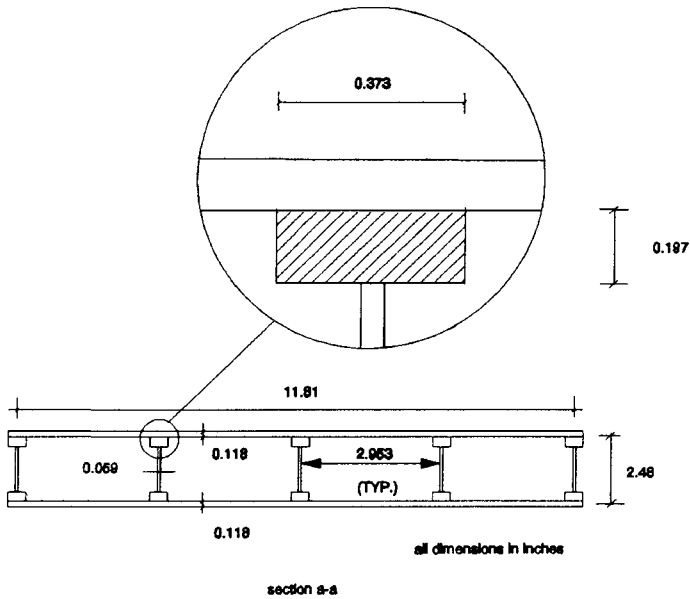
Fig. 3.7b   Details of the wing model of Fig. 3.7a.

Five identical construction spars and three identical ribs are used and bonded to the top and bottom skin sheets.

In this section, we will use the model designated as model number 2 in Ref. 24 for the present calculations. In this model, axial stress elements with two nodal points are used to represent the spar and rib cups. Rectangular membrane elements with four nodal points are used to model the spar and rib webs and the top and bottom skins. The nodal points have been localized at the intersection of the spars and the ribs and at the middle surface of the skins. A mesh of one element between spars, one element between ribs, and one element between spar and rib cups was used in the present investigation. The consistent mass technique as described in the simple problem cited above was used in the calculation for obtaining the mass matrix of the complete structure. Nastran finite element program was used for the present analysis.

Figures 3.8a–3.8d show the first four modes of the analysis performed. Modes one and four are predominantly bending modes. Mode two is the first fore-and-aft mode, and mode three is the first torsion mode of the wing model. Eigenvalue extraction is a time-consuming process. A method that tremendously reduces the computational cost in dynamic analysis for eigenvalues extraction is the selective inversion technique given in Chapter 1. We now apply this method to the problem at hand and compare the results obtained with the full finite element solution where the consistent mass technique was used. If, as is the usual case (for instance, the modal extraction is made for the purpose of performing a subsequent aeroelastic analysis), our interest is limited to the out-of-plane modes, we select the 15 nodal points on the upper skin and apply unit loads in the z direction to obtain a reduced flexibility matrix of the model. The masses are distributed on these 15 points, and

V4
C1

Z
Y
X
Output Set: Mode 1 3.772042 Hz
Deformed(0.771): Total Translation
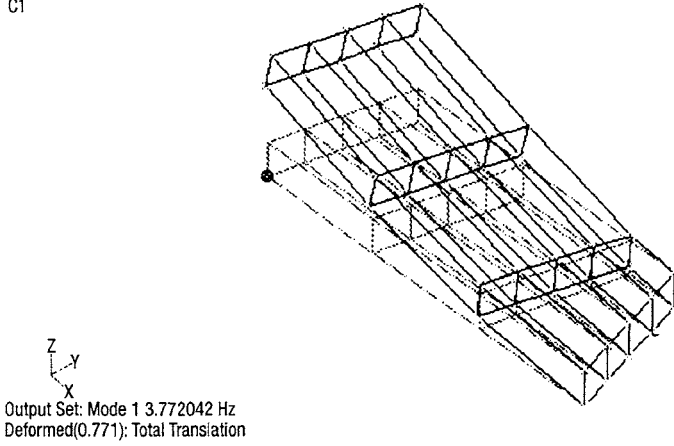
Fig. 3.8a   First mode of free vibration, first bending mode, f = 3.77 Hz.

the system mass matrix is therefore reduced to a diagonal matrix of order 15. The dynamic analysis is then performed as explained in Chapter 1. The results of the analysis are given in Table 3.1.

The results of Table 3.1 show that good agreement has been obtained using the selective inversion technique compared to the full finite element method, while the computational time has been tremendously reduced. If the in-plane modes are of interest, unit load should also be applied in the y direction at the respective points of the mass concentration in the formulation of the reduced flexibility matrix. In this case, the selective inversion technique will reproduce also the second free vibration mode, which is a fore-and-aft mode.

V4
C1

Z
Y
X
Output Set: Mode 2 11.4135 Hz
Deformed(0.781): Total Translation
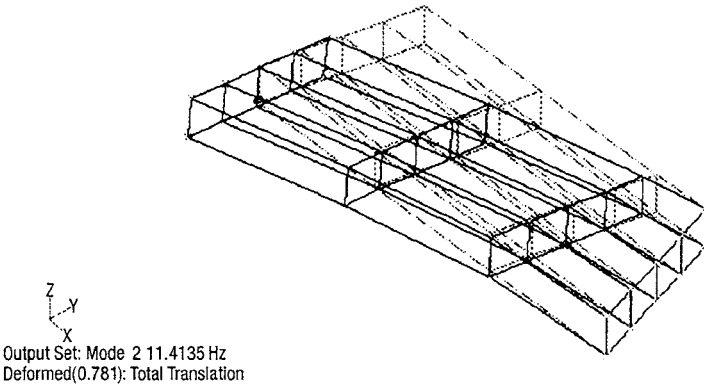
Fig. 3.8b   Second mode of free vibration, first fore-and-aft mode, f = 11.41 Hz.
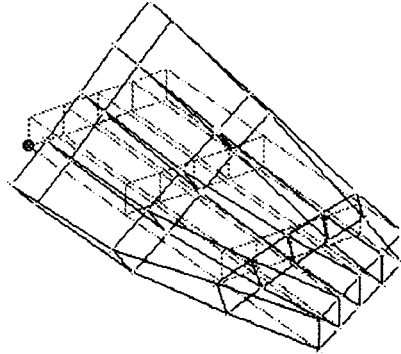
Output Set: Mode 3 13.93595 Hz
Deformed(0.993): Total Translation

Fig. 3.8c   Third mode of free vibration, first torsion mode, f = 13.93 Hz.

3.5.3   Free Vibration Analysis of a 15-deg Swept Untapered Wing Model

The structural configuration to be analyzed is shown in Fig. 3.9. It consists of a 0.041-in. thick aluminum sheet and has a chord of 2 in. measured perpendicular to the leading edge. The leading and trailing edges are beveled 0.25 in. to form a symmetrical hexagonal airfoil section perpendicular to the leading edge. It is required to perform a free vibration analysis to determine modal characteristics of the structure. These data are intended to be used in a subsequent aeroelastic analysis of the model. Experimental measurements of the frequencies and the mode shapes of this structural configuration were performed in Ref. 28 and thus will be used for the purpose of comparison with present analytical calculations.

Physical reasoning reveals that the lowest modes of this structural configuration will be due to out-of-plane motion with a highly coupled bending–torsion effect
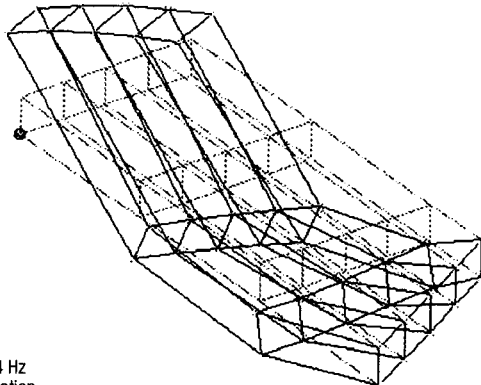
Output Set: Mode 4 18.47944 Hz
Deformed(0.692): Total Translation

Fig. 3.8d   Fourth mode of free vibration, second bending mode, f = 18.48 Hz.

**Table 3.1   Comparison of the free vibration frequencies
in Hz using the full finite element solution (FEM)
and the selective inversion technique (SIT)[a]**

Method	FEM	SIT
Degree of freedom	90	15
First mode	3.77	3.54
Second mode	11.41	——
Third mode	13.93	13.54
Fourth mode	18.48	17.43

[a]FEM is with the consistent mass matrix formulation and SIT is with
concentrated mass method.

due to the sweepback of the wing model. Furthermore, previous experience shows that the critical modes for aeroelastic analysis of this simple structural configuration will be limited to the first few lower natural modes. For these reasons we will use high-precision triangular bending elements, namely the T-18 element,[24] to represent adequately the stiffness part of the problem, and, for the inertia representation, we will use the lumped mass technique. The masses will be concentrated at the nodal points and will be considered to act only in the transverse direction. Rotary inertia effects will not be considered because their effect is considered to be of secondary nature for the present formulation. The finite element model used is shown in Fig. 3.9.

For the present configuration of the analysis, the best option to perform the dynamic solution of the problem is to use the selective inversion technique used in the previous example and described in Chapter 1. To this end, unit loads have
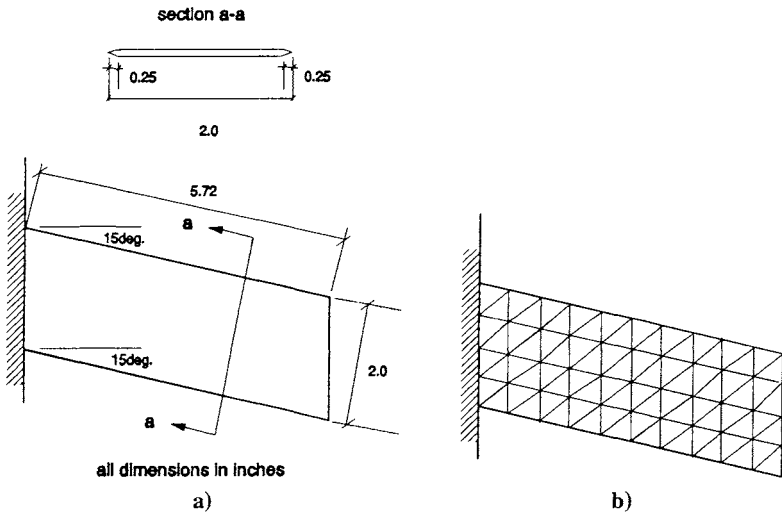
Fig. 3.9   Structural configuration and the finite element model of the 15-deg untapered swept-wing model.
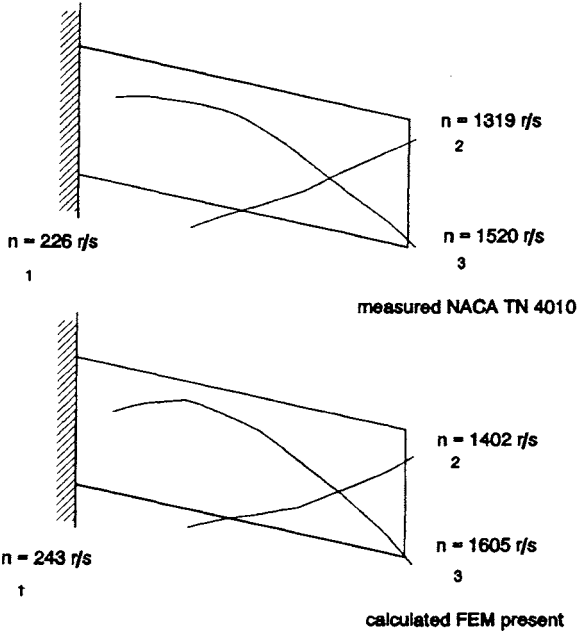
Fig. 3.10   First three natural free vibration modes of the structural model of the 15-deg untapered swept-wing model.

been applied at the 50 nodal points in the normal direction to obtain a reduced 50×50 flexibility matrix. This coupled with the 50 masses concentrated at the corresponding nodal points provides the dynamic representation of the problem. The direct iteration technique is then used to obtain the desired first eigenvalues and eigenvectors. The results of the analysis in terms of the first three vibration modes are shown in Fig. 3.10 and are compared with the experimental findings of Ref. 28. From these results, the following conclusions can be made. First, in terms of the precision attained, good achievements have been obtained. If we compare the calculated frequencies and measured values, we can see that the discrepancy is about 7%. This is reasonable due to the simplification introduced to the analysis, e.g., lumping and distribution of the masses to represent the inertia, and also to the experimental model, e.g., exact representation of the built-in conditions. Therefore, because of these limitations, no modifications or adjustments of the theoretical models are required or justified, and the results obtained in this dynamic analysis can be used directly in subsequent stability and response problems. Second, the lumped mass method coupled with the selective inversion technique to solve such dynamic problems is a powerful tool of analysis because the computational cost is tremendously reduced in the eigenvalue extraction process and good precision could be achieved when the method is used based on well-founded physical reasoning. Finally, from this simple example we can observe that the swept-back wing presents, in its natural vibration modes, a high degree of coupling between bending and torsion; therefore, the stiffness representation of such structures should reflect

such property. For instance, if beam elements are used to represent the structure configuration analyzed, these will never be capable of predicting adequately the vibration modes shown in Fig. 3.10. These vibration mode shapes have an important role to play in subsequent aeroelastic stability and response problems, where they are used in the calculation of generalized nonstationary airloads. Their accurate prediction is therefore mandatory before any attempt to perform such analyses.

3.5.4 Free Vibration Analysis of a T-Tail Model

In this section, a free vibration analysis of a T-tail model is presented. The main purpose of this analysis is a presentation of the modal characteristics of T-tail construction. These modal characteristics have an important role to play in subsequent aeroelastic and response problems. Again, the structure studied presents certain regularity and simplicity of the input data so that it can be easily reproduced or modified for further developments. At the same time, the structure considered possesses the main properties of T-tail construction so that the conclusions drawn can be generalized.

To facilitate the preparation of input data, vertical, left, and right horizontal tails have been considered of the same construction. Furthermore, each of these structures has the same structural properties as that of the wing model analyzed in Section 3.5.2. The three lifting surfaces have been joined by a boom. The boom is made of metal sheet construction. The thickness of the skin of the boom is the same as that of the tails. The boom has five spar elements equally spaced that are normal to the first rib of the horizontal tail. This construction has been considered to facilitate the preparation of input data. The finite element model made for this T-tail construction is the same as that of the wing model previously analyzed. The T-tail is fixed at the vertical tail root. Figure 3.11 presents the finite element model used in the present analysis.
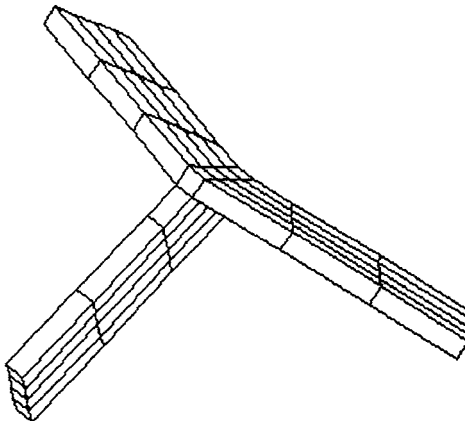
Fig. 3.11   Finite element model of the T-tail construction analyzed.

V3
L1
C1

Z
└-X
Y
Output Set: Mode 1 0.807481 Hz
Deformed(0.487): Total Translation
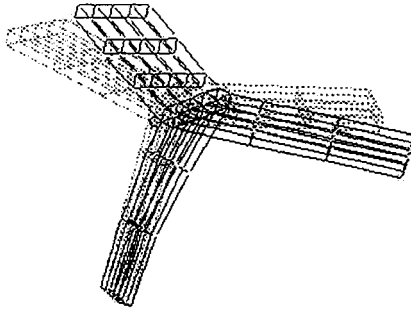
Fig. 3.12a   First mode of free vibration, f = 0.81 Hz, T-tail mode.

The Nastran finite element program has been used for the preparation of input data and the eigenvalue extraction problem. The output of the analysis is shown in Figs. 3.12a–3.12f. These figures correspond to the first six modes of free vibration. Figure 3.12a represents the first mode of free vibration of the T-tail unit. This mode is characterized by an asymmetric in-plane motion of the horizontal tail accompanied by a fin torsion and is normally the first mode found in T-tail construction. In aeroelastic analysis, this first mode has a very important role to play since it can cause a static instability at low speeds due to fin divergence. The second mode, shown in Fig. 3.12b, is mainly a fin bending with a one-node horizontal tail motion. In this mode, the horizontal tail moves almost as a rigid body. These first two modes are asymmetric modes. The third mode shape, depicted in Fig. 3.12c, is a two-node horizontal tail bending accompanied by a fore-and-aft motion of the fin and is a symmetric mode. The fourth mode, shown in Fig. 3.12d,

V3
L1
C1

Z
└-X
Y
Output Set: Mode 2 1.019493 Hz
Deformed(0.584): Total Translation
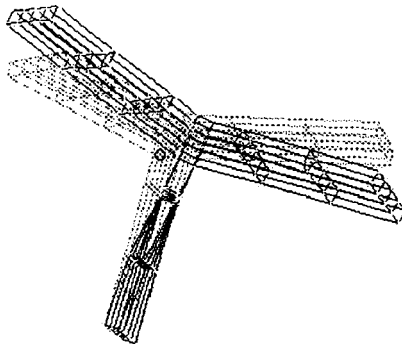
Fig. 3.12b   Second mode of free vibration, f = 1.02 Hz, vertical tail first bending and horizontal tail one node bending.

V3
L1
C1

Z
X
Y
Output Set: Mode 3 2.659375 Hz
Deformed(0.59): Total Translation
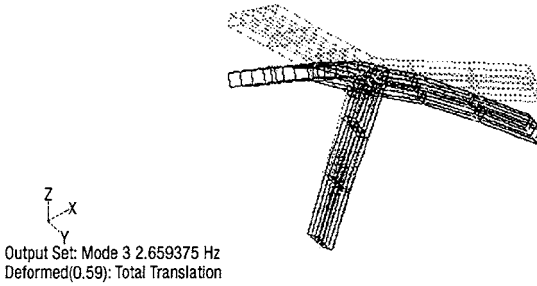
Fig. 3.12c   Third mode of free vibration, f = 2.66 Hz, vertical tail fore and aft and two nodes bending horizontal tail.

V3
L1
C1

Z
X
Y
Output Set: Mode 4 3.091983 Hz
Deformed(0.52): Total Translation
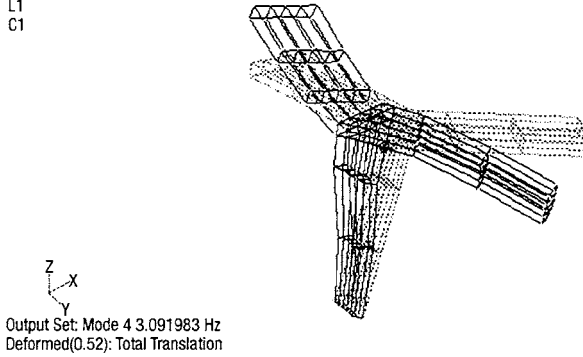
Fig. 3.12d   Fourth mode of free vibration, f = 3.09 Hz, vertical tail torsion.

V3
L1
C1

Z
X
Y
Output Set: Mode 5 4.880728 Hz
Deformed(0.526): Total Translation
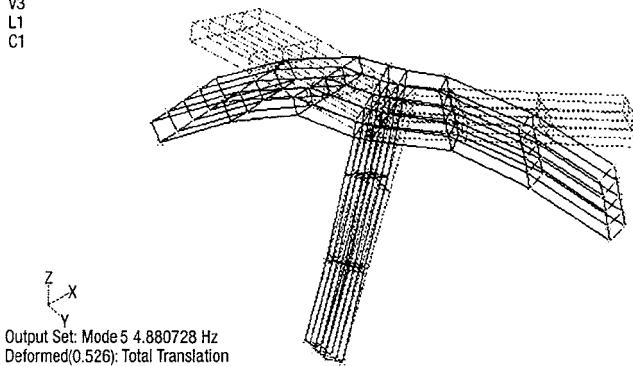
Fig. 3.12e   Fifth mode of free vibration, f = 4.88 Hz, horizontal tail symmetric torsion and vertical tail fore and aft.

V3
L1
C1

Y.   .Z
X
Output Set: Mode 6 10.84013 Hz
Deformed(0.842): Total Translation
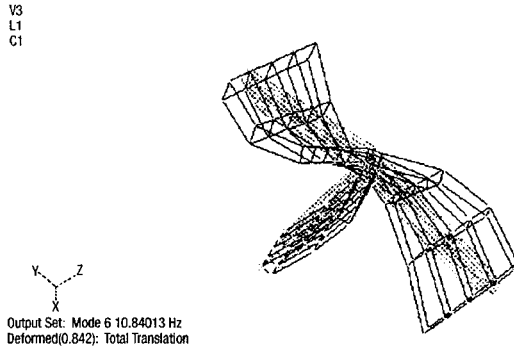
Fig. 3.12f   Sixth mode of free vibration, f = 10.84 Hz, vertical tail torsion and horizontal tail asymmetric torsion.

is an asymmetric mode with mainly a vertical tail torsion accompanied by an in-plane and out-of-plane bending of the horizontal stabilizer. The next mode, shown in Fig. 3.12e, is a symmetric mode with mainly a fore-and-aft motion of the fin and a symmetric horizontal tail torsion. The next mode, given in Fig. 3.12f, is an asymmetric mode characterized by a horizontal and vertical tail torsion. As can be shown from this example, the T-tail construction is a very complicated configuration from the dynamic point of view since in all modes the in-plane motion is almost accompanied by an out-of-plane motion, i.e., they are all coupled bending–torsion modes. Notice further that, in practical applications, more complications are introduced when the fuselage elasticity is introduced in the analysis.

References

[1] Newmark, N. M., "A Method of Computation for Structural Dynamics," *Journal of the Engineering Mechanics Division, ASCE*, Vol. 85, No. EM3, 1959, pp. 67–94.

[2] Wilson, E. L., and Penzien, J., "Evaluation of Orthogonal Damping Matrices," *International Journal for Numerical Methods in Engineering*, Vol. 4, No. 1, 1972, pp. 5–10.

[3] Bismarck-Nasr, M. N., and de Oliveira, A. M., "On Enhancement of the Accuracy in Direct Integration Dynamic Response Problems," *Earthquake Engineering and Structural Dynamics*, Vol. 20, No. 7, 1991, pp. 699–703.

[4] Bismarck-Nasr, M. N., "Finite Element Analysis of Aeroelasticity of Plates and Shells," *Applied Mechanics Reviews*, Vol. 45, No. 12, Part 1, 1992, pp. 461–482.

[5] Turner, M. J., Clough, R. W., Martin, H. C., and Topp, L. C., "Stiffness and Deflection Analysis of Complex Structures," *Journal of the Aeronautical Sciences*, Vol. 23, No. 9, 1956, pp. 805–824.

[6] Clough, R. W., "The Finite Element Method in Plane Stress Analysis," *Proceedings of the 2nd American Society of Civil Engineers Conference on Electronic Comp.*, Pittsburgh, PA, 1960.

[7] Argyris, J. H., "Energy Theorem and Structural Analysis," *Energy Theorem and Structural Analysis*, Butterworths, London, 1960.

[8] Argyris, J. H., "The Matrix Analysis of Structures with Cutouts and Modifications," *Proceedings of the 9th International Congress of Theoretical and Applied Mechanics*, Brussels, Belgium, 1956.

[9] Argyris, J. H., "The Matrix Theory of Statics," *Ingenieur Archiv*, Vol. 25, 1957, pp. 174–192.

[10] Argyris, J. H., "On the Analysis of Complex Elastic Structures," *Applied Mechanics Review*, Vol. 11, 1958, pp. 331–338.

[11] Argyris, J. H., "Continua and Discontinua," *Proceedings of the 1st Conference on Matrix Structural Mechanics*, AFFDL-TR-66-80, 1965, pp. 11–189.

[12] Courant, R., "Variational Methods for the Solutions of Problem of Equilibrium and Vibrations," *Bulletin of the American Mathematical Society*, Vol. 49, 1943, pp. 1–23.

[13] Zienkiewicz, O. C., *The Finite Element Method*, McGraw–Hill, New York, 1977.

[14] Desai, C. S., and Abel, J. F., *Introduction to the Finite Element Method*, Van Nostrand Reinhold, New York, 1972.

[15] Oden, J. T., *Finite Elements of Non-Linear Continua*, McGraw–Hill, New York, 1972.

[16] Martin, H. C., and Carey, G. F., *Introduction to the Finite Element Analysis*, McGraw–Hill, New York, 1973.

[17] Norrie, D. H., and De Vries, G., *The Finite Element Method*, Academic, New York, 1973.

[18] Strang, G., and Fix, G., *An Analysis of the Finite Element Method*, Prentice–Hall, Englewood Cliffs, NJ, 1973.

[19] Cook, R. D., *Concepts and Applications of the Finite Element Analysis*, Wiley, New York, 1974.

[20] Nath, B., *Fundamentals of the Finite Elements for Engineers*, Athlone Press, London, 1974.

[21] Gallagher, R. H., *Finite Element Analysis—Fundamentals*, Prentice–Hall, Englewood Cliffs, NJ, 1975.

[22] Huebner, K. H., *The Finite Element Method for Engineers*, Wiley, New York, 1975.

[23] Bathe, K. J., and Wilson, E. L., *Numerical Methods in Finite Element Analysis*, Prentice–Hall, Englewood Cliffs, NJ, 1976.

[24] Bismarck-Nasr, M. N., *Finite Elements in Applied Mechanics*, Abaeté, São Paulo, 1993.

[25] Noor, A. K., "Bibliography of Books and Monographs on Finite Element Technology," *Applied Mechanics Reviews*, Vol. 44, No. 6, 1991, pp. 307–317.

[26] Turner, M. J., Martin, H. C., and Weikel, R. C., "Further Development and Applications of the Stiffness Method," *Matrix Methods of Structural Analysis*, edited by B. Fraeijs de Veubeke, Macmillan, New York, 1964.

[27] Eggwertz, S., and Noton, B., "Stress and Deflexion Measurements on a Multi Cell Cantilever Box Beam with 30° Sweep," Aeronautical Research Institute of Sweden, Rept. 53, Stockholm, 1954.

[28] Hanson, P. W., and Tuovila, W. J., "Experimentally Determined Natural Vibration Modes of Some Cantilever-Wing Flutter Models by Using an Acceleration Method," NACA TN 4010, 1957.

Problems

3.1 The flexibility matrix of a wing built in at its root is given by

$$F = 10^{-8} \begin{bmatrix} 10 & 40 & 60 & 80 \\ 40 & 120 & 200 & 300 \\ 60 & 200 & 400 & 600 \\ 80 & 300 & 600 & 1000 \end{bmatrix} \text{ m/N}$$

90   STRUCTURAL DYNAMICS IN AERONAUTICAL ENGINEERING
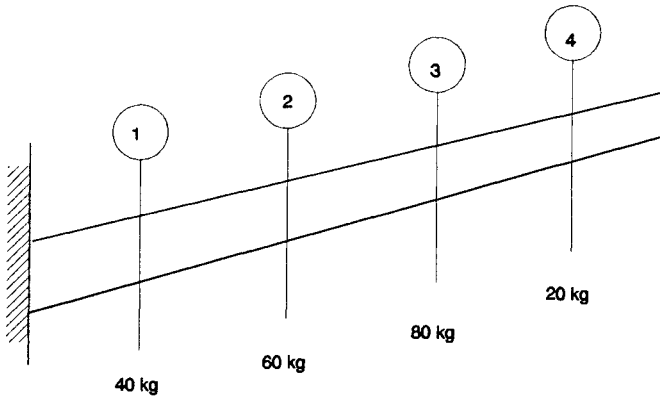
Fig. P3.1   Idealization of a wing built in at its root.

The flexibility matrix has been calculated according to the station numbering given in Fig. P3.1. The wing mass has been concentrated in the four stations as shown.

(a) Find the fundamental natural frequency of this idealized wing and the corresponding mode shape.

(b) Calculate the corresponding generalized mass and the generalized stiffness.

(c) Assuming a modal damping factor $\gamma = c/c_{cr} = 0.02$ for this mode, obtain the modal damping coefficient c and the maximum value of the modal gain ξ of this mode.

(d) Given an external applied force in the form $[F(t)]^T = 1000 \sin 20t[1 \ \ 1.5 \ \ 2 \ \ 3]^T$ N, calculate the generalized force of the first mode.

(e) Making the approximation of representing the structure by its first mode of vibration as a single-degree-of-freedom system and for the generalized force obtained in item (d), calculate the maximum displacements at the four points of the model of Fig. P3.1.

3.2   In a turboprop project, the natural frequency of the rudder tab is 27 Hz. While flying at V_C, the propeller induces a source of harmonic excitation with a forcing frequency equal to the natural frequency of the rudder tab, causing discomfort to the passengers and fatigue structural problems to the aircraft. To solve this problem, the following modifications have been proposed:

(a) Change the material of the tab from aluminum to steel, while keeping the same geometric properties of the tab (*Hint:* metallic materials have almost equal E/ρ ratios).

(b) Introduce to the tab system a hydraulic damper to reduce the level of vibrations.

(c) Project and include in the tab system a dynamic absorber.
Discuss the validity of these modifications.

3.3   The first bending and torsion mode shapes of the wing model analyzed in Section 3.5.2 using the selective inversion technique are given by (0.770, 0.765, 0.760, 0.753, 0.745, 0.383, 0.380, 0.374, 0.365, 0.356, 0.093, 0.091, 0.084, 0.072,

0.059) and $(-0.763, -0.341, 0.102, 0.543, 0.959, -0.761, -0.423, -0.063, 0.293,$ 0.622, -0.391, -0.241, -0.086, 0.053, and 0.173). The mode shapes have been normalized to unit generalized mass values. Consider now the application of a unit impulse in the transverse direction, at $t = 0$, with initial null conditions at point number seven, i.e., at the crossing of the second spar with the second rib. Because of the application of this external load, obtain

(a) The generalized force for the bending and torsion modes.

(b) Assuming zero damping, calculate the maximum displacement at the leading edge of the wing tip, considering that the structure is adequately represented by its two first transverse modes.

(c) Repeat item (b), assuming a modal damping ratio $\gamma = 0.02$ for both modes.

(d) From the results obtained, comment on the effect of damping on the response.

3.4 Repeat Problem 3.3 considering now that the external load is a unit step function having a duration of 1 s. Comment on these results compared with those of the previous case.

This page intentionally left blank

<div style="text-align:right">

4

</div>

Dynamics of Continuous Elastic Bodies

4.1 Introduction

In the preceding chapters, structural dynamic problems of discrete systems were exclusively treated. This chapter, on the other hand, concentrates on the dynamic behavior of continuous elastic bodies. This separation of structural dynamic problems into discrete and continuous systems does not mean that they have different dynamic behavior. The separation is merely a mathematical tool for the representation of the same physical system. Discrete systems lend themselves to direct application in practical problems of complex geometry and boundary conditions. This is the reason for the great emphasis made on discrete systems in previous chapters. On the other hand, some of the continuous elastic bodies problems have exact, closed-form analytical solutions. In spite of the limitation of these solutions to simple specific real problems, they have a great importance since they are directly used for parametric studies and present, in a clear and definite way, the effect of the different parameters involved in the problem. Furthermore, these exact solutions form the bases of comparisons and studies of performance and convergence of numerical discrete methods and therefore can predict the accuracy of these methods when applied to complex problems having no exact solutions. This chapter deals basically with free and forced vibrations of simple problems of beams, plates, and shells. The beams treated in this chapter are limited to slender beams; therefore, the effect of transverse shear and rotary inertias are not considered, and warping effects are neglected. The plates and shell structures considered are limited to thin thickness constructions. The shells considered in this chapter are of simple geometry so that only circular cylindrical and conical shells are studied.

4.2 Slender Beams

In this section, vibrations of slender beams are studied. The study will not consider transverse shear deformations, warping effects, and rotary inertias. The problem will be formulated using Hamilton's principle.

4.2.1 Equation of Motion

Strain energy of deformation. Consider the beam shown in Fig. 4.1. Three generalized degrees of freedom are considered, namely the axial displacement u, the transverse displacement w, and the rotation ϕ around the longitudinal axis x. The beam is subjected to an initial state of stress N_x, positive in compression, and rests on a continuous elastic foundation having a spring constant k per unit length, as shown in Fig. 4.1. The beam has a constant cross-sectional area A, a constant cross-sectional moment of inertia I about the axis y-y, and a constant cross-sectional torsional rigidity GI_t, where G is the shear modulus $= E/[2(1+\nu)]$, E is Young's
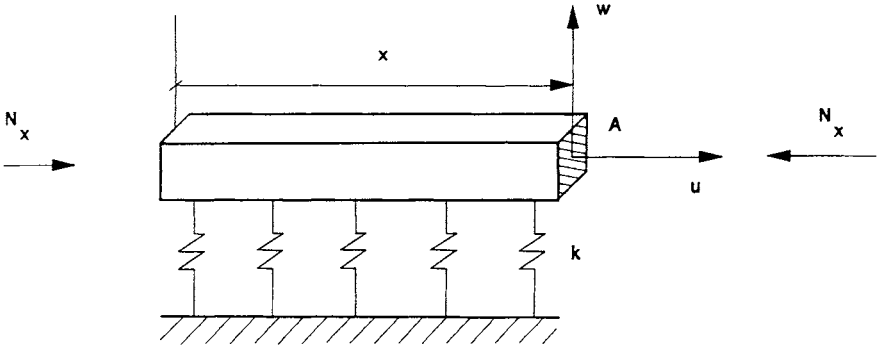
Fig. 4.1   Beam structure.

modulus, and v is Poisson's ratio. The strain energy of small deformations in the axial direction reads

$$U_x = \frac{1}{2} \int_0^L EA \left[\frac{\partial u}{\partial x} \right]^2 dx \qquad (4.1)$$

where L is the beam length.
The bending strain energy of small deformations reads

$$U_f = \frac{1}{2} \int_0^L EI \left[\frac{\partial^2 w}{\partial x^2} \right]^2 dx \qquad (4.2)$$

The torsional strain energy of small deformations reads

$$U_T = \frac{1}{2} \int_0^L GI_t \left[\frac{\partial \phi}{\partial x} \right]^2 dx \qquad (4.3)$$

The strain energy of deformation due to the elastic foundation reads

$$U_e = \frac{1}{2} \int_0^L kw^2 dx \qquad (4.4)$$

The strain energy due to the initial load N_x reads

$$U_i = \frac{1}{2} \int_0^L N_x \left[\frac{\partial w}{\partial x} \right]^2 dx \qquad (4.5)$$

Kinetic energy.   Considering the degrees of freedom u, w, and ϕ and neglecting the rotary inertia effects, the kinetic energy functional is expressed as

$$T = \frac{1}{2} \int_0^L \left\{ mA \left[\frac{\partial u}{\partial t} \right]^2 + mA \left[\frac{\partial w}{\partial t} \right]^2 + mI_p \left[\frac{\partial \phi}{\partial t} \right]^2 \right\} dx \qquad (4.6)$$

where m is the material mass density and I_p is the polar moment of inertia of the cross-sectional area.

Hamilton's principle.   Hamilton's principle for the problem at hand can be written as

$$\int_{t_1}^{t_2} \delta[T - U]\, \mathrm{d}t = 0 \qquad (4.7)$$

Substituting the functionals given in Eqs. (4.1–4.6) into Hamilton's principle [Eq. (4.7)] and applying the variational operation, we obtain the Euler–Lagrange equations governing the problem, i.e., the equations of motion for the case at hand as

$$\frac{\partial^2 u}{\partial x^2} + \frac{mA}{EA}\frac{\partial^2 u}{\partial t^2} = 0 \qquad (4.8)$$

$$\frac{\partial^2 \phi}{\partial x^2} + \frac{mI_p}{GI_t}\frac{\partial^2 \phi}{\partial t^2} = 0 \qquad (4.9)$$

$$EI\frac{\partial^4 w}{\partial x^4} + kw + N_x\frac{\partial^2 w}{\partial x^2} + mA\frac{\partial^2 w}{\partial t^2} = 0 \qquad (4.10)$$

and the corresponding boundary conditions for the problem. The boundary conditions will be treated in detail in subsequent sections.

Axial and torsional free vibrations.   Examining Eqs. (4.8) and (4.9), we notice that they represent the same differential equation; thus we can write both as

$$\frac{\partial^2 v}{\partial x^2} + \alpha^2\frac{\partial^2 v}{\partial t^2} = 0 \qquad (4.11)$$

where $v = u$ or ϕ and $\alpha^2 = m/E$ or mI_p/GI_t and we notice that α^2 is a real positive quantity. The solution of the partial differential equation [Eq. (4.11)] can be made by the method of separation of variables x and t for the case in consideration. Furthermore, we can prove that the time dependence is harmonic; thus we can write

$$v(x, t) = V(x)e^{i\omega t} \qquad (4.12)$$

where $V(x)$ is a real space function of x, ω is a real positive quantity, and $i = (-1)^{1/2}$. Substituting Eq. (4.12) into the differential equation [Eq. (4.11)], we obtain

$$\frac{\mathrm{d}^2 V}{\mathrm{d}x^2} - \alpha^2\omega^2 V = 0 \qquad (4.13)$$

The solution of Eq. (4.13) reads

$$V(x) = C_1 \sin\alpha\omega x + C_2 \cos\alpha\omega x \qquad (4.14)$$

where C_1 and C_2 are arbitrary constants to be determined from the boundary and initial conditions. In the sequel, several of these conditions will be analyzed.

Both ends fixed. For this condition, we have $V(x) = 0$ at $x = 0$ and $x = L$. Substituting these conditions in Eq. (4.14), we obtain $C_2 = 0$ and $C_1 \sin \alpha \omega L = 0$. Disregarding the trivial solution $C_1 = 0$, we obtain, $\sin \alpha \omega L = 0$; thus $\alpha \omega L = n\pi$, $n = 1, 2, 3, \ldots$. Therefore, the undamped natural frequencies of free vibration for the case when both ends are fixed are given by

$$\omega_n = \frac{n\pi}{\alpha L} \qquad n = 1, 2, 3, \ldots$$

$$= \frac{n\pi}{L} \sqrt{\frac{E}{m}} \qquad \text{for axial free vibrations}$$

$$= \frac{n\pi}{L} \sqrt{\frac{G I_t}{m I_p}} \qquad \text{for torsional free vibrations} \qquad (4.15)$$

and the mode shapes of free vibration read

$$V_n(x) = C_n \sin \frac{n\pi x}{L} \qquad n = 1, 2, 3, \ldots \qquad (4.16)$$

where C_n are now arbitrary constants to be determined from the initial conditions. Returning to Eq. (4.15), we observe that beams with the same geometrical properties will have their natural frequencies proportional to the speed of sound $(E/m)^{1/2}$. The speed of sound at room temperature in several metallic materials used in aeronautical construction are approximately given in Table 4.1. Surprisingly, these are close to each other. This is an important fact to be considered in design where, in some circumstances, we are faced with problems of increasing or decreasing the natural frequencies; thus changing the material used will not resolve the problem in such cases. This fact obtained from this simple case of extensional and torsional free vibrations will be extended in the sequel for other structures. Finally, it should be noted that modern composite materials used in aeronautical constructions, in general, do not possess this property of constant $(E/m)^{1/2}$.

Both ends free. For this condition, the stresses at both extremities are null. Now, the stresses are proportional to the strains, and these are proportional to dV/dx so that we can write the boundary conditions for the case at hand as $dV/dx = 0$ at $x = 0$ and $x = L$. Substituting these conditions in Eq. (4.14), we obtain

$$\alpha \omega [C_1 \cos \alpha \omega x - C_2 \sin \alpha \omega x] = 0 \qquad \text{for } x = 0 \text{ and } x = L \qquad (4.17)$$

Table 4.1   The speed of sound $(E/m)^{1/2}$ at room temperature in several metallic materials used in aeronautical construction

Material	$(E/m)^{1/2}$, m/s
Steels	4968
Aluminum alloys	5029
Magnesium alloys	5060
Titanium	4968

From Eq. (4.17), the following conditions are obtained

$$\alpha\omega = 0 \quad \text{and} \quad [C_1 \cos \alpha\omega x - C_2 \sin \alpha\omega x] \neq 0 \quad \text{for } x = 0 \text{ and } x = L$$

or

$$\alpha\omega \neq 0 \quad \text{and} \quad [C_1 \cos \alpha\omega x - C_2 \sin \alpha\omega x] = 0 \quad \text{for } x = 0 \text{ and } x = L$$

$$(4.18)$$

The first condition of Eq. (4.18) gives $\omega = 0$ and $C_1 \neq 0$, which corresponds to a rigid body motion. The second condition gives

$$C_2 \sin \alpha\omega L = 0 \qquad (4.19)$$

Eliminating the trivial solution $C_2 = 0$, we get

$$\omega_n = \frac{n\pi}{\alpha L} \qquad n = 1, 2, 3, \ldots$$

and the corresponding mode shapes read

$$V(x) = C_n \cos \frac{n\pi x}{L} \qquad n = 1, 2, 3, \ldots$$

Thus, we can write the complete solution of the problem as

$$\omega_n = \frac{n\pi}{\alpha L} \qquad n = 0, 1, 2, 3, \ldots \qquad (4.20)$$

and

$$V(x) = C_n \cos \frac{n\pi x}{L} \qquad n = 0, 1, 2, 3, \ldots \qquad (4.21)$$

One end clamped and the second end free. For this condition, we consider at the end $x = 0$, $V(x) = 0$, and at the end $x = L$, the stresses equal to zero, thus $dV/dx = 0$. Substituting these conditions in Eq. (4.14), we obtain

$$C_2 = 0 \quad \text{and} \quad -C_1 \alpha\omega \cos \alpha\omega L = 0 \qquad (4.22)$$

Eliminating the trivial solution $C_1 = 0$, we get, $\cos \alpha\omega L = 0$. Thus the modal characteristics for the problem at hand read

$$\omega_n = \frac{(2n-1)\pi}{2\alpha L} \qquad n = 1, 2, 3, \ldots \qquad (4.23)$$

and

$$V(x) = C_n \sin \frac{(2n-1)\pi x}{2L} \qquad n = 1, 2, 3, \ldots \qquad (4.24)$$

Transversal free vibrations. We consider first the case when $k = N_x = 0$, whose effect will be studied in the sequel. Under such conditions, Eq. (4.10) reads

$$EI \frac{\partial^4 w}{\partial x^4} + mA \frac{\partial^2 w}{\partial t^2} = 0 \qquad (4.25)$$

Using the method of separation of variables and for a harmonic solution, we can write

$$w(x, t) = W(x)\left[c_1 e^{i\omega t} + c_2 e^{-i\omega t}\right] \tag{4.26}$$

Substituting Eq. (4.26) into Eq. (4.25), we obtain

$$\frac{d^4 W}{dx^4} - a^4 W = 0 \tag{4.27}$$

where $a^4 = [mA/EI]w^2$. Writing $W(x) = Ce^{\lambda x}$, in Eq. (4.27), we get $\lambda^4 - a^4 = 0$. Thus, $\lambda_{1,2} = \pm a$ and $\lambda_{3,4} = \pm ia$. Hence we can write $W(x)$ as

$$W(x) = C_1 \sin ax + C_2 \cos ax + C_3 \sinh ax + C_4 \cosh ax \tag{4.28}$$

where C_1, C_2, C_3, and C_4 are constants to be determined from the boundary and initial conditions of the problem. In the sequel, these conditions will be analyzed.

Both ends simply supported. For this condition, we have $W(x) = 0$ and $M_x = EI[d^2 W/dx^2] = 0$ at $x = 0$ and $x = L$. Substituting the conditions for $x = 0$ into Eq. (4.28), we obtain

$$W(0) = C_2 + C_4 = 0$$

$$W''(0) = -C_2 + C_4 = 0$$

Thus, $C_2 = C_4 = 0$, and Eq. (4.28) reads

$$W(x) = C_1 \sin ax + C_3 \sinh ax \tag{4.29}$$

Substituting the conditions for $x = L$ into Eq. (4.29), we obtain

$$W(L) = C_1 \sin aL + C_3 \sinh aL = 0$$
$$W''(L) = a^2 \left[-C_1 \sin aL + C_3 \sinh aL\right] = 0 \tag{4.30}$$

or $C_3 \sinh aL = 0$ and $C_1 \sin aL = 0$. But $\sinh aL \neq 0$ for $aL \neq 0$, and eliminating the trivial solution $C_1 = 0$, we get $\sin aL = 0$. Thus $aL = n\pi$ and $n = 1, 2, 3, \ldots$. Therefore, the undamped natural frequencies and the corresponding mode shapes read

$$\omega_n = n^2 \pi^2 \sqrt{\frac{EI}{mAL^4}}$$
$$W(x) = C_n \sin \frac{n\pi x}{L} \tag{4.31}$$

where $n = 1, 2, 3, \ldots$ and C_n will be determined from the initial conditions.

Cantilever Beam. We consider a beam clamped at $x = 0$ and free at $x = L$. For the free end, the bending moment and shearing force are null, and, for the clamped end, the deflection and the rotation are null. Thus, the boundary conditions can be written as

$$W(0) = W'(0) = W''(L) = W'''(L) = 0 \tag{4.32}$$

Substituting the boundary conditions given by Eq. (4.32) for $x = 0$ into Eq. (4.28), we obtain

$$W(0) = C_2 + C_4 = 0 \qquad \text{and} \qquad W'(0) = C_1 + C_3 = 0 \qquad (4.33)$$

Using Eq. (4.33), we can write Eq. (4.28) as

$$W(x) = C_1 [\sin ax - \sinh ax] + C_2 [\cos ax - \cosh ax] \qquad (4.34)$$

Now using the boundary conditions for $x = L$, we obtain

$$2 + 2 \cos aL \cosh aL = 0 \qquad (4.35)$$

The solution of Eq. (4.35) gives

$$(aL)_1 = 1.875104 \qquad (aL)_2 = 4.69409 \qquad (aL)_3 = 7.85475$$
$$(aL)_n \approx \left(n - \tfrac{1}{2}\right)\pi \qquad \text{for } n \geq 4 \qquad (4.36)$$

and the undamped natural frequencies read

$$\omega_n = \zeta_n^4 \sqrt{\frac{EI}{mAL^4}} \qquad (4.37)$$

where

$$\zeta_1^2 = 1.875104 \qquad \zeta_2^2 = 4.69409 \qquad \zeta_3^2 = 7.85475$$
$$\zeta_n^2 \approx \left(n - \tfrac{1}{2}\right)\pi \qquad \text{for } n \geq 4 \qquad (4.38)$$

and the corresponding mode shapes read

$$W(x) = C_n \left[\left(\sin \zeta_n^2 x/L - \sinh \zeta_n^2 x/L\right) - g_n\left(\cos \zeta_n^2 x/L - \cosh \zeta_n^2 x/L\right)\right] \qquad (4.39)$$

where

$$g_n = \frac{\sin \zeta_n^2 + \sinh \zeta_n^2}{\cos \zeta_n^2 + \cosh \zeta_n^2} \qquad (4.40)$$

Both ends clamped.   For this condition, we have $W(x) = 0$ and $W'(x) = 0$ at $x = 0$ and $x = L$. Substituting these conditions into Eq. (4.28), we obtain

$$\begin{bmatrix} 0 & 1 & 0 & 1 \\ 1 & 0 & 1 & 0 \\ \sin aL & \cos aL & \sinh aL & \cosh aL \\ \cos aL & -\sin aL & \cosh aL & \sinh aL \end{bmatrix} \begin{Bmatrix} C_1 \\ C_2 \\ C_3 \\ C_4 \end{Bmatrix} = \begin{Bmatrix} 0 \\ 0 \\ 0 \\ 0 \end{Bmatrix} \qquad (4.41)$$

From the first two equations, we obtain

$$C_1 = -C_3 \qquad \text{and} \qquad C_2 = -C_4$$

Hence we can write the system of equations [Eq. (4.41)] as

$$\begin{bmatrix} (\sin aL - \sinh aL) & (\cos aL - \cosh aL) \\ (\cos aL - \cosh aL) & -(\sin aL + \sinh aL) \end{bmatrix} \begin{Bmatrix} C_1 \\ C_2 \end{Bmatrix} = \begin{Bmatrix} 0 \\ 0 \end{Bmatrix}$$

Thus the characteristic equation reads

$$1 - \cos aL \cosh aL = 0 \qquad (4.42)$$

The solution of Eq. (4.42) gives

$$(aL)_1 = 4.73004 \qquad (aL)_2 = 7.853204 \qquad (aL)_3 = 10.99560$$

$$(aL)_n \approx \left(n + \tfrac{1}{2}\right)\pi \qquad \text{for } n \geq 4 \qquad (4.43)$$

and the undamped natural frequencies read

$$\omega_n = \zeta_n^4 \sqrt{\frac{EI}{mAL^4}} \qquad (4.44)$$

where

$$\zeta_1^2 = 4.73004 \qquad \zeta_2^2 = 7.853204 \qquad \zeta_3^2 = 10.99560$$

$$\zeta_n^2 \approx \left(n + \tfrac{1}{2}\right)\pi \qquad \text{for } n \geq 4 \qquad (4.45)$$

and the corresponding mode shapes read

$$W(x) = C_n \left[\left(\sin \zeta_n^2 x/L - \sinh \zeta_n^2 x/L\right) - \eta_n \left(\cos \zeta_n^2 x/L - \cosh \zeta_n^2 x/L\right) \right] \qquad (4.46)$$

where

$$\eta_n = \frac{\sin \zeta_n^2 - \sinh \zeta_n^2}{\cos \zeta_n^2 - \cosh \zeta_n^2} \qquad (4.47)$$

4.2.2   Effect of the Elastic Support

The equation of motion considering the effect of an elastic support under no initial stress conditions for free vibrations reads

$$EI \frac{\partial^4 w}{\partial x^4} + kw + mA \frac{\partial^2 w}{\partial t^2} = 0 \qquad (4.48)$$

Assuming solutions in the form

$$w(x, t) = W(x)\cos(\omega t + \phi) \qquad (4.49)$$

we obtain

$$EI \frac{d^4 W}{dx^4} + kW - mA\omega^2 W = 0 \qquad (4.50)$$

or

$$\frac{d^4 W}{dx^4} - b^4 W = 0 \qquad (4.51)$$

where

$$b^4 = [mA\omega^2 - k]/EI \tag{4.52}$$

Comparing Eq. (4.51) with Eq. (4.27), we conclude that the modal forms will not be affected by the presence of the elastic support; only the frequencies will be modified and will suffer a constant shift. For example, for a beam simply supported at both ends, the undamped natural frequencies read

$$\omega^2 = \frac{n^4\pi^4 EI}{mAL^4} + \frac{k}{mA} \tag{4.53}$$

and the modal forms are the same as given by Eq. (4.31).

4.2.3 Initial Stress Effect

In this case, the equation of motion reads

$$EI\frac{\partial^4 w}{\partial x^4} + N_x\frac{\partial^2 w}{\partial x^2} + mA\frac{\partial^2 w}{\partial t^2} = 0 \tag{4.54}$$

Assuming solutions in the form

$$w(x, t) = W(x)\cos(\omega t + \phi) \tag{4.55}$$

we obtain

$$EI\frac{d^4 W}{dx^4} + N_x\frac{d^2 W}{dx^2} - mA\omega^2 W = 0 \tag{4.56}$$

and writing

$$W(x) = Ce^{sx} \tag{4.57}$$

we get

$$EIs^4 + N_xs^2 - mA\omega^2 = 0 \tag{4.58}$$

Thus,

$$s^4 + g^2s^2 - a^4 = 0 \tag{4.58a}$$

where $g^2 = N_x/EI$ and $a^4 = mA\omega^2/EI$. Hence

$$s^2 = -\frac{g^2}{2} \pm \sqrt{a^4 + \frac{g^4}{4}} \tag{4.59}$$

or $s_1^2 = -\delta^2$ and $s_2^2 = \varepsilon^2$, giving $s = \pm i\delta$ and $\pm\varepsilon$ where

$$\delta^2 = \left[a^4 + \frac{g^4}{4}\right]^{\frac{1}{2}} + \frac{g^2}{2}$$

$$\varepsilon^2 = \left[a^4 + \frac{g^4}{4}\right]^{\frac{1}{2}} - \frac{g^2}{2} \tag{4.60}$$

and the mode shapes can be written as

$$W(x) = C_1 \sin \delta x + C_2 \cos \delta x + C_3 \sinh \varepsilon x + C_4 \cosh \varepsilon x \qquad (4.61)$$

where C_1, C_2, C_3, and C_4 are constants to be determined from the boundary and initial conditions. We consider, as an example, the case when both beam ends are simply supported. The boundary conditions in this case are given by

$$W(0) = W''(0) = W(L) = W''(L) = 0 \qquad (4.62)$$

Substituting the boundary conditions of Eq. (4.62) into Eq. (4.61), we get

$$\begin{bmatrix} 0 & 1 & 0 & 1 \\ 0 & -\delta^2 & 0 & \varepsilon^2 \\ \sin \delta L & \cos \delta L & \sinh \varepsilon L & \cosh \varepsilon L \\ -\delta^2 \sin \delta L & -\delta^2 \cos \delta L & \varepsilon^2 \cosh \varepsilon L & \varepsilon^2 \sinh \varepsilon L \end{bmatrix} \begin{Bmatrix} C_1 \\ C_2 \\ C_3 \\ C_4 \end{Bmatrix} = \begin{Bmatrix} 0 \\ 0 \\ 0 \\ 0 \end{Bmatrix} \qquad (4.63)$$

The first equation of the system of equations [Eq. (4.63)] gives $C_2 = -C_4$. Substituting in the second equation, we obtain $(\delta^2 + \varepsilon^2)C_4 = 0$. But from Eq. (4.60), we conclude that $(\delta^2 + \varepsilon^2) \neq 0$; thus, $C_2 = C_4 = 0$. Using this result in the last two equations, we obtain

$$\begin{bmatrix} \sin \delta L & \sinh \varepsilon L \\ -\delta^2 \sin \delta L & \varepsilon^2 \sinh \varepsilon L \end{bmatrix} \begin{Bmatrix} C_1 \\ C_3 \end{Bmatrix} = \begin{Bmatrix} 0 \\ 0 \end{Bmatrix} \qquad (4.64)$$

Thus,

$$(\delta^2 + \varepsilon^2)[\sin \delta L \sinh \varepsilon L] = 0 \qquad (4.65)$$

Again, $(\delta^2 + \varepsilon^2) \neq 0$ and, because $\sinh \varepsilon L \neq 0$, we conclude that $\sin \delta L = 0$; thus, $\delta L = n\pi$ for $n = 1, 2, 3, \ldots$, and $C_3 = 0$. Therefore, the mode shapes can be written as

$$W(x) = C_n \sin \delta x = C_n \sin \frac{n\pi x}{L} \qquad n = 1, 2, 3, \ldots \qquad (4.66)$$

Using Eqs. (4.60) and (4.66), we get

$$\frac{n^2 \pi^2}{L^2} = \delta^2 = \left[a^4 + \frac{g^4}{4} \right]^{\frac{1}{2}} + \frac{g^2}{2} \qquad (4.67)$$

Thus,

$$a^4 = \left[\frac{n\pi}{L} \right]^4 + \left[\frac{n\pi g}{L} \right]^2 \qquad (4.68)$$

and using Eq. (4.58), the corresponding frequencies read

$$\omega_n^2 = \frac{EI}{mA} \left[\frac{n\pi}{L} \right]^4 \left(1 - \frac{L^2}{n^2 \pi^2} \frac{N_x}{EI} \right) \qquad (4.69)$$

From Eq. (4.69), we conclude that the effect of the initial stress N_x is to increase the natural frequencies for tension and reduce them for compression. Furthermore,

for an initial compressive prestress value, $N_x = EIn^2\pi^2/L^2$, the natural frequencies $\omega_n = 0$, thus defining the Euler buckling loads. The critical buckling load will be given for $n = 1$, or $N_{x\,cr} = EI\pi^2/L^2$. The same procedure detailed above will be applied for any other boundary conditions.

4.3 Flat Plates

4.3.1 Rectangular Flat Plates

In this section, the free vibration problem of thin rectangular flat plates is studied. Consider the structural configuration shown in Fig. 4.2. It consists of a rectangular flat plate subjected to an initial state of prestress loads N_{xx}, N_{yy}, and N_{xy}, positives as shown in Fig. 4.2 and resting on a continuous elastic support having a spring stiffness constant k (N/m^2).

We will consider small deformations and neglect the effects of transverse shear, rotary inertias, and in-plane inertias. In the analysis, only isotropic and homogeneous materials will be considered. Under such conditions, the strain energy of a small deformation functional can be written as

$$U = \frac{D}{2} \int_A \left[w_{,xx}^2 + w_{,yy}^2 + 2\nu w_{,xx} w_{,yy} + 2(1-\nu) w_{,xy}^2 \right] dA \qquad (4.70)$$

where w is the transverse displacement, ν is Poisson's ratio, $D = Eh^3/12(1-\nu^2)$ is the plate flexural rigidity, and h is the plate thickness, considered constant. The strain energy due to the initial state of stress reads

$$U_i = \frac{1}{2} \int_A \left[N_{xx} w_{,x}^2 + N_{yy} w_{,y}^2 + 2N_{xy} w_{,x} w_{,y} \right] dA \qquad (4.71)$$

where the initial prestresses are positive as shown in Fig. 4.2. The strain energy
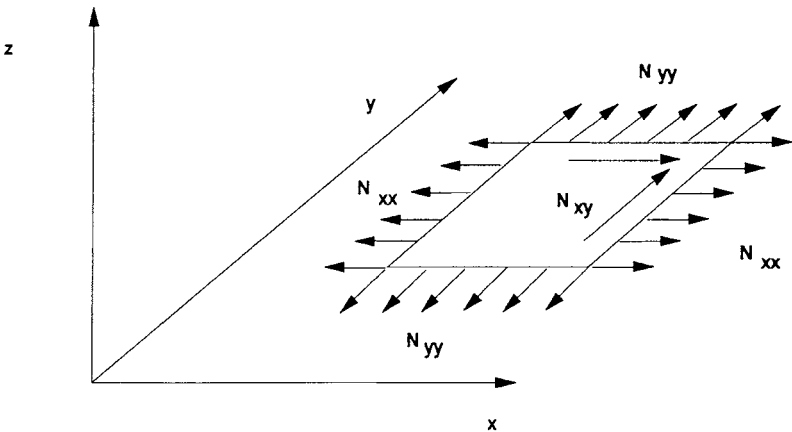
Fig. 4.2   Rectangular flat plate problem.

due to the elastic foundation reads

$$U_e = \frac{1}{2} \int_A k w^2 \, \mathrm{d}A \tag{4.72}$$

The kinetic energy reads

$$T = \frac{1}{2}\rho h \int_A w_{,t}^2 \, \mathrm{d}A \tag{4.73}$$

Hamilton's principle for the problem at hand reads

$$\int_{t_0}^{t_1} \delta(T - U - U_i - U_e) \, \mathrm{d}t = 0 \tag{4.74}$$

Performing the variational operation, the Euler–Lagrange equation governing the problem and corresponding boundary conditions are obtained. The Euler–Lagrange equation reads

$$D[w_{,xxxx} + w_{,yyyy} + 2w_{,xxyy}] + kw + N_{xx}w_{,xx} + N_{yy}w_{,yy}$$

$$+ 2N_{xy}w_{,xy} + \rho h w_{,tt} = 0 \tag{4.75}$$

On the boundaries, the natural boundary conditions are obtained as

$$D[w_{,xxx} + (2 - \nu)w_{,xyy}] = 0 = Q_x$$

$$D[w_{,xx} + \nu w_{,yy}] = 0 = M_x$$

$$\text{on } x = 0 \text{ and } x = a$$

and

$$D[w_{,yyy} + (2 - \nu)w_{,xxy}] = 0 = Q_y$$

$$D[w_{,yy} + \nu w_{,xx}] = 0 = M_y \tag{4.76}$$

$$\text{on } y = 0 \text{ and } y = b$$

The forced boundary conditions are given by

$$w = 0 \qquad w_{,x} = 0 \qquad \text{on } x = 0 \text{ and } x = a$$

and

$$w = 0 \qquad w_{,y} = 0 \qquad \text{on } y = 0 \text{ and } y = b \tag{4.77}$$

We notice that, on each edge of the plate, only two boundary conditions can be specified. In the sequel, some configurations will be analyzed in detail.

All edges simply supported and $N_{xy} = 0$.   In this case, the boundary conditions are given by

$$w = 0$$

$$M_x = D[w_{,xx} + \nu w_{,yy}] = 0$$

$$\text{on } x = 0 \text{ and } x = a$$

and

$$w = 0$$

$$M_y = D[w_{,yy} + vw_{,xx}] = 0 \tag{4.78}$$

$$\text{on } y = 0 \text{ and } y = b$$

Using the method of separation of variables, we can write solutions in the form

$$w(x, y, t) = W(x, y)e^{i\omega t} \tag{4.79}$$

Substituting Eq. (4.79) into Eq. (4.75) for $N_{xy} = 0$, we obtain

$$D[W_{,xxxx} + W_{,yyyy} + 2W_{,xxyy}] + kW + N_{xx}W_{,xx}$$

$$+ N_{yy}W_{,yy} - \rho h\omega^2 W = 0 \tag{4.80}$$

and we observe that solutions in the form

$$W(x, y) = \sum_{m,n=1}^{\infty} A_{m,n} \sin \frac{m\pi x}{a} \sin \frac{n\pi y}{b} \tag{4.81}$$

satisfy the boundary conditions [Eq. (4.78)]. Substituting these solutions into differential Eq. (4.80), we obtain

$$A_{m,n}\left\{ D\left[\left(\frac{m\pi}{a}\right)^4 + 2\left(\frac{m\pi}{a}\right)^2\left(\frac{n\pi}{b}\right)^2 + \left(\frac{n\pi}{b}\right)^4\right] \right.$$

$$\left. + N_x\left(\frac{m\pi}{a}\right)^2 + N_y\left(\frac{n\pi}{b}\right)^2 + k - \rho h\omega^2 \right\} = 0 \tag{4.82}$$

Eliminating the trivial solutions $A_{m,n} = 0$, the undamped natural frequencies of free vibration are obtained from Eq. (4.82) and read

$$\omega^2 = \frac{D}{\rho h}\left\{ \left[\left(\frac{m\pi}{a}\right)^2 + \left(\frac{n\pi}{b}\right)^2\right]^2 + \frac{N_x}{D}\left(\frac{m\pi}{a}\right)^2 + \frac{N_y}{D}\left(\frac{n\pi}{b}\right)^2 + \frac{k}{D} \right\} \tag{4.83}$$

and the mode shapes are given by Eq. (4.81). From these results, the following conclusions can be made:

1) The mode shapes, as can be observed from Eq. (4.81), are independent of k, N_x, and N_y.

2) The effect of the elastic support on the frequency spectrum is merely a constant shift for all the frequencies. This is an important result because, in many stability problems, the critical stability parameter is proportional to the difference between the square of two frequencies; therefore, it is anticipated that the elastic support will have no effect on the stability parameter for these problems.

3) In the absence of initial stress, i.e., $N_x = N_y = 0$, the fundamental mode is for $m = n = 1$.

4) For initial tension prestresses, i.e., when N_x and N_y are positive, the effect of prestress is an increase in the frequency value, and the fundamental mode is for $m = n = 1$.

5) For initial compression prestresses, i.e., when N_x and N_y are negative, the effect of the prestress is a decrease in the frequency value, and the fundamental mode is not necessary for $m = n = 1$ and depends on m, n, and a/b.

6) Buckling loads are obtained from Eq. (4.83), putting $\omega = 0$.

Rectangular plates with other boundary conditions. In the absence of initial shear prestress load and when two opposite edges are simply supported and the remaining two edges have any other boundary condition, analytical solutions can be obtained by writing for $w(x, y, t)$ expressions in the form

$$w(x, y, t) = W(x) \sin \frac{n\pi y}{b} e^{i\omega t} \tag{4.84}$$

where, in the expression given by Eq. (4.84), it has been assumed that the simply supported edges are on $y = 0$ and $y = b$. When Eq. (4.84) is used in Eq. (4.75), an ordinary differential equation in $W(x)$ of the fourth order is obtained. The solution of this equation will proceed in the same manner as was done in the previous item for the case of beams. Four arbitrary constants are obtained and are to be determined from the remaining boundary conditions in exactly the same manner as was done in the previous section.

For other boundary conditions, analytical solutions do not exist, and thus the problem is solved using numerical methods, i.e., Rayleigh–Ritz, Galerkin, finite difference, finite element methods, etc. As an example, we consider the case of no initial prestress and the absence of elastic support. For such cases, we can use the Rayleigh–Ritz method, writing solutions in the form

$$w(x, y, t) = X(x)Y(y)e^{i\omega t} \tag{4.85}$$

where $X(x)$ and $Y(y)$ are beam functions that satisfy the corresponding boundary conditions. Applying the Rayleigh–Ritz method, the frequency equation is obtained and can be written as

$$\omega^2 = \frac{\pi^2 D}{a^4 \rho h} \left\{ G_x^4 + G_y^4 \left(\frac{a}{b}\right)^4 + 2\left(\frac{a}{b}\right)^2 [\nu H_x H_y + (1 - \nu)J_x J_y] \right\} \tag{4.86}$$

where G, H, and J are functions of m and n and the boundary conditions. These functions have been tabulated and are given in Ref. 1.

4.3.2   Flat Plates with Other Geometry

Analytical solutions can be obtained for the case of circular plates simply supported on their edges and parallelogram plates with two opposite edges simply supported and any other condition on the remaining two edges. Such analytical solutions are treated in detail in Ref. 1. For other geometry and boundary conditions, numerical solutions are to be used. The most appropriate method for obtaining such solutions is the finite element method.

4.4 Shell Structures

4.4.1 Circular Cylindrical Shells

Strain energy of small deformation.   Consider the thin circular cylindrical shell of thickness h, radius R, and length L. The strain energy of small deformation can be written as

$$U = \frac{Eh}{2(1 - v^2)} \int_0^{2\pi} \int_0^{L/R} [U_{\text{DM}} + kU_{\text{MOD}}]dsd\theta \tag{4.87}$$

where U_{DM} is the integrand according to Donnell–Mushtari shell theory and is common in all the derived shell theories, U_{MOD} is a modification that differs according to the shell theory used, and k is a nondimensional thickness parameter defined as

$$k = h^2/12R^2 \tag{4.88}$$

and

$$s = x/R \tag{4.89}$$

The integrand according to the Donnell–Mushtari theory is given by[2,3]

$$U_{\text{DM}} = \left(\frac{\partial u}{\partial s} + \frac{\partial v}{\partial \theta} + w\right)^2 - 2(1 - v)\left[\frac{\partial u}{\partial s}w - \frac{1}{4}\left(\frac{\partial v}{\partial s} - \frac{\partial u}{\partial \theta}\right)^2\right]$$

$$+ k\left\{(\nabla^2)^2 - (1 - v)\left[\frac{\partial^2 w}{\partial s^2}\frac{\partial^2 w}{\partial \theta^2} - \left(\frac{\partial^2 w}{\partial s\partial\theta}\right)^2\right]\right\} \tag{4.90}$$

where $\nabla^2 = \partial^2/\partial s^2 + \partial^2/\partial\theta^2$. The modified integrand depends on the shell theory used. Some of these modifications are given below:

Goldenweiser–Novozhilov theory[4]   (see also Arnold–Warburton theory[5]):

$$U_{\text{MOD}} = -2\frac{\partial v}{\partial\theta}\nabla^2 w + \left(\frac{\partial v}{\partial\theta}\right)^2 - 2(1 - v)\left[-\frac{\partial v}{\partial\theta}\frac{\partial^2 w}{\partial s^2} + 2\frac{\partial v}{\partial s}\frac{\partial^2 w}{\partial s\partial\theta} - \left(\frac{\partial v}{\partial s}\right)^2\right] \tag{4.91}$$

Reissner–Nagdi–Berry theory[6,7]:

$$U_{\text{MOD}} = -2\frac{\partial v}{\partial\theta}\nabla^2 w + \left(\frac{\partial v}{\partial\theta}\right)^2 - 2(1 - v)\left[-\frac{\partial v}{\partial\theta}\frac{\partial^2 w}{\partial s^2} + \frac{\partial v}{\partial s}\frac{\partial^2 w}{\partial s\partial\theta} - \frac{1}{4}\left(\frac{\partial v}{\partial s}\right)^2\right] \tag{4.92}$$

Vlasov theory[8]:

$$U_{\text{MOD}} = (1 - v)\frac{\partial u}{\partial\theta}\frac{\partial^2 w}{\partial s\partial\theta} - 2\frac{\partial u}{\partial s}\frac{\partial^2 w}{\partial s^2} - 3(1 - v)\frac{\partial v}{\partial s}\frac{\partial^2 w}{\partial s\partial\theta}$$

$$- 2v\frac{\partial v}{\partial\theta}\frac{\partial^2 w}{\partial s^2} + w^2 + 2w\frac{\partial^2 w}{\partial\theta^2} \tag{4.93}$$

Other modified integrands are given in Ref. 2, some of which possess unsymmetric terms that have received much criticism in the literature, principally when used in dynamic problems. This leads to imaginary free vibration frequencies; thus, their use for the problem at hand is questionable.

Kinetic energy.   The kinetic energy, including in-plane inertias and neglecting rotary inertias, can be written as

$$T = \frac{1}{2} \int_0^{2\pi} \int_0^{L/R} \rho_m h \left[\left(\frac{\partial u}{\partial t} \right)^2 + \left(\frac{\partial v}{\partial t} \right)^2 + \left(\frac{\partial w}{\partial t} \right)^2 \right] R^2 \, ds \, d\theta \quad (4.94)$$

Strain energy caused by prestress.   We now consider the effect of initial prestress. In the formulation, only initial membrane direct stresses are considered, and thus initial in-plane shear, static bending, and transverse shear are not considered. Initial prestress in the case of circular cylindrical shells is caused by internal pressure p_m and an axial load p_x. Thus, we can write the initial prestress resultant loads as

$$N_{xx}^0 = \sigma_{xx} h = p_x / 2\pi R$$
$$N_{\theta\theta}^0 = \sigma_{\theta\theta} h = p_m R$$

$$(4.95)$$

The strain energy caused by prestress considered here thus reads[9,10]

$$U_i = \frac{1}{2} \int_0^L \int_0^{2\pi} \left[N_{xx}^0 \omega_{xx}^2 + N_{\theta\theta}^0 \omega_{\theta\theta}^2 + \left(N_{xx}^0 + N_{\theta\theta} \right) \omega_{zz}^2 \right] R \, d\theta \, dx \quad (4.96)$$

where the rotations are given by

$$\omega_{xx} = \frac{\partial w}{\partial x} = \frac{1}{R} \frac{\partial w}{\partial s}$$

$$\omega_{\theta\theta} = \frac{1}{R} \left(v - \frac{\partial w}{\partial \theta} \right)$$

$$\omega_{zz} = \frac{1}{2} \left(\frac{\partial u}{R \partial \theta} - \frac{\partial v}{\partial x} \right) = \frac{1}{2R} \left(\frac{\partial u}{\partial \theta} - \frac{\partial v}{\partial s} \right)$$

$$(4.97)$$

Substituting Eq. (4.97) into Eq. (4.96), we obtain

$$U_i = \frac{1}{2} \int_0^{L/R} \int_0^{2\pi} \left[N_{xx}^0 \left(\frac{\partial w}{\partial s} \right)^2 + N_{\theta\theta}^0 \left(v - \frac{\partial w}{\partial \theta} \right)^2 \right.$$

$$\left. + \left(N_{xx}^0 + N_{\theta\theta}^0 \right) \left(\frac{1}{2} \frac{\partial u}{\partial \theta} - \frac{1}{2} \frac{\partial v}{\partial s} \right)^2 \right] d\theta \, ds \quad (4.98)$$

Hamilton's principle. Hamilton's principle for the problem at hand can be written as

$$\int_{t_1}^{t_2} \delta(T - U - U_i)\,dt = 0 \tag{4.99}$$

where the functional T, U, and U_i are given by Eqs. (4.94), (4.87), and (4.98), respectively. Through application of Hamilton's principle, the following Euler–Lagrange equation is obtained:

$$[[L_0] + k[L_1]]\{q\} = \{0\} \tag{4.100}$$

where $[L_0]$ is the differential operator according to Donnell–Mushtari theory, $[L_1]$ is the differential operator incorporated according to the modified shell theory used, and $\{q\} = [u \; v \; w]^T$. The Donnell–Mushtari operator reads

$$L_{0_{11}} = \frac{\partial^2}{\partial s^2} + \frac{1-\nu}{2}\frac{\partial^2}{\partial \theta^2} - \rho\frac{1-\nu^2}{E}R^2\frac{\partial^2}{\partial t^2} - \frac{1-\nu^2}{4Eh}\left(N_{xx}^0 + N_{\theta\theta}^0\right)\frac{\partial^2}{\partial \theta^2}$$

$$L_{0_{12}} = \frac{1+\nu}{2}\frac{\partial^2}{\partial s\partial \theta} - \frac{1-\nu^2}{4Eh}\left(N_{xx}^0 + N_{\theta\theta}^0\right)\frac{\partial^2}{\partial \theta\partial s}$$

$$L_{0_{13}} = \nu\frac{\partial}{\partial s}$$

$$L_{0_{22}} = \frac{(1-\nu)}{2}\frac{\partial^2}{\partial s^2} + \frac{\partial^2}{\partial \theta^2} - \rho\frac{1-\nu^2}{E}R^2\frac{\partial^2}{\partial t^2}$$

$$\qquad - \frac{1-\nu^2}{4Eh}\left[N_{\theta\theta}^0 - \frac{1}{4}\left(N_{xx}^0 + N_{\theta\theta}^0\right)\frac{\partial^2}{\partial s^2}\right] \tag{4.101}$$

$$L_{0_{23}} = \frac{\partial}{\partial \theta} - \frac{1-\nu^2}{Eh}N_{\theta\theta}^0\frac{\partial}{\partial \theta}$$

$$L_{0_{33}} = 1 + k\nabla^4 + \rho\frac{1-\nu^2}{E}R^2\frac{\partial^2}{\partial t^2} + \frac{(1-\nu^2)}{Eh}\left[-N_{xx}^0\frac{\partial^2}{\partial s^2} - N_{\theta\theta}^0\frac{\partial^2}{\partial \theta^2}\right]$$

$$L_{0_{ij}} = L_{0_{ji}} \qquad i, j = 1, 2, 3$$

The modified operator $[L_1]$ according to the various modified shell theories given before is as follows.

Goldenweiser–Novozhilov theory[4]   (see also Arnold–Warburton theory[5]):

$$[L_1] = \begin{bmatrix} 0 & 0 & 0 \\[2mm] 0 & 2(1-\nu)\dfrac{\partial^2}{\partial s^2} + \dfrac{\partial^2}{\partial \theta^2} & -(2-\nu)\dfrac{\partial^3}{\partial s^2\partial \theta} - \dfrac{\partial^3}{\partial \theta^3} \\[3mm] 0 & -(2-\nu)\dfrac{\partial^3}{\partial s^2\partial \theta} - \dfrac{\partial^3}{\partial \theta^3} & 0 \end{bmatrix} \tag{4.102}$$

Reissner–Nagdi–Berry theory[6,7]:

$$[L_1] = \begin{bmatrix} 0 & 0 & 0 \\ 0 & \dfrac{(1-\nu)}{2}\dfrac{\partial^2}{\partial s^2} + \dfrac{\partial^2}{\partial \theta^2} & -\dfrac{\partial^3}{\partial s^2 \partial \theta} - \dfrac{\partial^3}{\partial \theta^3} \\ 0 & -\dfrac{\partial^3}{\partial s^2 \partial \theta} - \dfrac{\partial^3}{\partial \theta^3} & 0 \end{bmatrix} \tag{4.103}$$

Vlasov theory[8]:

$$[L_1] = \begin{bmatrix} 0 & 0 & -\dfrac{\partial^3}{\partial s^3} + \dfrac{(1-\nu)}{2}\dfrac{\partial^3}{\partial s \partial \theta^2} \\ 0 & 0 & -\dfrac{(3-\nu)}{2}\dfrac{\partial^3}{\partial s^2 \partial \theta} \\ -\dfrac{\partial^3}{\partial s^3} + \dfrac{(1-\nu)}{2}\dfrac{\partial^3}{\partial s \partial \theta^2} & -\dfrac{(3-\nu)}{2}\dfrac{\partial^3}{\partial s^2 \partial \theta} & (1+2\nu)\dfrac{\partial^2}{\partial \theta^2} \end{bmatrix}$$
$$\tag{4.104}$$

Furthermore, as stated before, some of other shell theories present terms that are unsymmetrical and thus are not adequate for the dynamic problems treated here because they lead to imaginary eigenvalues. For the static problems, Koiter[11] showed that all these theories are equivalents once the Kirchoff hypothesis and thin shell assumption have been made. We now consider a circular cylindrical shell freely supported on a diaphragm on both ends. The boundary conditions read

$$w = M_x = N_x = v = 0 \qquad \text{at } x = 0 \text{ and } x = L \tag{4.105}$$

Solutions that satisfy these boundary conditions can be written as

$$u = U_0 e^{i\omega t} \cos n\theta \cos \frac{m\pi x}{L}$$

$$v = U_0 e^{i\omega t} \sin n\theta \sin \frac{m\pi x}{L} \tag{4.106}$$

$$w = W_0 e^{i\omega t} \cos n\theta \sin \frac{m\pi x}{L}$$

Substituting Eq. (4.106) into the equations of motion [Eqs. (4.100)] for the case of no initial stresses, the following frequency equation is obtained

$$\Omega^6 - [K_2 + k\Delta K_2]\Omega^4 + [K_1 + k\Delta K_1]\Omega^2 - [K_0 + k\Delta K_0] = 0 \tag{4.107}$$

where $\Omega^2 = \rho(1 - \nu^2)R^2\omega^2/E$ and K_2, K_1, and K_0 are the terms according to Donnell–Mushtari theory and read

$$K_2 = 1 + \tfrac{1}{2}(3 - \nu)(n^2 + \lambda^2) + k(n^2 + \lambda^2)^2$$

$$K_1 = \tfrac{1}{2}(1 - \nu)\left[(3 + 2\nu)\lambda^2 + n^2 + (n^2 + \lambda^2)^2 + \frac{3 - \nu}{1 - \nu}k(n^2 + \lambda^2)^3\right] \tag{4.108}$$

$$K_0 = \tfrac{1}{2}(1 - \nu)[(1 - \nu^2)\lambda^4 + k(n^2 + \lambda^2)^4]$$

where $\lambda = m\pi R/L$ and $k = h^2/12R^2$. The ΔK_i elements are the terms corresponding to the modified shell theory used, and these, according to the various modified shell theories given before, are as follows.

Goldenweiser–Novozhilov theory[4]   (see also Arnold–Warburton theory[5]):

$$\Delta K_2 = 2(1 - \nu^2)\lambda^2 + n^2$$

$$\Delta K_1 = 2(1 - \nu)\lambda^2 + n^2 + 2(1 - \nu)\lambda^4 - (2 - \nu)\lambda^2 n^2 - \tfrac{1}{2}(3 + \nu)n^4$$

(4.109)

$$\Delta K_0 = \tfrac{1}{2}(1 - \nu)[4(1 - \nu^2)\lambda^4 + 4\lambda^2 n^2 + n^4 - 2(2 - \nu)$$

$$\times (2 + \nu)\lambda^4 n^2 - 8\lambda^2 n^4 - 2n^6]$$

Reissner–Nagdi–Berry theory[6,7]:

$$\Delta K_2 = \tfrac{1}{2}2(1 - \nu)\lambda^2 + n^2$$

$$\Delta K_1 = \tfrac{1}{2}(1 - \nu)\lambda^2 + n^2 + \tfrac{1}{2}(1 - \nu)\lambda^4 - \tfrac{1}{4}(1 + \nu)(3 - \nu)\lambda^2 n^2 - \tfrac{1}{2}(3 + \nu)n^4$$

$$\Delta K_0 = \tfrac{1}{2}(1 - \nu)\left[\tfrac{1}{2}(5 + 3\nu)\lambda^2 n^2 + n^4 - 2(2 + \nu)\lambda^4 n^2 - 2(3 + \nu)\lambda^2 n^4 - 2n^6\right]$$

(4.110)

Vlasov theory[8]:

$$\Delta K_2 = 1 - 2n^2$$

$$\Delta K_1 = \tfrac{1}{2}(3 - \nu)(\lambda^2 + n^2) - 2\nu\lambda^4 - (6 - 3\nu + \nu^2)\lambda^2 n^2 - (3 - \nu)n^4 \quad (4.111)$$

$$\Delta K_0 = \tfrac{1}{2}(1 - \nu)[(n^2 + \lambda^2)^2 + 2\nu\lambda^6 + 6\lambda^4 n^2 - 2(4 - \nu)\lambda^2 n^4 - 2n^6]$$

For other end conditions, numerical methods must be used for solving the problem, e.g., Rayleigh–Ritz method, finite difference methods, and finite element methods.

4.4.2   Conical Shells

Thin conical shells have been used extensively as adapter sections in rockets, supersonic aircrafts, and re-entry vehicles. Thus, a knowledge of their dynamic behavior is required. In this section, the problem formulation presented is based on Novozhilov's theory of thin shells,[4] specialized here for the case of a frustum of cone. The effect of internal pressure and axial membrane initial stresses are included; rotary inertia effects are neglected.

Strain energy of small deformation.   Consider the thin conical frustum shell shown in Fig. 4.3. The strain–displacement relationships, according to Novozhilov's theory of thin shells,[4] reduce for the case at hand to

$$\{\varepsilon\} = [A]\{q\} \qquad (4.112)$$
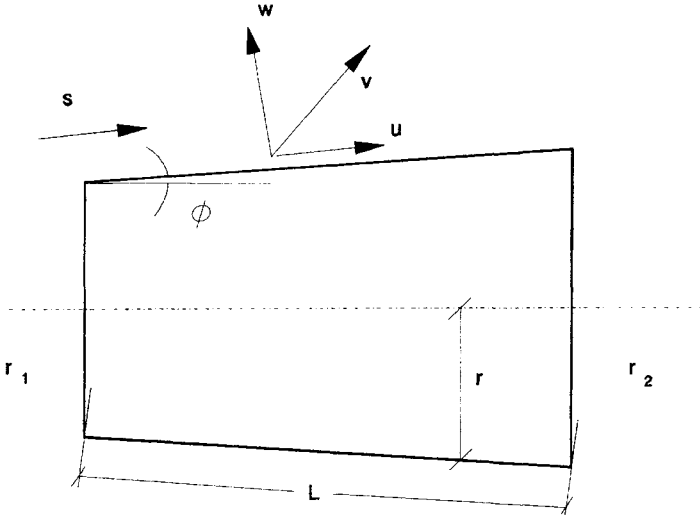
Fig. 4.3   Conical shell geometry.

where $\{\varepsilon\} = [\varepsilon_s\ \varepsilon_\theta\ \varepsilon_{s\theta}\ \chi_s\ \chi_\theta\ \chi_{s\theta}]^{\mathrm{T}}$ and $\{q\} = [u\ v\ w]^{\mathrm{T}}$. The differential operator $[A]$ reads

$$[A] = \begin{bmatrix} \dfrac{\partial}{\partial s} & 0 & 0 \\[2ex] \dfrac{\sin\phi}{r} & \dfrac{1}{r}\dfrac{\partial}{\partial\theta} & \dfrac{1}{r}\cos\phi \\[2ex] \dfrac{1}{r}\dfrac{\partial}{\partial\theta} & \dfrac{-\sin\phi}{r}+\dfrac{\partial}{\partial s} & 0 \\[2ex] 0 & 0 & \dfrac{-\partial^2}{\partial s^2} \\[2ex] 0 & \dfrac{\cos\phi}{r^2}\dfrac{\partial}{\partial\theta} & \dfrac{-\sin\phi}{r}\dfrac{\partial}{\partial s}-\dfrac{1}{r^2}\dfrac{\partial^2}{\partial\theta^2} \\[2ex] 0 & \dfrac{-2\sin\phi\cos\phi}{r^2}+\dfrac{2\cos\phi}{r}\dfrac{\partial}{\partial s} & \dfrac{2\sin\phi}{r^2}\dfrac{\partial}{\partial\theta}-\dfrac{2}{r}\dfrac{\partial^2}{\partial s\partial\theta} \end{bmatrix}$$

$$(4.113)$$

The stress–strain relations are given by

$$\{\sigma\} = [D]\{\varepsilon\}$$

where $\{\sigma\} = [n_s\ n_\theta\ n_{s\theta}\ m_s\ m_\theta\ m_{s\theta}]^{\mathrm{T}}$ and

$$[D] = \frac{Eh}{(1-v^2)}\begin{bmatrix} [d] & [0] \\ [0] & \alpha[d] \end{bmatrix}$$

$$(4.114)$$

and the $[d]$ matrix reads

$$[d] = \begin{bmatrix} 1 & v & 0 \\ v & 1 & 0 \\ 0 & 0 & (1-v)/2 \end{bmatrix} \qquad \alpha = h^2/12 \qquad (4.115)$$

where E is Young's modulus, v is Poisson's ratio, and h is the shell thickness. The strain energy of small deformation reads

$$U = \frac{1}{2} \int_0^{2\pi} \int_{s_1}^{s_2} \{\sigma\}^T \{\varepsilon\} r \, d\theta \, ds = U(u, v, w) \qquad (4.116)$$

Kinetic energy.   Neglecting the rotary inertia, the kinetic energy reads

$$T = \frac{1}{2} \int_0^{2\pi} \int_{s_1}^{s_2} \rho h \left[\left(\frac{\partial u}{\partial t}\right)^2 + \left(\frac{\partial v}{\partial t}\right)^2 + \left(\frac{\partial w}{\partial t}\right)^2 \right] r \, d\theta \, ds \qquad (4.117)$$

Strain energy caused by prestress.   In the formulation of the strain energy due to prestress, only direct membrane stresses will be considered in the analysis presented in this section. Consider the conical shell shown in Fig. 4.3, subjected to a prestress state of uniform axial load P_x, positive for traction, and a uniform internal pressure p_m. The prestress loads per unit length in the axial and meridional directions can be written as

$$N_{\theta\theta}^0 = \sigma_{\theta\theta} h = p_m s \tan \phi$$

$$N_{ss}^0 = \sigma_{ss} h = \frac{P_x}{2\pi r \sin\phi \cos\phi} + \frac{p_m}{2} s \tan\phi \qquad (4.118)$$

The strain energy caused by prestress can be written as

$$U_i = \frac{1}{2} \int_{s_1}^{s_2} \int_0^{2\pi} \{\eta\}^T [N]\{\eta\} r \, d\theta \, ds \qquad (4.119)$$

where $\{\eta\}$ is the rotation vector and reads

$$\{\eta\} = [\eta_s \eta_\theta \eta_n]^T = \begin{bmatrix} & & \dfrac{\partial}{\partial s} \\ & \dfrac{\cos\phi}{r} & -\dfrac{\partial}{r\partial\theta} \\ \dfrac{1}{2r}\dfrac{\partial}{\partial\theta} & -\dfrac{\partial}{2\partial s} + \dfrac{\sin\phi}{2}r & \end{bmatrix} \begin{Bmatrix} u \\ v \\ w \end{Bmatrix} \qquad (4.120)$$

and $[N]$ is the prestress load matrix and is given by

$$[N] = \begin{bmatrix} N_{ss}^0 & & \\ & N_{\theta\theta}^0 & \\ & & (N_{ss}^0 + N_{\theta\theta}^0) \end{bmatrix} \qquad (4.121)$$

Hamilton's principle.   Hamilton's principle for the problem at hand can be written as

$$\int_{t_1}^{t_2} \delta(T - U - U_i)\, dt = 0 \tag{4.122}$$

where the functional T, U, and U_i are given by Eqs. (4.117), (4.116), and (4.119), respectively. At this step, the Rayleigh–Ritz method or the finite element method can be invoked to obtain numerical solutions for the problem at hand. This will lead to a set of equations of motion with u, v, and w as the field variables with the corresponding boundary conditions.

Simplifications of the problem.   If the following simplifications were made: 1) the in-plane inertias are neglected, 2) the analysis is limited to the Donnell–Mushtari theory, 3) terms in u and v in the initial stress functional are neglected, and 4) an Airy stress function F defined as

$$N_{ss} = \frac{1}{s^2 \sin^2 \phi} \frac{\partial^2 F}{\partial \theta^2} + \frac{1}{s} \frac{\partial F}{\partial s}$$

$$N_{\theta\theta} = \frac{\partial^2 F}{\partial s^2} \tag{4.123}$$

$$N_{\theta s} = \frac{1}{s \sin \phi} \left[\frac{1}{s} \frac{\partial F}{\partial \theta} - \frac{\partial^2 F}{\partial \theta \partial s} \right]$$

is introduced, it can be shown that the differential equations governing the problem are reduced to

$$D\nabla^4 w + \nabla_R^2 F = -\rho h \frac{\partial^2 w}{\partial t^2} + N_{ss}^0 \frac{\partial^2 w}{\partial s^2} + N_{\theta\theta} \left[\frac{1}{s^2 \sin^2 \phi} \frac{\partial^2 w}{\partial \theta^2} + \frac{1}{s} \frac{\partial w}{\partial s} \right]$$

$$\nabla^4 F - Eh\nabla_R^2 w = 0 \tag{4.124}$$

where $D = Eh^3/12(1 - \nu^2)$ and

$$\nabla^2 = \frac{\partial^2}{\partial s^2} + \frac{1}{s} \frac{\partial w}{\partial s} + \frac{1}{s^2 \sin^2 \phi} \frac{\partial^2}{\partial \theta^2}$$

$$\nabla_R^2 = \frac{1}{s \tan \phi} \frac{\partial^2}{\partial s^2} \tag{4.125}$$

We note that, in Eqs. (4.124), the first equation is an equation of motion in w, while the second equation is a compatibility equation. Furthermore, the field variables have been reduced to two functions, namely w and F, which facilitates considerably the solution of the problem. The solution of Eqs. (4.124) can be made using the Galerkin method to obtain numerical results for the problem at hand. Such solutions have been extensively treated in the literature.[2]

4.5   Response to Initial Conditions

As an example for the determination of the structural response to initial conditions, we will consider the case of longitudinal vibration of a cantilever beam subjected to the application of an initial displacement v_0 at the free end at time $t = t_0$. The process of solution as described below can then be extended in the same manner for the determination of the structural response due to the application of initial conditions for any other special case.

From the results obtained in Section 4.2, we can write the solution of the problem as

$$v(x, t) = \sum_{n=1,2,\dots}^{\infty} C_n \sin \frac{(2n - 1)\pi x}{2L} \cos(\omega_n t - \phi_n) \qquad n = 1, 2, 3, \dots \quad (4.126)$$

The initial conditions for the problem at hand read

$$v(x, 0) = v_0 \frac{x}{L} \qquad \text{and} \qquad \frac{\partial v}{\partial t}(x, 0) = 0 \qquad (4.127)$$

Applying the second initial condition of Eq. (4.127) into Eq. (4.126), we get

$$\sum_n - C_n \omega_n \sin(2n - 1)\frac{\pi x}{2L} \sin(-\phi_n) = 0 \qquad (4.128)$$

We therefore conclude from Eq. (4.128) that $\sin \phi_n = 0$, thus $\phi_n = 0$. This was expected since no structural damping was considered in the formulation. Applying now the first initial condition of Eq. (4.127) into Eq. (4.126), we get

$$v_0 \frac{x}{L} = \sum_n C_n \sin(2n - 1)\frac{\pi x}{2L} \qquad (4.129)$$

To determine the coefficients C_n, we multiply both sides of Eq. (4.129) by $\sin[(2i - 1)\pi x/2L]$ and integrate from 0 to L to obtain

$$\int_0^L v_0 \frac{x}{L} \sin(2i - 1)\frac{\pi x}{2L} \, dx = \frac{L}{2} C_i \qquad (4.130)$$

because

$$\int_0^L \sin(2i - 1)\frac{\pi x}{2L} \sin(2n - 1)\frac{\pi x}{2L} \, dx = 0 \qquad \text{for } i \neq n$$

$$= \frac{L}{2} \qquad \text{for } i = n \qquad (4.131)$$

Integrating the left-hand side of Eq. (4.130), we obtain

$$\frac{L}{2} C_i = \frac{4 v_0 L (-1)^{i+1}}{[(2i - 1)\pi]^2} \qquad (4.132)$$

Now using Eqs. (4.126) and (4.132), we get

$$v(x, t) = \frac{8v_0}{\pi^2} \sum_n C_n \frac{(-1)^{n+1}}{(2n-1)^2} \sin\frac{(2n-1)\pi x}{2L} \cos(\omega_n t) \qquad n = 1, 2, 3, \ldots \tag{4.133}$$

where ω_n is given by Eq. (4.23) and reads

$$\omega_n = \frac{(2n-1)\pi}{2\alpha L} \qquad \alpha = \sqrt{\frac{m}{E}} \qquad n = 1, 2, 3, \ldots \tag{4.134}$$

The procedure described above can be applied in the same manner to obtain the structural response due to initial conditions for all the cases treated in the present chapter.

4.6 Response to External Excitations

In this section, the modal transformation is used to obtain the structural response due to external excitations. As an example, we will treat the same simple problem of the cantilever rod considered in the previous section. The procedure can be generalized and applied to all cases treated in the present chapter. The equation of motion for the problem at hand can be written as

$$\frac{\partial^2 u}{\partial x^2} + \frac{m}{E}\frac{\partial^2 u}{\partial t^2} = \frac{f(t, x)}{EA} \tag{4.135}$$

Without loss of the generality, we can write Eq. (4.135) as

$$\frac{\partial^2 u}{\partial x^2} + \frac{m}{E}\frac{\partial^2 u}{\partial t^2} = p(x)F(t) \tag{4.136}$$

Now, make the modal transformation

$$u(x, t) = \sum_n \phi_n(x)q_n(t) \tag{4.137}$$

where ϕ_n are the modal functions and q_n are the modal amplitudes. For the case at hand, the modal functions read

$$\phi_n(x) = \sin\frac{(2n-1)\pi x}{2L} \qquad n = 1, 2, 3, \ldots \tag{4.138}$$

Substituting Eq. (4.137) into Eq. (4.136), we obtain

$$\sum_n -\frac{(2n-1)^2\pi^2}{4L^2} \sin\frac{(2n-1)\pi x}{2L} q_n(t)$$

$$+ \frac{m}{E} \sum_n \sin\frac{(2n-1)\pi x}{2L} q_n''(t) = p(x)F(t) \tag{4.139}$$

Multiplying both sides of Eq. (4.139) by $\sin(2i-1)\pi x/2L$ and integrating from 0 to L, we get

$$-\frac{(2n-1)^2\pi^2}{8L}q_n(t) + \frac{mL}{2E}q_n''(t) = F(t)\int_0^L \sin\frac{(2n-1)\pi x}{2L}p(x)\,\mathrm{d}x \tag{4.140}$$

We now notice that the equations for $q_n(t)$ are uncoupled due to the orthogonality property of the natural modes. Given the function $p(x)$, the integral in Eq. (4.140) can be evaluated analytically or numerically. The solution of Eq. (4.140) will be obtained using Duhamel's method for a single degree of freedom. Once the solutions $q_n(t)$ have been obtained, these will be used in Eq. (4.137) to determine the displacement functions $u(x, t)$. For initial conditions different from the null conditions, the solution of the present section should be superposed with that of the preceding section to obtain the complete solution of the problem. The method of solution presented in this section can be applied to all the problems of structural response due to external applied loads of elastic continuum bodies presented in this chapter.

References

[1] Leissa, A. W., *Vibration of Plates*, NASA SP-160, 1969.

[2] Leissa, A. W., *Vibration of Shells*, NASA SP-228, 1973.

[3] Donnell, L. H., "A Discussion of Thin Shell Theory," *Proceedings of the 5th International Congress Applied Mechanics*, 1938.

[4] Novozhilov, V. V., *The Theory of Thin Elastic Shells*, Noordhoff International Leyden, The Netherlands, 1964.

[5] Arnold, R. N., and Warburton, G. B., "The Flexural Vibrations of Thin Cylinders," *Journal of the Engineering Institution of Mechanical Engineers*, Proceedings Vol. 167A, 1953, pp. 62–80.

[6] Nagdi, P. M., "A Survey of Recent Progress in the Theory of Elastic Shells," *Applied Mechanics Reviews*, Vol. 9, No. 9, 1956, pp. 365–368.

[7] Reissner, E., "A New Derivation of the Equations of the Deformation of Elastic Shells," *American Journal of Mathematics*, Vol. 63, No. 1, 1941, pp. 177–184.

[8] Vlasov, V. Z., "Basic Differential Equations in the General Theory of Elastic Shells," NASA TM-1241, 1951.

[9] McNeal, R. H., "Nastran Theoretical Manual," NASA SP-221, 1972.

[10] Bismarck-Nasr, M. N., "Finite Element Method Applied to the Supersonic Flutter of Circular Cylindrical Shells," *Internal Journal for Numerical Methods in Engineering*, Vol. 10, No. 2, 1976, pp. 423–435.

[11] Koiter, W. T., "A Consistent First Approximation in the General Theory of Thin Elastic Shells," *Proceedings Symposium on the Theory of Thin Elastic Shells*, Delft, The Netherlands, 1959, North-Holland, Amsterdam, 1960.

Problems

4.1 Consider the axial free vibrations of a uniform cantilever rod with a concentrated mass at the free end. Obtain the characteristic equation and the corresponding eigenvalues and eigenvectors. Discuss and comment on the effect of the tip mass.

4.2 Structural beams are neither clamped nor simply supported; actually, they can be considered as partially fixed. Consider a simply supported beam having a discrete rotational spring with a stiffness rotational constant $k_\theta = \beta(EI/L)$ at both ends. Obtain the equation of motion, the characteristic equation, and the

corresponding eigenvalues and eigenvectors. Discuss the effect of β, where $0 \leq \beta \leq \infty$ is the parameter that controls the rotational restraint.

4.3   Determine the permanent solution of a uniform cantilever beam having an external excitation harmonic force $P \sin \omega t$ at its free end.

4.4   A square plate simply supported at all edges is subjected to a sudden force P, applied at a time $t = 0$ at its central point. Find the maximum displacement of the plate.

4.5   A square plate is simply supported on two opposite edges and is clamped at the other two edges. Find an exact expression for the undamped free vibration natural frequencies and the corresponding mode shapes.

4.6   Obtain the undamped free vibration natural frequencies and the corresponding mode shapes of a circular plate simply supported at the outer boundary.

4.7   Obtain the first three undamped natural frequencies of a circular cylindrical shell freely supported at both ends. Consider a radius $R = 1$ m, a length $L = 4$ m, a thickness $h = 8$ mm, and steel material.

5
Nonlinear Systems

5.1 Introduction

The progress achieved in the past decades in the applied mechanics field is attributed to the representation of complex physical problems by simple mathematical equations. In many applications, these equations are nonlinear. In spite of this fact, simplifications consistent with the physical situation permit, in most cases, a linearization process that simplifies the mathematical solution of the problem while conserving the precision of the physical results. However, in few cases, the linear solutions are not sufficient to describe adequately the problem at hand because new physical phenomena are introduced and can be explained only if nonlinearity is considered.

This chapter begins with an enumeration of simple examples of nonlinear systems in structural dynamics. Physical properties of nonlinear systems are then introduced. The available exact solutions of nonlinear systems are then given, and approximate solutions are discussed in detail.

5.2 Simple Examples of Nonlinear Systems

5.2.1 Simple Pendulum in Free Vibrations

Consider the simple pendulum in free vibrations shown in Fig. 5.1. The equation of motion of the pendulum can be written as

$$mL^2\theta'' + mgL \sin\theta = 0 \tag{5.1}$$

Equation (5.1) is nonlinear due to the presence of the term $\sin\theta$. For small oscillations about the position of equilibrium, we can make the approximation $\sin\theta \approx \theta$, and we obtain a linearized equation in the form

$$mL^2\theta'' + mgL\,\theta = 0 \tag{5.2}$$

with its well-known linear solution. When the values of θ are not small, we can write $\sin\theta$ in its series expansion, and Eq. (5.1) can be written as

$$mL^2\theta'' + mgL\,\theta - mgL\frac{\theta^3}{3!} + mgL\frac{\theta^5}{5!} - \cdots = 0 \tag{5.3}$$

The solution of Eq. (5.3) will be given in the next sections.

5.2.2 Systems with Nonlinear Spring Characteristics

For a linear system, the force in the spring reads

$$F = kx \tag{5.4}$$
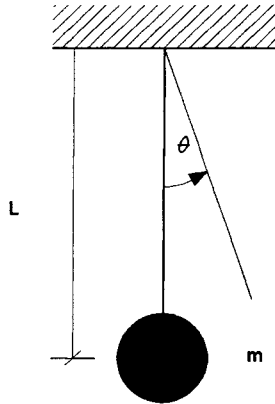
Fig. 5.1   Simple pendulum in free vibrations.

In many situations, the force–displacement relationship of the spring deviates from linearity, and we can have a soft or a hard spring as shown in Fig. 5.2. We can write the force–displacement relationship for the hard and the soft spring as

$$F_1 = k_0 x + k_1 x^3 + O(x^5)$$

$$F_2 = k_0 x - k_1 x^3 + O(x^5)$$

(5.5)

Notice that the stiffness terms in Eq. (5.5) are odd functions, i.e.,

$$F(x) = -F(-x)$$

(5.6)
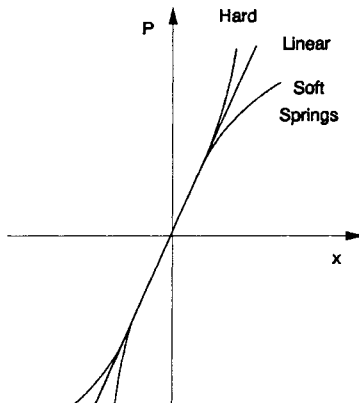
Fig. 5.2   Linear and nonlinear spring characteristics.

5.2.3 Nonlinear Viscous Damping

The damping force for a linear system reads

$$F_s = cx' \tag{5.7}$$

In many practical applications, the damping forces are more adequately represented by forces that are proportional to the velocity squared and in a direction opposite to the motion. Mathematically, this model can be written as

$$F_s = c\,|x'|\,x' \tag{5.8}$$

and thus represents systems with nonlinear damping effects.

5.3 Physical Properties of Nonlinear Systems

5.3.1 Undamped Free Vibrations

Physical considerations reveal that, for a mechanical system with nonlinear stiffness in free vibrations, the period (and thus the frequency) of the response will be a function of the amplitude of vibration. This is expected mathematically since $k = k(x)$ and therefore $T = T(x)$. It is to be emphasized that the natural frequency is a constant and is a property of the mechanical system, despite whether the system is linear. The frequency of response in free vibration of a linear system is constant and is equal to the natural frequency of the system, while a nonlinear system in free vibration responds with a frequency that is a function of the amplitude of vibration. As an example (the proof will be given in the next sections), for the dependence of the period of free vibration on the amplitude of the response, it can be shown that the period of the simple pendulum of Fig. 5.1 is given by

$$T = T_0 \left[1 + \frac{1}{4}\left(\sin\frac{\theta}{2}\right)^2 + \frac{9}{64}\left(\sin\frac{\theta}{2}\right)^4 + \frac{25}{256}\left(\sin\frac{\theta}{2}\right)^6 + \cdots \right] \tag{5.9}$$

where T_0 is the period of the linear system. A plot of T/T_0 vs θ is shown in Fig. 5.3.

The curves plotted in Fig. 5.3 clearly show that the linear solution gives an error of the order of 1% compared to the nonlinear solution up to values of $\theta = 30$ deg and the rapid convergence of the nonlinear solution taking few terms in the series expansion.

5.3.2 Damped Free Vibrations

Consider a nonlinear damped system having a hard spring nonlinearity characteristic in free vibrations. The system equation of motion can be written as

$$mx'' + cx' + k_0 x + k_1 x^3 = 0 \tag{5.10}$$

With initial conditions different from zero and an initial displacement value in the nonlinear regime, physical considerations and Eq. (5.10) reveal that the response will appear as the curve sketched in Fig. 5.4. We notice that, for nonlinear amplitude values, we will have smaller periods of response (thus higher frequencies)
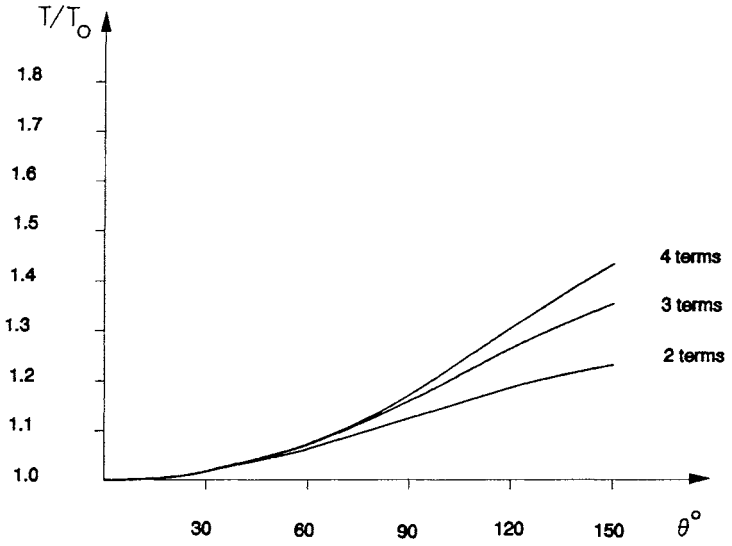
Fig. 5.3   Period of free vibrations of a simple pendulum.
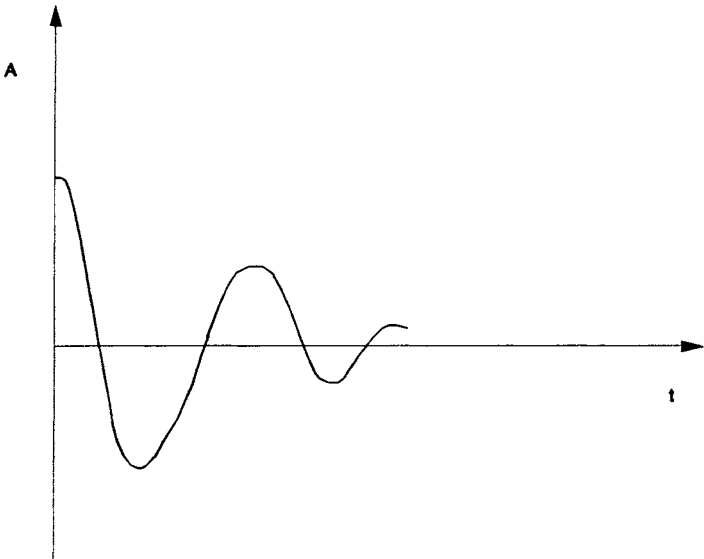
Fig. 5.4   Damped free vibration response of a nonlinear system.

compared to the linear part. Thus, we expect that the amplitude of the response will begin with a certain value in the nonlinear regime, and the system will oscillate with frequencies higher than the damped natural frequency; with the increase of time, the amplitude of the response will decrease due to the system damping. As a result, we will have an amplitude response oscillating with a decrease in amplitude and frequency values until it reaches the linear amplitude where the system responds with a damped amplitude and a constant frequency equal to the system damped natural frequency.

5.3.3 Forced Vibrations

Consider an undamped linear single degree of freedom with a harmonic external excitation. The equation of motion of the system reads

$$x'' + \omega_n^2 x = \frac{P}{m} \cos \omega t \tag{5.11}$$

The amplitude of the permanent response is sketched in Fig. 5.5. We notice that for $P = 0$, i.e., for free vibration, we will have a harmonic response with a frequency of response equal to the undamped natural frequency of the system. For $P \neq 0$, we will have response curves characterized by the resonance phenomena studied in Chapter 2. Consider now the nonlinear system for the free vibration problem due to the conclusions drawn in the preceding sections. We expect that the amplitude of the response when plotted against the frequency of excitation will have the form sketched in Fig. 5.6, for soft and hard springs, respectively.
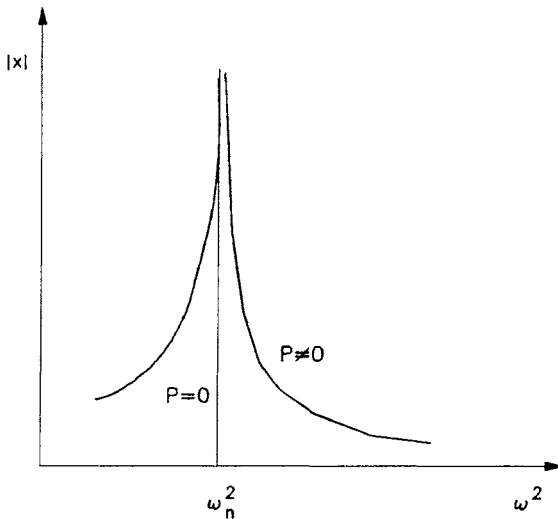
Fig. 5.5   Permanent response amplitude of a linear undamped system due to harmonic external excitation.
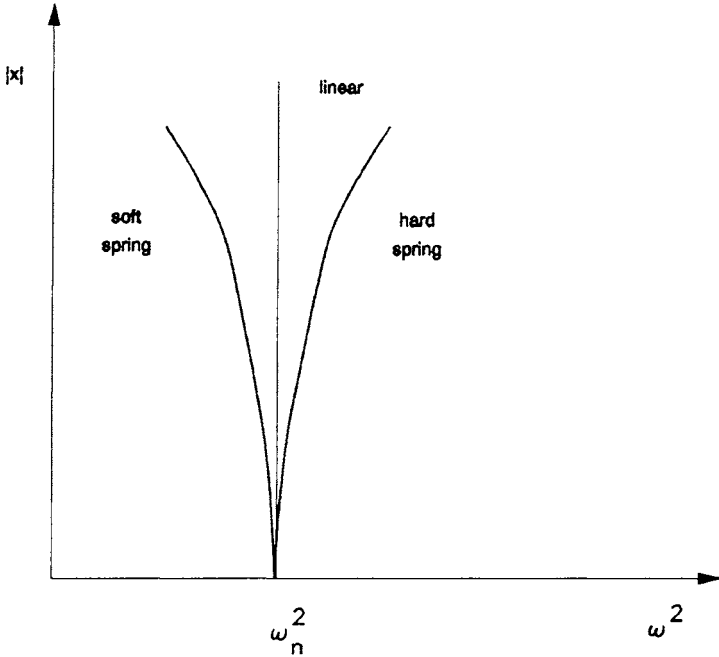
Fig. 5.6   Free vibration response of linear and nonlinear systems.

Again, physical considerations reveal that, for the forced responses of the nonlinear system, we will have the curves sketched in Figs. 5.7 and 5.8, for soft and hard springs, respectively. As in the linear system, we will expect that, for the nonlinear system, the presence of the damping in the system will limit the amplitude of oscillation at the points of maximum frequency responses as shown in the figures.

5.3.4 Stability

Consider a single-degree-of-freedom nonlinear system with hard spring stiffness characteristics. We perform a harmonic external excitation test on the system, varying continuously the excitation frequency and recording the corresponding response amplitude. We start the test from very low frequency value and increase gradually the external excitation frequency. During this test and due to the physical properties of the nonlinear hard spring system previously discussed, the response amplitude will follow curve 1A'CC'2 shown in Fig. 5.9. We notice the sudden change of the amplitude of the response at the point of maximum response C to the position C' as given in Fig. 5.9. Consider now the test realized from a high frequency value and with a gradual decrease in the external harmonic excitation frequency. The response amplitude will follow curve 2C'AA'1 shown in Fig. 5.9. We notice the sudden change of the amplitude of the response at the point A to the
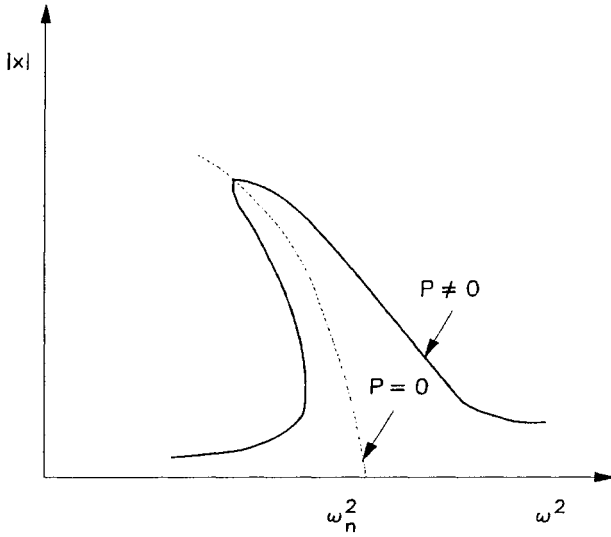
Fig. 5.7   Forced vibration response of nonlinear soft spring systems.
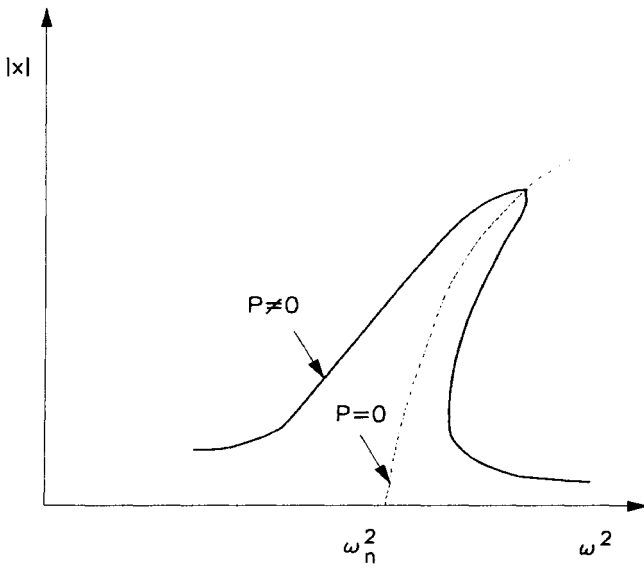
Fig. 5.8   Forced vibration response of nonlinear hard spring systems.
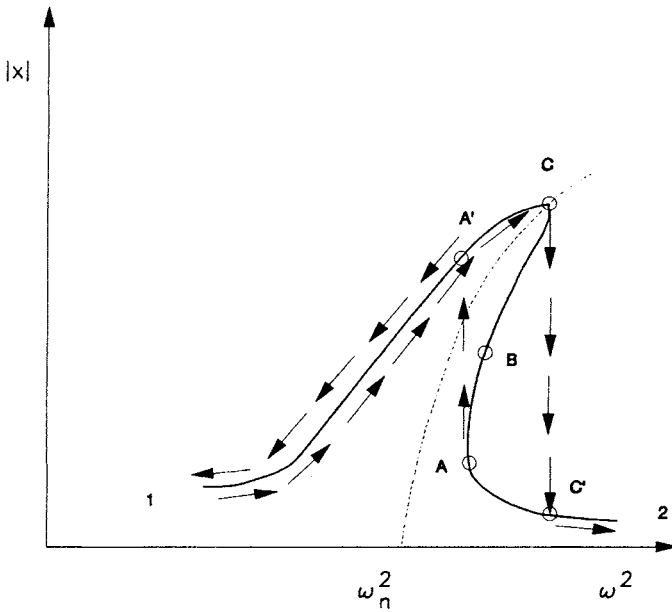
Fig. 5.9   Stability problem in nonlinear systems.

position A′ as given in Fig. 5.9. From these tests, we can conclude that path ABC will never be reached during these experiments.

Consider now the starting of the experiment with initial conditions localized on a point of curve ABC. Slight perturbations from this initial condition will show that the experiment will follow either the upper branch or the lower branch, depending on a decrease or increase in the external excitation frequency. We thus define path ABC as being an unstable path. This is a characteristic of the dynamic system that can be explained only if nonlinearity is considered in the analysis. We finally observe that in practice we will not have a sudden jump from C to C′ or A to A′; instead, the system will perform some limited number of oscillation cycles until reaching the other branch. In practice, therefore, the vertical lines CC′ and AA′ are transformed to slightly inclined lines. The instability phenomenon is frequently observed during ground vibration harmonic testing performed for the determination of the nonlinear modal characteristics of control systems and external stores in aeronautical applications. The above discussion has been made for a hard spring system; the same conclusions in a similar manner can be drawn for a soft spring with the curves now inclined to the left.

5.3.5 Superposition

For linear systems, the superposition process is valid, i.e., if x_1 is the response due to an external excitation F_1 and x_2 is the response due to an external excitation F_2, we will have for an excitation $F_1 + F_2$ a response of $x_1 + x_2$. For nonlinear systems, the superposition process is not valid. This is obvious, because the force–displacement relationship is not linear.

5.4 Solutions of the Equation of Motion of a Single-Degree-of-Freedom Nonlinear System

5.4.1 Exact Solutions

Very few nonlinear differential equations have exact solutions. In this section, we say that an exact solution to a differential equation is obtained if the solution of the response can be written in a closed-form analytical expression or in an analytical expression that permits the determination of the response to any predefined desired precision. Exact mathematical solutions of nonlinear systems are studied not only because of their importance for the cases where they exist but also because these exact solutions can be used in the studies of the performance and convergence of nonlinear numerical algorithm solvers that are to be used for the solution of the problems that do not have exact solutions. This fact will be emphasized in detail in the subsequent sections.

Free vibration. Consider an undamped single-degree-of-freedom system with stiffness nonlinearity in free vibration. The related equation of motion can be written as

$$x'' + \phi^2 f(x) = 0 \tag{5.12}$$

In Eq. (5.12), the symbol ϕ^2 has been used to emphasize the fact that physical considerations reveal that it is a real positive quantity for the case at hand. The function $f(x)$ is, in general, any real odd function of the displacement x. Again, the function $f(x)$ is a real odd function based on physical considerations. Equation (5.12) can be written as

$$\frac{d(x')^2}{dx} + 2\phi^2 f(x) = 0 \tag{5.13}$$

Integrating, we obtain

$$(x')^2 = 2\phi^2 \int_x^X f(\xi)\, d\xi \tag{5.14}$$

where ξ is the dummy variable of the integration and X corresponds to the amplitude when the velocity x' is null. We now write Eq. (5.14) as

$$x' = \frac{dx}{dt} = \sqrt{2}\phi \sqrt{\int_x^X f(\xi)\, d\xi} \tag{5.15}$$

or

$$dt = \frac{dx}{\sqrt{2}\phi \sqrt{\int_x^X f(\xi)\, d\xi}} \tag{5.16}$$

Integrating, we obtain

$$t - t_0 = \frac{1}{\sqrt{2}\phi} \int_0^x \frac{d\zeta}{\sqrt{\int_\zeta^X f(\xi)\, d\xi}} \tag{5.17}$$

Table 5.1   Values of the elliptic functions $\psi(n)$

n	1	3	5	7
$\psi(n)$	1.5708	1.8541	2.1035	2.3282

where ζ is the dummy variable of the integration and t_0 corresponds to the time for $x = 0$. Now, because $f(x)$ is an odd function and because the solution is periodic, we can consider the period T as being four times the integration of the displacement from 0 to X, which in turn is the amplitude that corresponds to $x' = 0$, and we obtain

$$T = \frac{4}{\phi\sqrt{2}} \int_0^X \frac{d\zeta}{\sqrt{\int_x^X f(\xi)\,d\xi}} \tag{5.18}$$

An exact solution for Eq. (5.18) will be obtained if we can evaluate the integration in the right-hand side in a closed-form analytical expression. We now consider the case where we can write $f(x)$ as

$$f(x) = x^n \qquad n = 1, 3, 5, \ldots \tag{5.19}$$

Using Eqs. (5.19) and (5.18), we obtain

$$T = \frac{4}{\phi} \sqrt{\frac{n+1}{2}} \int_0^X \frac{d\zeta}{\sqrt{X^{n+1} - \zeta^{n+1}}} \tag{5.20}$$

and making the transformation $u = \zeta/X$, we get

$$T = \frac{4}{\phi\sqrt{X^{n+1}}} \left[\sqrt{\frac{n+1}{2}} \int_0^1 \frac{du}{\sqrt{1 - u^{n+1}}} \right] = \frac{4}{\phi\sqrt{X^{n+1}}} \psi(n) \tag{5.21}$$

where $\psi(n)$ are the elliptic functions[1] and can be calculated to any desired precision. Table 5.1 gives the values of $\psi(n)$ up to four digits after the decimal point.

We now consider the case when $f(x)$ is given by

$$f(x) = x^n + \mu x^m \qquad m > n > 0$$
$$m = 3, 5, 7, \ldots \qquad n = 1, 3, 5, \ldots \tag{5.22}$$

Making the substitution of Eq. (5.22) into Eq. (5.18), we obtain

$$T = \frac{4}{\phi\sqrt{X^{n-1}}} \left[\sqrt{\frac{n+1}{2}} \int_0^1 \frac{du}{\sqrt{(1+v) - (u^{n+1} + vu^{m+1})}} \right] \tag{5.23}$$

where

$$v = \mu X^{m-n} \left\{ \frac{n+1}{m+1} \right\} \tag{5.24}$$

The integral in Eq. (5.23) can be calculated to any desired precision[1] for specific values of n, m, and ν. The extension to the case of a higher-order polynomial is straightforward.

Forced vibration. There is no exact solution for the general case of forced vibration of a nonlinear dynamic single-degree-of-freedom system. The solutions are therefore obtained using numerical methods that will be discussed in the next section.

5.4.2 Numerical Solutions

Duffing method. In this section, we consider a single degree of freedom having stiffness nonlinearity up to a cubic term and excited by an external harmonic force. The equation of motion can be written as

$$x'' + \phi^2(x \pm \mu^2 x^3) = p \cos \omega t \tag{5.25}$$

Equation (5.25) is called the Duffing equation. In this equation, the term $\phi^2 \mu^2$ is considered very small compared to unity. The positive sign in this equation is for the hard spring, and the negative sign is for the soft spring nonlinearity. We will treat only the case of the positive sign, because once a solution has been obtained for the hard spring the solution for the case of a soft spring is directly given by changing the sign of μ^2 in the solution. The Duffing method starts by assuming as a first iteration for the nonlinear solution an approximation given by the linear solution, i.e., we write as a first iteration a solution in the form

$$x_1 = A \cos \omega t \tag{5.26}$$

Substituting Eq. (5.26) into Eq. (5.25), we obtain

$$x_2'' = -\phi^2 A \cos \omega t - \mu^2 \phi^2 A^3 \cos^3 \omega t + p \cos \omega t \tag{5.27}$$

Now writing

$$\cos^3 \omega t = \tfrac{1}{4}[3 \cos \omega t + \cos 3\omega t] \tag{5.28}$$

in Eq. (5.27) and integrating twice, we obtain

$$x_2 = \frac{1}{\omega^2}\left\{\left[\phi^2 A + \frac{3}{4}\mu^2\phi^2 A^3 - p\right]\cos \omega t + \frac{\mu^2\phi^2 A^3}{36}\cos 3\omega t\right\} \tag{5.29}$$

where null integration constants have been assumed for periodic solutions. The solution [Eq. (5.29)] can be considered as a better approximation than the first iteration given by Eq. (5.26) for the solution of the Duffing equation. We can now start an iteration process by substituting the solution to Eq. (5.29) into the Duffing equation and integrating twice to obtain a better approximation for the solution and repeat the iteration process until a desired accuracy. We notice that this process is convergent only for small values of $\phi^2\mu^2$ and, for such quasilinear systems, the convergence is very rapid. Now, comparing Eqs. (5.26) and (5.29) and equating the coefficient of the term $\cos \omega t$, we obtain

$$A = \frac{1}{\omega^2}\left[\phi^2 A + \frac{3}{4}\mu^2\phi^2 A^3 - p\right] \tag{5.30}$$

or

$$\omega^2 = \phi^2 \left[1 + \frac{3}{4}\mu^2 A^2 \right] - \frac{p}{A} \tag{5.31}$$

We conclude the following:

1) For the linear system, we have $\phi^2 = \omega_n^2$.

2) For free vibration, $p = 0$, and we have $\omega^2 = \phi^2[1 + (3/4)\mu^2 A^2]$, showing that the response frequency is a function of the amplitude of free vibration and the related curve has the form given in Fig. 5.6.

3) We notice that, for the linear system if the external excitation is harmonic, the response is also harmonic with the same frequency. For the nonlinear system and in view of Eq. (5.29) for an external harmonic excitation, terms of upper harmonics exist in the solution.

4) Successive iterations using the Duffing method will show the presence of the terms $\cos 5\omega t$, $\cos 7\omega t$, etc., with decreasing amplitude as the superharmonic value increases.

Perturbation methods.   Consider again the Duffing equation

$$x'' + \phi^2(x \pm \mu^2 x^3) = p \cos \omega t \tag{5.32}$$

Writing $\omega t = \theta$ in Eq. (5.32), we get

$$\omega^2 x'' + \phi^2(x \pm \mu^2 x^3) - p \cos \theta = 0 \tag{5.33}$$

where the derivatives are now with respect to θ, i.e., $x' = dx/d\theta$. Let now the initial condition be given as

$$x(0) = A \qquad x'(0) = 0 \qquad \text{for } t = 0 \tag{5.34}$$

which corresponds to a periodic solution. We consider again the term $\phi^2\mu^2$ as being very small compared to unity, and we write

$$\phi^2\mu^2 = \varepsilon \qquad p = \varepsilon p_0 \tag{5.35}$$

where ε is a small quantity. We can now write $x(\theta)$ and ω as a series expansion in ε in the form

$$x(\theta) = x_0(\theta) + \varepsilon x_1(\theta) + \varepsilon^2 x_2(\theta) + \cdots \tag{5.36}$$

and

$$\omega = \omega_0 + \varepsilon\omega_1 + \varepsilon^2\omega_2 + \cdots \tag{5.37}$$

Deriving twice Eq. (5.36), we get

$$x''(\theta) = x_0''(\theta) + \varepsilon x_1''(\theta) + \varepsilon^2 x_2''(\theta) + \cdots \tag{5.38}$$

and the boundary conditions read

$$x_i(0) = x_i'(0) = 0 \qquad i = 1, 2, 3, \ldots \tag{5.39}$$

Substituting Eq. (5.35) into Eq. (5.33), we obtain

$$\omega^2 x'' + \phi^2 x + \varepsilon x^3 - \varepsilon p_0 \cos\theta = 0 \tag{5.40}$$

Substituting now Eqs. (5.36–5.38) into Eq. (5.40), we obtain an equation that can be written in the form

$$[\ ]\varepsilon^0 + [\ ]\varepsilon^1 + [\ ]\varepsilon^2 + \cdots = 0 \tag{5.41}$$

Equation (5.41) is valid for any value of ε; therefore, the only condition for the sum of all the terms to be equal to zero is that all the individual coefficients of ε^n must vanish individually. Equating the first term, i.e., the coefficient of ε^0, to zero, we get

$$\omega_0^2 x_0'' + \phi^2 x_0 = 0 \tag{5.42}$$

Equation (5.42) is subjected to the boundary conditions given by Eq. (5.34) and the solution of Eq. (5.42) thus reads

$$x_0(t) = A \cos\omega t \tag{5.43}$$

and we obtain

$$\omega_0^2 = \phi^2 \tag{5.44}$$

Equating the second term, i.e., the coefficient of ε^1, to zero, we get

$$\left[\omega_0^2 x_1'' + 2\omega_0\,\omega_1 x_0'' + \phi^2 x_1 + x_0^3 - p_0 \cos\theta\right] = 0 \tag{5.45}$$

Substituting the value of x_0, already calculated from Eq. (5.43), into Eq. (5.45), we obtain

$$\omega_0^2 x_1'' + \phi^2 x_1 = \left[2\omega_0\,\omega_1 A - \tfrac{3}{4}A^3 + p_0\right]\cos\theta - \tfrac{1}{4}A^3 \cos 3\theta \tag{5.46}$$

Equation (5.46) is a second-order ordinary differential equation in x_1 having a general solution composed of two parts, the homogeneous solution x_{11} and the particular integral x_{12}. The homogeneous solution x_{11} reads

$$x_{11} = A_1 \sin\theta + B_1 \cos\theta \tag{5.47}$$

where A_1 and B_1 are constants that will be determined from the initial conditions of x_1. The particular integral x_{12} reads

$$x_{12} = 2\theta\left[2\frac{\omega_1}{\omega_0}A - \frac{3}{4\omega_0^2}A^3 + \frac{p_0}{\omega_0^2}\right]\cos\theta - \frac{A^3}{32\,\omega_0^2}\cos 3\theta \tag{5.48}$$

Now, because $\theta = \omega t$, we observe that the first term in Eq. (5.48) increases exponentially with time. This contradicts the physical solution that must be periodic; therefore, the only condition for this term to vanish is that the bracket term be set to zero. In the perturbation method of solution, we call such terms secular terms, and they are equated to zero in each step. Furthermore, from this condition, the value of ω_1 can be determined, and we write

$$\omega_1 = \frac{1}{2\phi}\left[\frac{3}{4}A^2 - \frac{p_0}{A}\right] \tag{5.49}$$

and the total solution x_1, which is the sum of x_{11} and x_{12}, reads

$$x_1 = A_1 \sin \theta + B_1 \cos \theta - \frac{A^3}{32 \, \phi^2} \cos 3\theta \tag{5.50}$$

Applying now the initial boundary conditions given by Eq. (5.39) into Eq. (5.50), we obtain

$$x_1 = \frac{A^3}{32 \, \phi^2} [\cos 3\theta - \cos \theta] \tag{5.51}$$

Now using Eqs. (5.43) and (5.51), we get the first approximation for the solution of x as

$$x = x_0 + \varepsilon x_1 = A \cos \theta + \frac{A^3 \varepsilon}{32 \, \phi^2} [\cos 3\theta - \cos \theta] \tag{5.52}$$

and the first approximation for the value of ω as

$$\omega = \omega_0 + \omega_1 = \phi^2 + \frac{\varepsilon}{2\phi} \left[\frac{3}{4} A^2 - \frac{p_0}{A} \right] \tag{5.53}$$

Substituting now the value of θ by ωt and ε^2 by $\mu^2 \phi^2$ in Eqs. (5.52) and (5.53), we obtain

$$x = \frac{1}{\omega^2} \left\{ \left[\phi^2 A + \frac{3}{4} \mu^2 \phi^2 A^3 - p \right] \cos \omega t + \frac{\mu^2 \phi^2 A^3}{36} \cos 3 \, \omega t \right\} \tag{5.54}$$

and

$$\omega^2 = \phi^2 \left[1 + \frac{3}{4} \mu^2 A^2 \right] - \frac{p}{A} \tag{5.55}$$

Comparing Eqs. (5.54) and (5.55) with the Duffing solution given by Eqs. (5.29) and (5.30), we conclude that the first approximation in both methods is the same. The extension of the perturbation method as given above for higher iterations is straightforward. Finally, we observe the great advantage of the perturbation method, which is the transformation of the nonlinear problem to a series of solutions of linear problems.

Galerkin method.   The Galerkin method is a powerful tool for obtaining numerical solutions for linear and nonlinear problems in structural dynamics. Furthermore, in nonlinear problems, the method has no limitation to the small nonlinearity condition as in the Duffing and perturbation methods. The basis of the application of the method for nonlinear problems is given in the sequel.

Consider the equation of motion of a single-degree-of-freedom nonlinear system, which can be written as

$$E = E(x'', x', x, t) = 0 \tag{5.56}$$

In the Galerkin method, we write approximate solutions for the differential Eq. (5.56) in the form

$$x(t) = a_1 \psi_1(t) + a_2 \psi_2(t) + \cdots + a_n \psi_n(t) \tag{5.57}$$

where $\psi_i(t)$ are arbitrary continuous and differentiable functions that satisfy all the boundary conditions of the problem, a_i are arbitrary unknown constants to be determined, and $i = 1, 2, \ldots, n$. For the case at hand, when we are solving problems of periodic responses, the boundary conditions of the problem are $\psi_i(t) = 0$ at the beginning and at the end of the period. Now, if the approximate solution [Eq. (5.57)] is substituted into the differential Eq. (5.56), in general, a residue will be obtained, except for the case when the trial functions are the exact solutions of the problem, and, in this case, the differential equation is identically satisfied. In the Galerkin method, the error is minimized by multiplying the residue by the trial function, i.e., we consider the trial functions as being the weighting functions in a weight residual minimization process and force the integration of the product over the domain (the period for the case at hand) to vanish. This process will furnish n nonlinear algebraic equations in the form

$$\int_0^T \psi_i E(x'', x', x, t)\, dt = 0 \qquad i = 1, 2, 3, \ldots, n \tag{5.58}$$

which can be solved using any nonlinear simultaneous algebraic equation algorithm solver, e.g., the Newton method, and the coefficients a_i are thus determined. In the sequel, some applications of the Galerkin method will be given.

Rayleigh–Ritz method. The Rayleigh–Ritz method starts by formulating the problem using a variational approach, Hamilton's principle for the case at hand, which can be written as

$$I = \int_{t_1}^{t_2} F(x', x, t)\, dt \tag{5.59}$$

Again, approximate solutions for the problem are sought in the form

$$x(t) = a_1\psi_1(t) + a_2\psi_2(t) + \cdots + a_n\psi_n(t) \tag{5.60}$$

where $\psi_i(t)$ must satisfy only the forced boundary conditions.[2] Substituting the approximate solution [Eq. (5.60)] into the variational functional and performing the related integrations, the functional will be transformed to a function of the arbitrary constants a_i that can be written as

$$I = I(a_1, a_2, a_3, \ldots, a_n) \tag{5.61}$$

The functional maximization is thus transformed to the minimization of the function given by Eq. (5.61), and this condition can be written as

$$\frac{\partial I}{\partial a_i} = 0 \qquad i = 1, 2, \ldots, n \tag{5.62}$$

Again, the set of equations [Eq. (5.62)] represents n nonlinear algebraic equations whose solutions will produce the values of the unknown coefficients a_i. Consider now Eqs. (5.62) and (5.59). We can write

$$\frac{\partial I}{\partial a_i} = \int_{t_0}^{t_1} \left[\frac{\partial F}{\partial x}\frac{dx}{da_i} + \frac{\partial F}{\partial x'}\frac{dx'}{da_i}\right] dt = 0 \tag{5.63}$$

or

$$\frac{\partial I}{\partial a_i} = \int_{t_0}^{t_1} \left[\frac{\partial F}{\partial x} \psi_i + \frac{\partial F}{\partial x'} \psi_i' \right] dt = 0 \tag{5.64}$$

Integrating the second integral by parts, we obtain

$$\frac{\partial I}{\partial a_i} = \left[\frac{\partial F}{\partial x'} \psi_i \right]_{t_0}^{t_1} + \int_{t_0}^{t_1} \left[\frac{\partial F}{\partial x} - \frac{d}{dt} \frac{\partial F}{\partial x'} \right] \psi_i \, dt = 0 \tag{5.65}$$

The first term of the right-hand side of Eq. (5.65) vanishes since $\psi_i = 0$ at the initial of the period t_0 and at the end of the period t_1. Equation (5.65) thus reads

$$\frac{\partial I}{\partial a_i} = \int_{t_0}^{t_1} \left[\frac{\partial F}{\partial x} - \frac{d}{dt} \frac{\partial F}{\partial x'} \right] \psi_i \, dt = 0 \tag{5.66}$$

Now, the term between brackets in Eq. (5.66) is the Euler–Lagrange equation governing the problem, i.e., the equation of motion for the case at hand. Thus, we can write Eq. (5.66) as

$$\int_{t_0}^{t_1} \left[E(x'', x', x, t) \psi_i \right] dt = 0 \tag{5.67}$$

Comparing now Eqs. (5.58) and (5.67), we conclude that the Galerkin and Rayleigh–Ritz methods are equivalent for the problem at hand. This equivalence can always be shown whenever a variational principle exists for the problem in consideration.

As an example of the application of the Galerkin and/or the Rayleigh–Ritz methods, for a nonlinear single-degree-of-freedom system, we consider the equation

$$x'' + \phi^2 x^n = 0 \qquad n = 1, 3, 5, \ldots \tag{5.68}$$

This equation has an exact closed-form solution given by Eq. (5.21). We apply now the Galerkin method of solution using only one trial function for the approximate solution in the form

$$x = A \cos \omega t = A \cos \theta \tag{5.69}$$

where $\theta = \omega t$. Applying the Galerkin method to Eq. (5.68), we obtain

$$\int_0^{2\pi} \left[-\omega^2 A \cos^2 \theta + \phi^2 A^n \cos^{n+1} \theta \right] d\theta = 0 \tag{5.70}$$

or

$$\frac{\omega^2 \pi}{\phi^2 A^{n-1}} = \int_0^{2\pi} \cos^{n+1} \theta \, d\theta \tag{5.71}$$

To evaluate the integral in Eq. (5.71), we use the relations

$$\int_0^{2\pi} \cos^m \theta \, d\theta = \frac{m-1}{m} \int_0^{2\pi} \cos^{m-2} \theta \, d\theta$$

$$\int_0^{2\pi} \cos^2 \theta \, d\theta = \pi \qquad m = 4, 6, 8, \ldots \tag{5.72}$$

Table 5.2   Galerkin one-term solution $\zeta(n)$
compared with the exact solution $\psi(n)$

n	1	3	5	7
$\zeta(n)$	1.5708	1.8138	1.9869	2.1241
$\psi(n)$	1.5708	1.8541	2.1035	2.3282

and because $\omega = 2\pi/T$, we obtain for the period T the following expression

$$T = \frac{4}{\phi\sqrt{A^{n-1}}}\zeta(n) \tag{5.73}$$

where

$$\zeta(n) = \frac{\pi^{\frac{3}{2}}}{2\sqrt{\int_0^{2\pi}\cos^{n+1}\theta\,d\theta}} \tag{5.74}$$

The values of $\zeta(n)$ are given in Table 5.2 and are compared with the exact solution given by the elliptic functions $\psi(n)$.

From the results of Table 5.2, we observe that for $n = 1$, i.e., for the linear case, the Galerkin solution corresponds to the exact solution. As the value of n increases, i.e., with the increase of the nonlinearity effect, the precision of the Galerkin method deteriorates; if more precision is required, we will have to incorporate to the numerical solution more and more terms. Furthermore, the numerical solution for the period T is always less than the exact solution; hence, the numerical frequency is always higher than the exact solution. This property can always be shown and proved when the numerical solution uses the Rayleigh–Ritz method, which for the case at hand is equivalent to the Galerkin solution.[2]

5.4.3 Damped Systems

We consider in this section a viscous damped single degree of freedom with nonlinear stiffness characteristics subjected to an external harmonic excitation. The governing equation of motion can be written as

$$mx'' + cx' + k_0 f(x) - p\cos\omega t = 0 \tag{5.75}$$

Because no exact solution of the differential Eq. (5.75) exists, we will use the Galerkin method to obtain a numerical approximate solution for the problem. As a first approximation, we will use only one term in the Galerkin method, and we write

$$x = A\cos[\omega t - \theta] \tag{5.76}$$

Notice that a phase angle θ has been incorporated to the solution due to the presence of the damping term. Substituting the approximate solution [Eq. (5.76)] into the differential Eq. (5.75) and applying the Galerkin method, we obtain an

equation in the form

$$[A_1]\cos \omega t + [A_2]\sin \omega t = 0 \tag{5.77}$$

where

$$A_1 = -m\omega^2 A \cos \theta + c\omega A \sin \theta + k_0 A F(A)\cos \theta - p$$

$$A_2 = -m\omega^2 A \sin \theta - c\omega A \cos \theta + k_0 A F(A)\sin \theta \tag{5.78}$$

and

$$F(A) = \frac{1}{\pi A} \int_0^{2\pi} f(A \cos \sigma)\cos \sigma \, d\sigma \tag{5.79}$$

We now observe that Eq. (5.77) is valid for any value ωt; therefore, $A_1 = A_2 = 0$. Applying this condition and using Eqs. (5.78) and (5.79), we obtain

$$[F(A) - \Omega^2]^2 + 4\gamma^2 \Omega^2 = \left[\frac{p/k_0}{A} \right]^2 \tag{5.80}$$

and

$$\tan \theta = \frac{2\gamma \Omega}{F(A) - \Omega^2} \tag{5.81}$$

where

$$\Omega^2 = \omega^2 \frac{m^2}{k_0^2} \qquad \text{and} \qquad \gamma = \frac{c}{2\sqrt{mk_0}} \tag{5.82}$$

and we observe the following:
1) The linear system is obtained when $F(A) = 1$.
2) For the undamped nonlinear system in free vibration, i.e., $c = 0$ and $p = 0$, we obtain from Eq. (5.80) $\gamma = 0$; thus, $\theta = 0$ or π, and from Eq. (5.80) we get

$$F(A) = \Omega^2 \tag{5.83}$$

For the case when $f(x)$ is given by an odd polynomial function of x, Eq. (5.83) will produce the curves previously given in Fig. 5.6.
3) For the undamped forced vibration system, i.e., $c = 0$ (thus $\gamma = 0$) and $p \neq 0$, we obtain from Eq. (5.80) $\theta = 0$ or π, and we write

$$\Omega^2 = F(A) \pm \left[\frac{p/k_0}{A} \right] \tag{5.84}$$

For the case when $f(x)$ is given by an odd polynomial function of x, Eq. (5.84) will produce the curves previously given in Figs. 5.7 and 5.8, with peaks tending to infinity.
4) For the damped response, Eq. (5.80) can be written as

$$\Omega^2 = F(A) - 2\gamma^2 \pm \sqrt{\left[\frac{p/k_0}{A} \right]^2 - 4\gamma^2 \left[F(A) - \gamma^2 \right]} \tag{5.85}$$
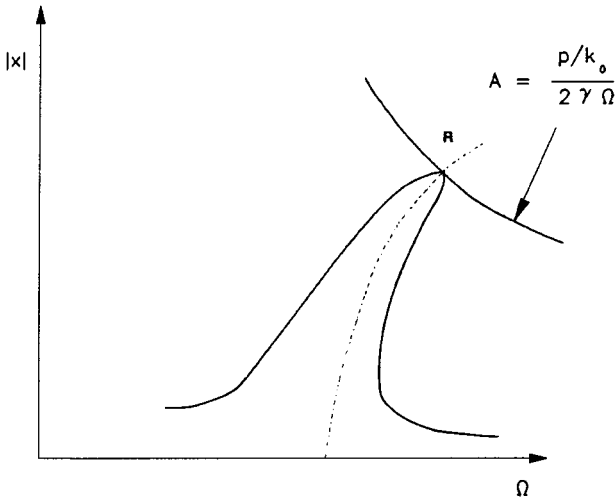
Fig. 5.10   Damped nonlinear single-degree-of-freedom system.

For the case when $f(x)$ is given by an odd polynomial function of x, Eq. (5.85) will produce the curves previously given in Figs. 5.7 and 5.8.

5) Of special interest is the determination of the point of maximum amplitude of the response for the nonlinear damped system. We will approximate this point by the point denominated R in Fig. 5.10, i.e., the crossing point of the response curve with the undamped free vibration curve. At this point, both Eqs. (5.83) and (5.85) are satisfied. Solving these two equations simultaneously, we obtain

$$\Omega^2 = \frac{1}{4\gamma^2} \left[\frac{p}{k_0 A} \right]^2 \tag{5.86}$$

or

$$\frac{A}{p/k_0} = \frac{1}{2\gamma\Omega} \tag{5.87}$$

Equation (5.87) is a hyperbola in the $|A| - \Omega$ plane and can be plotted knowing only the linear terms as can be seen from Eq. (5.87). The point R will thus be determined from the crossing of this curve with the curve $F(A) = \Omega^2$, as shown in Fig. 5.10.

5.5   Multidegree-of-Freedom Nonlinear Systems

The step-by-step numerical integration methods given in Chapter 3 are directly extended for the analysis of arbitrary nonlinear systems with multiple degrees of freedom. As in the linear case, the time-history response is divided into short, normally equal time increments, and the response is calculated at the end of the time interval for a linearized system having properties determined at the beginning of the interval. The system nonlinear properties are then modified at the end of the interval to conform to the state of deformations and stresses at that time. The

mass matrix is usually constant in most practical applications so that its inverse is evaluated once at the beginning of the solution procedure. The stiffness and the damping matrices are modified at the beginning of each step. Therefore, during each step of the nonlinear solution, a triangular decomposition of the equivalent stiffness matrix must be done to obtain the end displacements and velocities. As in the linear case, the acceleration vectors are obtained solving the equations of motion at the beginning of the interval to avoid accumulation of errors during the solution procedure. The modal transformation technique can be used in the solution of the nonlinear system with multiple degrees of freedom; however, in this case, the related matrices are coupled, but the system will have a smaller number of equations compared to the original system written in the physical coordinates. The step-by-step integration procedures are applied to the transformed smaller system of equations.

The Rayleigh–Ritz and Galerkin methods given in the previous section for the solution of the single-degree-of-freedom system are directly extended for application in the solution of multidegree-of-freedom nonlinear systems.

The perturbation methods given in the previous section for the solution of the single-degree-of-freedom system are also directly extended for application in the solution of multidegree-of-freedom nonlinear systems with small nonlinearity effects. The perturbation methods are in general superior to the step-by-step numerical integration methods, especially when the external excitation is harmonic or in the solution of nonlinear dynamic stability problems with small nonlinearity because only few linear solutions are needed to obtain the nonlinear problem response. The step-by-step numerical integration methods are most useful for arbitrary general cases and especially when the external excitation is of short duration.

References

[1]*Handbook of Mathematical Functions with Formulas, Graphs and Mathematical Tables*, 8th ed., edited by M. Abramowitz and I. A. Stegnun, Dover, New York, 1972.

[2]Bismarck-Nasr, M. N., *Finite Elements in Applied Mechanics*, Abaeté, São Paulo, 1993.

Problems

5.1   The equation of motion of a nonlinear single-degree-of-freedom system in free vibration is given by $mx'' + kx^5 = 0$. Given $m = 1$ kg and $k = 9$ N/m^5, plot the period–amplitude curve of the system.

5.2   Free-play in airplane control surface tabs can be modeled as a nonlinear damped single degree of freedom having a stiffness characteristic k defined as $k = 0$ for $-\delta_0 \leq x \leq \delta_0$ and $k = k_0$ for $-\delta_0 > x > \delta_0$, where $2\delta_0$ is defined as the system free-play and $x = x(t)$ is the system response. Neglecting the damping effect, obtain the system response in free vibrations due to initial conditions given by $x_0 = 0$ and $x_0' = v$ at $t = t_0$. Comment on the results obtained in terms of the dependence of the frequency of oscillation on the free-play and the initial velocity values. Include then the damping in the equation of motion and discuss its effect on the system response.

6
Random Vibrations

6.1 Introduction

Consider the record of a measured variable $x(t)$, illustrated in Fig. 6.1, which can represent for instance the displacement of a point in a structure as a function of time. In Fig. 6.1a, we can conclude that the variable $x(t)$ is predominantly harmonic, while $x(t)$ of Fig. 6.1b is predominantly irregular. If we repeat the process of measuring and recording the response of the displacement several times and if in all cases we obtain the same responses in both processes, we define such processes as being deterministic processes. Now if, in the process of Fig. 6.1a, during the repeated measurements of the records at each time, we obtain a different angle of phase and if, in the process of Fig. 6.1b, the responses are different from each other during the repeated measurements, we call such processes random processes. Random processes are characterized by the fact that their behavior cannot be predicted in advance and therefore can be treated only in a statistical manner. We will begin this chapter by studying random processes and their statistical properties. In the sequence, we will study the response of linear systems due to random excitations. For more detail on random vibrations, the reader can consult Refs. 1–5.

6.2 Classification of Random Processes

6.2.1 Stationary Random Processes

Consider n records of a random variable as given in Fig. 6.2. We define the complete set of $x_k(t)$, $k = 1, 2, \ldots, n$ as a random process, and each record of the set will be called a sample of the random process. Consider now the values of $x_k(t)$ for the instant of time $t = t_1$; we can write the mean value of the random process at that instant of time as

$$\mu_x(t_1) = \frac{1}{n} \sum_{k=1}^{n} x_k(t_1) \tag{6.1}$$

For an instant of time $t = t_2$ separated from t_1 by an interval of time τ, we can write a statistical measurement of the behavior of the mean value in relation to a shift τ as a function $R_x(t_1, t_1 + \tau)$, given by

$$R_x(t_1, t_1 + \tau) = \lim_{n \to \infty} \frac{1}{n} \sum_{k=1}^{n} x_k(t_1) x_k(t_1 + \tau) \tag{6.2}$$

We call $R_x(t_1, t_1 + \tau)$ the autocorrelation function. In the same manner, we can define higher-order autocorrelation functions for more than one shift, say $\tau, \sigma, \ldots$.

139
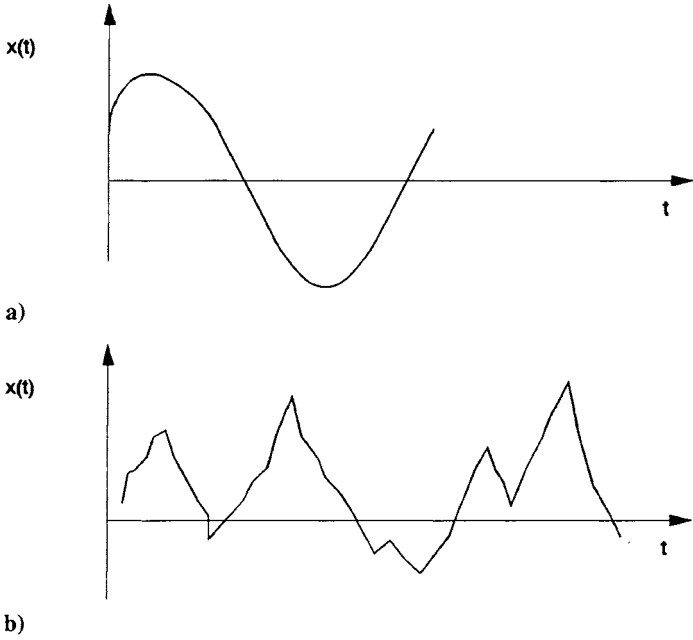
Fig. 6.1   Record of a variable as a function of time.
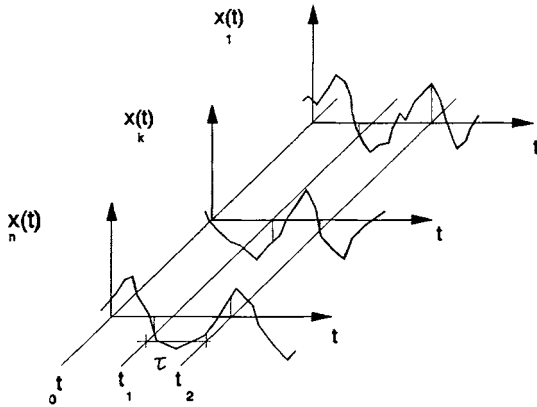
Fig. 6.2   Time history of a random process.

For example, for two shifts, we can write an expression in the form

$$R_x(t_1, t_1 + \tau, t_1 + \sigma) = \lim_{n \to \infty} \frac{1}{n} \sum_{k=1}^{n} x_k(t_1)x_k(t_1 + \tau)x_k(t_1 + \sigma) \qquad (6.3)$$

In general, $\mu_x(t_1)$, $R_x(t_1, t_1 + \tau)$, $R_x(t_1, t_1 + \tau, t_1 + \sigma)$, etc., will be functions of t_1 where the mean values have been calculated. Now if in a random process these mean values do not depend on t_1, i.e., $\mu_x(t_1) = \mu_x = \text{const}$ and $R_x(t_1, t_1 + \tau) = R_x(\tau)$ and $R_x(t_1, t_1 + \tau, t_1 + \sigma) = R_x(\tau, \sigma)$, etc., we call the random process a process that is heavily stationary. If, however, only the mean value and the first autocorrelation function do not depend on t_1, we define the random process as a slightly stationary process. In general, the higher autocorrelation functions are not calculated, and the slightly stationary processes are, in general, considered as heavily stationary. In the following, we will make no more distinction between the heavily stationary and the slightly stationary definition, and we will consider the processes having $\mu_x = \text{const}$ and $R_x = R_x(\tau)$ as stationary processes.

6.2.2 Ergodic Random Processes

Consider a stationary random process. For each sample of the process, we can write the mean value and the autocorrelation function in relation to the time as

$$\mu_x(k) = \lim_{T \to \infty} \frac{1}{T} \int_{-T/2}^{T/2} x_k(t)\, dt \qquad (6.4)$$

and

$$R_x(k, \tau) = \lim_{T \to \infty} \frac{1}{T} \int_{-T/2}^{T/2} x_k(t)x_k(\tau + \tau)\, dt \qquad (6.5)$$

In general, $\mu_x(k)$ and $R_x(k, \tau)$ will be different for each sample. In the case when $\mu_x(k) = \mu_x = \text{const}$ and $R_x(k, \tau) = R_x(\tau)$, i.e., all the values are the same for all samples, we say that the process is ergodic, and we notice that the concept of heavily stationary and slightly stationary processes are extended to stationary ergodic processes. In the following, we will make no more distinction between the heavily ergodic stationary and the slightly ergodic stationary definition, and we will consider both as stationary ergodic processes. We note further that a stationary process is not necessarily ergodic, while an ergodic process is by defintion a stationary process. In the following, we will further limit our study to ergodic stationary processes. For an ergodic process, we will define the mean square value as

$$\psi_x^2 = \lim_{T \to \infty} \frac{1}{T} \int_{-T/2}^{T/2} x(t)^2\, dt \qquad (6.6)$$

and the variance as

$$\sigma_x^2 = \lim_{T \to \infty} \frac{1}{T} \int_{-T/2}^{T/2} [x(t) - \mu_x]^2\, dt \qquad (6.7)$$

The standard deviation will be defined as the positive square root value of σ_x^2. Now, using Eq. (6.7), we can write

$$\sigma_x^2 = \lim_{T \to \infty} \frac{1}{T} \int_{-T/2}^{T/2} \left[x^2(t) - 2\mu_x x(t) + \mu_x^2 \right] dt$$

$$= \lim_{T \to \infty} \frac{1}{T} \int_{-T/2}^{T/2} x^2(t)\, dt - 2\mu_x \lim_{T \to \infty} \frac{1}{T} \int_{-T/2}^{T/2} x(t)\, dt$$

$$+ \mu_x^2 \lim_{T \to \infty} \frac{1}{T} \int_{-T/2}^{T/2} dt$$

$$= \psi_x^2 - 2\mu_x \mu_x + \mu_x^2 = \psi_x^2 - \mu_x^2 \qquad (6.8)$$

i.e., the variance is equal to the mean square value minus the mean value squared.

6.3 Probability Distribution and Density Functions

Consider a sample of an ergodic process as shown in Fig. 6.3. We define the probability distribution function as

$$P(x) = \text{Prob}\,[x(t) < x] = \lim_{T \to \infty} \frac{1}{T} \sum_i \Delta t_i \qquad (6.9)$$

and we conclude from Fig. 6.3 that $P(-\infty) = 0$, $P(\infty) = 1$, and $0 \le P(x) \le 1$. We will define the probability density function as

$$p(x) = \lim_{\Delta x \to 0} \frac{P(x + \Delta x) - P(x)}{\Delta x} = \frac{dP(x)}{dx} \qquad (6.10)$$
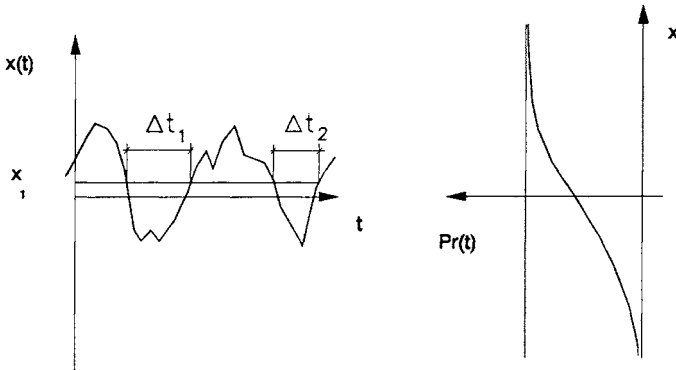
Fig. 6.3   Probability distribution function.

We observe that $P(x)$ is a nondimensional function, while $p(x)$ has dimension x^{-1}, and we verify the following relations:

$$P(x_1 < x < x_2) = \int_{x_1}^{x_2} p(x)\,dx$$

$$p(-\infty) = p(\infty) = 0$$

$$P(x) \geq 0 \qquad (6.11)$$

$$P(x) = \int_{-\infty}^{x} p(\xi)\,d\xi$$

$$P(\infty) = \int_{-\infty}^{\infty} p(\xi)\,d\xi = 1$$

In many statistical applications where the number of samples is very great and none of the samples represents a significant weight in the process, the probability density function can be represented by the so-called Gaussian distribution. The probability density function for the Gaussian or normal distribution reads

$$p(x) = \frac{1}{\sigma_x\sqrt{2\pi}}\, e^{-\frac{(x-\underline{x})^2}{2\sigma_x^2}} \qquad (6.12)$$

and thus the probability distribution function is given by

$$P(x) = \frac{1}{\sigma_x\sqrt{2\pi}} \int_{-\infty}^{x} e^{-\frac{(x-\underline{x})^2}{2\sigma_x^2}}\,dx \qquad (6.13)$$

where the parameters $\underline{x}$ and σ_x are the mean and the standard deviation of the distribution, respectively. If the mean value $\underline{x}$ of the Gaussian distribution is zero and making the transformation $\xi = x/\sigma$, the probability distribution function reads

$$P(\xi) = \frac{1}{\sqrt{2\pi}} \int_{0}^{\xi} e^{-\frac{\xi^2}{2}}\,d\xi \qquad (6.14)$$

6.4 Description of the Mean Values in Terms of the Probability Density Function

Considering a stationary random process $\{x(t)\}$ for a continuous function $g(x)$, we can write the mean value $\underline{g(x)}$ as

$$\underline{g(x)} = \frac{1}{n}\sum_{1}^{n}{}_{n\to\infty} g(x) = \sum_{1}^{n}{}_{n\to\infty} g(x)\frac{1}{n} \qquad (6.15)$$

We note that $\{1/n\}$ represents the probability of the process to have the value of $g(x)$. Thus, we can write

$$\underline{g(x)} = \sum_{-\infty}^{\infty}{}_{\Delta x\to 0} g(x)p(x)\Delta x = \int_{-\infty}^{\infty} g(x)p(x)\,dx \qquad (6.16)$$

We call $\underline{g(x)}$ the mean value or the mathematical expectation, and we write

$$\underline{g(x)} = E[g(x)] \tag{6.17}$$

Thus, we can write for the mean values the following expressions in terms of the probability density function:

1) For the mean value $g(x) = x$,

$$E[x] = \underline{x} = \int_{-\infty}^{\infty} x p(x)\, dx \tag{6.18}$$

2) For the mean square value $g(x) = x^2$,

$$E[x^2] = \underline{x^2} = \int_{-\infty}^{\infty} x^2 p(x)\, dx \tag{6.19}$$

3) For the variance $g(x) = (x - \underline{x})^2$,

$$\sigma_x^2 = E[(x - \underline{x})^2] = \int_{-\infty}^{\infty} (x - \underline{x})^2 p(x)\, dx$$

$$\underline{x^2} - (\underline{x})^2 = E[x^2] - (E[x])^2 \tag{6.20}$$

6.5 Properties of the Autocorrelation Function

The autocorrelation function for an ergodic process reads

$$R_x(\tau) = \lim_{T \to \infty} \frac{1}{T} \int_{-T/2}^{T/2} x(t)x(t + \tau)\, dt \tag{6.21}$$

1) Now consider the function $R_x(-\tau)$, which can be written as

$$R_x(-\tau) = \lim_{T \to \infty} \frac{1}{T} \int_{-T/2}^{T/2} x(t)x(t - \tau)\, dt \tag{6.22}$$

Making the transformation $t - \tau = \lambda$, we get

$$R_x(-\tau) = \lim_{T \to \infty} \frac{1}{T} \int_{-T/2-\tau}^{T/2-\tau} x(\lambda + \tau)x(\lambda)\, d\lambda \tag{6.23}$$

and because the integration is made for $T \to \infty$, we can write

$$R_x(-\tau) = \lim_{T \to \infty} \frac{1}{T} \int_{-T/2}^{T/2} x(\lambda + \tau)x(\lambda)\, d\lambda$$

$$= \lim_{T \to \infty} \frac{1}{T} \int_{-T/2}^{T/2} x(t + \tau)x(t)\, dt \tag{6.24}$$

and thus we conclude from Eqs. (6.21) and (6.24) that

$$R_x(\tau) = R_x(-\tau) \tag{6.25}$$

Hence we conclude that the autocorrelation function is an even function.

2) Consider the integral

$$\lim_{T\to\infty} \frac{1}{T} \int_{-T/2}^{T/2} [x(t) \pm x(t+\tau)]^2 \, dt \geq 0$$

$$= \lim_{T\to\infty} \frac{1}{T} \int_{-T/2}^{T/2} [x(t)]^2 \, dt \pm 2 \lim_{T\to\infty} \frac{1}{T} \int_{-T/2}^{T/2} x(t)x(t+\tau) \, dt$$

$$+ \lim_{T\to\infty} \frac{1}{T} \int_{-T/2}^{T/2} [x(t+\tau)]^2 \, dt \geq 0 \qquad (6.26a)$$

or

$$\lim_{T\to\infty} \frac{1}{T} \int_{-T/2}^{T/2} [x(t) \pm x(t+\tau)]^2 \, dt = R_x(0) \pm 2R_x(\tau) + R_x(0) \geq 0 \quad (6.26b)$$

Thus,

$$R_x(0) \geq |R_x(\tau)| \qquad (6.27)$$

Hence we conclude that the maximum value of $R_x(\tau)$ will be for $\tau = 0$ and is equal to ψ_x^2 because

$$R_x(0) = \lim_{T\to\infty} \frac{1}{T} \int_{-T/2}^{T/2} [x(t)]^2 \, dt = \psi_x^2 \qquad (6.28)$$

6.6 Power Spectral Density Function

Consider the sample $f(t)$ of an ergodic process and its autocorrelation function, which can be written as

$$R_f(\tau) = \lim_{T\to\infty} \frac{1}{T} \int_{-T/2}^{T/2} f(t)f(t+\tau) \, dt \qquad (6.29)$$

We define a new function $S_f(\omega)$ as the Fourier transform of the autocorrelation function that will be called the power spectral density function, and we write

$$S_f(\omega) = \int_{-\infty}^{\infty} R_f(\tau)e^{-i\omega\tau} \, d\tau \qquad (6.30)$$

This implies that the autocorrelation function is the inverse Fourier transform of $S_f(\omega)$, or

$$R_f(\tau) = \frac{1}{2\pi} \int_{-\infty}^{\infty} S_f(\omega)e^{i\omega\tau} \, d\omega \qquad (6.31)$$

and we observe the following:

1) $S_f(\omega)$ does not furnish any new information since $R_f(\tau)$ is its Fourier transform, and thus the information contained in one is the same as the information contained in its transform. However, $S_f(\omega)$ gives us the information in the frequency domain while $R_f(\tau)$ gives us the information in the time domain, and, depending on the application, one may be more convenient than the other.

2) From Eq. (6.31), we notice that since $R_f(\tau)$ has dimension $[x^2]$, the dimension of $S_f(\omega)$ is $[x^2]$ per unit frequency.

6.7   Properties of the Power Spectral Density Function

6.7.1   The Power Spectral Density Function Is a Positive Function

Consider Eq. (6.31) for τ equal to zero, which reads

$$R_f(0) = \psi_f^2 = \frac{1}{2\pi} \int_{-\infty}^{\infty} S_f(\omega)\,d\omega \tag{6.32}$$

Because ψ_f^2 is definitely positive, we conclude that $S_f(\omega)$ is a positive function. Furthermore, if $f(t)$ is a function measured in volts, the mean square value ψ_f^2 will represent the potential dissipated in a resistance of 1 Ω. Thus, $S_f(\omega)/2\pi$ will represent the power spectral density of the potential, and, from physical considerations, we also conclude that $S_f(\omega) \geq 0$.

6.7.2   The Power Spectral Density Function Is an Even Function

Considering Eq. (6.30) and because $R_f(\tau) = R_f(-\tau)$, we can write

$$S_f(\omega) = \int_{-\infty}^{\infty} R_f(-\tau)e^{-i\omega\tau}\,d\tau \tag{6.33}$$

Making the transformation $\tau = -\sigma$, Eq. (6.33) reads

$$S_f(\omega) = - \int_{\infty}^{-\infty} R_f(\sigma)e^{i\omega\sigma}\,d\sigma = \int_{-\infty}^{\infty} R_f(\sigma)e^{i\omega\sigma}\,d\sigma = S_f(-\omega) \tag{6.34}$$

and we conclude that $S_f(\omega)$ is an even function of ω.

6.7.3   Representation of the Power Spectral Density Function in the Positive Domain

Consider Eq. (6.30), which can be written as

$$S_f(\omega) = \int_{-\infty}^{\infty} R_f(\tau)e^{-i\omega\tau}\,d\tau$$

$$= \int_{-\infty}^{\infty} R_f(\tau)[\cos\omega\tau - i\sin\omega\tau]\,d\tau$$

$$= \int_{-\infty}^{\infty} R_f(\tau)\cos\omega\tau\,d\tau - i \int_{-\infty}^{\infty} R_f(\tau)\sin\omega\tau\,d\tau \tag{6.35}$$

The second integral vanishes because $R_f(\tau)$ is an even function of τ, and we write

$$S_f(\omega) = \int_{-\infty}^{\infty} R_f(\tau)\cos\omega\tau\,d\tau$$

and, because $R_f(\tau)$ is an even function of τ, we get

$$S_f(\omega) = 2 \int_0^{\infty} R_f(\tau)\cos\omega\tau\,d\tau \tag{6.36}$$

Because $R_f(\tau)$ is a real function, we conclude that $S_f(\omega)$ is a real even function. Using Eq. (6.31), we can write

$$R_f(\tau) = \frac{1}{\pi} \int_0^\infty S_f(\omega)\cos\omega\tau \, d\omega \qquad (6.37)$$

The set of Eqs. (6.36) and (6.37) are known as Wiener–Khintchine equations and represent, except for the factor 2, a pair of cosine Fourier transforms. The great advantage of working with Eqs. (6.36) and (6.37) is that they do not contain negative frequencies.

6.8 White Noise and Narrow and Large Bandwidth

The power spectral density function provides the necessary information on the frequency decomposition of a random process. Now if the frequency decomposition is concentrated in turns of a peak frequency ω_0 as shown in Fig. 6.4a, we call such distribution a narrow bandwidth distribution. This is in contrast to the distribution given in Fig. 6.4b, where we have an equal frequency distribution in a large band, and we call such distribution a large bandwidth distribution. Now, if $S_f(\omega)$ is a constant for all the frequency decompositions, i.e., from $-\infty$ to ∞ as shown in Fig. 6.4c, we define such distribution as white noise; this is in comparison with the white light distribution, which has a plain spectral
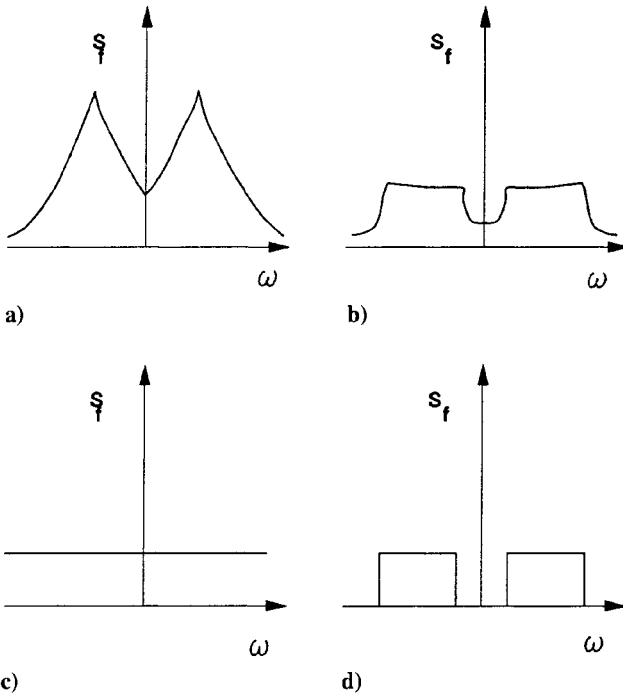
Fig. 6.4   Narrow, large bandwidth and white noise distributions.

distribution in the large visible band frequency. In many practical cases, processes having distributions as shown in Fig. 6.4d with an equal distribution in a large band of frequency can be considered as white noise distribution for practical purposes.

6.9 Single-Degree-of-Freedom Response

The response $x(t)$ of a linear single-degree-of-freedom system due to an external applied load $f(t)$, whether a deterministic or random excitation, can be written in terms of Duhamel's convolution integral as

$$x(t) = \int_0^t f(t)h(t - \tau)\,d\tau = \int_0^t f(t - \lambda)h(\lambda)\,d\lambda \qquad (6.38)$$

Now, for random excitation, we can extend the integration to $-\infty$, and we write

$$x(t) = \int_{-\infty}^t f(t - \lambda)h(\lambda)\,d\lambda \qquad (6.39)$$

Making the transformation $t - \lambda = \sigma$, we get

$$x(t) = -\int_\infty^0 f(\sigma)h(t - \sigma)\,d\sigma = \int_0^\infty f(\sigma)h(t - \sigma)\,d\sigma$$

$$= \int_0^\infty f(t - \tau)h(\tau)\,d\tau \qquad (6.40)$$

Again, for random excitation, we can extend the integration to $-\infty$, and we write

$$x(t) = \int_{-\infty}^\infty f(t - \tau)h(\tau)\,d\tau = \int_{-\infty}^\infty f(\tau)h(t - \tau)\,d\tau \qquad (6.41)$$

The Fourier transform of the response reads

$$X(\omega) = \int_{-\infty}^\infty x(t)e^{-i\omega t}\,dt \qquad (6.42)$$

and using Eqs. (6.41) and (6.42), we obtain

$$X(\omega) = \int_{-\infty}^\infty e^{-i\omega t}\left[\int_{-\infty}^\infty f(t - \tau)h(\tau)\,d\tau\right]dt$$

$$= \int_{-\infty}^\infty f(\tau)\left[\int_{-\infty}^\infty e^{-i\omega t}h(t - \tau)\,dt\right]d\tau \qquad (6.43)$$

Now making the transformation $\sigma = t - \tau$ in the internal integration, we obtain

$$X(\omega) = \int_{-\infty}^\infty f(\tau)\left[\int_{-\infty}^\infty e^{-i\omega(\sigma+\tau)}h(\sigma)\,d\sigma\right]d\tau$$

$$= \int_{-\infty}^\infty f(\tau)e^{-i\omega\tau}\,d\tau \int_{-\infty}^\infty e^{-i\omega\sigma}h(\sigma)\,d\sigma \qquad (6.44)$$

or

$$X(\omega) = F(\omega) \int_{-\infty}^{\infty} e^{-i\omega\sigma} h(\sigma)\,d\sigma \tag{6.45}$$

where $F(\omega)$ is the Fourier transform of $f(t)$. Now, for the single-degree-of-freedom response, we deduced in Chapter 2 the relation

$$X(\omega) = H(\omega)F(\omega) \tag{6.46}$$

Thus, we conclude from Eqs. (6.45) and (6.46) that

$$H(\omega) = \int_{-\infty}^{\infty} e^{-i\omega\sigma} h(\sigma)\,d\sigma \tag{6.47}$$

This shows that the complex frequency response function $H(\omega)$ is the Fourier transform of the unit impulsive function $h(t)$.

Considering now a random ergodic excitation $f(t)$ to a single-degree-of-freedom mechanical system, we can write the mean value of the response $\underline{x}$ as

$$\underline{x} = E[x(t)] = E \int_{-\infty}^{\infty} h(\lambda)f(t-\lambda)\,d\lambda \tag{6.48}$$

and, because the system is linear, we can invert the order of the mean and the integration operations to write

$$\underline{x} = E[x(t)] = \int_{-\infty}^{\infty} E[h(\lambda)f(t-\lambda)\,d\lambda] \tag{6.49}$$

Now the mean operation is made on time. Hence, we obtain

$$\underline{x} = E[x(t)] = \int_{-\infty}^{\infty} h(\lambda)[Ef(t-\lambda)]\,d\lambda \tag{6.50}$$

and, because the process is ergodic, we have

$$E[f(t-\lambda)] = \underline{f} \tag{6.51}$$

Thus,

$$\underline{x} = E[x(t)] = \underline{f} \int_{-\infty}^{\infty} h(\lambda)\,d\lambda = \text{const} \tag{6.52}$$

Using Eq. (6.47) for $\omega = 0$, we get

$$\underline{x} = H(0)\underline{f} = \text{const} \tag{6.53}$$

In the sequel, we will calculate the autocorrelation function of the response to a single degree of freedom due to an ergodic external excitation. Using Eq. (6.41), we can write

$$x(t) = \int_{-\infty}^{\infty} f(\lambda_1)h(t-\lambda_1)\,d\lambda_1$$

$$x(t+\tau) = \int_{-\infty}^{\infty} f(\lambda_2)h(t+\tau-\lambda_2)\,d\lambda_2 \tag{6.54}$$

150   STRUCTURAL DYNAMICS IN AERONAUTICAL ENGINEERING

and, for the autocorrelation function, we write

$$R_x(\tau) = E[x(t)x(t + \tau)]$$

$$= E\left[\int_{-\infty}^{\infty} f(\lambda_1)h(t - \lambda_1)\,d\lambda_1 \int_{-\infty}^{\infty} f(\lambda_2)h(t + \tau - \lambda_2)\,d\lambda_2\right]$$

$$= \iint_{-\infty}^{\infty} h(\lambda_1)h(\lambda_2)E[f(t - \lambda_1)f(t + \tau - \lambda_2)]\,d\lambda_1\,d\lambda_2 \tag{6.55}$$

Again, because the excitation process is ergodic, we can write

$$E[f(t - \lambda_1)f(t + \tau - \lambda_2)] = R_f(\tau + \lambda_1 - \lambda_2) \tag{6.56}$$

Thus, the autocorrelation function can be written as

$$R_x(\tau) = \iint_{-\infty}^{\infty} h(\lambda_1)h(\lambda_2)R_f(\tau + \lambda_1 - \lambda_2)\,d\lambda_1\,d\lambda_2 \tag{6.57}$$

From Eqs. (6.53) and (6.57), we conclude that the mean value of the response and the autocorrelation function of the response of an ergodic external excitation do not depend on the time t. Hence, we conclude that the response of an ergodic excitation is also an ergodic process. In the sequel, we will calculate the power spectral density function of the response. Using the definition of the power spectral density function and Eq. (6.57), we can write

$$S_x(\omega) = \int_{-\infty}^{\infty} R_x(\tau)e^{-i\omega\tau}\,d\tau$$

$$= \iint_{-\infty}^{\infty} e^{-i\omega\tau}[h(\lambda_1)h(\lambda_2)R_f(\tau + \lambda_1 - \lambda_2)\,d\lambda_1\,d\lambda_2]\,d\tau \tag{6.58}$$

but the autocorrelation function of the excitation R_f is the inverse Fourier transform of S_f. Thus, we can write

$$R_f(\tau + \lambda_1 - \lambda_2) = \frac{1}{2\pi}\iint_{-\infty}^{\infty} S_f e^{i\omega(\tau+\lambda_1-\lambda_2)}\,d\omega \tag{6.59}$$

Substituting Eq. (6.59) into Eq. (6.58), we get

$$S_x(\omega) = \int_{-\infty}^{\infty} e^{-i\omega\tau}$$

$$\times \left\{\frac{1}{2\pi}\int_{-\infty}^{\infty} S_f(\omega)\left[\left[\int_{-\infty}^{\infty} h(\lambda_1)e^{i\omega\lambda_1}\,d\lambda_1\right]\right.\right.$$

$$\times \left.\left.\left[\int_{-\infty}^{\infty} h(\lambda_2)e^{-i\omega\lambda_2}\,d\lambda_2\right]\right]e^{i\omega\tau}d\omega\right\}\,d\tau \tag{6.60}$$

Using Eq. (6.47), we obtain

$$S_x(\omega) = \int_{-\infty}^{\infty} e^{-i\omega\tau}\left\{\frac{1}{2\pi}\int_{-\infty}^{\infty} S_f(\omega)H(-\omega)H(\omega)e^{i\omega\tau}\,d\omega\right\}\,d\tau \tag{6.61}$$

Because $H(-\omega)$ is the conjugate of $H(\omega)$, we can write

$$H(\omega)H(-\omega) = |H(\omega)|^2 \tag{6.62}$$

Substituting Eq. (6.62) into Eq. (6.61), we obtain

$$S_x(\omega) = \int_{-\infty}^{\infty} e^{-i\omega\tau} \left\{ \frac{1}{2\pi} \int_{-\infty}^{\infty} S_f(\omega)|H(\omega)|^2 e^{i\omega\tau}\,d\omega \right\} d\tau \tag{6.63}$$

Comparing Eqs. (6.58) and (6.63), we conclude that

$$R_x(\tau) = \frac{1}{2\pi} \int_{-\infty}^{\infty} S_f(\omega)|H(\omega)|^2 e^{i\omega\tau}\,d\omega \tag{6.64}$$

but from definition, we have

$$R_x(\tau) = \frac{1}{2\pi} \int_{-\infty}^{\infty} S_x(\omega) e^{i\omega\tau}\,d\omega \tag{6.65}$$

Comparing Eqs. (6.64) and (6.65), we conclude that

$$S_x(\omega) = |H(\omega)|^2 S_f(\omega) \tag{6.66}$$

Equation (6.66), which represents an algebraic relation between three functions, is a very important relation in structural dynamics. Knowing two of these functions through calculations or from experimental work, the third one can be easily obtained from Eq. (6.66). For instance, during ground vibration tests, $S_f(\omega)$ and $S_x(\omega)$ are obtained experimentally; thus, using Eq. (6.66), we can obtain $H(\omega)$, which in turn will determine all the modal characteristics of the mechanical system. On the other hand, knowing, for instance, the modal dynamic properties of a mechanical system $H(\omega)$, we can calculate $S_x(\omega)$ due to a statistically known function, e.g., the power spectral density function of continuous turbulence gust $S_f(\omega)$. From $S_x(\omega)$ and its inverse Fourier transform $R_x(\tau)$, we can calculate the statistical mean values of the response. Finally, knowing the modal dynamic properties of a mechanical system $H(\omega)$ and through repeated measurements of the responses $S_x(\omega)$ to an unknown external random excitation, we can use Eq. (6.66) to construct a model for $S_f(\omega)$, which can be used in future design.

6.10   Response to a White Noise

Consider a single-degree-of-freedom mechanical system subjected to an external random ergodic excitation having a power spectral density function given by a white noise with intensity S_0. Thus, we can write

$$S_f(\omega) = S_0 \tag{6.67}$$

Using Eq. (6.66), we can write the power spectral density function of the response as

$$S_x(\omega) = |H(\omega)|^2 S_0 \tag{6.68}$$

Now, for a single-degree-of-freedom system, the complex frequency response function $H(\omega)$ reads

$$H(\omega) = \frac{1/k}{(1 - \Omega^2) + 2i\gamma\Omega} \tag{6.69}$$

Hence,

$$|H(\omega)|^2 = H(\omega)H(-\omega)$$

$$= \frac{(1/k)^2}{[(1 - \Omega^2)^2 + 4\gamma^2\Omega^2]} \tag{6.70}$$

Substituting Eq. (6.70) into Eq. (6.68), we obtain

$$S_x(\omega) = \frac{(1/k)^2 S_0}{[(1 - \Omega^2)^2 + 4\gamma^2\Omega^2]} \tag{6.71}$$

The autocorrelation function of the response can be obtained from the inverse Fourier transform of $S_x(\omega)$ and reads

$$R_x(\tau) = \frac{1}{2\pi} \int_{-\infty}^{\infty} \frac{(1/k)^2 S_0 e^{i\omega\tau}\,d\omega}{[(1 - \Omega^2)^2 + 4\gamma^2\Omega^2]}$$

$$= \frac{1}{\pi} \int_0^{\infty} \frac{(1/k)^2 S_0 e^{i\omega\tau}\,d\omega}{[(1 - \Omega^2)^2 + 4\gamma^2\Omega^2]} \qquad \text{for } \tau \geq 0 \tag{6.72}$$

Integrating, we obtain

$$R_x(\tau) = \frac{S_0\omega_n e^{-\gamma\omega_n\tau}}{4\gamma k^2} \left[\cos\omega_d\tau + \frac{\gamma}{(1 - \gamma^2)^{\frac{1}{2}}} \sin\omega_d\tau \right] \qquad \text{for } \tau \geq 0 \tag{6.73}$$

and the mean square value of the response reads

$$\psi_x^2 = R_x(0) = \frac{S_0\omega_n}{4\gamma k^2} \tag{6.74}$$

6.11 Multidegree-of-Freedom Systems

6.11.1 Statistical Properties of Multirandom Processes

Cross probability distribution of random processes.   Consider the random processes $x(t)$ and $y(t)$. We can define the cross probability function or the second-order probability distribution function as

$$P(x, t) = \text{Prob}[x(t) \leq x; y(t) \leq y] \tag{6.75}$$

or, in terms of the specific probability distribution function, we can write

$$P(x, y) = \int_{-\infty}^{x} \int_{-\infty}^{y} p(\xi, \eta)\,d\xi\,d\eta \tag{6.76}$$

Therefore, we conclude that

$$\text{Prob}\,[x_1 \le x(t) \le x_2; y_1 \le y(t) \le y_2] = \int_{x_1}^{x_2} \int_{y_1}^{y_2} p(\xi, \eta)\, d\xi\, d\eta \qquad (6.77)$$

and we verify that

$$p(x, y) \ge 0$$

$$\int_{-\infty}^{\infty} \int_{-\infty}^{\infty} p(x, y)\, dx\, dy = 1 \qquad (6.78)$$

and we conclude that the specific probability distribution functions of the first order can be obtained from the specific probability distribution function of the second order because

$$\text{Prob}\,[x_1 \le x(t) \le x_2; -\infty \le y(t) \le \infty] = \int_{x_1}^{x_2} \left[\int_{-\infty}^{\infty} p(x, y)\, dy \right] dx$$

$$= \int_{x_1}^{x_2} p(x)\, dx \qquad (6.79)$$

where

$$p(x) = \int_{-\infty}^{\infty} p(x, y)\, dy \qquad (6.80)$$

In a similar manner, we conclude that

$$p(y) = \int_{-\infty}^{\infty} p(x, y)\, dx \qquad (6.81)$$

and two random variables are statistically independent if

$$p(x, y) = p(x)p(y) \qquad (6.82)$$

The mean value or the mathematical expectation of a continuous function $g(x, y)$ can be written as

$$E[g(x, y)] = \int_{-\infty}^{\infty} \int_{-\infty}^{\infty} g(x, y)p(x, y)\, dx\, dy \qquad (6.83)$$

Therefore, the mean values of $x(t)$ and $y(t)$ read

$$\underline{x} = E[x] = \int_{-\infty}^{\infty} \int_{-\infty}^{\infty} xp(x, y)\, dx\, dy = \int_{-\infty}^{\infty} xp(x)\, dx$$

$$\underline{y} = E[y] = \int_{-\infty}^{\infty} \int_{-\infty}^{\infty} yp(x, y)\, dx\, dy = \int_{-\infty}^{\infty} yp(y)\, dy \qquad (6.84)$$

The covariance of two random processes C_{xy} is defined as

$$C_{xy} = E[(x - \underline{x})(y - \underline{y})] = \int_{-\infty}^{\infty} \int_{-\infty}^{\infty} (x - \underline{x})(y - \underline{y})p(x, y)\, dx\, dy$$

$$= \underline{xy} - \underline{x}\,\underline{y} \qquad (6.85)$$

and the variances C_{xx} and C_{yy} read

$$C_{xx} = E[(x - \underline{x})^2] = \underline{x^2} - \{\underline{x}\}^2 = \sigma_{xx}^2$$

$$C_{yy} = E[(y - \underline{y})^2] = \underline{y^2} - \{\underline{y}\}^2 = \sigma_{yy}^2$$

(6.86)

Writing now,

$$\int_{-\infty}^{\infty} \int_{-\infty}^{\infty} \left[\frac{x - \underline{x}}{\sigma_x} \pm \frac{y - \underline{y}}{\sigma_y} \right]^2 \geq 0$$

(6.87)

we obtain

$$\frac{\sigma_x^2}{\sigma_x^2} \pm \frac{2C_{xy}}{\sigma_x \sigma_y} + \frac{\sigma_y^2}{\sigma_y^2} \geq 0$$

(6.88)

and we conclude that

$$\sigma_x \sigma_y \geq |C_{xy}|$$

(6.89)

and we define the correlation coefficient ρ_{xy} as

$$\rho_{xy} = \frac{C_{xy}}{\sigma_x \sigma_y}$$

(6.90)

and we conclude that $\rho_{xy} \, \varepsilon \, [-1, 1]$. When $C_{xy} = 0$, we will have two random variables that are statistically uncorrelated.

Statistical cross properties of stationary random processes. Consider two stationary random processes $x(t)$ and $y(t)$; following the same procedure and the same definitions previously given for a single stationary random process, we can write the mean values of the two stationary random processes as

$$\mu_x(t_1) = \mu_x = \text{const}$$

$$\mu_y(t_1) = \mu_y = \text{const}$$

$$C_{xx}(t_1, t_1 + \tau) = C_{xx}(\tau)$$

(6.91)

$$C_{yy}(t_1, t_1 + \tau) = C_{yy}(\tau)$$

$$C_{xy}(t_1, t_1 + \tau) = C_{xy}(\tau)$$

The autocorrelation functions $R_{xx}(\tau)$ and $R_{yy}(\tau)$ and the cross correlation function $R_{xy}(\tau)$, in terms of the specific probability distribution function $p(x, y)$, can

be expressed as

$$R_{xx}(\tau) = E[x_k(t)x_k(t + \tau)]$$

$$= \int_{-\infty}^{\infty} \int_{-\infty}^{\infty} x_k(t)x_k(t + \tau)p\{x_k(t)x_k(t + \tau)\}dx_k(t)dx_k(t + \tau)$$

$$R_{yy}(\tau) = E[y_k(t)y_k(t + \tau)]$$

$$= \int_{-\infty}^{\infty} \int_{-\infty}^{\infty} y_k(t)y_k(t + \tau)p\{y_k(t)y_k(t + \tau)\}dy_k(t)dy_k(t + \tau)$$

(6.92)

$$R_{xy}(\tau) = E[x_k(t)y_k(t + \tau)]$$

$$= \int_{-\infty}^{\infty} \int_{-\infty}^{\infty} x_k(t)y_k(t + \tau)p\{x_k(t)y_k(t + \tau)\}dx_k(t)dy_k(t + \tau)$$

and the covariance functions read

$$C_{xx}(\tau) = E[(x_k(t) - \mu_x)(x_k(t + \tau) - \mu_x)] = R_{xx}(\tau) - \mu_x^2$$

$$C_{yy}(\tau) = E[(y_k(t) - \mu_y)(y_k(t + \tau) - \mu_y)] = R_{yy}(\tau) - \mu_y^2 \quad (6.93)$$

$$C_{xy}(\tau) = E[(x_k(t) - \mu_x)(y_k(t + \tau) - \mu_y)] = R_{xy}(\tau) - \mu_x\mu_y$$

and we conclude that the covariance functions are identical to the cross correlation functions when the first mean values μ_x and μ_y are null. As was previously deduced for a single stationary random process, we can easily prove that

$$R_{xx}(\tau) = R_{xx}(-\tau) \qquad R_{yy}(\tau) = R_{yy}(-\tau) \qquad R_{xy}(\tau) = R_{xy}(-\tau)$$

(6.94)

$$R_{xx}(0) \geq |R_{xx}(\tau)| \qquad R_{yy}(0) \geq |R_{yy}(\tau)| \qquad R_{xx}(0)R_{yy}(0) \geq [R_{xy}(\tau)]^2$$

Statistical cross properties of ergodic random processes. Consider two stationary ergodic random processes $x(t)$ and $y(t)$; following the same procedure and the same definitions previously given for a single stationary random process, we can conclude that the statistical mean values of the two stationary ergodic random processes are given by the expressions in Eqs. (6.91–6.94) using only one sample and integrated in the time domain.

Power spectral density functions. Following the same procedure and the same definitions previously given for a single stationary random process, we can define the power spectral density functions of two stationary ergodic random processes as the Fourier transforms of their autocorrelation and cross correlation

functions, and we write

$$S_{xx}(\omega) = \int_{-\infty}^{\infty} R_{xx}(\tau)e^{-i\omega\tau}\,\mathrm{d}\tau$$

$$S_{yy}(\omega) = \int_{-\infty}^{\infty} R_{yy}(\tau)e^{-i\omega\tau}\,\mathrm{d}\tau \tag{6.95}$$

$$S_{xy}(\omega) = \int_{-\infty}^{\infty} R_{xy}(\tau)e^{-i\omega\tau}\,\mathrm{d}\tau$$

and, using the inverse Fourier transform definition, we write

$$R_{xx}(\tau) = \frac{1}{2\pi} \int_{-\infty}^{\infty} S_{xx}(\omega)e^{i\omega\tau}\,\mathrm{d}\omega$$

$$R_{yy}(\tau) = \frac{1}{2\pi} \int_{-\infty}^{\infty} S_{yy}(\omega)e^{i\omega\tau}\,\mathrm{d}\omega \tag{6.96}$$

$$R_{xy}(\tau) = \frac{1}{2\pi} \int_{-\infty}^{\infty} S_{xy}(\omega)e^{i\omega\tau}\,\mathrm{d}\omega$$

and we verify that

$$S_{xx}(\omega) = S_{xx}(-\omega) \qquad S_{yy}(\omega) = S_{yy}(-\omega) \qquad S_{xy}(\omega) = S_{xy}(-\omega) \tag{6.97}$$

Consider two stationary ergodic random processes $x(t)$ and $y(t)$; for a single ergodic random process we have proved that the complex frequency response function is the Fourier transform of the response due to a unit impulse excitation. Thus, for two ergodic random processes r and s, we can write

$$H_r(\omega) = \int_{-\infty}^{\infty} h_r(t)e^{-i\omega t}\,\mathrm{d}t$$

$$H_s(\omega) = \int_{-\infty}^{\infty} h_s(t)e^{-i\omega t}\,\mathrm{d}t \tag{6.98}$$

Now, let f be the external excitation, q the system response, and F and Q their Fourier transforms. Thus, we can write

$$Q_r(\omega) = |H_r(\omega)|F_r(\omega)$$

$$Q_s(\omega) = |H_s(\omega)|F_s(\omega) \tag{6.99}$$

The cross correlation function of the response reads

$$R_{q_r q_s}(\tau) = \lim_{T\to\infty} \frac{1}{T} \int_{-T/2}^{T/2} q_r(t)q_s(t+\tau)\,\mathrm{d}t$$

$$= \int_{-\infty}^{\infty}\int_{-\infty}^{\infty} h_r(\lambda_r)h_s(\lambda_s)R_{f_r f_s}(\tau+\lambda_r-\lambda_s)\,\mathrm{d}\lambda_r\lambda_s \tag{6.100}$$

where $R_{q_r q_s}$ is the cross correlation function of the excitation. Applying the Fourier transform to Eq. (6.100), we obtain

$$S_{q_r q_s}(\omega) = \int_{-\infty}^{\infty} R_{q_r q_s}(\tau)\, e^{-i\omega\tau} \, d\tau \qquad (6.101)$$

and using Eqs. (6.99) and (6.100) in Eq. (6.101), we get

$$S_{q_r q_s}(\omega) = H_r^*(\omega)\, H_s(\omega)\, S_{f_r f_s}(\omega) \qquad (6.102)$$

where $H_r^*(\omega)$ is the conjugate of $H_r(\omega)$.

6.11.2 System Response to Multirandom Excitation

Consider the equations of motion of an nth degree-of-freedom linear system subject to an external excitation ergodic force vector $P(t)$,

$$[M]\{x''\} + [C]\{x'\} + [K]\{x\} = \{P(t)\} \qquad (6.103)$$

The system being linear, the response $x(t)$ will be also ergodic. Making the modal transformation,

$$\{x\} = [N]\{q\} \qquad (6.104)$$

where $[N]$ is the matrix of the autonormal modes (i.e., we are using eigenvectors normalized to obtain a unit generalized mass matrix), the generalized mass, generalized stiffness, and generalized damping matrices read

$$[N]^T[M][N] = \lceil I \rfloor$$

$$[N]^T[K][N] = \lceil \omega_i^2 \rfloor \qquad (6.105)$$

$$[N]^T[C][N] = \lceil 2\omega_i \gamma_i \rfloor$$

where ω_i and γ_i are the undamped natural frequency and the modal damping ratio of the mode i, respectively. Using Eqs. (6.103–6.105), we obtain the system uncoupled equations of motion in the form

$$q_i'' + 2\gamma_i \omega_i q_i' + \omega_i^2 q_i = f_i(t) \qquad (6.106)$$

where $f_i(t)$ is the modal generalized force and reads

$$f_i(t) = [N]^T\{P(t)\} \qquad (6.107)$$

The Fourier transforms of the modal amplitude $q_i(t)$ and the generalized force $f_i(t)$ read

$$Q_i(\omega) = \int_{-\infty}^{\infty} q_i(t) e^{i\omega t} \, dt$$

$$\qquad (6.108)$$

$$F_i(\omega) = \int_{-\infty}^{\infty} f_i(t) e^{i\omega t} \, dt$$

Applying now the Fourier transform to Eq. (6.106), we obtain

$$Q_r(\omega) = H_r(\omega) F_r(\omega) \qquad (6.109)$$

where

$$H_r(\omega) = \frac{1}{1 - \Omega^2 + 2i\gamma_r\Omega} \quad \text{and} \quad \Omega = \frac{\omega}{\omega_r} \qquad (6.110)$$

We proceed now to calculate the cross correlation matrix $[R_{x_i x_j}(\tau)]$, and we write

$$\left[R_{x_i x_j}(\tau)\right] = \lim_{\tau \to \infty} \frac{1}{T} \int_{-T/2}^{T/2} \{x(t)\} \{x(t+\tau)\}^T \, dt \qquad (6.111)$$

and, making the modal transformation, we obtain

$$\left[R_{x_i x_j}(\tau)\right] = [N] \left[R_{q_r q_s}(\tau)\right] [N]^T \qquad (6.112)$$

where

$$\left[R_{q_r q_s}(\tau)\right] = \lim_{\tau \to \infty} \frac{1}{T} \int_{-T/2}^{T/2} \{q_r(t)\} \{q_s(t+\tau)\}^T \, dt \qquad (6.113)$$

Now, writing Eq. (6.102) in matrix form, we get

$$\left[S_{q_r q_s}(\omega)\right] = \lceil H^*(\omega)\rfloor \left[S_{f_r f_s}(\omega)\right] \lceil H(\omega)\rfloor \qquad (6.114)$$

and, using the inverse Fourier transform definition, we write

$$\left[R_{q_r q_s}(\tau)\right] = \frac{1}{2\pi} \int_{-\infty}^{\infty} \lceil H^*(\omega)\rfloor \left[S_{f_r f_s}(\omega)\right] \lceil H(\omega)\rfloor e^{i\omega\tau} \, d\omega \qquad (6.115)$$

where $[S_{f_r f_s}(\omega)]$ are related to the generalized modal forces. The inverse Fourier transform of $[S_{f_r f_s}(\omega)]$ reads

$$\left[S_{f_r f_s}(\omega)\right] = \int_{-\infty}^{\infty} \left[R_{f_r f_s}(\tau)\right] e^{-i\omega\tau} \, d\tau \qquad (6.116)$$

where $[R_{f_r f_s}(\tau)]$ are related to the generalized modal amplitude and, in the physical degree-of-freedom base, read

$$\left[S_{f_r f_s}(\omega)\right] = [N] \int_{-\infty}^{\infty} \left[R_{P_r P_s}(\tau)\right] e^{-i\omega\tau} \, d\tau [N]^T \qquad (6.117)$$

Thus,

$$\left[S_{f_r f_s}(\omega)\right] = [N] \left[S_{P_r P_s}(\omega)\right] [N]^T \qquad (6.118)$$

The solution thus proceeds as follows: having the Fourier transform matrix $[S_{P_r P_s}(\omega)]$ of the correlation matrix $[R_{P_r P_s}(\tau)]$ in the physical base, Eq. (6.118) is used to obtain the power spectral density matrix in the modal base. This in turn is used in Eq. (6.115) to obtain $[R_{q_r q_s}(\tau)]$. Finally, using Eq. (6.112), the correlation matrix $[R_{x_r x_s}(\tau)]$ in the physical degree of freedom x is deduced, and its Fourier transform will produce the power spectral density function $[S_{x_r x_s}(\omega)]$ in the physical degree of freedom x. We further notice that, in ground vibration tests, if $[S_{F_r F_s}(\omega)]$ is a white noise, the information contained in $[S_{x_r x_s}(\omega)]$ will furnish directly the structure modal properties, i.e., the modal generalized mass, stiffness, damping, and corresponding mode shape.

References

[1] Clough, R. W., and Penzien, J., *Dynamics of Structures*, McGraw–Hill, New York, 1975.

[2] Meirovitch, L., *Elements of Vibration Analysis*, McGraw–Hill, New York, 1975.

[3] Harris, C. M., and Crede, C. E., *Shock and Vibration Handbook*, 2nd ed., McGraw–Hill, New York, 1976.

[4] Bendat, J. S., and Piersol, A. G., *Random Data: Analysis and Measurement Procedures*, Wiley, New York, 1971.

[5] Warburton, G. W., *The Dynamical Behaviour of Structures*, 2nd ed., Pergamon, Oxford, England, UK, 1976.

Problems

6.1 A damped single-degree-of-freedom linear system is excited by a random ergodic external force having a power spectral density function given by $S_f(\omega) = S_0$ for $(-\omega_0, \omega_0)$ and $S_f(\omega) = 0$ for $\omega \leq -\omega_0$ and $\omega \geq \omega_0$. The system has a damping ratio $c/c_{cr} = 0.05$ and a natural undamped frequency equal to $-\omega_0/2$. Find the power spectral density function of the response.

6.2 Given the function $x(t) = A \sin(2\pi/T)t$ find its autocorrelation and power spectral density functions.

6.3 A periodic function $y(t)$ with a period T is defined as $y(t) = A$ for $0 \leq t \leq T/2$ and $y(t) = 0$ for $T/2 \leq t \leq T$. Find its autocorrelation and power spectral density functions.

6.4 Obtain the cross correlation functions of the functions $x(t)$ and $y(t)$ given in Problems 6.2 and 6.3 and their cross power spectral density functions.

This page intentionally left blank

<div align="right">

7

</div>

The Typical Section in Aeroelasticity

7.1 Single-Degree-of-Freedom Stability

Consider the single-degree-of-freedom mechanical system shown in Fig. 7.1. The system consists of a concentrated mass m (kg), a spring with a spring constant k (N/m), and a dashpot having a viscous damping coefficient c (N·s/m). The external applied load is $F(t)$ (N), and the displacement $x(t)$ (m) is measured from the position of equilibrium. The potential energy stored at any instant of time t measured from the position of equilibrium can be written as

$$U = \int_0^x kx \, \mathrm{d}x = \frac{1}{2} kx^2 \tag{7.1}$$

The kinetic energy of the mass m reads

$$T = \tfrac{1}{2}mx'^2 \tag{7.2}$$

where $x' = \mathrm{d}x/\mathrm{d}t$. The system dissipation function can be expressed as

$$D = \tfrac{1}{2}cx'^2 \tag{7.3}$$

Applying Lagrange's equation of motion,

$$(\mathrm{d}L/\mathrm{d}x)' - \mathrm{d}L/\mathrm{d}x + \mathrm{d}D/\mathrm{d}x' = Q \tag{7.4}$$

where $L = T - U$ and Q is the generalized force corresponding to the degree of freedom x, we obtain

$$mx'' + cx' + kx = F(t) \tag{7.5}$$

This single-degree-of-freedom mechanical system has been studied in detail in Chapter 2. For a structural dynamic system, m, c, and k are real positive constants. We learned in courses on structural dynamics that the system is stable, in the sense that, if the system is subjected to an initial disturbance, following for instance an impulsive force $F(t) = F_0\delta(t)$ where $\delta(t)$ is a Dirac–delta function, the response of the system $x(t)$ decays asymptotically to zero. Furthermore, we know that when the damping ratio $\gamma^2 < 1$, $[\gamma = c/c_{cr} = c/2(km)^{1/2}]$. Therefore, when $c^2 < 4km$, the response is a damped oscillation, having a frequency of oscillation given by the damped natural frequency of the mechanical system $\omega_d = \omega_0(1 - \gamma^2)^{1/2}$, where $\omega_0 = (k/m)^{1/2}$ is the mechanical system undamped natural frequency. A typical response in such a case is shown in Fig. 7.2.

Whereas, when $c^2 > 4km$, the response is again stable but is a nonoscillatory motion. A typical response in such a case is shown in Fig. 7.3.

Now, consider the same mechanical system shown in Fig. 7.1, with the inclusion of nonconservative forces, i.e., forces that do not derive from a potential and are

<div align="center">

161

</div>
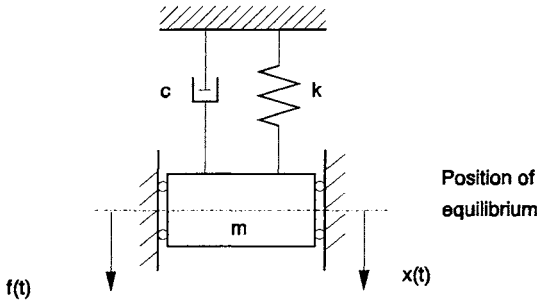
Fig. 7.1   Single-degree-of-freedom mechanical system.

inherent to the system, i.e., they are not externally applied loads in the sense that their presence is due to the change in the position of the generalized coordinate. In aeroelasticity, we call such forces incremental aerodynamic forces due to motion. Let these forces be proportional to the displacement and the velocity of the single-degree-of-freedom mechanical system. The equation of motion in this case can be written as

$$mx'' + cx' + kx = F(t) + c_1 x' + k_1 x \qquad (7.6)$$

or

$$mx'' + c_{\text{eff}}x' + k_{\text{eff}}x = F(t) \qquad (7.7)$$

where $c_{\text{eff}} = c - c_1$ is the effective damping of the system configuration and $k_{\text{eff}} = k - k_1$ is the effective stiffness of the system configuration. Consider first the case when $k_1 = 0$ and $c_1 \neq 0$. Now if c_1 is real and positive and is less than c, the behavior of the system is as previously discussed and is stable. If c_1 is real, positive, and greater than c, we say that the system has a negative effective damping, and
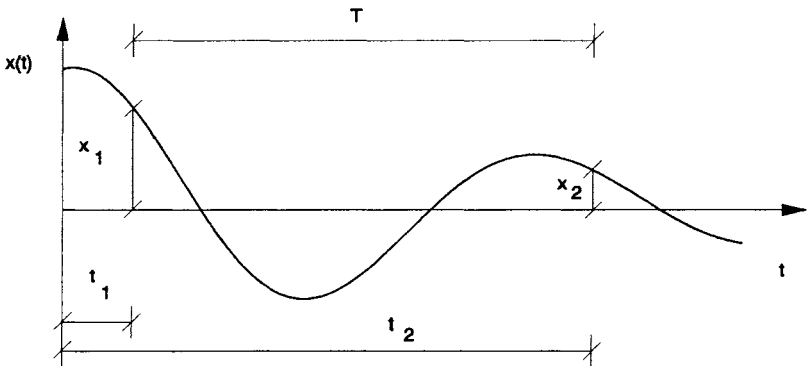
Fig. 7.2   Response of a single-degree-of-freedom mechanical system due to an external disturbance when the damping parameter c^2 is less than $4km$ and $T = 2\pi/\omega_d = 1/f_d$. Curve is plotted for $\gamma = 0.15$.
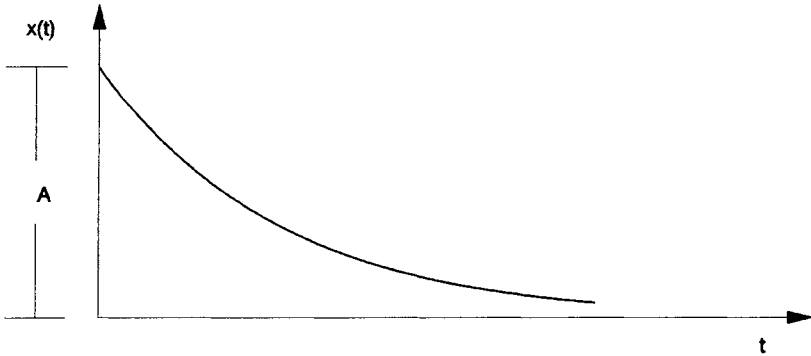
Fig. 7.3   Response of a single-degree-of-freedom mechanical system due to an external disturbance when the damping parameter c^2 is greater than $4km$.

the system response will be oscillatory divergent if $c_{eff}^2 < 4km$ or will be a pure nonoscillatory divergent motion if $c_{eff}^2 > 4km$. Typical responses in such cases are shown in Figs. 7.4 and 7.5.

Such systems have been called dynamically unstable systems or possess a flutter-type instability. It is instructive to notice that the instability is inherent to the system configuration, i.e., it is a system configuration property and has nothing to do with the external applied force $F(t)$ or the nature of its origin. The instability is a property of the system and depends only on the parameter c_1, which in turn is a system configuration property. Furthermore, we notice that the borderline of the stability is at the configuration when c_{eff} is zero. In this case, we have a simple harmonic motion response with a frequency equal to the undamped natural frequency of the mechanical system. We call this condition the critical condition, and it separates the stable behavior, i.e., $c_{eff} > 0$, from the unstable behavior, i.e., $c_{eff} < 0$. Finally,
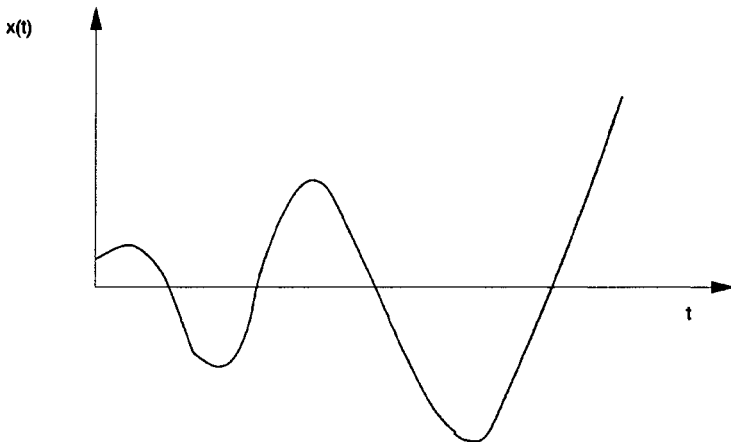
Fig. 7.4   Response of a single-degree-of-freedom unstable system due to an external disturbance when the damping c_{eff} is negative and c^2 is less than $4km$.
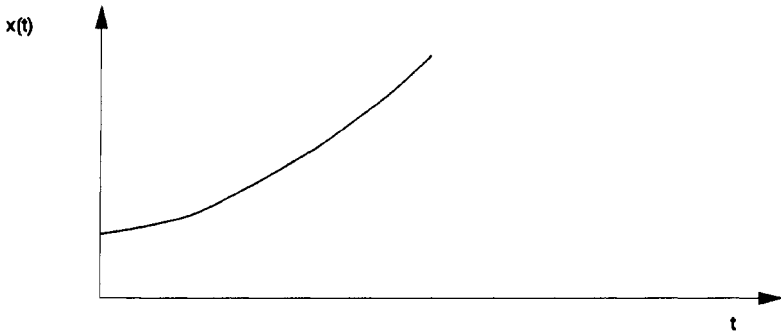
Fig. 7.5   Response of a single-degree-of-freedom unstable system due to an external disturbance when the damping c_{eff} is negative and c^2 is greater than $4km$.

it should be observed that situations as shown in Fig. 7.5 are scarcely encountered in practice, principally in aeroelasticity where c_1 is generally a function of the vehicle forward speed. Therefore, physically the situation of Fig. 7.4 will happen before (i.e., at a lesser forward speed) that of Fig. 7.5.

We now consider the case when c_{eff} is positive and $k_1 \neq 0$. When k_{eff} is real and positive, the system is stable as discussed in the beginning of this section, and the system behavior is as shown in Fig. 7.2 and 7.3. Now, when k_{eff} is less than 0, i.e., $k_1 > k$, the solution of the differential equation shows that the system is unstable, i.e., the response due to an initial disturbance will grow exponentially with time in a pure nonoscillatory divergent motion. The borderline of the stability will be obtained when $k_{\text{eff}} = 0$ and again will be called the critical condition, i.e., the condition that separates the stable system configuration from the unstable system configuration. This phenomenon has been called static divergence or static aeroelastic phenomenon. This denomination bears its origin from the fact that the instability can be explained using the effective stiffness term alone. However, the phenomenon is clearly a dynamic one. For it to happen, we must have $k_1 > k$, and $k_1 x$ is due to motion; therefore, the instability bears its origin from a dynamic phenomenon.

From this simple exposition, based on the behavior of a single-degree-of-freedom mechanical system in the presence of nonconservative forces, several important facts have been observed:

1) The equation of motion is written from an initial state of equilibrium.

2) The stability of the system is studied from this initial state of equilibrium.

3) The problem of stability of motion is a system configuration property and has nothing to do with the origin of the external applied force.

4) The borderlines of stability are obtained when $c_{\text{eff}} = 0$ or $k_{\text{eff}} = 0$.

In the next section, we will study the origin of the nonconservative forces as applied in aeroelasticity for a simple structural configuration, namely the typical section.

7.2   The Typical Section

In this section, the quasisteady aerodynamic assumption for the representation of the incremental nonstationary aerodynamic loads will be made. According to this assumption, the aerodynamic characteristics of an airfoil motion are equal at
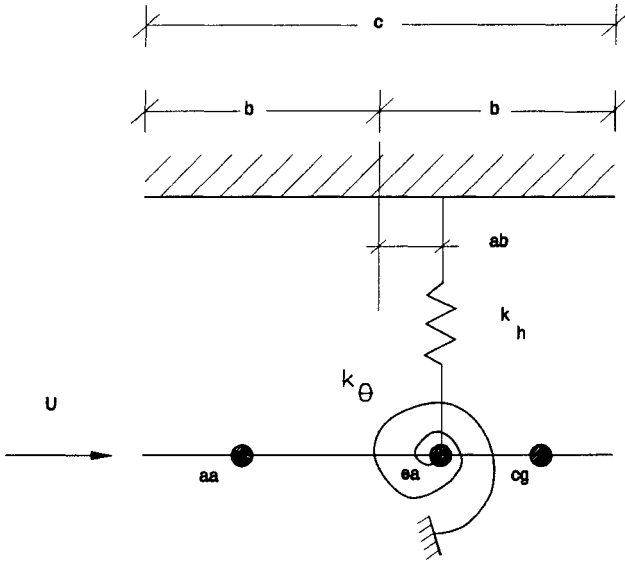
Fig. 7.6 Typical section system in an initial state of equilibrium.

any instant of time to the characteristics of the same airfoil, moving with constant linear and angular velocities equal to the actual instantaneous values. The quasi-steady aerodynamic assumption introduces great simplifications to the problem formulation, while the main physical features of the problem are not masked by mathematical complications. These simplifications are later removed, and the non-stationary incremental loads will be formulated using a linearized potential theory. Furthermore, limitations in this section will be made to two-dimensional flows. Treatment of finite span effect will be made using the strip theory assumption, and, according to this theory, the aerodynamic characteristics at any spanwise station will be considered as the same as if the airfoil sections were situated in a two-dimensional flow, with no spanwise interactions. Again, later these simplifications will be removed.

Consider a flat plate in a potential flow with a velocity at infinity U in the x-direction parallel to the plate as shown in Fig. 7.6. Let the plate have two degrees of freedom as shown in Fig. 7.7, a vertical translation h, and a rotation θ of the elastic axis of the airfoil. The translation coordinate h will be measured positive downward and the rotational degree of freedom θ is taken positive for nose-up motion. Both coordinates are measured from the initial position of equilibrium of the flat plate.

The potential energy functional at any instant of time, measured from the initial state of equilibrium, can be written as

$$U = \int_0^h k_h h \, \mathrm{d}h + \int_0^\theta k_\theta \theta \, \mathrm{d}\theta$$

$$= \tfrac{1}{2} k_h h^2 + \tfrac{1}{2} k_\theta \theta^2 \tag{7.8}$$
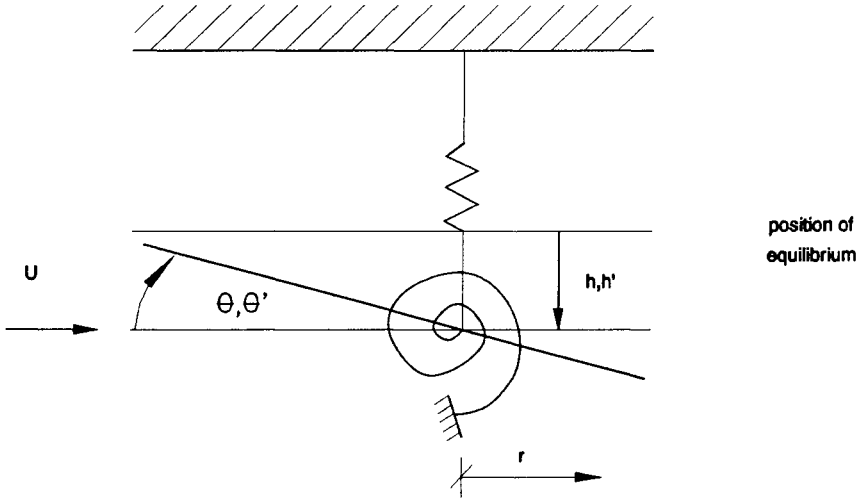
Fig. 7.7   Typical section system configuration after an external disturbance.

For an element of mass dm of the plate located at a position r, measured from the elastic axis position ea, we can write an expression of the kinetic energy as

$$dT = \tfrac{1}{2}(h' + r\theta')^2 dm \tag{7.9}$$

Integrating for the whole section, we obtain

$$T = \tfrac{1}{2}mh'^2 + S_w h'\theta' + \tfrac{1}{2}I_\theta \theta'^2 \tag{7.10}$$

where $m = \int dm$ = total mass per unit span, $S_w = \int r\,dm$ = static mass moment per unit span about the elastic axis, and $I_\theta = \int r^2 dm$ = moment of inertia about the elastic axis per unit span. Considering that the system possesses a viscous structural damping, we can write for the structural damping representation a dissipation function as

$$D = \tfrac{1}{2}c_h h'^2 + \tfrac{1}{2}c_\theta \theta'^2 \tag{7.11}$$

Using the quasisteady aerodynamic theory, we can write expressions for the incremental aerodynamic lift L and the incremental aerodynamic moment M about the elastic axis ea as

$$Q_h = -L = -\frac{1}{2}\rho U^2 c \frac{dc_L}{d\alpha}\alpha$$

$$M = M_{aa} + L\left(\frac{b}{2} + ab\right) \tag{7.12}$$

In the first equation of Eq. 7.12, the generalized force Q_h is positive downward, and the lift L is positive upward for a positive incremental angle of attack α, and ρ is the free stream air density. In the second equation of Eq. 7.12, M_{aa} is the aerodynamic moment about the aerodynamic center due to incremental airloads,

and the aerodynamic center has been assumed as acting at the 1/4 chordwise position. The incremental angle of attack α is due to the incremental angle of rotation θ, the incremental vertical velocity h', and the incremental rotational velocity θ' and, at any chordwise station r, can be written as

$$\alpha_x = \theta + \frac{h'}{U} + \frac{\theta'r}{U} \tag{7.13}$$

For the complete two-dimensional airfoil section, a correct total vortex strength is obtained by regarding the vortices as concentrated at the 1/4 chordwise position and calculating the velocity at the 3/4 chordwise position where the boundary condition of tangency of flow is applied. This fact remains even when the quasi-steady assumption is removed for two-dimensional flows. Accordingly, we can write the incremental angle of attack of the complete airfoil α using Eq. (7.13) for r computed at the 3/4 chordwise position to obtain

$$\alpha = \theta + \frac{h'}{U} + \frac{\theta'b}{U}\left[\frac{1}{2} - a\right] \tag{7.14}$$

Using Eqs. (7.14) and (7.12), we obtain

$$-Q_h = L = \frac{1}{2}\rho U^2 c \frac{dc_L}{d\alpha}\left[\theta + \frac{h'}{U} + \frac{\theta'b}{U}\left(\frac{1}{2} - a\right)\right]$$

$$M = M_{aa} + \frac{1}{2}\rho U^2 \frac{c^2}{2}\frac{dc_L}{d\alpha}\left(a + \frac{1}{2}\right)\left[\theta + \frac{h'}{U} + \frac{\theta'b}{U}\left(\frac{1}{2} - a\right)\right] \tag{7.15}$$

where M_{aa} is the incremental aerodynamic moment about the 1/4 chordwise position and is positive for nose-up rotation. According to the quasisteady theory, we can write M_{aa} as

$$M_{aa} = \frac{1}{2}\rho U^2 c^2 c_{mac}\theta' = -\frac{1}{2}\rho U^2 c^2 \frac{b\pi}{4U}\theta' \tag{7.16}$$

The work done by the incremental aerodynamic load W reads

$$W = \int Q_h h \, dt + \int M\theta \, dt \tag{7.17}$$

Therefore,

$$-\delta W = \int L\delta h \, dt - \int M\delta\theta \, dt \tag{7.18}$$

Notice that in the above formulation the generalized coordinates were taken as h and θ, which are the deflection and the rotation about the elastic axis. This simplifies extremely the formulation of the potential energy functional expression. If the generalized coordinates were taken as the deflection and the rotation about the center of mass, the expression of the kinetic energy functional would be simplified and no coupling term would appear in the kinetic energy functional expression; however, on the other hand, the potential energy functional expression will be more complicated. In the next chapters, we will see that, if the structural modal base were taken as genaralized coordinates, both the stiffness and the mass contribution

functional expressions will be uncoupled; however, the generalized incremental aerodynamic loads will be more complicated. In spite of these facts, we will adopt in the present chapter the classical formulation of the typical section, as presented above, and other formulations and their relative merits will be discussed in the next chapters. Applying now the Lagrange equations of motion,

$$\left[\frac{\partial L}{\partial x'}\right] - \frac{\partial L}{\partial x} + \frac{\partial D}{\partial x'} = Q_x \tag{7.19}$$

where $L = T - U$ and $x = h$ or θ, we obtain the equations of motion cast in the form

$$mh'' + S_w\theta'' + k_h h + c_h h' + c_{1h'}h' + k_{1\theta}\theta + c_{1\theta'}\theta' = f_h(t)$$
$$I_\theta\theta'' + S_w h'' + k_\theta\theta + c_\theta\theta' + c_{2h'}h' + k_{2\theta}\theta + c_{2\theta'}\theta' = f_\theta(t) \tag{7.20}$$

where $f_h(t)$ and $f_\theta(t)$ are the external generalized incremental applied loads in the x and θ degrees of freedom, respectively, and

$$c_{1h'} = \frac{f}{U} \qquad k_{1\theta} = f \qquad c_{1\theta'} = [1 - g]\frac{fb}{U}$$

$$c_{2h'} = -fg\frac{b}{U} \qquad k_{2\theta} = -fgb \qquad c_{2\theta'} = -[1 - g]\frac{fgb^2}{U} + \frac{fb^2}{4U} \tag{7.21}$$

and

$$f = \frac{1}{2}\rho U^2 c\frac{dc_L}{d\alpha} \qquad g = \left[\frac{1}{2} + a\right] \tag{7.22}$$

We now examine the response of the typical section subjected to initial conditions in free vibration, i.e., for $f_h(t) = f_\theta(t) = 0$. In such conditions, the equations of motion Eq. (7.20) read

$$mh'' + S_w\theta'' + k_h h + c_h h' + c_{1h'}h' + k_{1\theta}\theta + c_{1\theta'}\theta' = 0$$
$$I_\theta\theta'' + S_w h'' + k_\theta\theta + c_\theta\theta' + c_{2h'}h' + k_{2\theta}\theta + c_{2\theta'}\theta' = 0 \tag{7.23}$$

When $U = 0$, i.e., in the absence of aerodynamic effects, and if the structural damping is neglected, Eq. (7.23) reduces to

$$mh'' + S_w\theta'' + k_h h = 0$$
$$I_\theta\theta'' + S_w h'' + k_\theta\theta = 0 \tag{7.24}$$

For a nontrivial solution, the determinate of Eq. (7.24) vanishes, and we can write the system characteristic equation as

$$s^4 - [\omega_h^2 + \omega_\theta^2]s^2 + \omega_h^2\omega_\theta^2 - \mu s^4 = 0 \tag{7.25}$$

where

$$\omega_h^2 = (k_h/m) \qquad \omega_\theta^2 = k_\theta/I_\theta \qquad \mu = S_w^2/mI_\theta \tag{7.26}$$

ω_h and ω_θ are the inertia uncoupled, undamped natural frequencies of the typical section, and μ represents the inertia coupling between the translational and the rotational degrees of freedom, respectively. Notice that physical considerations

reveal that ω_h, ω_θ, and μ are real positive numbers. Furthermore, μ is less than 1 since $m I_\theta > S_w^2$. Solving the characteristic Eq. (7.26), we obtain the undamped natural frequencies of the typical section, which can be written as

$$s_i^2 = \frac{\left[\omega_h^2 + \omega_\theta^2\right] \pm \sqrt{\left[\omega_h^2 - \omega_\theta^2\right]^2 + 4\mu\omega_h^2\omega_\theta^2}}{2\left[1 - \mu\right]} \qquad i = 1, 2 \qquad (7.27)$$

Clearly, the undamped natural frequencies of the typical section given by Eq. (7.27) are real positive numbers. Furthermore, their numerical values are less than the rotational uncoupled undamped natural frequency ω_θ and greater than the translational uncoupled undamped natural frequency ω_h.

We examine now the case when U is different from zero, and, for simplicity and without loss of the generality, we consider that $S_w = 0$ since its effect can be analyzed separately. Under such conditions, the elastic axis coincides with the typical section center of gravity position, and the equation of motion [Eq. (7.23)] is uncoupled and reads

$$mh'' + [c_h + c_{1h'}] h' + k_h h = 0$$
$$I_\theta \theta'' + [c_\theta + c_{2\theta'}] \theta' + [k_\theta + k_{2\theta}] \theta = 0 \qquad (7.28)$$

Examining the first equation of Eq. (7.28), we observe that the structural damping c_h is always a real positive number; $c_{1h'}$ is always a real positive number because $c_{1h'} = f/U$, and k_h is always a real positive number. Therefore, from physical considerations, we conclude that the equivalent damping term in the first equation of Eq. (7.28) is definitively a real positive number, and we conclude that the uncoupled translational degree of freedom can never present an instability based on the considerations previously discussed in Section 7.1. Examining the second equation of Eq. (7.28), we observe that the structural damping c_θ is always a real positive number; however, $c_{2\theta'}$ can be positive or negative, and k_θ is always a real positive number, while $k_{2\theta}$ can be positive or negative. We therefore conclude that the uncoupled rotational degree of freedom of the typical section can present all types of instabilities discussed in Section 7.1. We first examine the equivalent stiffness term, which can be written as

$$k_{\theta\,\text{eff}} = k_\theta + k_{2\theta} = k_\theta - fgb = k_\theta - \frac{1}{2}\rho U^2 c \frac{dc_L}{d\alpha} \left[\frac{1}{2} + a\right] b \qquad (7.29)$$

Examination of Eq. (7.29) shows that, when $a \leq -1/2$, i.e., when the elastic axis is located at the aerodynamic center position or in front of it, static divergence can never occur for the typical section. Static divergence can happen when g is positive, and the critical condition of instability reads

$$k_\theta - \frac{1}{2}\rho U^2 c \frac{dc_L}{d\alpha} \left[\frac{1}{2} + a\right] b = 0 \qquad (7.30)$$

Using Eq. (7.30), we obtain the static divergence velocity, which can be written as

$$U_{\text{div}}^2 = \frac{2k_\theta}{2b^2\rho \left[a + \frac{1}{2}\right] \frac{dc_L}{d\alpha}} \qquad (7.31)$$
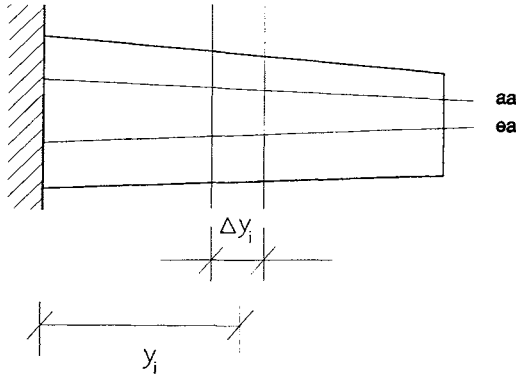
Fig. 7.8   Strip theory nomenclature. (aa is the aerodynamic axis, and ea is the elastic axis.)

and using, for the typical section, $dc_L/d\alpha = 2\pi$, we obtain

$$U_{\text{div}}^2 = \frac{k_\theta}{b^2 \rho \pi \, [1 + 2a]}$$

$$= \frac{I_\theta \omega_\theta^2}{b^2 \rho \pi \, [1 + 2a]} \tag{7.32}$$

Equation (7.32) represents a simple relation for the static divergence speed of the typical section, where the effects of altitude, rotational frequency or rotational stiffness, and the numerical value considered for $dc_L/d\alpha$ on the divergence speed are evident. We are now in a position to extend our application for the practical case of the computation of the divergence speed of a lifting surface, under the limitations of the quasisteady aerodynamic theory, using strip theory aerodynamic simplification. The strip theory approximation, for lifting surfaces of high aspect ratio, consists in dividing the lifting surface in chordwise strips, of small but finite width, and assuming that in each strip the flow is two dimensional and does not interact with the flow in other strips of the lifting surface. The chord length of the strip is taken as being its geometric mean value. Consider the lifting surface shown in Fig. 7.8, divided into strips having spanwise strip width Δy_i, mean chord strip c_i, and strip spanwise position y_i.

For each strip, we can write

$$k_{2\theta} = -\frac{1}{2}\rho U^2 c_i \frac{dc_L}{d\alpha}\left[\frac{1}{2} + a_i\right] b_i \Delta y_i \tag{7.33}$$

For each strip, $dc_L/d\alpha = 2\pi$, and writing $\lambda_i = \rho\pi U^2$, we obtain

$$k_{2\theta} = -\lambda A_i \tag{7.34}$$

where A_i is a strip geometric constant and reads

$$A_i = b_i^2 \Delta y_i \, [1 + 2a_i] \tag{7.35}$$

Equation (7.34) can be written in matrix form for the complete lifting surface as

$$\lceil k_{2\theta_i} \rfloor \{\theta_i\} = -\lambda \lceil A_i \rfloor \{\theta_i\} \tag{7.36}$$

where $\lceil k_{2\theta_i} \rfloor$ and $\lceil A_i \rfloor$ are diagonal matrices with elements given by the corresponding strip values. Furthermore, from the engineering theory of elasticity, we can write a matrix form expression for the torsional moment about the elastic axis for the complete lifting surface as

$$\{T_i\} = [k_\theta] \{\theta_i\} = [B]^{-1} \{\theta_i\} \tag{7.37}$$

where $[k_\theta]$ is the torsional stiffness matrix and $[B_i]$ is the torsional flexibility matrix. Notice that the torsional flexibility matrix is more easily obtained than the torsional stiffness matrix through finite element or engineering theory calculations and also in experimental measurements. Now using Eqs. (7.36) and (7.37), the critical condition for the lifting surface reads

$$[B]^{-1} \{\theta_i\} - \lambda \lceil A \rfloor \{\theta_i\} = \{0\} \tag{7.38}$$

or

$$\{\theta_i\} - \lambda [C] \{\theta_i\} = \{0\} \tag{7.39}$$

where $[C] = [B]\lceil A \rfloor$. Equation (7.39) can be written as a standard eigenvalue problem cast in the form

$$\left[[C] - \frac{1}{\lambda}\lceil I \rfloor\right] \{\theta_i\} = \{0\} \tag{7.40}$$

where again $\lambda_i = \rho \pi U^2$. The solution of the eigenvalue problem [Eq. (7.40)], using for instance a power iteration direct eigenvalue extraction algorithm, will furnish as a first eigenvalue the lowest value of λ and therefore the lowest static divergence speed of the lifting surface. We next examine the typical section for $S_w = 0$ and coupled degrees of freedom. In such a condition, the equation of motion [Eq. (7.23)] reads

$$mh'' + k_h h + c_h h' + c_{1h'} h' + k_{1\theta}\theta + c_{1\theta'}\theta' = 0 \tag{7.41}$$
$$I_\theta \theta'' + k_\theta \theta + c_\theta \theta' + c_{2h'} h' + k_{2\theta}\theta + c_{2\theta'}\theta' = 0$$

The set of equations [Eq. (7.41)] admits solutions in the form

$$h = \underline{h}_0 e^{st} \qquad \theta = \underline{\theta}_0 e^{st} \tag{7.42}$$

where $\underline{h}_0$ and $\underline{\theta}_0$ are in general complexes. Substituting the solutions to Eq. (7.42) into the Eq. (7.41), two simultaneous homogeneous algebraic equations in $\underline{h}_0$ and $\underline{\theta}_0$ are obtained, and, for the nontrivial solution, the determinant must be zero, giving the characteristic equation of the system, which can be written as

$$s^4 [mI] + s^3 [mc_{\theta\,\text{eff}} + I c_{h\,\text{eff}}] + s^2 [mk_{\theta\,\text{eff}} + c_{h\,\text{eff}} c_{\theta\,\text{eff}} + k_h I - c_{2h'} c_{1\theta'}]$$
$$+ s [c_{h\,\text{eff}} k_{\theta\,\text{eff}} + k_h c_{\theta\,\text{eff}} - c_{2h'} k_{1\theta}] + [k_h k_{\theta\,\text{eff}}] = 0 \tag{7.43}$$

A system instability will be obtained if the real part of one of the roots of Eq. (7.43) is positive. It can be shown that the necessary and sufficient condition for system stability is obtained when all the roots and the root discriminant R are of the same sign. The root discriminant R reads

$$a_4 \left[a_1 a_2 a_3 - a_0 a_3^2 - a_4 a_1^2 \right] \tag{7.44}$$

where a_i in Eq. (7.44) are the coefficients of s^i of Eq. (7.43). Examining the coefficients of s^i of Eq. (7.43), we observe that a_4 and a_3 are always positive from physical considerations. The coefficient a_0 is negative only if $k_{\theta \, \text{eff}}$ is negative, and this gives the static divergence condition of stability as previously discussed. We further notice that in such a case, i.e., at the divergence critical condition, one of the roots of the characteristic Eq. (7.43) will be zero, characterizing the fact that the critical point of divergence occurs at a zero frequency. The only coefficients left to be examined are a_1 and a_2. We examine first the coefficient a_1 for a possible condition of instability. Using Eqs. (7.21) and (7.43), we can write for an instability $a_1 \leq 0$, or

$$(c_h + c_{1h'})(k_\theta + k_{2\theta}) + k_h(c_\theta + c_{2\theta'}) - c_{2h'} k_{1\theta} \leq 0 \tag{7.45}$$

Omitting for the moment the structural damping terms, because their effect is always stabilizing, we can write the condition of instability given by Eq. (7.45) as

$$c_{1h'}(k_\theta + k_{2\theta}) + k_h c_{2\theta'} - c_{2h'} k_{1\theta} \leq 0 \tag{7.46}$$

Numerical evaluation of Eq. (7.46) will furnish the critical flutter velocity of the typical section under such conditions; furthermore, if structural damping is considered, Eq. (7.45) will furnish the critical flutter condition when such damping is assumed. We now consider the case when $a = -1/2$ and neglect the structural damping effect. Under such conditions, $k_{2\theta}$ and $c_{2h'}$ are null because $g = 0$, and Eq. (7.46) reads

$$\frac{f}{U} \left[k_\theta + k_h \frac{b^2}{4} \right] \leq 0 \tag{7.47}$$

Physically, the term between brackets is always positive so that the flutter condition can take place only for $f = 0$, i.e., $U = 0$. This implies that if the system velocity is plotted against system damping, when the structural damping is neglected, these curves start with a zero system damping at zero velocity. From this discussion, we conclude that a typical section with a coincident aerodynamic axis, center of gravity, and elastic axis position can never have a flutter- or divergent-type instability. We next examine the case when the c.g. does not coincide with the elastic center, i.e., $S_w \neq 0$, and we neglect the structural damping since its effect is conservative in the stability sense. We further consider that the elastic and aerodynamic axes are at the same position, to concentrate only on the effect of the c.g. on the stability of the typical section. Under such conditions, the equations of motion [Eq. (7.23)] read

$$\begin{aligned}
mh'' + S_w \theta'' + k_h h + c_h h' + k_{1\theta} \theta + c_{1\theta'} \theta' = 0 \\
I_\theta \theta'' + S_w h'' + k_\theta \theta + c_{2h'} h' + k_{2\theta} \theta + c_{2\theta'} \theta' = 0
\end{aligned} \tag{7.48}$$

Again, Eq. (7.48) admits solutions in the form

$$h = \underline{h}_0 e^{st} \qquad \theta = \underline{\theta}_0 e^{st} \tag{7.49}$$

Substituting the solutions in Eq. (7.49) into Eq. (7.48), two algebraic homogeneous equations are obtained, and, except for the trivial solution, we obtain the problem characteristic equation, which can be written as

$$s^4 [mI_\theta - S_w] + s^3 \left[m\frac{fb^2}{4U} + I_\theta \frac{f}{U} - S_w \frac{fb}{U} \right]$$

$$+ s^2 \left[mk_\theta + k_h I_\theta + f^2 \frac{b^2}{4U^2} - f S_w \right] + s \left[k_h \frac{fb^2}{4U} + k_\theta \frac{f}{U} \right] + k_h k_\theta = 0 \tag{7.50}$$

Examination of Eq. (7.50) shows that, if S_w is negative, the typical section will never have instability because all the coefficients and the Routh discriminant are of the same sign. In other words, a typical section having elastic and aerodynamic axes coincidents and the c.g. position located at the elastic axis or in front of it will never present problems of aeroelastic instabilities, whether of a static nature or of a dynamic nature, i.e., divergence or flutter. If S_w is positive, the coefficient of s^4 is still positive because $mI_\theta > S_w$; the coefficient of s^3 gives instability only for $f = 0$, as previously discussed. Thus, the only coefficient that can give instability is the coefficient of s^2. The other remaining coefficients, the coefficients of s^1 and s^0, are positives from physical considerations. The instability condition can thus be written as

$$mk_\theta + k_h I_\theta + \frac{f^2 b^2}{4U^2} - s_w f \le 0 \tag{7.51}$$

and the critical flutter instability condition can be written as

$$f_{1,2} = \frac{S_w \pm \sqrt{S_w^2 - 4[mk_\theta + I_\theta k_h]}}{2b^2/4U^2} \tag{7.52}$$

Equation (7.52) can be solved numerically to determine the critical flutter speed under such conditions. For the clarity of the exposition, the structural damping has been neglected in most of the analyses presented in the present section. However, as has been demonstrated in Section 7.1, its effect is always stabilizing in the sense that the critical instability speed with the structural damping considered in the analysis is always higher than critical instability speed when the structural damping is neglected. In the present section, the simple quasisteady aerodynamic theory has been used exclusively, and, as has been demonstrated, this theory, despite its simplicity, has shown its ability to explain the cause of the various types of instabilities of aeroelastic nature and effects of various parameters involved in the problem. In the next section, we will use a more elaborate aerodynamic theory for the problem formulation and discuss its relative merit compared with the simple quasisteady aerodynamic theory.

7.3   Typical Section Using Unsteady Linearized Potential Theory

The exact determination of the aerodynamic forces acting on an airfoil moving in an unsteady motion about the initial state of equilibrium is complex and very detailed. At each instant of time, the change in the airfoil position results in a change in the circulation about the airfoil, causing a change in the vortex shed from the trailing edge. These vortex sheds produce vertical velocities on the airfoil and affect the aerodynamic incremental nonstationary airloads on the lifting section, rendering the problem extremely complicated to be physically analyzed and mathematically represented. On the other hand, as has been demonstrated in Section 7.1, at the critical point of dynamic instability the motion of the system is a pure harmonic oscillation. This fact promoted the development to establish the formulation of the incremental nonstationary aerodynamic loads acting on an airfoil performing simple harmonic motion, which limits the type of unsteadiness; however, it presents the exact solution at the critical instability point.

The first studies made were performed by Birnhaum,[1] Wagner,[2] Küssner,[3] and Glauert[4] and later by Theodorsen[5] and Ellenberger[6] in the period from 1924 to 1939. In 1940, Küssner[7] in Germany and Theodorsen and Garrick[8] in the United States published, in a comprehensible and easily used manner, the incremental aerodynamic forces and moments acting on a two-dimensional airfoil performing a simple harmonic motion. Theodorsen obtained the incremental lift and moment for the incompressible case, using the linearized potential solutions of the individual types of motion, i.e., individual solutions due to θ, θ', h', etc. Assuming linearity to sum the individual solutions and applying the Bernoulli theorem, he obtained the total incremental lift as

$$L_{e.a.} = \pi \rho b^3 \left\{ -\frac{h''}{b} - \frac{2U}{b^2} C(k)h' + a\theta'' + \left[2\left(a - \frac{1}{2}\right) C(k) - 1 \right] \right.$$
$$\left. \times \frac{U}{b}\theta' - \frac{2U^2}{b^2} C(k)\theta \right\} \tag{7.53}$$

and the incremental moment about the elastic axis of the typical section as

$$M_{e.a.} = \pi \rho b^4 \left\{ -\frac{a}{b}h'' + \frac{2Ug}{b^2} C(k)h' - \left(\frac{1}{8} + a^2\right)\theta'' \right.$$
$$\left. + \left[2\left(\frac{1}{4} - a^2\right) C(k) - \frac{1}{2} + a \right] \frac{U}{b}\theta + \frac{2gU^2}{b^2} C(k)\theta \right\} \tag{7.54}$$

where $C(k)$ is the Theodorsen function and is given by

$$C(k) = F(k) + iG(k) = \frac{H_1^{(2)}(k)}{H_1^{(2)}(k) + iH_0^{(2)}(k)} = \frac{K_1(ik)}{K_0(ik) + K_1(ik)} \tag{7.55}$$

where $H_0^{(2)}$ and $H_1^{(2)}$ are the Hankel functions of the second kind and order zero and one, respectively; K_0 and K_1 are the modified Bessel functions of the second kind and order zero and one, respectively; and $F(k)$ and $G(k)$ are the real and imaginary parts of the Theodorsen function. All these functions are functions of
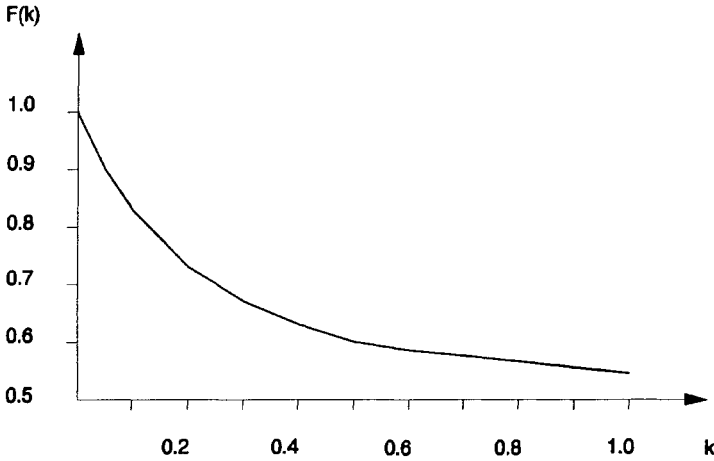
Fig. 7.9 Real part of the Theodorsen function $F(k)$ plotted vs the reduced frequency $k = \omega b / U$.

the nondimensional or reduced frequency parameter k, which is defined as

$$k = \frac{b\omega}{U} \tag{7.56}$$

where ω is the frequency of oscillation of the typical section. Hankel functions and the modified Bessel functions of the second kind can be found in a tabulated or power series form in several handbooks on mathematical functions (for example, Ref. 9). The real and imaginary parts of the Theodorsen functions $F(k)$ and $G(k)$ are well-behaved analytical functions and are a combination of Bessel functions as stated above. The real and imaginary parts of the Theodorsen function F and G are given in Figs. 7.9 and 7.10, respectively, and are plotted against the reduced frequency parameter k for values of $k < 1$. Table 7.1 is a short compilation of the functions $F(k)$ and $G(k)$. Several approximate expressions for the real and imaginary parts of the Theodorsen function are available in the literature. A simple and precise formula for the evaluation of these functions was obtained by Jones[10] and reads

$$C(k) = 1 - \frac{0.165}{1 - \frac{0.0455}{k}i} - \frac{0.335}{1 - \frac{0.3}{k}i} \qquad \text{for } k \leq 0.5$$

$$C(k) = 1 - \frac{0.165}{1 - \frac{0.041}{k}i} - \frac{0.335}{1 - \frac{0.32}{k}i} \qquad \text{for } k > 0.5 \tag{7.57}$$

The maximum percentage error in the formula for the first part of Eq. (7.57) is 2.7% and for the second part of Eq. (7.57) is -2.1%.

Now, because the motion is harmonic, we can write solutions in the form

$$h = \underline{h}_0 e^{i\omega t} \qquad \theta = \underline{\theta}_0 e^{i\omega t} \tag{7.58}$$

The solutions in Eq. (7.58), when substituted in Eqs. (7.53) and (7.54), give expressions for the total incremental lift and the incremental moment about the elastic

-G(k)
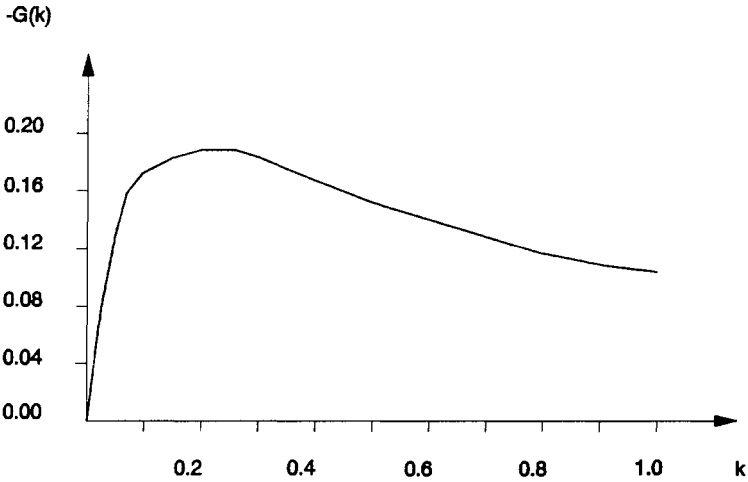
Fig. 7.10   Imaginary part of the Theodorsen function $G(k)$ plotted vs the reduced frequency $k = \omega b / U$.

axis of the typical section and read

$$L_{e.a.} = \pi \rho \omega^2 b^3 \left[L_h \frac{h}{b} + [L_\alpha - g L_h]\theta \right]$$

$$M_{e.a.} = \pi \rho \omega^2 b^4 \left[[M_h - g L_h]\frac{h}{b} + [M_\alpha - g(L_\alpha + M_h) + g^2 L_h]\theta \right]$$

(7.59)

The coefficients L_h, L_α, M_h, and M_α have been published in many references (for instance, Refs. 11 and 12).

7.3.1   Theodorsen Solution of the Flutter Determinant

In the following section, a solution of the stability equations as proposed by Theodorsen is given. Using the expressions of the incremental oscillatory airloads given by Eq. (7.59) and substituting the harmonic solutions in Eq. (7.58) into the equations of motion, we can write

$$\begin{bmatrix} A & B \\ C & D \end{bmatrix} \begin{Bmatrix} \underline{h_0/b} \\ \underline{\theta_0} \end{Bmatrix} = \begin{Bmatrix} 0 \\ 0 \end{Bmatrix}$$

(7.60)

Table 7.1   Theodorsen function $C(k) = F(k) + i G(k)$

k	F	$-G$	k	F	$-G$
∞	0.5000	0	0.80	0.5541	0.1165
10.00	0.5006	0.0124	0.50	0.5979	0.1507
6.00	0.5017	0.0206	0.20	0.7276	0.1886
4.00	0.5036	0.0305	0.05	0.9090	0.1305
1.00	0.5394	0.1003	0	1.000	0

where

$$A = \mu\left[1 - \left[\frac{\omega_\theta}{\omega}\right]^2\left[\frac{\omega_h}{\omega_\theta}\right]^2[1 + ic_h]\right] + L_h$$

$$B = \mu x_\alpha + L_\alpha - L_h g$$

$$C = \mu x_\alpha + \tfrac{1}{2} - L_h g$$

$$D = \mu r_\alpha^2\left[1 - \left[\frac{\omega_\alpha}{\omega}\right]^2[1 + ic_\alpha]\right] + L_h g^2 + M_\alpha - L_\alpha g - \frac{1}{2}g$$

(7.61)

and

$$\mu = \frac{m}{\pi\rho b^2} \qquad r_\alpha^2 = \frac{I_\alpha}{mb^2}$$

(7.62)

x_α is the distance between the c.g. and the elastic axis and is positive for the c.g. aft of the elastic axis. For a nontrivial solution to Eq. (7.60), we write

$$\Delta = \begin{vmatrix} A & B \\ C & D \end{vmatrix} = \Delta_R + i\Delta_I = 0$$

(7.63)

where Δ_R and Δ_I are the real and imaginary parts of the determinant, respectively. The solution starts by assuming a value for $k(k = \omega b/U)$. Compute the aerodynamic coefficients or use the aerodynamic tables to get the values of these coefficients for the predefined value of k. Write $X = 1/\omega^2$, solve $\Delta_R = 0$, and get the corresponding X_R. Solve $\Delta_I = 0$, get the corresponding X_I, and repeat the whole process for different values of k. Plot curves of X_R and X_I vs k. At the intersection of the two curves, we have the same $X(X = 1/\omega^2)$. Determine this value of ω and the corresponding k. From this value of k, determine the corresponding velocity U. These values of ω and U are the critical flutter conditions of the problem.

7.3.2 Some Parametric Studies Using Two-Dimensional Potential Theory for the Typical Section

The critical flutter velocities of the typical section have been calculated for different configurations to perform a parametric study of the various parameters involved in the problem. The results of the analyses are shown in Figs. 7.11–7.13.

From the results of Figs. 7.11–7.13, we can observe the following:

1) With the increase of ω_h/ω_α, the flutter velocity decreases, with the minimum velocity obtained at $\omega_h/\omega_\alpha = 1$ stemming the fact that the flutter instability occurs due to the coupling of the two frequencies; therefore, the minimum velocity is obtained when $\omega_h = \omega_\alpha$.

2) The effect of the air density on the flutter velocity is an increase of U_F with the decrease of ρ, i.e., it is conservative to perform the flutter calculations at sea level.

3) With the increase of x_α, the flutter velocity decreases, and, with the increase of r_a^2, i.e., an increase in the torsional rigidity, the flutter velocity increases, as was expected based on previous considerations.
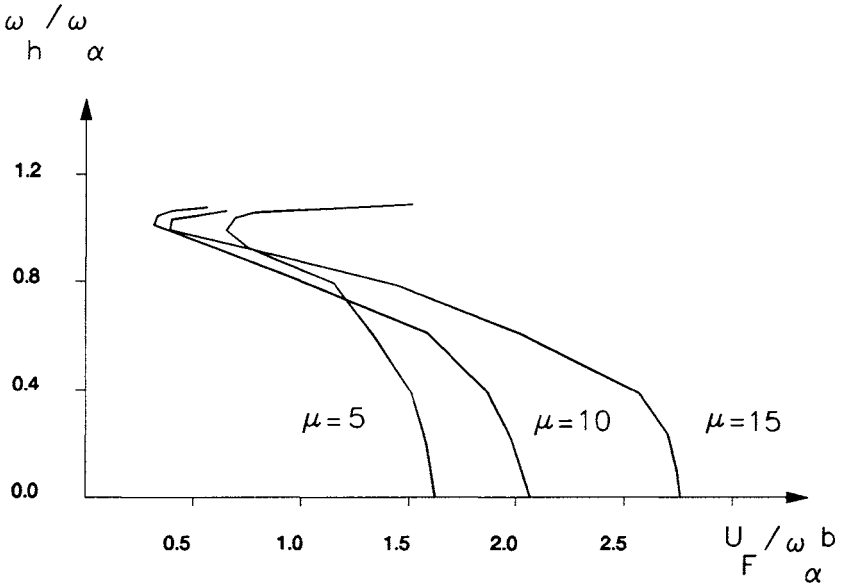
Fig. 7.11   Parametric study to show the effect of the frequency ratio ω_h/ω_α and the mass parameter $\mu = m/\pi\rho b^2$ on the nondimensional flutter velocity $U_F/\omega_\alpha b$. Curves are plotted for $a = -0.2, r_\alpha^2 = 1/3$, and $x_\alpha = 0.1$.

Fig. 7.12   Parametric study to show the effect of the static mass parameter $x_\alpha = S_w/mb$ on the nondimensional flutter velocity $U_F/\omega_\alpha b$. Curves are plotted for $\omega_h/\omega_\alpha = 0.30$, $a = -0.3$, $\mu = 10$, and $r_\alpha^2 = 0.25$.

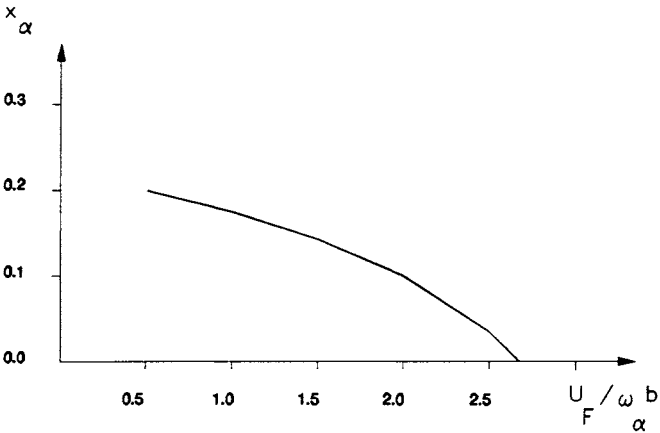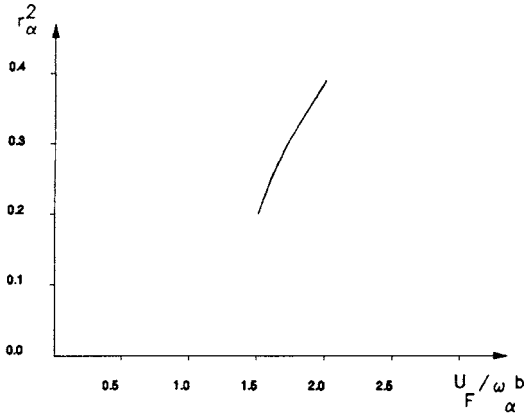**Fig. 7.13 Parametric study to show the effect of the moment of inertia parameter $r_\alpha^2 = I_\alpha/mb^2$ on the nondimensional flutter velocity $U_F/\omega_\alpha b$. Curves are plotted for $\omega_h/\omega_\alpha = 0.30, a = -0.2, \mu = 10,$ and $x_\alpha = 0.10$.**

7.3.3 Extension to Three-Dimensional Lifting Surfaces Strip Theory

The typical section theory can be extended directly for the computation of the aeroelastic stability of the straight wing of high aspect ratio and no considerable mass concentration at low speeds using the strip theory aerodynamic simplification. Again, the strip theory approximation for lifting surfaces of high aspect ratio consists in dividing the lifting surface in spanwise strips of small but finite width and in assuming that in each strip the flow is two dimensional and does not interact with the flow in other strips of the lifting surface. The chord length of the strip is taken as being its geometric mean value. Consider again the lifting surface shown in Fig. 7.8, divided into strips having spanwise strip width Δ_{yi}, mean chord strip c_i, and strip spanwise position y_i. We will use the following notation for each strip:

$m(y_i)$ = mass per unit width at station i
$I(y_i)$ = moment of inertia about the elastic axis (e.a.) per unit width at station i
$S_w(y_i)$ = static mass moment about the e.a. per unit width at station i

For each strip at station y_i, we can write for the deflection and the rotation expressions in the form

$$h(y, t) = f(y)\underline{h}$$
$$\theta(y, t) = \theta(y)\underline{\theta} \tag{7.64}$$

where $f(y)$ and $\theta(y)$ are assumed uncoupled modes in bending and in torsion, normalized to unit values at the wing tip. The expression of strain energy of deformation for the half-wing can be written as

$$U = \frac{1}{2} \int_0^l EI(y) \left[\frac{\partial^2}{\partial y^2} [f(y)\underline{h}] \right]^2 dy + \frac{1}{2} \int_0^l GJ(y) \left[\frac{\partial}{\partial y} [\theta(y)\underline{\theta}] \right]^2 dy \tag{7.65}$$

where $EI(y) =$ bending stiffness at station i, $GJ(y) =$ torsional stiffness at station i, and $l =$ total length of the half-wing span.

Now defining k_h and k_θ as

$$k_h = \int_0^l EI(y)\left[\frac{\partial^2}{\partial y^2}[f(y)]\right]^2 dy$$

$$k_\theta = \int_0^l GJ(y)\left[\frac{\partial}{\partial y}[\theta(y)]\right]^2 dy \qquad (7.66)$$

the expression of strain energy of deformation for the half-wing reads

$$U = \tfrac{1}{2}k_h \underline{h}^2 + \tfrac{1}{2}k_\theta \underline{\theta}^2 \qquad (7.67)$$

Defining now the uncoupled natural frequencies in bending and in torsion as ω_h and ω_θ, respectively, we can write the strain energy expression as

$$U = \tfrac{1}{2}M\omega_h^2 \underline{h}^2 + \tfrac{1}{2}I_\theta \omega_\theta^2 \underline{\theta}^2 \qquad (7.68)$$

where M and I_θ are the generalized mass for the bending and the torsional modes, respectively, and are given by

$$M = \int_0^l m(y)[f(y)]^2 dy$$

$$I_\theta = \int_0^l I(y)[\theta(y)]^2 dy \qquad (7.69)$$

The expression of kinetic energy of the half-wing can be written as

$$T = \tfrac{1}{2}M\underline{h}'^2 + \tfrac{1}{2}I_\theta \underline{\theta}'^2 + S\underline{h}'\,\underline{\theta}' \qquad (7.70)$$

where S is the total static mass moment and is given by

$$S = \int_0^l S_w f(y)\theta(y)\,dy \qquad (7.71)$$

Considering that the wing structure possesses a viscous structural damping, we can write for the structural damping representation a dissipation function as

$$D = \tfrac{1}{2}c_h \underline{h}'^2 + \tfrac{1}{2}c_\theta \underline{\theta}'^2 \qquad (7.72)$$

At any station y_i, we can write for the lift and the aerodynamic moment about the elastic axis the same expressions given by Eq. (7.59), replacing h and θ by $f(y)\underline{h}$ and $\theta(y)\underline{\theta}$, respectively, and thus the incremental aerodynamic loads at station y_i can be written as

$$L_{e.a.} = \pi\rho\omega^2 b^3\left[L_h f(y)\frac{h}{b} + [L_\alpha - gL_h]\theta(y)\underline{\theta}\right]$$

$$M_{e.a.} = \pi\rho\omega^2 b^4\left[[M_h - gL_h]f(y)\frac{h}{b} + [M_\alpha - g(L_\alpha + M_h) + g^2 L_h]\theta(y)\underline{\theta}\right]$$

$$(7.73)$$

and for the entire half-wing, we can write the generalized incremental aerodynamic loads as

$$Q_h = \int_0^l L' f(y)\,dy$$

$$Q_\theta = \int_0^l M' \theta(y)\,dy$$

(7.74)

The integrations in Eq. (7.74) are evaluated numerically considering constant values for each strip. The aerodynamic loads can thus be written as

$$\left\{ \begin{matrix} Q_h \\ Q_\theta \end{matrix} \right\} = \pi \rho \omega^2 \begin{bmatrix} A_{hh} & A_{h\theta} \\ A_{\theta h} & A_{\theta\theta} \end{bmatrix} \left\{ \begin{matrix} \underline{h} \\ \underline{\theta} \end{matrix} \right\}$$

(7.75)

where

$$A_{hh} = \int_0^l L_h b^2 [f(y)]^2 \,dy$$

$$A_{h\theta} = \int_0^l b^3 f(y)\theta(y)[L_\theta - gL_h]\,dy$$

(7.76)

$$A_{\theta h} = \int_0^l b^3 f(y)\theta(y)[M_h - gL_h]\,dy$$

$$A_{\theta\theta} = \int_0^l b^4 [\theta(y)]^2 \left[M_\theta - g(L_\theta + M_h) + \left(a + \frac{1}{2}\right)^2 L_h \right] dy$$

Applying the Lagrange equations of motion, we obtain for free vibration the following equation for the complete half-wing

$$\left[M + \pi\rho A_{hh} - M(1 + ic_h)\left[\frac{\omega_h}{\omega}\right]^2 \right] \underline{h} + [S + \pi\rho A_{h\theta}]\underline{\theta} = 0$$

$$[S + \pi\rho A_{\theta h}]\underline{h} + \left[I_\theta + \pi\rho A_{\theta\theta} - I_\theta(1 + ic_\theta)\left[\frac{\omega_\theta}{\omega}\right]^2 \right]\underline{\theta} = 0$$

(7.77)

The solution then proceeds in the same way using the Theodorsen method of solution as given in Section 7.2 for the case of the two-dimensional typical section.

7.4 Typical Section with Control Surface

Consider the typical section shown in Fig. 7.14, where we have included in the section a control surface giving a third degree of freedom. The same notation used for the typical section with two degrees of freedom is adopted, and we consider that the control surface hingeline is located at a distance cb from the origin, and the leading edge of the control surface is located at a distance eb from the origin. Furthermore, we consider that the third degree of freedom is the control surface rotation and will be denoted by β, measured relative to the main surface rotation and positive for nose up as indicated in the figure.

The same theory used for the typical section with two degrees of freedom can now be extended to the case of three degrees of freedom without too much difficulty.
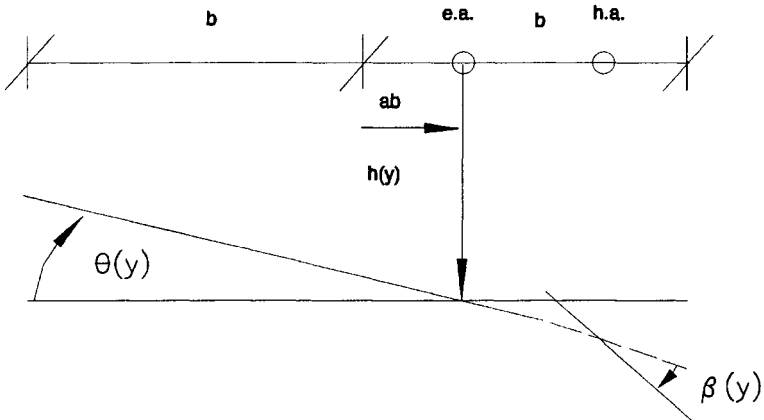
Fig. 7.14   Typical section with a control surface showing notations and definitions. (h.a. is the hinge axis position.)

In the following section, we will present directly the extension to the three-degree-of-freedom typical section using the strip theory for a complete half-wing. The following notation will be adopted:

$m(y)$ = mass per unit width at station i

$I(y_i)$ = moment of inertia about the e.a. per unit width at station i

$S_w(y_i)$ = static mass moment about the e.a. per unit width at station i

$I_\beta(y_i)$ = control surface mass moment of inertia about the e.a. at station i

$S_\beta(y_i)$ = control surface static moment about the e.a. per unit width at station i

For each strip at station y_i, we can write for the deflection the main surface rotation and the control surface rotation expressions in the form

$$h(y, t) = f(y)\underline{h}$$
$$\theta(y, t) = \theta(y)\underline{\theta} \tag{7.78}$$
$$\beta(y, t) = \beta(y)\underline{\beta} \approx \underline{\beta}$$

where it has been assumed that the rotation of the aileron is a rigid body rotation about its hingeline, i.e., the angle β is assumed to be a constant spanwise through the control surface extension. The strain energy of small deformation of the complete half-wing can be written as

$$U = \frac{1}{2} \int_0^l EI(y) \left[\frac{\partial^2}{\partial y^2} [f(y)\underline{h}] \right]^2 dy + \frac{1}{2} \int_0^l GJ(y) \left[\frac{\partial}{\partial y} [\theta(y)\underline{\theta}] \right]^2 dy + \frac{1}{2} k_\beta \beta^2 \tag{7.79}$$

where the same notation has been used as in Section 7.3. Furthermore, using Eq. (7.66), we can write the expression of the potential energy as

$$U = \frac{1}{2} M \omega_h^2 \underline{h}^2 + \frac{1}{2} I_\theta \omega_\theta^2 \underline{\theta}^2 + \frac{1}{2} I_\beta \omega_\beta^2 \underline{\beta}^2 \tag{7.80}$$

where ω_β is the rotational frequency of the control surface, M and I_θ are given in Eq. (7.69), and I_β is given by

$$I_\beta = \int_{l_1}^l I_\beta(y)\,dy \tag{7.81}$$

where l_1 is the distance from the half-wing root to the inboard control edge spanwise. Including a viscous structural damping in the analysis, we can write a dissipation function in the form

$$D = \tfrac{1}{2}c_h\underline{h}'^2 + \tfrac{1}{2}c_\theta\underline{\theta}'^2 + \tfrac{1}{2}c_\beta\underline{\beta}'^2 \tag{7.82}$$

The kinetic energy can be written as

$$T = \tfrac{1}{2}M\underline{h}'^2 + \tfrac{1}{2}I_\theta\underline{\theta}'^2 + S\underline{h}'\,\underline{\theta}' + \tfrac{1}{2}I_\beta\underline{\beta}'^2 + S_\beta\underline{h}'\,\underline{\beta}' + P_{\theta\beta}\underline{\theta}'\,\underline{\beta}' \tag{7.83}$$

where

$$S_\beta = \int_{l_1}^l S_\beta(y)f(y)\,dy$$

$$P_{\theta\beta} = \int_{l_1}^l [S_\beta(y)(c-a)b + I_\beta(y)]f(y)\,dy \tag{7.84}$$

and the remaining constants are as defined before. The aerodynamic loads for strips without control surfaces are the same as given in Section 7.3. The aerodynamic loads for strips with control surfaces were given by Theodorsen[8] in terms of the Theodorsen function and involve other functions due to the presence of the control surface. These can further be written in terms of other constants for three degrees of freedom as has been done in the Section 7.3 for two degrees of freedom to facilitate the computation using tabulated procedures. These coefficients for three degrees of freedom have been tabulated in several textbooks and manuals, e.g., Refs. 11–13. The aerodynamic loads, i.e., lift at the aerodynamic center, moment at the aerodynamic center, and aerodynamic moment about the hingeline, for a strip with control surface per unit span can be written as

$$L' = \pi\rho\omega^2 b^3\left\{L_h f(y)\frac{h}{b} + [L_\alpha - gL_h]\theta(y)\underline{\theta} + [L_\beta - dL_z]\underline{\beta}\right\}$$

$$M' = \pi\rho\omega^2 b^4\left\{[M_h - gL_h]f(y)\frac{h}{b} + [M_\alpha - g(L_\alpha + M_h) + g^2L_h]\theta(y)\underline{\theta}\right.$$

$$\left. + [gL_\beta - dM_z + dgL_z]\underline{\beta}\right\} \tag{7.85}$$

$$T' = \pi\rho\omega^2 b^4\left\{[T_h - dP_h]f(y)\frac{h}{b} + [T_\alpha - d(P_\alpha - gT_h + gdP_h)]\theta(y)\underline{\theta}\right.$$

$$\left. + [T_\beta - d(P_\beta + T_z) + d^2 P_z]\underline{\beta}\right\}$$

where

$$g = \left[\tfrac{1}{2} + a\right] \qquad d = [c - e] \tag{7.86}$$

The aerodynamic coefficients in Eq. (7.85) are given in Refs. 11–13. The integrations in Eq. (7.86) are evaluated numerically considering constant values for each strip. The aerodynamic loads can thus be written as

$$
\begin{Bmatrix} Q_h \\ Q_\theta \\ Q_\beta \end{Bmatrix} = \pi \rho \omega^2 \begin{bmatrix} A_{hh} & A_{h\theta} & A_{h\beta} \\ A_{\theta h} & A_{\theta\theta} & A_{\theta\beta} \\ A_{\beta h} & A_{\beta\theta} & A_{\beta\beta} \end{bmatrix} \begin{Bmatrix} \underline{h} \\ \underline{\theta} \\ \underline{\beta} \end{Bmatrix} \tag{7.87}
$$

where

$$
A_{hh} = \int_0^l b^2 [f(y)]^2 L_h \, dy
$$

$$
A_{h\theta} = \int_0^l b^3 f(y) \theta(y) [L_\theta - g L_h] \, dy
$$

$$
A_{\theta h} = \int_0^l b^3 f(y) \theta(y) [M_h - g L_h] \, dy
$$

$$
A_{\theta\theta} = \int_0^l b^4 [\theta(y)]^2 [M_\theta - g(L_\theta + M_h) + g^2 L_h] \, dy
$$

$$
A_{h\beta} = \int_{l_1}^l b^3 f(y) [L_\beta - d L_z] \, dy \tag{7.88}
$$

$$
A_{\theta\beta} = \int_{l_1}^l b^4 \theta(y) [M_\beta - g L_\beta - d M_z + dg L_z] \, dy
$$

$$
A_{\beta h} = \int_{l_1}^l b^3 f(y) [T_h - d P_h] \, dy
$$

$$
A_{\beta\theta} = \int_{l_1}^l b^4 f(y) [T_\theta - d P_\theta - g T_h - gd P_h] \, dy
$$

$$
A_{\beta\beta} = \int_{l_1}^l b^4 [T_\beta - d(P_\beta + T_z) + d^2 P_z] \, dy
$$

The Lagrange equations of motion can be written as

$$
\frac{d}{dt} \left[\frac{\partial T}{\partial \xi'} \right] + \frac{\partial U}{\partial \xi} + \frac{\partial D}{\partial \xi'} = Q_\xi \tag{7.89}
$$

where $\xi = h, \theta$, or β. Applying the Lagrange equations of motion for a harmonic solution in the form

$$
h = \underline{h} e^{i\omega t}
$$

$$
\theta = \underline{\theta} e^{i\omega t} \tag{7.90}
$$

$$
\beta = \underline{\beta} e^{i\omega t}
$$

we obtain

$$
\begin{bmatrix} A & B & C \\ D & E & F \\ G & H & I \end{bmatrix} \begin{Bmatrix} \underline{h} \\ \underline{\theta} \\ \underline{\beta} \end{Bmatrix} = \begin{Bmatrix} 0 \\ 0 \\ 0 \end{Bmatrix} \tag{7.91}
$$

where

$$
A = \left[M + \pi \rho A_{hh} - M \left[\frac{\omega_h}{\omega} \right]^2 [1 + i c_h] \right]
$$

$$
B = S + \pi \rho A_{h\theta}
$$

$$
C = S_\beta + \pi \rho A_{h\beta}
$$

$$
D = S_\beta + \pi \rho A_{h\beta}
$$

$$
E = \left[I_\theta + \pi \rho A_{\theta\theta} - I_\theta \left[\frac{\omega_\theta}{\omega} \right]^2 [1 + i c_\alpha] \right] \tag{7.92}
$$

$$
F = P_{\theta\beta} + \pi \rho A_{\theta\beta}
$$

$$
G = S_\beta + \pi \rho A_{\beta h}
$$

$$
H = P_{\beta\theta} + \pi \rho A_{\beta\theta}
$$

$$
I = I_\beta + \pi \rho A_{\beta\beta} - I_\beta (1 + i c_\beta) \left[\frac{\omega_\beta}{\omega} \right]^2
$$

The solution of the problem can proceed in the same way as given in Section 7.3 using the Theodorsen method of solution for the determination of the flutter velocities's critical values.

7.5 Control Surface Reversal and Efficiency

In this section, we will extend the application of the strip aerodynamic theory given in Section 7.4 to an important problem of aeroelasticity, namely the problem of control reversal and efficiency. We will limit the presentation to the case of the aileron reversal and efficiency because the extension to other control surfaces is straightforward. The ailerons control the rolling moment of an airplane. Because of an aileron nose-up rotation on the right half-wing, an increase in the corresponding lift on the right half-wing will occur. At the same time, we will have a decrease in the left half-wing due to the nose-down rotation of the left aileron. The net result is a rolling moment rotation about the fuselage axis. Now, the nose-up rotation of the right aileron creates a sectional aerodynamic moment about the elastic axis, tending to decrease the angle of attack due to the flexibility of the wing and vice versa for the left half-wing. This causes a reduction in the net rolling moment about the fuselage centerline of the airplane compared to the rolling moment produced by a rigid wing. While the wing stiffness is constant, the aerodynamic load increases with the increase of the airplane speed; therefore, it is expected that at a given speed the effect of the actuation of the ailerons will be null, and beyond this speed the effect of the aileron actuation will be reversed. Our purpose in this section is to present a method of calculation of the critical reversal speed and the aileron efficiency using the strip aerodynamic theory previously presented. The aileron efficiency will be defined as the ratio of the rolling moment with the wing flexibility

considered to the rolling moment produced considering the wing completely rigid. The airfoil incremental sectional lift per unit span can be written as

$$L' = 2\pi\rho U^2 \left[b\theta + b\frac{\partial c_l}{\partial \beta}\beta \right] \tag{7.93}$$

where ρ is the air density, U is the airplane speed, b is the sectional half chord, θ is the incremental angle of attack at the wing section in consideration, β is the aileron deflection at the corresponding section, and a theoretical lift coefficient $= 2\pi$ has been assumed for simplicity of the representation. Assuming that β is constant spanwise, we can write the total rolling moment (R.M.) as

$$\text{R.M.} = 4\pi\rho U^2 \left[\sum_{\text{wing}} b_i y_i \Delta y_i \theta_i + \beta \sum_{\text{aileron}} b_i \frac{T_{10}}{\pi} y_i \Delta y_i \right] \tag{7.94}$$

where T_{10} is a function of the ratio of the aileron chord and the airfoil chord; the evaluation of T_{10} will be given in the sequel. At the reversal speed, the rolling moment is null; therefore, using Eq. (7.94), we can write

$$\beta = -\frac{\sum\limits_{\text{wing}} b_i y_i \Delta y_i \theta_i}{\sum\limits_{\text{aileron}} b_i \dfrac{T_{10}}{\pi} y_i \Delta y_i} \tag{7.95}$$

The incremental aerodynamic moment at station i due to the aileron deflection can be written as

$$\Delta M_i = \lambda \left\{ 2gb_i^2\theta_i + \left[2g\frac{T_{10}}{\pi} - \frac{T_4 + T_{10}}{\pi} \right]_i b_i^2 \beta \right\} \Delta y_i \tag{7.96}$$

Substituting Eq. (7.95) into Eq. (7.96), we obtain

$$\Delta M_i = \lambda \left\{ 2gb_i^2\theta_i - \left[2g\frac{T_{10}}{\pi} - \frac{T_4 + T_{10}}{\pi} \right]_i b_i^2 \frac{\sum\limits_{\text{wing}} b_i y_i \Delta y_i}{\sum\limits_{\text{aileron}} b_i \dfrac{T_{10}}{\pi} y_i \Delta y_i} \theta_i \right\} \Delta y_i \tag{7.97}$$

and, for the complete half-wing, we can write in a matrix form

$$\{\Delta M_i\} = \lambda [F]\{\theta_i\} \tag{7.98}$$

where $[F]$ is a diagonal matrix with the corresponding strip elements given by Eq. (7.97). Again the rotational angles $\{\theta_i\}$ are related to the torsional moments $\{\Delta M_i\}$ through the matrix of influence coefficients $[B]$, and we write

$$\{\theta_i\} = [B]\{\Delta M_i\} \tag{7.99}$$

Using Eqs. (7.98) and (7.99), we can write

$$\{\theta_i\} = \lambda[B][F]\{\theta_i\} = \lambda[G]\{\theta_i\} \tag{7.100}$$

Table 7.2 Numerical values of T_4 and T_{10}
as functions of e

e	T_4	T_{10}
0.0	−1.57080	2.57080
0.1	−1.37112	2.46562
0.2	−1.17348	2.34922
0.3	−0.97993	2.22004
0.4	−0.79266	2.07578
0.5	−0.61418	1.91323
0.6	−0.44730	1.72731
0.7	−0.29550	1.50954

where $[G] = [B][F]$. Equation (7.100) represents an eigenvalue problem; the lowest eigenvalue will furnish the lowest reversal velocity. The aerodynamic coefficients T_4 and T_{10} were calculated by Theodorsen[8] as functions of e, the aileron chord over the total main airfoil chord. Table 7.2 is a short table of these coefficients.

References

[1]Birnhaum, W., "Der Schlagflügelpropeller und die Kleinen Schwingungen Elastischer Befestigter Tragflügel," *Z. Flugtech. und Motorluftschift*, Vol. 15, 1924, pp. 128–134.

[2]Wagner, H., "Über die Entstehung des Dynamischer Auftriebes von Tragflügeln," *ZAMM*, Vol. 5, 1925, pp. 17–35.

[3]Küssner, H. G., "Allgemeine Tragflachentheorie," *Luftfahrtforschung*, Vol. 17, No. 11–12, 1940, pp. 370–379.

[4]Glauert, H., "The Accelerated Motion of a Cylindrical Body Through a Fluid," *Aeronautical Research Council R & M*, No. 1215, 1929.

[5]Theodorsen, T., *General Theory of Aerodynamic Instability and the Mechanism of Flutter*, NACA Rept. No. 496, 1935.

[6]Ellenberger, G., "Bestimmung der Luftkräfte auf Einen Ebenen Tragflügel mit Querruder," *ZAMM*, Vol. 16, 1936, pp. 199–226.

[7]Küssner, H. G., "Schwingungen von Flugzeugflügeln," *Luftfahrtforschung*, Vol. 4, No. 2, 1929, pp. 41–62.

[8]Theodorsen, T., and Garrick, E., *Mechanism of Flutter. A Theoretical and Experimental Investigation of the Flutter Problem*, NACA Rept. No. 485, 1940.

[9]*Handbook of Mathematical Functions with Formulas, Graphs and Mathematical Tables*, 8th ed., edited by M. Abramowitz and I. A. Stegnun, Dover, New York, 1972.

[10]Jones, W. P., "Aerodynamic Forces on Wings in Non-Uniform Motion," *Aeronautical Research Council R & M*, No. 2117, 1945.

[11]Scalan, R. H., and Rosenbaum, R., *Introduction to the Study of Aircraft Vibration and Flutter*, 2nd ed., Macmillan, New York, 1960.

[12]Smilg, B., and Wasserman, L. S., *Application of Three-Dimensional Flutter Theory to Aircraft Structures*, U.S. Army Air Force, Tech. Rept. No. 4798, 1942.

[13]*Manual on Aeroelasticity*, AGARD, Vol. I–VII, NATO, first edited in 1959, edited by W. P. Jones, 1961, edited by R. Mazet, 1968, and continuously updated.

Problems

7.1 For a typical section, the following information is given: $I_\theta = 32.00 \, \text{kg·m}^2/\text{m}$, $\omega_\theta = 20$ Hz, $b = 1$ m, $\rho = 1.226$ kg/m^3, $c_{l\alpha} = 2\pi$, and $a = -0.3$ (i.e., elastic axis position at 35% of the section chord). Find the sectional divergence speed.

7.2 During the preliminary design stage, aeroelastic analyses are performed using a sectional $c_{l\alpha} = 2\pi$, a quasistationary aerodynamic theory, and calculations are performed at sea level. Justify such proceedings.

7.3 For a half-wing, the following information is given: wing-half span $= 6.096$ m and elastic axis position at 35% of the sectional chord. The half-wing has been modeled using the six geometric data in Table P7.3.

Table P7.3

Strip	1	2	3	4	5	6
y, m	0.096	1.8288	3.0734	4.0894	4.8514	5.6642
Δy, m	1.2192	1.2192	1.2700	0.7620	0.7620	0.8636
b, m	1.4473	1.2954	1.1398	1.0128	0.9175	0.8159

The torsional influence coefficient matrix, corresponding to the above-mentioned strips, is given by the following (in rad/N·m):

$B_{1,1} = 0.02304 \times 10^{-6}$ $B_{2,2} = 0.4954 \times 10^{-6}$ $B_{3,3} = 1.33646 \times 10^{-6}$
$B_{4,4} = 2.21207 \times 10^{-6}$ $B_{5,5} = 2.97248 \times 10^{-6}$ $B_{6,6} = 3.83657 \times 10^{-6}$
$B_{i,j} = B_{i,i}$ for $j > i$ $i = 1, 2, 3, \ldots$ and $j = 2, 3, 4, \ldots$ $B_{j,i} = B_{i,j}$

Find the half-wing divergence speed at sea level.

7.4 At 3/4 half-span position of a cantilever wing, the following information is given: $m = 31.814$ kg/m, $I_\alpha = 15.30$ kg·m, $s_\alpha = 6.78$ kg, $\omega_h = 62.2$ rad/seg, $\omega_\alpha = 100.64$ rad/seg, $b = 0.95$ m, $c_{l\alpha} = 2\pi$, $a = -0.3$ (i.e., elastic axis at 35% of the sectional chord), and $g_h = g_\alpha = 0.02$, assuming $\rho = 1.226$ kg/m^3. Obtain the following:

(a) The aeroelastic stability determinant for $1/k = 2.0$, given that, for $1/k = 2.0$, we have $L_h = 0.972 - 2.3961 \, i$, $L_\alpha = -4.8860 - 3.1860 \, i$, and $M_\alpha = 0.3750 - 2.0000 \, i$. Find the values of X_R and X_I for this condition.

(b) The aeroelastic stability determinant for $1/k = 2.5$, given that, for $1/k = 2.5$, we have $L_h = 0.1752 - 3.1250 \, i$, $L_\alpha = -8.1375 - 3.5625 \, i$, and $M_\alpha = 0.3750 - 2.5000 \, i$. Find the values of X_R and X_I for this condition.

(c) Calculate the flutter frequency and velocity using the Theodorsen method of solution.

<div align="right">

8
Aeroelasticity of Flight Vehicles

</div>

8.1 Introduction

This chapter deals with the problem of aeroelasticity of flight vehicles. The problem formulation is first presented. Emphasis is made on the aeroelastic modal base representation of the problem. Discrete aerodynamic theories, which are closely related to the finite element method, are then presented. The various methods of the solution of the aeroelastic equations, namely the k, p, and $p–k$ methods, are discussed.

8.2 Problem Formulation

Consider the elastic flight vehicle shown in Fig. 8.1. The vehicle is flying in a state of equilibrium under the action of a set of external loads. In the presence of some external disturbance, e.g., a gust or a sudden pilot-induced action on the control of the flight vehicle, the vehicle can start to perform a perturbed motion with transverse deflections $w(x, y, z, t)$. These in turn will create a distribution of incremental airloads $\Delta p(x, y, z, t)$ on the flight vehicle. We are interested in the study of the stability of the flight vehicle due to such motion. The theoretical formulation of the problem can be made using an energy approach using Hamilton's principle, and we write

$$\int_{t_0}^{t_1} \delta(T - U)\,dt + \int_{t_0}^{t_1} \delta W\,dt = 0 \tag{8.1}$$

where T is the kinetic energy, U is the strain energy of small deformations, W is the work done by the external incremental nonstationary airloads, t is the time, and δ is the variational operator. Using a set of generalized coordinates $\{q\}$ and applying Hamilton's principle, the equations of motion are obtained and can be written as

$$[M]\{q''\} + [B]\{q'\} + [K]\{q\} = \{F\} \tag{8.2}$$

where an internal damping has been incorporated and is represented by the term $[B]\{q'\}$ in the equation of motion and $\{F\}$ is the vector of the external nonstationary aerodynamic load corresponding to the generalized coordinates $\{q\}$. The finite element method is now the most adequate means of structural representation of complex structures. This, if done, will furnish the left-hand side of Eq. (8.2). The problem of the structural representation has been treated in detail in previous chapters. The number of unknowns in Eq. (8.2) is, however, enormous, and the solution of the aeroelastic problem for the complete vehicle in the physical degrees of freedom would be prohibitive even with the use of high-speed digital computers

$\triangle$ p(x,y,z,t)

external
disturbance

$\triangle$ w(x,y,z,t)
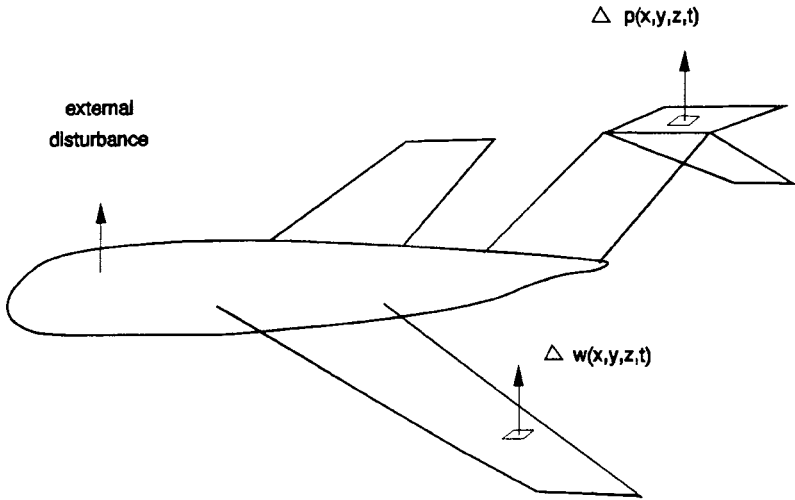
Fig. 8.1   Flight vehicle in the presence of an external disturbance.

now available. A method that has proved to be efficient for the solution of aeroelastic problems is the modal base transformation. This has been given in detail in Chapter 3. The modal transformation not only facilitates the problem formulation, but, most important, it gives a clear physical interpretation in subsequent analysis of the stability problem.

Thus making the modal transformation

$$\{q\} = [Q]\{\eta\} \tag{8.3}$$

in Eq. (8.2), where $[Q]$ is the matrix of the eigenvectors of the associated conservative system retained in the analysis and $\{\eta\}$ is the vector of the modal amplitudes, and premultiplying by $[Q]^T$, we obtain

$$[\mu]\{\eta''\} + [\beta]\{\eta'\} + [\gamma]\{\eta\} = \{\phi\} \tag{8.4}$$

The matrices $[\mu]$ and $[\gamma]$ are the generalized mass and stiffness matrices and are diagonal matrices as has been given in Chapter 3. The damping matrix $[\beta]$ is not in general diagonal. However, for slightly damped structures such as used in aeronautical constructions, the modal damping forces are much less than the inertia and stiffness terms so that we can make the approximation of neglecting the modal damping coupling and assume that the generalized damping matrix is diagonal. The value of the individual damping mode can be obtained from ground vibration tests or can be estimated from previous experience of similar structures. The right-hand side of Eq. (8.3) represents the generalized aerodynamic nonstationary incremental airloads written in the modal coordinates. The formulation of these loads will be treated in the next sections.

8.3   Incremental Nonstationary Aerodynamic Loads

In this section the formulation of nonstationary airloads is presented. The formulation used is based on integral representation methods because they are the most suitable for numerical solution of the problem. For other methods of representation and more details on nonstationary airloads formulation, the reader is referred to excellent textbooks available on the subject, e.g., Refs. 1–6. The integral equation relating the pressure and the normalwash distribution in unsteady potential (subsonic or supersonic) three-dimensional flows was first derived by Küssner[7] and reads

$$\frac{w(x, y, z)}{U} = \frac{1}{8\pi} \iint_A \left[\frac{\Delta p(\xi, \eta, \zeta) K(x, y, z, \xi, \eta, \zeta, k, M)}{qr^2} \right] d\xi\, d\eta \qquad (8.5)$$

where $w(x, y, z)$ is the normalwash velocity at point x, y, z; U is the free stream velocity of the unperturbated flow assumed in the x direction; and $\Delta p(\xi, \eta, \zeta)$ is the nonstationary aerodynamic pressure difference at point ξ, η, ζ. The free stream dynamic pressure is denoted by q and is equal to $\rho U^2/2$ where ρ is the free stream air density. The Kernel function of the integral K is a function of the relative position, the free stream Mach number M, and the reduced frequency k. Other notations are as given in Fig. 8.2. The Kernel function of the integral Eq. (8.5) for three-dimensional problems can be written as

$$K = e^{\frac{-i\omega x_0}{U}} [K_1 T_1 + K_2 T_2] \qquad (8.6)$$

where T_1 and T_2 are geometric relations and are given by

$$T_1 = \cos(\gamma_r - \gamma_s)$$

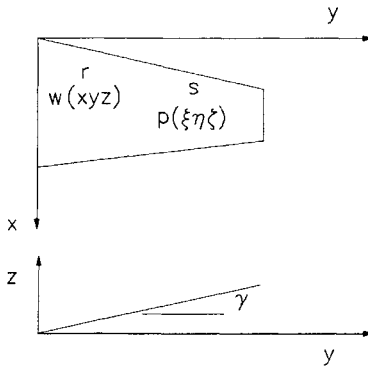$$T_2 = \frac{(z_0 \cos \gamma_r - y_0 \sin \gamma_r)(z_0 \cos \gamma_s - y_0 \sin \gamma_s)}{r^2} \qquad (8.7)$$

Fig. 8.2   Notations of the three-dimensional aeroelastic problem.

where

$$x_0, y_0, z_0 = x - \xi, y - \eta, z - \zeta$$

$$r = [(y - \eta)^2 + (z - \zeta)^2]^{\frac{1}{2}}$$

(8.8)

and the subscripts r and s stand for receiving and sending points, respectively. The functions K_1 and K_2 were evaluated by Landahl[8] and Albano and Rodden[9] and are given by

$$K_1 = \frac{Mre^{-iku}}{R(1+u^2)^{\frac{1}{2}}} + N_{3/2}$$

$$K_2 = -\frac{ikM^2r^2e^{-iku}}{R^2(1+u^2)^{\frac{1}{2}}} - \frac{Mre^{-iku}[(1+u^2)\beta^2r^2 + 2R^2 + MRru]}{R^3(1+u^2)^{\frac{3}{2}}} - 3N_{5/2}$$

(8.9)

where

$$R = \left(x_0^2 + \beta^2 r^2\right)^{\frac{1}{2}}$$

$$u = \frac{(Mr - x_0)}{\beta^2 r}$$

$$N_{3/2} = \int_u^{\infty} \frac{e^{-ikv}}{(1+v^2)^{\frac{3}{2}}} \, dv$$

(8.10)

$$N_{5/2} = \int_u^{\infty} \frac{e^{-ikv}}{(1+v^2)^{\frac{5}{2}}} \, dv$$

$$\beta = (1 - M^2)^{\frac{1}{2}}$$

Since Küssner[7] introduced the integral equation relating the pressure and the normalwash distribution in unsteady potential three-dimensional flows, many authors investigated his integral equation to reduce it to a form suitable for digital computation. The main contributions are from Watkins,[10] Laschka,[11] Vivian and Andrew,[12] Landahl,[8] Albano and Rodden,[9] and Rowe et al.[13] Basically there exist in the literature two methods of solution.

The first method known as the collocation method consists in choosing a set of admissible functions to represent the pressure difference. These functions are multiplied by undetermined coefficients, and their combination is assumed to represent the pressure difference. To determine these coefficients, a set of collocation points are chosen on the lifting surface and Eq. (8.5) is forced to be satisfied at these points. Obviously, the number of collocation points must be

equal to the number of terms taken in the series. Seen from this point of view, this collocation method is nothing more than a finite element method applied to the whole domain. The great disadvantages of this method reside in the choice of the independent functions, the huge amount of integrations involved in the solution, limitations of the method to planar lifting surfaces, and difficulty of the treatment of the problem of control surfaces. However, for planar surfaces, reasonable solutions were obtained, including control surfaces in Refs. 14 and 15.

The second method is a discrete method that has proved to be versatile, can treat nonplanar surfaces, and can be applied to problems with control surfaces without difficulties. One procedure of these discrete methods is the doublet lattice method originally proposed by Albano and Rodden[9] and is now widely used in aeroelastic numerical computations. This method will be briefly described in the following section. In the doublet lattice method, the lifting surfaces are divided into panel segments. Each panel is constructed such that the two side edges are parallel to the unperturbated flow, which in turn is assumed to be in the x direction of the system of coordinates as shown in Fig. 8.3. In the fourth mean chord location of each element, a constant strength acceleration doublet with unknown intensity is assumed to be positioned. The boundary conditions are applied at the 3/4 position of the mean chord of each element. Thus, at the control point r, we can write for
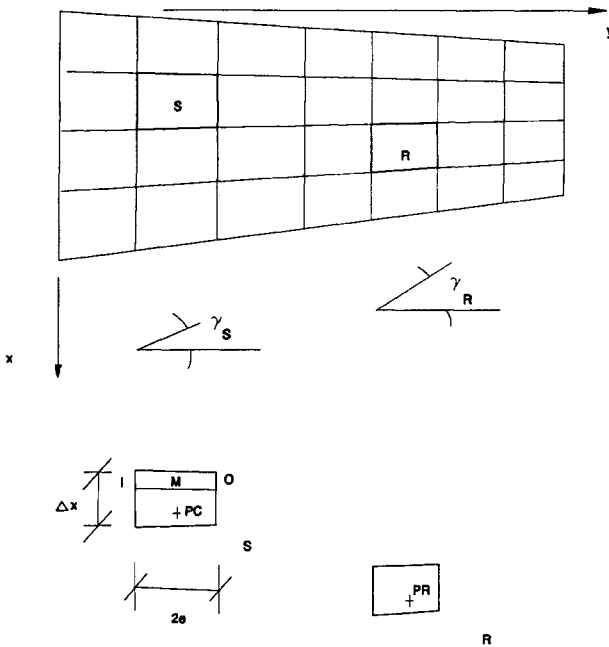

Fig. 8.3   Notations of the doublet lattice method.

the contribution of all the elements

$$\frac{w(x, y, z)}{U} = \sum_{j=1}^{n} \frac{f_j}{4\pi \rho U^2} \int_{l_j} K \, d\mu \qquad (8.11)$$

where f_j is the intensity of the doublet of the element j, l_j is the span of the element j, and the integration is performed along the span of the element j. The aerodynamic pressure difference for the element j can be written as

$$P_j = \frac{\text{force}}{\text{element area}} = \frac{f_j l_j}{a_j} \qquad (8.12)$$

where a_j is the area of the element j. Using Eqs. (8.11) and (8.12), the integral Eq. (8.5) is transformed to an algebraic equation, and we write

$$\left\{ \frac{w}{U} \right\} = [D] \left\{ \frac{P}{\rho U^2/2} \right\} \qquad (8.13)$$

and the elements of the matrix $[D]$ are given by

$$D_{ij} = \frac{1}{8\pi} \frac{a_j}{l_j} \int_{l_j} K \, d\mu \qquad (8.14)$$

Finally, the matrix $[D]$ is inverted, and we obtain a relation between the pressure difference vector and the downwash vector in the form

$$\left\{ \frac{P}{\rho U^2/2} \right\} = [A] \left\{ \frac{w}{U} \right\} \qquad (8.15)$$

where $[A] = [D]^{-1}$.

8.3.1   Evaluation of the Aerodynamic Influence Coefficient Matrix

To evaluate numerically the aerodynamic influence coefficient matrix, we proceed to use the scheme first proposed by Albano and Rodden,[9] and we write a quadratic variation of the doublet intensity along the 1/4 chord position of the element span. The integral of Eq. (8.14) can then be written as

$$I_{ij} = \int_{l_j} K \, d\mu = \int_{-e}^{e} \frac{A\eta^2 + B\eta + C}{(\eta - \eta_0)^2 + \zeta_0^2} \, d\eta \qquad (8.16)$$

where $e = l_j \cos \lambda_j / 2$, λ_j is the local sweeping angle of the element j, and

$$\eta_0 = [y_r - y_{sm}] \cos \gamma_s + [z_r - z_{sm}] \sin \gamma_s$$

$$\zeta_0 = -[y_r - y_{sm}] \sin \gamma_s + [z_r - z_{sm}] \cos \gamma_s$$

$$A = [\kappa_i - 2\kappa_m + \kappa_0]/2e^2 \qquad B = [\kappa_0 - \kappa_i]/2e \qquad C = \kappa_m \qquad (8.17)$$

$$\kappa = r_1^2 K$$

The subscripts i, m, and o indicate values at the internal, middle, and external extremities of the line doublet as shown in Fig. 8.3, and the coordinates η and ζ are given by

$$\eta = y \cos \gamma_s + z \sin \gamma_s$$
$$\zeta = -y \sin \gamma_s + z \cos \gamma_s \tag{8.18}$$

We can thus perform the integration analytically, and the results read

$$I_{ij} = \left[\left(\eta_0^2 - \zeta_0^2 \right) A + \eta_0 B + C \right] |\zeta_0|^2 \tan^{-1} \frac{2e|\zeta_0|}{r_1^2 - e^2}$$

$$+ [0.5B + \eta_0 A] \, \ell_n \frac{r_1^2 - 2\eta_0 e + e^2}{r_1^2 + 2\eta_0 e + e^2} + 2eA \tag{8.19}$$

where $r_1 = (\eta_0^2 + \zeta_0^2)^{1/2}$ and, for the case of planar condition, i.e., $\zeta_0 \to 0$, the integral reads

$$I_{ij} = \left[\eta_0^2 A + \eta_0 B + C \right] \left[\frac{1}{\eta_0 - e} - \frac{1}{\eta_0 + e} \right] + [0.5B + \eta_0 A] \, \ell_n \frac{\eta_0 - e}{\eta_0 + e} + 2eA \tag{8.20}$$

To compute the constants A, B, and C, the Kernel function K must be obtained at the three points i, m, and o. This will be treated in the next section.

8.3.2 Evaluation of the Kernel Function in Subsonic Flows

The first attempt to evaluate the integrals involved in the nonelementary part of the Kernel function [Eq. (8.9)] was made by Watkins et al.,[10] who approximated the algebraic part of the integrand by a four-term exponential approximation, adjusted tentatively to fit the algebraic part. The integrals can then be evaluated in a closed form. This approximation, made well before the advent of high-speed digital computations, has an accuracy of two digits. Later on, Laschka[11] presented an analytical solution in terms of infinite series. The solution was obtained by expanding the exponential term of the integrand in its power series solution and then applying successive integrations by parts to obtain the infinite power series solution. This series solution has the defect of very slow convergence, limiting its application to a limited range of the values of the arguments. For this reason, Laschka also presented a numerical solution similar to that of Watkins et al., which includes an 11-term exponential approximation. The integrals performed using the Laschka approximation have an accuracy of the order of three digits. A similar numerical solution was presented by Dat and Malfois[16] approximating the algebraic part of the integrand by a series of fraction terms having constant numerators. The accuracy of this solution and the computational effort involved are similar to the Laschka approximation. The exponential approximation of the algebraic part of the integrand was again used by Desmarais,[17] who used the least-squares technique to minimize the error in approximation. The precision of the integrals evaluated using Desmarais's approximation with 12 terms is of the order of three to four digits. By increasing the number of terms, better precision will be achieved; however,

the process would be very costly in terms of computational time and will be subject to accumulation errors. Asymptotic expansion of the Laschka series was given by Ueda[18] for large values of the arguments. In Ref. 19 an exact solution of related integrals coupled with a costly efficient numerical evaluation was presented. The problem was first transformed to a solution of a differential equation. The functional solutions of the differential equation were given, and efficient evaluation of these functions were then described. This procedure is detailed below.

The differential equation.   The nonelementary part of the Kernel function given in Eq. (8.5) can be written as

$$N_{3/2} = \int_u^\infty \frac{e^{-ikv}}{[1+v^2]^{\frac{3}{2}}}\, dv = \int_0^\infty \frac{e^{-ikv}}{[1+v^2]^{\frac{3}{2}}}\, dv - \int_0^u \frac{e^{-ikv}}{[1+v^2]^{\frac{3}{2}}}\, dv$$

$$N_{5/2} = \int_u^\infty \frac{e^{-ikv}}{[1+v^2]^{\frac{5}{2}}}\, dv = \int_0^\infty \frac{e^{-ikv}}{[1+v^2]^{\frac{5}{2}}}\, dv - \int_0^u \frac{e^{-ikv}}{[1+v^2]^{\frac{5}{2}}}\, dv$$

$$(8.21)$$

Notice that the first integrals of the second form in Eq. (8.21) are readily available in terms of the modified Bessel and Struve functions. Consider now the integral

$$N_\nu(u) = \int_u^\infty \frac{e^{-ikv}}{[1+v^2]^\nu}\, dv \qquad \nu = 1/2, 3/2, 5/2, \ldots$$

$$= N_{R_\nu}(u) + i N_{I_\nu}(u) \tag{8.22}$$

where

$$N_{R_\nu}(u) = \int_u^\infty \frac{\cos(kv)}{[1+v^2]^\nu}\, dv$$

$$(8.23)$$

$$N_{I_\nu}(u) = -\int_u^\infty \frac{\sin(kv)}{[1+v^2]^\nu}\, dv$$

In the integrals depicted in Eqs. (8.22) and (8.23), we consider k as a constant, nonnegative parameter, and we notice that it is sufficient to consider only nonnegative values of the arguments u, because of the symmetry properties of the arguments, and it can be easily shown that

$$N_{R_\nu}(-u) = \frac{2\pi^{\frac{1}{2}}}{\Gamma(\nu)}(k/2)^\mu K_\mu(k) - N_{R_\nu}(u)$$

$$(8.24)$$

$$N_{I_\nu}(-u) = N_{I_\nu}(u) \qquad \mu = 0, 1, 2, \ldots$$

where $K_\mu(u)$ is the modified Bessel function of the second kind and the order μ. Now using Poisson–Basset[20] and Nicholson–Watson[21] integrals, the functions in

Eq. (8.23) for $u = 0$ read

$$N_{R_\nu}(0) = \int_0^\infty \frac{\cos(kv)}{[1+v^2]^\nu} = \pi^{\frac{1}{2}}(k/2)^\mu \frac{K_\mu(k)}{\Gamma(\nu)} \tag{8.25a}$$

$$N_{I_\nu}(0) = -\int_0^\infty \frac{\sin(kv)}{[1+v^2]^\nu} = -\pi^{\frac{1}{2}}(1-\nu)(k/2)^\mu \frac{I_{-\mu}(k) - L_{-\mu}(k)}{2}$$

$$\mu = \frac{2\nu - 1}{2} = 0, 1, 2, \ldots \tag{8.25b}$$

where $I_\mu(k)$ is the modified Bessel function of the first kind and the order μ, and $L_\mu(k)$ is the modified Struve function of the order μ. We now define a function $F_\nu(u)$ as

$$F_\nu(u) = N_{R_\nu}(u)\sin(ku) + N_{I_\nu}(u)\cos(ku) \tag{8.26}$$

Through differentiation of Eq. (8.26), we obtain

$$F_\nu'(u) = k\left[N_{R_\nu}(u)\cos(ku) - N_{I_\nu}(u)\sin(ku)\right] \tag{8.27}$$

and

$$F_\nu''(u) + k^2 F_\nu(u) = -\frac{k}{[1+u^2]^\nu} \tag{8.28}$$

The boundary conditions on the differential Eq. (8.28) can be obtained from Eqs. (8.27), (8.28), and (8.25) and read

$$F_\nu(0) = -\frac{\pi^{\frac{1}{2}}}{2}\Gamma(1-\nu)(k/2)^\mu[I_{-\mu}(k) - L_{-\mu}(k)] \tag{8.29}$$

and

$$F_\nu'(0) = \frac{\pi^{\frac{1}{2}}}{\Gamma(\nu)}(k/2)^\mu k K_\mu(k) \tag{8.30}$$

Furthermore, Eqs. (8.26) and (8.27) can be inverted to read

$$N_{R_\nu} = F_\nu(u)\sin(ku) + \frac{1}{k}F_\nu'(u)\cos(ku)$$

$$N_{I_\nu} = F_\nu(u)\cos(ku) - \frac{1}{k}F_\nu'(u)\sin(ku) \tag{8.31}$$

We notice that the problem of the evolution of the integrals given in Eq. (8.22) is now transformed to the solution of the differential Eq. (8.28), subjected to the boundary conditions in Eqs. (8.29) and (8.30). The integrals are then obtained from Eq. (8.31).

Recurrence relations of the functions $N_\nu(u)$ *and* $F_\nu(u)$.   Recurrence relations of the functions $N_\nu(u)$ and $F_\nu(u)$ can be obtained through integrating Eq. (8.23) and making use of Eqs. (8.26) and (8.27) to read

$$4\nu(1+\nu)N_{R_{\nu+2}}(u) = k^2 N_{R_\nu}(u) + 2\nu(2\nu+1)N_{R_{\nu+1}}(u)$$

$$+ \frac{k\sin(ku)}{(1+u^2)^\nu} - \frac{2\nu u\cos(ku)}{(1+u^2)^{\nu+1}}$$

$$4\nu(1+\nu)N_{I_{\nu+2}}(u) = k^2 N_{I_\nu}(u) + 2\nu(2\nu+1)N_{I_{\nu+1}}(u)$$

$$+ \frac{k\cos(ku)}{(1+u^2)^\nu} + \frac{2\nu u\sin(ku)}{(1+u^2)^{\nu+1}} \tag{8.32}$$

$$4\nu(1+\nu)F_{\nu+2}(u) = k^2 F_\nu(u) + 2\nu(2\nu+1)F_{\nu+1}(u) + \frac{k}{(1+u^2)^\nu}$$

$$4\nu(1+\nu)F'_{\nu+2}(u) = k^2 F'_\nu(u) + 2\nu(2\nu+1)F'_{\nu+1}(u) - \frac{2\nu u k}{(1+u^2)^{\nu+1}}$$

Integral representation of the function $F_\nu(u)$.   The Laplace transform of the differential Eq. (8.28) reads

$$(s^2+k^2)F_\nu(s) = sF_\nu(0) + F'_\nu(0) - k\int_0^\infty \frac{e^{-su}}{[1+u^2]^\nu}\,du \tag{8.33}$$

Consider now the Lipschitz–Hankel–Gegenbauer integral[22]

$$\frac{\pi^{\frac{1}{2}}}{2^\mu\Gamma(\nu)}\int_0^\infty t^\mu J_\mu(t)e^{-ut}\,dt = \frac{1}{[1+u^2]^\nu} \qquad \mathrm{Re}(\mu) > -1/2 \tag{8.34}$$

and, for the case treated here, $\mu = 0, 1, 2, 3, \ldots$. Using now Eqs. (8.33) and (8.34), we obtain

$$(s^2+k^2)F_\nu(s) = sF_\nu(0) + F'_\nu(0) - \frac{k\pi^{\frac{1}{2}}}{2^\mu\Gamma(\nu)}\int_0^\infty \frac{t^\mu J_\mu(t)}{[t+s]}\,dt \tag{8.35}$$

Applying the Laplace transform, we obtain

$$F_\nu(u) = -\frac{k\pi^{\frac{1}{2}}}{2^\mu\Gamma(\nu)}\int_0^\infty \frac{t^\mu J_\mu(t)e^{-ut}}{t^2+k^2}\,dt - \frac{\pi^{\frac{1}{2}}\sin(ku)}{2^\mu\Gamma(\nu)}\int_0^\infty \frac{t^{\mu+1}J_\mu(t)}{t^2+k^2}\,dt$$

$$+ \frac{k\pi^{\frac{1}{2}}\cos(ku)}{2^\mu\Gamma(\nu)}\int_0^\infty \frac{t^\mu J_\mu(t)}{t^2+k^2}\,dt + \frac{F'_\nu\sin(ku)}{k} + F_\nu(0)\cos(ku) \tag{8.36}$$

Now making use of the Hankel–Nicholson integrals[23]

$$\int_0^\infty \frac{J_0(t)}{t^2 + k^2}\, dt = \frac{\pi}{2k}[I_0(k) - L_0(k)]$$

$$\int_0^\infty \frac{t J_1(t)}{t^2 + k^2}\, dt = -\frac{\pi}{2}[I_{-1}(k) - L_{-1}(k)]$$

$$\int_0^\infty \frac{t J_0(t)}{t^2 + k^2}\, dt = K_0(k)$$ (8.37)

$$\int_0^\infty \frac{t^2 J_1(t)}{t^2 + k^2}\, dt = k K_1(k)$$

and using the recurrence relations $F_\nu(u)$ and the recurrence relations of the Bessel functions, we finally obtain an integral representation for the function $F_\nu(u)$ as

$$F_\nu(u) = -\frac{k\pi^{\frac{1}{2}}}{e^\mu \Gamma(\nu)} \int_0^\infty \frac{t^\mu J_\mu(t) e^{-ut}}{t^2 + k^2}\, dt$$ (8.38)

$$\mu = \frac{2\nu - 1}{2} = 0, 1, 2, 3, \ldots$$

Furthermore, examination of Eqs. (8.28) and (8.38) shows that

$$\int_0^\infty \frac{t^\mu J_\mu(t)}{t^2 + k^2}\, dt = -\frac{\Gamma(\nu)\Gamma(1 - \nu)k^{\mu-1}}{2}[I_{-\mu}(k) - L_{-\mu}(k)]$$ (8.39)

and

$$\int_0^\infty \frac{t^{\mu+1} J_\mu(t)}{t^2 + k^2}\, dt = k^\mu K_\mu(k)$$ (8.40)

$$\mu = \frac{2\nu - 1}{2} = 0, 1, 2, 3, \ldots$$

so that the upper limitation on the Hankel–Nicholson integral, i.e., $-1/2 < \mu < 5/2$ for Eq. (8.39) and $-1 < \mu < 3/2$ for Eq. (8.40) (e.g., Refs. 23–26) are now liberated as given by Eqs. (8.39) and (8.40). Obviously, the present case treats only nonnegative integers for the values of μ.

Evaluation of the function $F_\nu(u)$ *Solution for* $u > 1$.   Consider the integral representation of the function $F_{1/2}(u)$

$$F_{1/2}(u) = -k \int_0^\infty \frac{e^{-ut} J_0(t)}{t^2 + k^2}\, dt = -\int_0^\infty \frac{e^{-ukt} J_0(kt)}{t^2 + 1}\, dt$$ (8.41)

Expanding the Bessel function in Eq. (8.41) in its ascending power series, we get

$$F_{1/2}(u) = -\sum_{n=0.1}^\infty (-)^n \frac{(k/2)^{2n}}{(n!)^2} \int_0^\infty \frac{t^{2n} e^{-ukt}}{(t^2 + 1)}\, dt$$ (8.42)

Through Laplace transform, the first term of Eq. (8.42) can be integrated and is given by

$$\int_0^\infty \frac{e^{-ukt}}{t^2+1}\, dt = f(ku) \tag{8.43}$$

where $f(ku)$ is the first auxiliary function of the trigonometric integral functions. Applying Laplace transform differentiating rule for the other terms of Eq. (8.42), we obtain

$$F_{1/2}(u) = -\sum_{n=0}^\infty (-)^n \frac{(k/2)^{2n}}{(n!)^2} \frac{d^{2n} f(ku)}{d(ku)^{2n}} \tag{8.44}$$

Deriving, we get

$$F_{1/2}(u) = -f(ku) - \sum_{n=1}^\infty \frac{(k/2)^{2n}}{(n!)^2}\left[f(ku) + \sum_{m=1}^n \frac{(-)^m (2m-2)!}{(ku)^{2m-1}} \right] \tag{8.45a}$$

$$F_{1/2}(u) = -f(ku) I_0(k) + \sum_{n=0}^\infty \frac{(-)^n (2n)!}{(2u)^{2n+1}}\left[\sum_{m=0}^\infty \frac{(k/2)^{2m+1}}{[(n+m+1)!]^2} \right] \tag{8.45b}$$

Applying the Cauchy ratio test for the series given in Eqs. (8.45), it can be shown that the series are convergent for all values of k and $u > 1$. We notice that for high values of k the series in Eq. (8.45a) is highly convergent since the series coefficient terms are the asymptotic expansion of $f(ku)$. Furthermore, for low values of k, the coefficient of the series in Eq. (8.45b) tends rapidly to zero. For numerical computation of the function $F_{1/2}(u)$, only very few terms will be needed for attaining a desired accuracy using the series in Eq. (8.45). This subject will be treated in detail below. Applying the same procedure as given above for the integral representation of the function $F_{3/2}(u)$, we obtain

$$F_{3/2}(u) = k \sum_{n=1}^\infty \frac{(k/2)^{2n-1}}{(n-1)!\,(n!)}\left[f(ku) + \sum_{m=1}^n \frac{(-)^m (2m-2)!}{(ku)^{2m-1}} \right] \tag{8.46}$$

and

$$F_{3/2}(u) = k f(ku) I_1(k) - k \sum_{n=0}^\infty \frac{(-)^n (2n)!}{(2u)^{2n+1}}\left[\sum_{m=0}^\infty \frac{(k/2)^{2m}}{(n+m)!\,(n+m+1)!} \right] \tag{8.47}$$

with the same consideration on the convergence as stated above for $F_{1/2}(u)$. Having obtained $F_{1/2}(u)$ and $F_{3/2}(u)$, a higher order of $F_\nu(u)$ can be obtained from the recurrence relation in Eq. (8.32).

Solution for u < 1.   Consider again the integral representation of the function $F_{1/2}(u)$

$$F_{1/2}(u) = -\int_0^\infty \frac{e^{-ukt} J_0(kt)}{t^2+1}\, dt \tag{8.48}$$

Expanding the exponential term in its ascending power series, we obtain

$$F_{1/2}(u) = -\sum_{n=0}^{\infty} (-)^n \left[\frac{(ku)^n}{n!} \right] \int_0^\infty \frac{t^n J_0(kt)}{t^2 + 1} \, dt \tag{8.49}$$

Now using the recurrence relations of the Bessel and Struve functions and Eqs. (8.39) and (8.40), it can be shown that

$$\int_0^\infty \frac{t^{2m} J_0(kt)}{t^2 + 1} \, dt = (-)^m \left(\frac{d}{k \, dk} \right)^m [(\pi/2)k^m [I_{-m}(k) - L_{-m}(k)]] \tag{8.50}$$

and

$$\int_0^\infty \frac{t^{2m+1} J_0(kt)}{t^2 + 1} \, dt = \left(\frac{d}{k \, dk} \right)^m [k^m K_m(k)] \tag{8.51}$$

Equations (8.50) and (8.51) can be considered as operation transforms for the Hankel functions for powers of t. The derivatives of the modified Bessel functions in Eqs. (8.50) and (8.51) are readily available[24] and are given by

$$\left(\frac{d}{k \, dk} \right)^n [k^m I_m(k)] = k^{m-n} I_{m-n}(k) \tag{8.52}$$

and

$$\left(\frac{d}{k \, dk} \right)^n [k^m K_m(k)] = (-)^n k^{m-n} K_{m-n}(k) \tag{8.53}$$

Furthermore, using the recurrence relations for the modified Struve function and through successive differentiation, the following derivative operation on the modified Struve function is obtained

$$\left(\frac{d}{k \, dk} \right)^m [k^m L_{-m}(k)] = L_0(k) + \frac{2}{\pi} \sum_1^m c_n \tag{8.54}$$

where

$$c_n = \sum_{m=1}^n \frac{(2m-3)^2 (2m-5)^2 \cdots 3^2 \, 1^2}{k^{2m-1}} \tag{8.55}$$

and

$$\left(\frac{d}{k \, dk} \right)^m \left[k^{m+1} L_{-m-1}(k) \right] = kL_{-1}(k) - \frac{2}{\pi} \sum_1^m c_n \tag{8.56}$$

where

$$c_n = \sum_{m=1}^n \frac{(2m-1)(2m-3)^2 (2m-5)^2 \cdots 3^2 \, 1^2}{k^{2m-1}} \tag{8.57}$$

Notice that the relation in Eq. (8.54) will be used for the evaluation of $F_{1/2}(u)$ and the relation in Eq. (8.56) for the evaluation of $F_{3/2}(u)$. Furthermore, generalization

for a higher power of $F_\nu(u)$ is straightforward. Using now the relations in Eqs. (8.50–8.55) in Eq. (8.49) and grouping terms, we obtain

$$F_{1/2}(u) = -\frac{\pi}{2}\left[I_0(k) - L_0(k)\right]\cos(ku) + K_0(k)\sin(ku) + \sum_{n=1}^{\infty}\frac{(-)^n(ku)^{2n}}{(2n)!}c_n$$

$$(8.58)$$

where

$$c_n = \sum_{m=1}^{n}\frac{(2m - 3)^2(2m - 5)^2\cdots 3^2\, 1^2}{k^{2m-1}}$$

$$(8.59)$$

Notice that the coefficients c_n in Eq. (8.58) are the asymptotic terms of $(\pi/2)$ $\times[I_0(k) - L_0(k)]$. Applying the Cauchy ratio test for the series given in Eq. (8.58), it can be shown that the series are convergent for all values of k and $u < 1$. Furthermore, the computation of $F_{1/2}(u)$ using Eq. (8.58) is highly convergent, and few terms are needed for a desired accuracy for its range of application. Again the subject is discussed in detail in the next sections. Following the same procedure given above, a series representation for $F_{3/2}(u)$ convergent for all values of k and $u < 1$, with the same considerations on convergence, is obtained and reads

$$F_{3/2}(u) = -\frac{\pi k}{2}\left[I_{-1}(k) - L_{-1}(k)\right]\cos(ku) + kK_1(k)\sin(ku) + \sum_{n=1}^{\infty}\frac{(-)^n(ku)^{2n}}{(2n)!}c_n$$

$$(8.60)$$

where

$$c_n = \sum_{m=1}^{n}\frac{(2m - 1)(2m - 3)^2(2m - 5)^2\cdots 3^2\, 1^2}{k^{2m-1}}$$

$$(8.61)$$

Notice that the coefficients c_n in Eq. (8.61) are the asymptotic terms of $(\pi k/2)$ $\times[I_{-1}(k) - L_{-1}(k)]$. Having obtained $F_{1/2}(u)$ and $F_{3/2}(u)$, a higher order of $F_\nu(u)$ can be obtained from the recurrence relation in Eq. (8.32).

Solution convergent for all values of u.   A power series expansion convergent for all values of k and u for the function $F_\nu(u)$ can be obtained from Eq. (8.26) through the expansion of the trigonometric functions of N_R and N_I and integration term by term. The results are given by

$$F_{1/2}(u) = [K_0(k) - VI_0(k) + B_0]\sin(ku)$$

$$-\left[\frac{\pi}{2}\{I_0(k) - TL_0(k)\} - C_0\right]\cos(ku)$$

$$(8.62)$$

and

$$F_{3/2}(u) = [K_1(k) - VI_1(k) - B_1]k\,\sin(ku)$$

$$+\left[\frac{\pi}{2}\{I_1(k) - TL_{-1}(k)\} - C_1\right]k\,\cos(ku)$$

$$(8.63)$$

where

$$T = (1 + u^2)^{\frac{1}{2}} \qquad V = \ell_n\left[(1 + u^2)^{\frac{1}{2}} + u\right]$$

$$B_i = uT \sum_{m=0}^{\infty} (-)^m \left[\frac{(2u)^{2m}(m!)^2}{(2m+1)!}\right] b_{i,m} \qquad i = 0, 1$$

$$C_i = \frac{Tku^2}{2} \sum_{m=0}^{\infty} (-)^m \left[\frac{(u/2)^{2m}(2m+1)!}{m!(m+1)!}\right] c_{i,m} \qquad i = 0, 1$$

$$b_{0,m} = \sum_{n=0}^{\infty} \frac{(k/2)^{2m+2n+1}}{[(m+n+1)!]^2}$$

$$b_{1,m} = \sum_{n=0}^{\infty} \frac{(k/2)^{2m+2n+1}}{(m+n+1)!(m+n)!}$$

$$c_{0,m} = \sum_{n=0}^{\infty} \frac{(2k)^{2m+2n+2}[(m+n+1)!]^2}{[(2m+2n+3)!]^2}$$

$$c_{1,m} = \frac{1}{k} \sum_{n=0}^{\infty} \frac{(2k)^{2m+2n+2}[(m+n+1)!]^2}{(2m+2n+2)!(2m+2n+3)!}$$

The series given by Eqs. (8.62) and (8.63) when used in Eq. (8.26) bear similarity with the Laschka's series.[11] Hence, their convergence is very slow. Their practical use is therefore limited to small values of the arguments k and u.

Asymptotic expansion for large values of k.   Asymptotic expansion for large values of k for $F_{1/2}(u)$ and $F_{3/2}(u)$ can be obtained from Eqs. (8.58) and (8.60), respectively, through successive derivations, making use of the differential Eq. (8.28). Performing these operations after three steps, we obtain

$$F_{1/2}(u) = -\left(\frac{\pi}{2}\right)[I_0(k) - L_0(k)]\cos(ku) + K_0(k)\sin(ku)$$

$$- \frac{1}{k(1+u^2)^{\frac{1}{2}}} \left\{1 + \frac{1-2u^2}{k^2(1+u^2)^2} + \frac{3(3-24u^2+8u^4)}{k^4(1+u^2)^4}\right\}$$

$$+ \left\{\frac{1}{k} + \frac{1}{k^3} + \frac{3^2 \cdot 1}{k^5}\right\}$$

$$- \frac{uk^2}{2!} \left\{\frac{1}{k} + \frac{1}{k^3} + \frac{3^2 \cdot 1}{k^5} + \frac{5^2 \cdot 3^2 \cdot 1}{k^7}\right\} + \cdots \qquad (8.64)$$

If more steps are performed, each of the algebraic terms will be increased by one more element for each step. We notice that, for large values of k, the series terms are the asymptotic terms of $(\pi/2)[I_0(k) - L_0(k)]$ so that they cancel the first term in

Eq. (8.64). Furthermore, for large values of k, the modified Bessel function $K_0(k)$ tends to zero much more rapidly than the remaining terms so that we can write

$$F_{1/2}(u) = -\frac{1}{k(1+u^2)^{\frac{1}{2}}}\left[1 + \frac{2-u^2}{k^2(1+u^2)^2} + \frac{3(3-24u^2+8u^4)}{k^4(1+u^2)^4} + \cdots\right] \quad (8.65)$$

Following the same procedure, we obtain an asymptotic expansion for large values of k for the function $F_{3/2}(u)$ as

$$F_{3/2}(u) = -\frac{1}{k(1+u^2)^{\frac{3}{2}}}\left[1 + \frac{3\cdot 1^2(1-4u^2)}{k^2(1+u^2)^2}\right.$$

$$\left. + \frac{5\cdot 3^2\cdot 1^2(1-12u^2+8u^4)}{k^4(1+u^2)^4} + \cdots\right] \quad (8.66)$$

The relations given by Eqs. (8.65) and (8.66) can be used efficiently for the calculation of the functions for large values of k and u. Notice that if Eq. (8.66) and its derivative are used in Eq. (8.31), the asymptotic relations for $N_{R3/2}$ and $N_{I3/2}$ given by Ueda[18] are recovered. Furthermore, for $u = 0$, Eqs. (8.65) and (8.66) give the asymptotic relations for $(\pi/2)[I_0(k) - L_0(k)]$ and $(\pi k/2)[I_{-1}(k) - L_{-1}(k)]$, respectively.

Numerical integration.   Consider the integral representation of the function $F_{1/2}(u)$

$$F_{1/2}(u) = -k\int_0^\infty \frac{J_0(t)e^{-ut}}{t^2+k^2}\,dt \quad (8.67)$$

Using the Laguerre integration scheme, we write

$$F_{1/2}(u) = -k\sum_{i=1}^n \frac{w_i e^{x_i}J_0(x_i)e^{-ux_i}}{x_i^2+k^2} + R_n$$

$$= -k\sum_{i=1}^n \frac{a_i e^{-ux_i}}{x_i^2+k^2} + R_n \quad (8.68)$$

where x_i are the ith zeros of the Laguerre polynomials $L_n(x)$ and w_i are the weight functions given by

$$w_i = \frac{(n!)^2 x_i}{(n+1)^2 L_{n+1}^2(x_i)} \quad (8.69)$$

and the remainder R_n is given by

$$R_n = \frac{(n!)^2}{(2n)!}f^{2n}(\xi) \quad 0 \le \xi \le \infty \quad f(\xi) = \frac{J_0(\xi)e^{\xi(1-u)}}{\xi^2+k^2} \quad (8.70)$$

and

$$a_i = w_i e^{x_i}J_0(x_i) \quad (8.71)$$

Similarly, for the function $F_{3/2}(u)$, we write

$$F_{3/2}(u) = -k \int_0^\infty \frac{t J_1(t) e^{-ut}}{t^2 + k^2} \, dt$$

$$= -k \int_0^\infty \frac{J_1(t) e^{-ut}}{t} \, dt + k^3 \int_0^\infty \frac{J_1(t) e^{-ut}}{t(t^2 + k^2)} \, dt$$

$$= -k\left[(1 + u^2)^{\frac{1}{2}} - u\right] + k^3 \int_0^\infty \frac{J_1(t) e^{-ut}}{t(t^2 + k^2)} \, dt \tag{8.72}$$

It is beneficial to use the second form in Eq. (8.72) for numerical integration rather than working directly on the first form, since this will enhance the convergence. Using now the Laguerre scheme, we obtain

$$F_{3/2}(u) = -k\left[(1 + u^2)^{\frac{1}{2}} - u\right] + k^3 \sum_1^n \frac{b_i e^{-ux}}{x_i^2 + k_i^2} + R_n \tag{8.73}$$

where

$$b_i = \frac{w_i e^{x_i} J_1(x_i)}{x_i} \tag{8.74}$$

The abscissa x_i and the weight function w_i are as given before, and the remainder is given by

$$R_n = \frac{(n!)^2}{(2n)!} f^{2n}(\xi) \qquad 0 \le \xi \le \infty \qquad f(\xi) = \frac{J_1(\xi) e^{\xi(1-u)}}{\xi^2 + k^2} \tag{8.75}$$

Examining the remainders given by Eqs. (8.70) and (8.75), we observe that the accuracy of the approximation is not only a function of the number of terms used but is also dependent on $f^{2n}(\xi)$, which is a function of the arguments k and u. Furthermore, for k less than 1 and u less than 0.5, it can be easily shown that many terms are needed for obtaining a reasonable accuracy. However, the numerical integration can be explored outside this region, and this is where the series solutions need many terms for convergence.

A scheme for the numerical evaluation of the function $F_\nu(u)$. In this section, a numerical scheme is given for evaluating the functions $F_{1/2}(u)$ and $F_{3/2}(u)$; formulas for their derivatives are also given for completeness. These functions are well-behaved functions and are plotted in Figs. 8.4 and 8.5 for a wide range of the arguments k and u. In what follows, the scheme given preserves an accuracy of six digits; if more precision is required, one should increase the number of terms in the related formulas and/or subdivide the region of the application of the formulas into smaller regions. In the scheme presented, we first divide the region of $0 \le k \le 20$ into three subregions, namely, $0 \le u \le 0.5$, $0.5 \le u \le 2.0$, and $2.0 \le u \le \infty$, and then the asymptotic relations are used for the computation of the functions for $k \ge 20$ and all values of u.
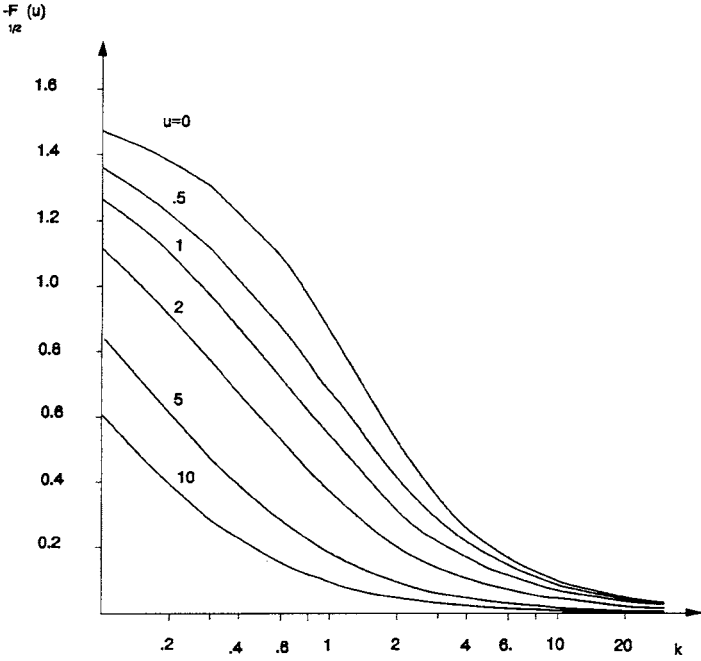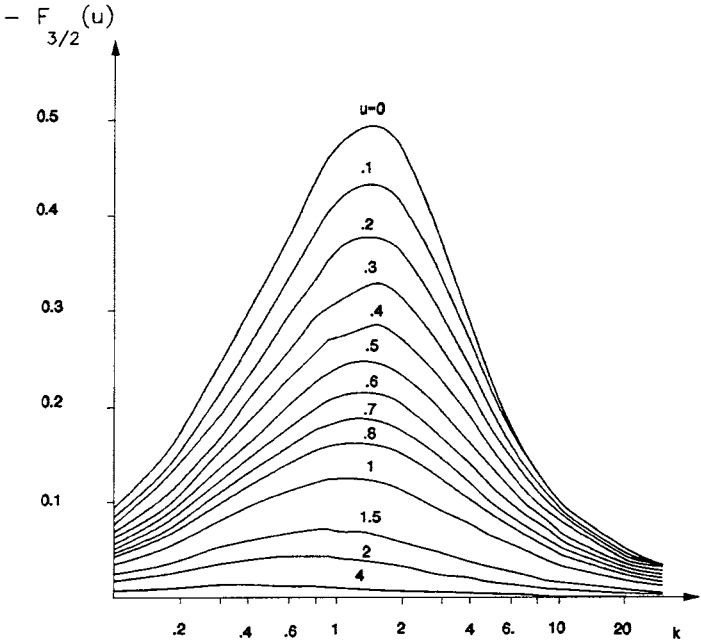
Fig. 8.4   The function $F_{1/2}(u)$.

Fig. 8.5   The function $F_{3/2}(u)$.

$F_{1/2}(u)$ *for* $0 \le k \le 20$ *and* $0 \le u \le 0.5$. We rearrange Eq. (8.58) and write it in the form

$$F_{1/2}(u) = K_0(k)\sin(ku) - k[uV - T + 1] - \alpha\left[1 - \frac{(ku)^2}{2}\right]$$

$$-\sum_{n=1}^{6}(-)^{n+1}\frac{(ku)^{2n+2}c_n}{(2n+2)!} \qquad + |\varepsilon| \le 5.56 \times 10^{-7} \qquad (8.76)$$

and

$$\frac{F'_{1/2}(u)}{k} = K_0(k)\cos(ku) - V + \alpha uk$$

$$-\sum_{n=1}^{7}(-)^{n+1}\frac{(ku)^{2n+1}c_n}{(2n+2)!} \qquad + |\varepsilon| \le 1.70 \times 10^{-7} \qquad (8.77)$$

where

$$V = \ell_n\left[(1 + u^2)^{\frac{1}{2}} + u\right] \qquad T = (1 + u^2)^{\frac{1}{2}}$$

$$\alpha = \frac{\pi}{2}[I_0(k) - L_0(k)] \qquad c_n = \alpha - \sum_{m=1}^{n}\frac{(2m-3)^2(2m-5)^2\cdots 3^2\,1^2}{k^{2m-1}}$$

Notice that the second term in Eq. (8.76) is the summation of the last terms in the series coefficients. This has been done to enhance the computation. Furthermore, for $k = 0$, the function $F_{1/2}(u)$ equals $-\pi/2$.

$F_{1/2}(u)$ *for* $0 \le k \le 20$ *and* $0.5 \le u \le 2.0$. For the range $0 \le k \le 2.0$, use Eq. (8.62) with eight terms; this will give an error less than or equal to 5.04×10^{-7}. An efficient way to compute the coefficients is given below

$$b_{0.7} = \frac{(k/2)^{16}}{(8!)^2} + \frac{(k/2)^{18}}{(9!)^2} + \frac{(k/2)^{20}}{(10!)^2}$$

$$b_{0,n-1} = b_{0,n} + \frac{(k/2)^{2n}}{(n!)^2} \qquad n = 7, 6, \ldots, 1$$

$$I_0(k) = b_{0,0} + 1$$

$$\qquad\qquad\qquad\qquad\qquad\qquad\qquad\qquad\qquad (8.78)$$

$$c_{0.7} = \frac{(2k)^{16}(8!)^2}{(17!)^2} + \frac{(2k)^{18}(9!)^2}{(19!)^2}$$

$$c_{0,n-1} = c_{0,n} + \frac{(2k)^{2n}(n!)^2}{[(2n+1)!]^2} \qquad n = 7, 6, \ldots, 1$$

$$L_0(k) = (2k/\pi)[c_{0,0} + 1]$$

Notice that $I_0(k)$ and $L_0(k)$ need not be evaluated because they are calculated while computing the coefficients of the series. The derivative of the function is

Table 8.1   Numerical values of x_i, a_i, and b_i

i	x_i	a_i	b_i
1	0.09330 78120 17	0.23905 69913 45	0.11965 87667 94
2	0.49269 17403 02	0.52662 26292 37	0.27163 83275 27
3	1.21559 54120 71	0.58837 99267 46	0.36647 62188 37
4	2.26994 95262 04	0.08791 10490 84	0.29384 44207 34
5	3.66762 27217 51	−0.62548 12307 17	2.88742 83313 50E−2
6	5.42533 66274 14	−0.06314 30242 51	−0.12354 70297 47
7	7.56591 62266 13	0.60151 60522 86	4.68073 69972 70E−02
8	10.12022 85680 19	−0.69170 86091 13	3.65190 79983 40E−3
9	13.13028 24821 76	0.69758 05409 60	−1.04830 62950 40E−2
10	16.65440 77083 30	−0.73526 20426 41	−8.16025 42979 40E−3
11	20.77647 88994 49	——	3.44468 02171 80E−2
12	25.62389 42267 29	——	−8.94957 68520 20E−3

given by

$$F'_{1/2}(u) = [K_0(k) - VI_0(k) + B_0]\cos(ku) + \left[\frac{\pi}{2}[I_0(k) - TL_0(k)] + C_0\right]\sin(ku)$$

(8.79)

For the range $2 \leq k \leq 20$, use the Laguerre integration scheme with 10 terms and the following formulas:

$$F_{1/2}(u) = -\sum_{i=1}^{10} \frac{a_i e^{-ux_i}}{x_i^2 + k_i^2} \qquad + |\varepsilon| \leq 2.18 \times 10^{-6}$$

(8.80)

and

$$F'_{1/2}(u) = \sum_{i=1}^{10} \frac{x_i a_i e^{-ux_i}}{x_i^2 + k_i^2} \qquad + |\varepsilon| \leq 1.47 \times 10^{-6}$$

(8.81)

The numerical values of a_i and x_i are given in Table 8.1.

$F_{1/2}(u)$ for $0 \leq k \leq 20$ and $2.0 \leq u \leq \infty$. For the range $0 \leq k \leq 2.0$, use Eq. (8.45) with six terms; this will give an error less than or equal to 2.85×10^{-7}. An efficient way to compute the coefficients is as follows:

$$c_5 = \frac{(k/2)}{(6!)^2} + \frac{(k/2)^3}{(7!)^2}$$

$$c_{n-1} = c_n(k/2)^2 + \frac{k/2}{(n!)^2} \qquad n = 5, 4, \ldots, 1$$

(8.82)

$$I_0(k) = c_0(k/2) + 1$$

and

$$F'_{1/2}(u) = kg(ku)I_0(k) - 2\sum_{n=0}^{6} \frac{(-)^n (2n+1)! c_n}{(2u)^{2n+2}} \qquad + |\varepsilon| \leq 3.74 \times 10^{-7}$$

(8.83)

For the range $2 \leq k \leq 10.0$, use Eq. (8.45) with seven terms

$$F_{1/2}(u) = -\sum_{n=0}^{6} \frac{(k/2)^{2n} c_n}{(n!)^2} \qquad + |\varepsilon| \leq 4.03 \times 10^{-7}$$

(8.84)

where

$$c_0 = f(ku)$$

$$c_n = c_{n-1} + \frac{(-)^n (2n-2)!}{(ku)^{2n-1}} \qquad n = 1, 2, \ldots, 6$$

and the derivative is given by

$$\frac{F'_{1/2}(u)}{k} = \sum_{n=0}^{7} \frac{(k/2)^{2n} d_n}{(n!)^2} \qquad + |\varepsilon| \leq 1.67 \times 10^{-7}$$

(8.85)

where

$$d_0 = g(ku)$$

$$d_n = d_{n-1} + \frac{(-)^n (2n-1)!}{(ku)^{2n}} \qquad n = 1, 2, \ldots, 7$$

For the range $10 \leq k \leq 20$, use the asymptotic expansion given in Eq. (8.65); this will give an error less than or equal to 6.96×10^{-8}, and the derivative is given by

$$F'_{1/2}(u) = \frac{u}{k(1+u^2)^{\frac{3}{2}}} \left[1 + \frac{3^2(3-2u^2)}{3k^2(1+u^2)^2} + \frac{3^2 \cdot 5^2 (15 - 40u^2 - 8u^4)}{15k^4(1+u^2)^4} \right]$$

(8.86)

The error in the calculation using Eq. (8.86) is less than or equal to 1.54×10^{-8}.

$F_{1/2}(u)$ *for* $k \geq 20$ *and* $0 \leq u \leq \infty$.   Use the asymptotic expansion given by Eq. (8.65). For the computation of $F_{1/2}(u)$; the error will be less than or equal to 2.04×10^{-7}. For the derivative, use Eq. (8.86); this will give an error less than or equal to 2.80×10^{-8}.

$F_{3/2}(u)$ *for* $0 \leq k \leq 20$ *and* $0 \leq u \leq 0.5$.   We rearrange Eq. (8.60) and write it in the form

$$F_{3/2}(u) = kK_1(k)\sin(ku) - k\left[(1+u^2)^{\frac{1}{2}} - 1\right] + \alpha \left[1 - \frac{(ku)^2}{2} \right]$$

$$+ \sum_{n=1}^{7} (-)^{n+1} \frac{(ku)^{2n+2} c_n}{(2n+2)!} \qquad +|\varepsilon| \leq 1.94 \times 10^{-7}$$

(8.87)

and

$$\frac{F'_{3/2}(u)}{k} = kK_1(k)\cos(ku) - \left[\frac{u}{(1+u^2)^{\frac{1}{2}}}\right] - \alpha uk$$

$$+ \sum_{n=1}^{7}(-)^{n+1}\frac{(ku)^{2n+1}c_n}{(2n+2)!} \qquad +|\varepsilon| \le 2.68 \times 10^{-7} \tag{8.88}$$

where

$$c_n = \alpha + \sum_{m=1}^{n}\frac{(2m-1)(2m-3)^2(2m-5)^2 \cdots 3^2 1^2}{k^{2m-1}}$$

$$\alpha = \frac{\pi k}{2}[I_1(k) - L_1(k)]$$

Notice that, for $k = 0$, we have $F_{3/2} = 0$ and $F'_{3/2}(u) = 1 - u/(1+u^2)^{1/2}$.

$F_{3/2}(u)$ *for* $0 \le k \le 20$ *and* $0.5 \le u \le 2.0$.   We use Eq. (8.63) with nine terms for the range of $0 \le k \le 2$; this will give an error less than or equal to 3.29×10^{-7} for the computation of $F_{3/2}(u)$ and $F'_{3/2}(u)/k$. An efficient way to compute the coefficients is given below

$$b_{1.8} = \frac{(k/2)^{17}}{8!9!} + \frac{(k/2)^{19}}{9!10!}$$

$$b_{1.n-1} = b_{1.n} + \frac{(k/2)^{2n-1}}{n!(n-1)!} \qquad n = 8, 7, \ldots, 1$$

$$I_1(k) = b_{1.0}$$

$$c_{1.8} = (1/k)\left[\frac{(2k)^{18}(9!)^2}{18!19!} + \frac{(2k)^{20}(10!)^2}{20!21!}\right] \tag{8.89}$$

$$c_{1.n-1} = c_{1.n} + \frac{(2k)^{2n}(n!)^2}{k(2n!)(2n+1)!} \qquad n = 8, 7, \ldots, 1$$

$$L_{-1}(k) = (2/\pi)[kc_{1.0} + 1]$$

Notice that $I_1(k)$ and $L_{-1}(k)$ need not be evaluated because they are obtained while computing the coefficients of the series. The formula for the derivative is given by

$$F'_{3/2}(u) = -\frac{u}{(1+u^2)^{\frac{1}{2}}} + [K_1(k) + VI_1(k) - B_1]\cos(ku)$$

$$+ \left[\frac{\pi}{2}[I_1(k) - TL_{-1}(k)] + C_1\right]\sin(ku) \tag{8.90}$$

For the range $2 \leq k \leq 20$, use the Laguerre integration scheme with 12 terms and the following formulas:

$$F_{3/2}(u) = -k[(1+u^2)^{\frac{1}{2}} - u] + k^3 \sum_{i=1}^{12} \frac{b_i e^{-ux_i}}{x_i^2 + k_i^2} \qquad +|\varepsilon| \leq 2.39 \times 10^{-6} \quad (8.91)$$

and

$$\frac{F'_{3/2}(u)}{k} = \left[1 - \frac{u}{(1+u^2)^{\frac{1}{2}}}\right] + k^2 \sum_{i=1}^{12} \frac{x_i b_i e^{-ux_i}}{x_i^2 + k_i^2} \qquad +|\varepsilon| \leq 1.96 \times 10^{-6}$$

$$(8.92)$$

The values of b_i and x_i are given in Table 8.1.

$F_{3/2}(u)$ *for* $0 \leq k \leq 20$ *and* $2.0 \leq u \leq \infty$. For the range $0 \leq k \leq 2.0$, use Eq. (8.46) written in the form

$$F_{3/2}(u) = -k\left[(1 + u^2)^{\frac{1}{2}} - u\right] + kf(ku)I_1(k) - k\sum_{n=0}^{4} \frac{(-)^n (2n)! c_n}{(2u)^{2n+1}}$$

$$(8.93)$$

$$+|\varepsilon| \leq 4.84 \times 10^{-7}$$

and

$$\frac{F'_{3/2}(u)}{k} = \left[1 - \frac{u}{(1 + u^2)^{\frac{1}{2}}}\right] + kg(ku)I_1(k) + 2\sum_{n=0}^{5} \frac{(-)^n (2n + 1)! c_n}{(2u)^{2n+2}}$$

$$(8.94)$$

$$+|\varepsilon| \leq 2.31 \times 10^{-7}$$

where

$$c_5 = \frac{(k/2)^2}{6!7!} + \frac{(k/2)^4}{7!8!} + \frac{(k/2)^6}{8!9!}$$

$$c_{n-1} = (k/2)^2 \left[c_n + \frac{1}{n!(n + 1)!}\right]$$

$$I_1(k) = [c_0 + 1](k/2)$$

For the range $2 \leq k \leq 10.0$, use Eq. (8.46) with seven terms

$$F_{3/2}(u) = -k \sum_{n=1}^{7} \frac{(k/2)^{2n-1} c_n}{n!(n - 1)!} \qquad +|\varepsilon| \leq 7.36 \times 10^{-7} \qquad (8.95)$$

where

$$c_1 = f(ku) - \frac{1}{ku}$$

$$c_n = c_{n-1} + \frac{(-)^n (2n - 2)!}{(ku)^{2n-1}} \qquad n = 2, 3, \ldots, 7$$

and the derivative is given by

$$\frac{F'_{3/2}(u)}{k} = k \sum_{n=1}^{8} \frac{(k/2)^{2n} d_n}{n!(n-1)!} \quad + |\varepsilon| \le 6.68 \times 10^{-7} \qquad (8.96)$$

where

$$d_1 = -g(ku) + \frac{1}{(ku)^2}$$

$$d_n = d_{n-1} + \frac{(-)^{n+1}(2n-1)!}{(ku)^{2n}} \qquad n = 2, 3, \ldots, 7$$

For the range $10 \le k \le 20$, use the asymptotic expansion given by Eq. (8.66); this will give an error less than or equal to 1.31×10^{-7}, and the derivative is given by

$$F'_{3/2}(u) = \frac{3u}{k^2(1+u^2)^{\frac{5}{2}}}\left[1 + \frac{5(3-4u^2)}{k^2(1+u^2)^2} + \frac{7\cdot5\cdot3\cdot(5-20u^2-8u^4)}{k^4(1+u^2)^4}\right] \qquad (8.97)$$

The error in the derivative calculation using Eq. (8.97) is less than or equal to 1.03×10^{-7}.

$F_{3/2}(u)$ *for* $k \le 20$ *and* $0 \le u \le \infty$. Use the asymptotic expansion given by Eq. (8.66). For the computation of $F_{3/2}(u)$, the error will be less than or equal to 1.50×10^{-6}. For the derivative, use Eq. (8.97); this will give an error less than or equal to 1.64×10^{-8}.

8.3.3 Evaluation of the Kernel Function in Supersonic Flows

The integral equation relating the incremental pressure difference and the normalwash distribution in unsteady potential flows [Eq. (8.5)] is valid whether the flow is subsonic or supersonic.[27] The difference between the two regimes lies in the Kernel function of the integral equation. For both regimes, the nonelementary part of the Kernel can be written as

$$I_v(u_1, u_2) = \int_{u_1}^{u_2} \frac{e^{-ikv}}{(1+v^2)^v} \, dv \qquad (8.98)$$

The limits of the integration in Eq. (8.98) read as follows:
For the subsonic case

$$u_1 = (MR - x_0)/\beta^2 r \qquad (8.99)$$

and

$$u_2 = \infty \qquad (8.100)$$

For the supersonic case

$$u_1 = (x_0 - MR)/B^2 r \qquad (8.101)$$

and

$$u_2 = (x_0 + MR)/B^2 r \tag{8.102}$$

where $\beta = (1 - M^2)^{1/2}$ and $B = (M^2 - 1)^{1/2}$, and other notations are as previously defined. The extension of the subsonic case[19] to the supersonic case was presented in Ref. 28 and is summarized below. In a supersonic regime, the disturbances are restricted to the region of their aft cone so that x_0 is always positive and $x_0 > Br$. Therefore, in the limits of integrations of Eqs. (8.101) and (8.102), u_2 is always positive, whereas u_1 can be positive or negative. For values of $x_0 < Br$, there is no disturbance; hence the Kernel is null. Writing now for the supersonic case, use Eq. (8.98) in the following form:

$$I_\nu(u_1, u_2) = \int_{u_1}^{\infty} \frac{e^{-ikv}}{(1 + v^2)^\nu} \, dv - \int_{u_2}^{\infty} \frac{e^{-ikv}}{(1 + v^2)^\nu} \, dv \tag{8.103}$$

and define[28]

$$\psi_\nu(u) = F_\nu(u) + i F_\nu'/k$$
$$\psi_\nu^*(u) = F_\nu(u) - i F_\nu'/k \tag{8.104}$$

After several algebraic manipulations, it can be shown that

$$I_\nu(u_1, u_2) = i e^{-iku_1} \psi_\nu^*(u_1) - i e^{-iku_2} \psi_\nu^*(u_2) \qquad u_1 > 0 \tag{8.105}$$

and

$$I_\nu(u_1, u_2) = \frac{2\pi^{\frac{1}{2}}}{\Gamma(\nu)} (k/2)^\mu K_\mu(k) + i e^{ik|u_1|} \psi_\nu(|u_1|) - i e^{-iku_2} \psi_\nu(u_2) \qquad u_1 < 0 \tag{8.106}$$

Equations (8.105) and (8.106) give a simple and direct way for the evaluation of the nonelementary part of the supersonic Kernel in terms of the real function $F_\nu(u)$.

Simple and direct expressions for the evaluation of the nonelementary part of the Kernel function of the integral equation relating the pressure and the normalwash distribution in subsonic and supersonic nonstationary flow have been detailed above. The expressions provided represent an exact solution of the problem, i.e., the expressions can be obtained to any desired accuracy. The details have been given for two reasons. First, they are not available elsewhere; second, they constitute the bases of numerical methods for obtaining the nonstationary airloads needed for aeroelastic stability and response problems. Therefore, these expressions must be calculated with a higher degree of precision since they are used in further approximations and numerical processes in subsequent aeroelastic and response problems.

8.4 Modal Transformation

Once the aerodynamic matrices have been calculated, we can use Eq. (8.14) to relate the pressure distribution and the normalwash distribution, and we write

$$\{F_A\} = -\{p_i a_i\} = \frac{1}{2} \rho U^2 \lceil a_i \rfloor [A] \left\{ \frac{w}{U} \right\} \tag{8.107}$$

where $\lceil a_i \rfloor$ is a diagonal matrix composed of the area of the respective aerodynamic elements and $\{F_A\}$ is the vector of the resulting incremental aerodynamic loads assumed to act at the control point of the aerodynamic elements. Other symbols are as defined before. The normalwash vector $\{w/U\}$ is related to the surface deflection vector $\{z\}$ for a small disturbance theory by the following equation:

$$\left\{\frac{w}{U}\right\} = \frac{1}{U}\left\{\frac{\partial}{\partial t}\{z\} + U\left\{\frac{\partial z}{\partial x}\right\}\right\} \qquad (8.108)$$

The modal transformation can now be used, and we write $\{z\}$ in terms of the modal amplitude $\{\eta\}$ as

$$\{z\} = [\phi]\{\eta\} \qquad (8.109)$$

where $[\phi]$ is the modal matrix with columns composed of the modal values at aerodynamic control points. Special techniques must be used for surface interpolation of the modal values at aerodynamic control points from the finite element structural nodal points results. Using now Eqs. (8.107) and (8.108), we obtain

$$\left\{\frac{w}{U}\right\} = \frac{1}{U}\{[\phi]\{\eta'\} + U[\phi_{,x}]\{\eta\}\} \qquad (8.110)$$

Finally, the system's equations of motion read

$$\lceil\mu\rfloor\{\eta''\} + \lceil\beta\rfloor\{\eta'\} + \lceil\gamma\rfloor\{\eta\} = -\frac{\rho U}{2}[a_i][A]\{[\phi]\{\eta'\} + U[\phi_{,x}]\{\eta\}\} \qquad (8.111)$$

8.5   Solution of the Aeroelastic Stability Equations

In this section the various methods of the solution of the aeroelastic stability equations are discussed. Basically these methods can be classified into three main groups, namely the p methods, the k methods, and the p–k methods.

8.5.1   The p Methods

In many cases of aeroelastic stability formulation, the aerodynamic incremental nonstationary airloads matrix assumes the form

$$[A] = [A_1]pa_1 + [A_0]a_2 \qquad (8.112)$$

where $[A_1]$ and $[A_0]$ are constant real matrices; a_1 and a_2 are parameters that are in general functions of the unperturbated flow velocity, density, and Mach number; and p is the aeroelastic eigenvalue. This occurs for instance when quasistatic, quasisteady, or simple forms of unsteady aerodynamic loads are assumed in the formulation. The matrix $[A_1]$ represents the aerodynamic damping effect, and the matrix $[A_0]$ represents the aerodynamic stiffness effect. We first consider the structural undamped case, when the quasistatic aerodynamic theory is used in the analysis. In such a case, the equation of aeroelastic stability [Eq. (8.111)] can be written as

$$[\lceil\mu\rfloor p^2 + \lceil\gamma\rfloor + a_2[A_0]]\{\eta\} = 0 \qquad (8.113)$$

The limits of the integration in Eq. (8.98) read as follows:

Notice that it is not necessary to use the modal base formulation for the solution of the problem; however, if this is done the solution of the problem is greatly simplified. We observe that the matrices in Eq. (8.113) are real; therefore, the eigenvalue roots are real, or if complex they appear in pairs of complex conjugate roots. Because of the exponential nature of the solution assumed, the borderline of the stability will be at the coalescence of two eigenvalues just before presenting the first pair of complex conjugate roots. This type of aeroelastic stability is known as flutter due to coalescence of modes. The lowest value of a_2 for which the first coalescence of modes takes place will determine the critical flutter speed of the problem. Traditionally, the problem solution is made by numerically tracing the problem eigenvalues vs the velocity and observing numerically the point of the modes's coalescence. This will require the solution of an eigenvalue problem at each iterative step. The method presented in Ref. 29 permits us to obtain directly the stability points without the need for the iterative eigenvalue solution. This method of solution is given in the following section.

Equation (8.113) represents a parametric eigenvalue problem, with p being the eigenvalue and a_2 considered as the parameter of the problem. We observe that not all the modes of Eq. (8.113) can contribute to a fluttering condition. Flutter occurs physically due to the interaction between at least two degrees of freedom. Mathematically, this is expressed through the coupling of terms of the matrix $[A_0]$ of Eq. (8.113). Therefore, the problem can be simplified by eliminating from Eq. (8.113) all individual modes having null columns and/or rows except for a nonzero diagonal element. These modes do not contribute to or affect the fluttering condition. They can only give rise to static divergences, and these can easily be treated through the solution of their individual single-degree-of-freedom equations. The remaining modes are then separated into groups that interact aerodynamically. Each of these groups represents a system of equations similar to Eq. (8.113), but of a reduced order, and can be treated separately for the examination of the aeroelastic stability.

We next examine under what conditions each of these smaller systems are flutter prone. As the value of a_2 increases, the roots of the reduced characteristic equation change until reaching a point where complex conjugate roots appear. Under such conditions, one of the root pairs will give an unstable motion. The borderline of stability will be obtained at the point of coalescence of two roots. Now, the characteristic equation of each reduced system can be written as

$$\mu^n + c_1\mu^{n-1} + \cdots + c_{n-1}\mu + c_n = 0 \qquad (8.114)$$

where n is the number of modes with aerodynamic interaction. The coefficients of the characteristic equation read

$$c_1 = T_1$$

$$c_j = -\frac{1}{j}\left[c_{j-1}T_1 + c_{j-2}T_2 + \cdots + c_1 T_{j-1} + T_j\right] \qquad (8.115)$$

$$j = 2, 3, \ldots, n$$

where T_j are the traces of the power j of the reduced $[\gamma + a_2 A_0]$ matrix. Let the roots of Eq. (8.114) be μ_i, where $i = 1, 2, \ldots, n$. Using now the Encke notation,[30]

the coefficients in Eq. (8.115) are written as

$$c_j = \left[\mu_i^j\right] \tag{8.116}$$

On the borderline of stability, Eq. (8.114) has a pair of repeated roots. Let this pair of roots be λ and denote the rest of the roots by ν_i and $i = 1, 2, \ldots, n - 2$. Doing so, the coefficients of Eq. (8.116) read

$$c_j = \lambda^2\left[\nu_i^{j-2}\right] + 2\lambda\left[\nu_i^{j-1}\right] + \left[\nu_i^j\right] \tag{8.117}$$

where again the Encke notation has been used, with $[\nu_i^0]$ and $[\nu_i^j] = 0$ for $j < 0$ and $j > n - 2$. Equation (8.117) represents a system of n equations in n unknowns, namely, λ, a_2, and the $n - 2$ Encke roots. Eliminating the Encke roots $[\nu_i^j]$ from these equations, we obtain

$$c_{n-1} - \sum_{i-1}^{n-1} (-)^{i+1}[i+1]\lambda^j c_{n-i-1} = 0 \tag{8.118}$$

and

$$c_n - \sum_{i-1}^{n-1} (-)^{i+1}[i]\lambda^{j+1} c_{n-i-1} = 0 \tag{8.119}$$

This represents two equations in two unknowns, λ and a_2. Their solution determines the fluttering parameters of the aeroelastic problem, namely, λ_{fl} and $a_{2\,fl}$. As a numerical application, we consider the supersonic flutter of a simply supported flat plate. Using the quasistatic aerodynamic theory, applying the Galerkin method for the problem formulation, and taking the free vibration modes as trial functions, we can write the equation of motion as

$$[\mu[I] + \lceil\gamma\rfloor + \Lambda[A]]\{q\} = 0 \tag{8.120}$$

The matrices in Eq. (8.120) are given by

$$\lceil\gamma\rfloor = \lceil(m^2 + n^2\beta^2)\rfloor$$

$$[A_{ij}] = \left[\frac{ij}{2(i^2 - j^2)}\right] \quad \text{for } i + j = 3, 5, 7, \ldots \text{ and } = 0 \text{ otherwise}$$

and

$$\mu = \omega^2\rho h a^4/D\pi^4$$

$$\Lambda = 16a^3 q/\pi^4 D[M^2 - 1]^{\frac{1}{2}}$$

$$\beta = a/b$$

For the numerical application, we consider the case of a square plate. Taking a two-mode approximation in the Galerkin formulation, with $n = 1$ and $m = 1, 2$,

and applying Eqs. (8.118) and (8.119), we obtain

$$\lambda = (\gamma_1 + \gamma_2)/2 = -14.50$$

$$\Lambda = 3(\gamma_1 - \gamma_2)/2 = 31.50$$

For a four-mode Galerkin formulation, with $n = 1$ and $m = 1, 2, 3, 4$, the coefficients c_i are given by

$$c_1 = -418$$

$$c_2 = 40,281 + 1.223387\Lambda^2$$

$$c_3 = -877,000 - 172.23056\Lambda^2 \tag{8.121}$$

$$c_4 = 2,890,000 + 3745.1849\Lambda^2 + 0.1337469\Lambda^4$$

Notice that the calculation of these coefficients is made only once at the beginning of the computations, and the computation effort required is less than that required for the computation of a single eigenvalue iteration step using the classical methods of solution. Having obtained the coefficients, we apply again Eqs. (8.118) and (8.119) to obtain two equations in λ and Λ, and these are solved numerically. The results obtained for various modes using the Galerkin formulation are shown in Table 8.2. In this table, only the first coalescence is given since higher coalescences produce higher values of Λ and thus have no practical use. Furthermore, notice that modes of different n are uncoupled aerodynamically.

A similar solution for the case of quasisteady aerodynamic loads, i.e., when the aerodynamic damping is considered in the analysis, was presented in Ref. 31. This solution is summarized in the following. In such a case, the equations of motion can be written as

$$[-p^2[I] + [\xi^2] - \lambda[A_0] - i\gamma p[A_1]]\{q_0\} \tag{8.122}$$

where solutions in the form $\{q\} = \{q_0\}e^{i\omega t}$ have been assumed and the mode shapes have been normalized to a unit generalized mass value. This has been done to simplify the exposition. Again, Eq. (8.122) represents a parametric eigenvalue problem, with p considered as the problem eigenvalue. The characteristics of Eq. (8.122) can be written as

$$p^{2n} + ic_1 p^{2n-1} + c_2 p^{2n-2} + \cdots + c_{2n} = 0 \tag{8.123}$$

Table 8.2   Flutter solution of a square flat simply supported plate in the presence of a supersonic flow

n	m	$-\lambda$	Λ_{cr}
1	2	14.50	31.50
1	4	18.71	41.58
1	6	18.84	42.04
1	8	18.94	42.00

where n is the order of the system. Because the matrices in Eq. (8.122) are all real, it follows that the coefficients of Eq. (8.123) are real and are functions of the aerodynamic parameter Λ and the damping factor γ. Now, on the borderline of stability, the roots p of Eq. (8.123) are real so that we can separate Eq. (8.123) into two equations for the real and the imaginary parts to read

$$k^{2n} + c_2 k^{2n-2} + \cdots + c_{2n} = 0 \tag{8.124}$$

$$c_1 k^{2n-1} + c_3 k^{2n-3} + \cdots + c_{2n-1}k = 0 \tag{8.125}$$

where k is real. The static divergence condition is obtained from Eq. (8.124) as

$$c_{2n} = 0 \tag{8.126}$$

The flutter condition is then obtained by solving Eqs. (8.124) and (8.125) for $k \neq 0$, giving two equations in two unknowns, namely, the flutter velocity V_F and the flutter frequency ω_F. The coefficients c_i of Eqs. (8.124) and (8.125) often assume simple forms, and this will be shown in the application presented in the sequel.

We also consider in this section the problem of aeroelasticity of plates and shells with rectangular planform freely supported on all edges. In such cases, an exact solution for the free vibration analysis is available. The aeroelastic stability equation for the case at hand can be written as

$$[-k^2[I] + [\xi^2] - \lambda[A] - i\lambda gk\,[I]]\{q_0\} = 0 \tag{8.127}$$

where λ and g are the dynamic pressure and the aerodynamic damping parameters and the mode shape has been normalized to obtain a unit generalized mass matrix. It can be shown by expansion that the coefficients of Eqs. (8.124) and (8.125) can be expressed as

$$c_m = \sum_{j}^{L} \frac{d_{(m-j)/2}[\lambda g]^j e_j}{j!} \tag{8.128}$$

where

$$j = 0,\, 2,\, 4,\, \ldots \quad \text{and} \quad L = \frac{m+2}{2} \quad \text{for } m \text{ even}$$

$$j = 1,\, 3,\, 5,\, \ldots \quad \text{and} \quad L = \frac{m+1}{2} \quad \text{for } m \text{ odd}$$

and

$$e_j = \prod_{i=1}^{j} \frac{(2n + 2i - m - j)}{2} \quad \text{for } j = 1, 2, 3, \ldots$$

$$= 1 \quad \text{for } j = 0 \tag{8.129}$$

The coefficients d_i in Eq. (8.128) are obtained from the characteristic equation coefficients when only in-quadrature aerodynamic loads are considered, which have been treated in the previous section. As a numerical application, we consider a simply supported flat square plate of dimension a, thickness h, material mass

density ρ, and flexural rigidity D. The dynamic pressure parameter λ and the aerodynamic damping parameter g are given by

$$\lambda = \frac{8Qa^3}{D\pi^4(M^2-1)^{\frac{1}{2}}}$$

$$g = \frac{M^2-2}{M^2-1}\frac{\pi^2}{Va}\sqrt{\frac{D}{\rho h}}$$

(8.130)

and the aeroelastic eigenvalue k is related to the flutter frequency ω through the relation

$$k^2 = \left[\frac{\rho h a^4}{D\pi^4}\right]\omega^2$$

(8.131)

Using a four-mode solution with a half-sine wave in the cross stream direction and a number of half-sine waves equal to 1, 2, 3, and 4 in the streamwise direction, the coefficient c_i can be determined in terms of g and λ. The flutter condition can then be obtained by solving Eqs. (8.124) and (8.125) simultaneously for different values of the damping factor. Notice the simplification introduced by the present formulation, where all the flutter velocities and flutter frequencies are obtained directly from the solution of these two equations. Furthermore, the present formulation can provide first the least instability, i.e., the first flutter velocity, if this is the prime factor of the analysis. Figure 8.6 gives the results of the numerical calculations performed for different values of the damping factor g. From these curves, it can be observed that the inclusion of the aerodynamic
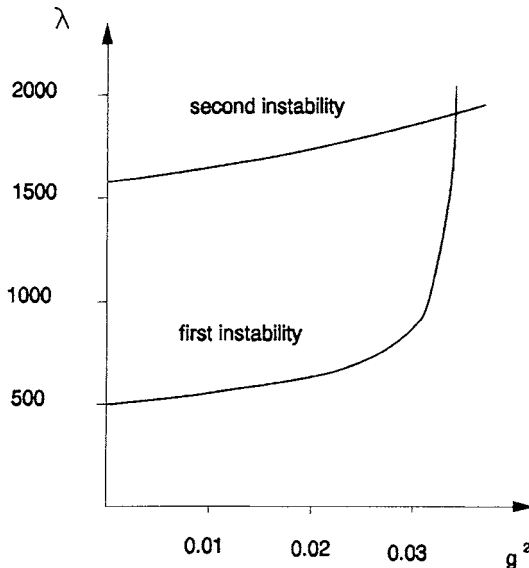

Fig. 8.6   Flutter dynamic pressure vs aerodynamic damping parameter of a flat plate.

damping for this type of problem is always conservative. Moreover, for high values of damping, higher modes can be more critical than the first ones, even for this simple problem, and therefore a convergence study of the solution must be made by including more modes in the analysis when high values of aerodynamic damping are present. Finally, it is to be observed that practical values of g^2 range between 0 and 0.03.

8.5.2   The k Methods

The aerodynamic matrix cannot always be put in the form previously given in Eq. (8.112). In general, the aerodynamic matrix elements are complicated functions of the reduced frequency k and the Mach number M. In such cases, iterative methods of solution must be used. The k methods of solution are the most widely used methods in such cases. In this section, this is briefly discussed. The equation of aeroelastic stability in the modal base can be written as

$$\left[\lceil\mu\rfloor p^2 + \lceil\beta\rfloor p + \lceil\gamma\rfloor - \tfrac{1}{2}\rho U^2 [A]\right]\{q\} = \{0\} \tag{8.132}$$

where the aerodynamic matrix is composed, in general, of complex element functions of the reduced frequency and Mach number.

In the k method of solution, an artificial structural damping $ig\gamma$ is added to the equation of aeroelastic stability [Eq. (8.132)] to read

$$\left[\lceil\mu\rfloor p^2 + \lceil\beta\rfloor p + (1+ig)\lceil\gamma\rfloor - \tfrac{1}{2}\rho U^2[A]\right]\{q\} = \{0\} \tag{8.133}$$

and a pure harmonic solution is sought for the system in Eq. (8.133). In such a case, physically the only points that are correct are when the damping in the system is zero. This gives the flutter points. Thus, for Eq. (8.133) solutions in the form

$$\{q\} = \{q_0\}e^{i\omega t} \tag{8.134}$$

where ω is assumed real, multiplying Eq. (8.133) by $(1+ig)$ and grouping terms, we obtain

$$\left[\left[-\mu + \frac{\rho}{2}\left(\frac{c}{2k}\right)^2 A\right]\frac{\omega^2}{1+ig} + [\beta]\frac{i\omega}{(1+ig)^{1/2}} + [\gamma]\right]\{q_0\} = \{0\} \tag{8.135}$$

where the term $[\beta]$ has been multiplied by $(1+ig)^{1/2}$, which is valid only at the flutter point, i.e., for $g = 0$, and c is the reference length used for nondimensionalizing the reduced frequency. The problem solution then proceeds as follows:

1) For fixed given values of ρ, M, and k, compute the aerodynamic matrix $[A]$.

2) Solve the eigenvalue problem, with $\omega^2/[1 + ig]$ regarded as the eigenvalue of the problem.

3) For each mode used in the analysis, compute the frequency, damping, and velocity.

4) Repeat steps 2) and 3) for different values of the reduced frequency k.

5) Numerically trace the frequency and damping vs the velocity.

6) Flutter instabilities are obtained at the points when a damping curve crosses the zero line.

7) Static divergence instabilities are obtained at the points when a frequency curve crosses the zero line.

8) Repeat steps 1) to 7) for different values of Mach number.

9) Obtain a matching between the velocity and the Mach number for the fluttering conditions.

10) Repeat the complete algorithm for different altitudes.

The disadvantage of the k method, described above, is that no interpretation about the system damping can be obtained because the solution is only valid for a pure harmonic motion, i.e., at the flutter condition. On the other hand, for a given set of $k-M-\rho$, all the modal values are obtained from a single eigenvalue solution.

8.5.3 The p–k Methods

In the p-k methods of solution, we separate the aerodynamic matrix into a real matrix and an imaginary matrix and write the equation of aeroelastic stability in the form

$$\left[\mu p^2 + \left(\beta - \frac{\rho c V}{4k} A_I \right) p + \left(\gamma - \frac{\rho V^2}{2} A_R \right) \right] \{q_0\} = \{0\} \quad (8.136)$$

Where A_R and A_I are the real and imaginary parts of the aerodynamic matrix; p is the problem eigenvalue and is considered complex. The problem solution then proceeds as follows:

1) For fixed given values of ρ, begin the calculation for a fixed value of a velocity V and therefore a Mach number M.

2) Assume for the first mode a root $p_1 = \delta_1 + ik_1$.

3) Compute the aerodynamic matrix for this k_1 value.

4) Solve the eigenvalue problem and obtain the computed first root as $p_2 = \delta_2 + ik_2$.

5) Repeat steps 3) and 4) until a desired accuracy is achieved.

7) Repeat this process for all the modes.

8) Repeat the algorithm for all the required velocities.

The great advantage of the method resides in the fact that the damping calculated is a true damping value and can be used for comparison with experimental values. Furthermore, the matching of velocity and Mach number is avoided. The big disadvantage of the method is that it is a time-consuming process due to the lengthy iterations required.

8.6 Applications

8.6.1 Flutter Analysis of a 15-deg Swept-Wing Model

We consider the 15-deg swept untapered wing model previously analyzed in Chapter 3 for free vibration. This wing model has been tested in the tunnel, and the experimental results are given in Ref. 32.

For the aeroelastic analysis of this model, we use the doublet lattice method and a regular mesh of 4 elements chordwise and 10 elements spanwise. The first three modes obtained in Chapter 3 are used in the aeroelastic analysis. These mode shapes are surface splinned to produce modal deflections and slopes at the 3/4 points of the elements of the doublet lattice model. The analysis is performed using a Mach number equal to 0.45. The k method of solution is used for the aeroelastic problem solution. The results of the analysis in terms of frequency
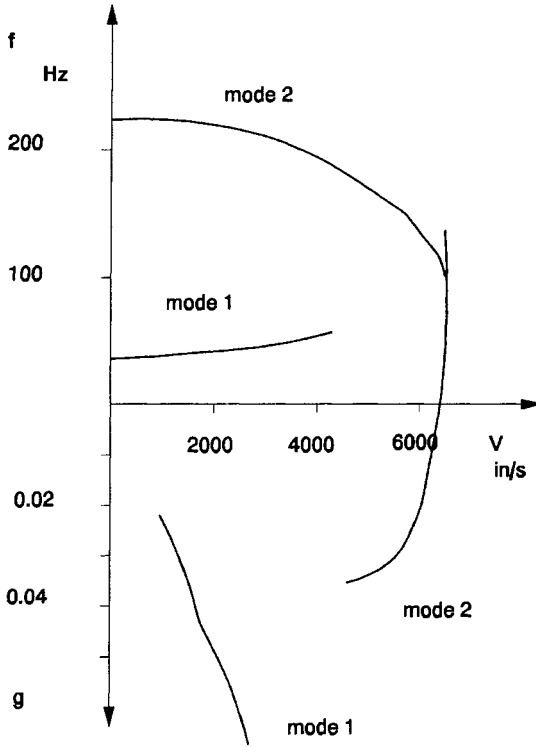
Fig. 8.7   Theoretical aeroelastic analysis for a 15-deg swept-wing model using the doublet lattice and k method of solution.

and damping vs the velocity are given in Fig. 8.7. From this figure, we obtain the calculated flutter velocity as 6400 in./s, and the corresponding flutter frequency is 120 Hz. The corresponding measured values of Ref. 32 are 6100 in./s and 121 Hz, respectively. From these results, it can be concluded that good agreement has been achieved between measured and calculated values.

8.6.2   Hypersonic Flutter of a Cantilever Wing

As a second example, we consider the hypersonic flutter of the cantilever wing studied in Ref. 33 and reported in Ref. 5. The same example has been analyzed in detail in Refs. 29 and 31 using the direct methods of solution given in these references. The results of these analyses are summarized in the following. All the analyses have been performed for the first three modes of free vibration, namely the first bending, the first torsion, and the first chordwise modes, based on experimental measurements of these. Aerodynamic piston theory was used in all the analyses. As was given in Ref. 29, we first omit the aerodynamic damping from the analysis, and, using the data of Ref. 5, we write the equations of aeroelastic stability as

$$[\mu[I] + \lceil \gamma \rfloor + \Lambda[A]]\{q\} = 0 \qquad (8.137)$$

where

$$\mu_i = -(\omega/\omega_2)^2$$

$$\gamma_i = \omega_i^2/\omega_2^2$$

$$\Lambda = (U/b\omega_2)^2$$

and

$$[A] = \begin{bmatrix} 0 & -0.0425 & -0.00668625 \\ 0 & -0.0075 & -0.05517185 \\ 0 & 0 & -0.01125 \end{bmatrix} \tag{8.138}$$

The frequencies are nondimensionalized for the torsional natural frequency ω_2, and other notations are as defined before. The analysis reported in Ref. 33 was done for several values of the chordwise frequency ratio $\Lambda_3 = \omega_3/\omega_2$. Examining the aerodynamic matrix $[A]$ given in Eq. (8.138), we conclude that, based on the frequency coalescence theory, no flutter can take place for these data because there is no aerodynamic coupling among the modes. Only static divergence can occur, and these conditions of static divergence can be obtained by solving the following individual equations for $\mu = 0$:

$$-\mu + 0.2195 = 0$$

$$-\mu + 1 - 0.0075\Lambda = 0 \tag{8.139}$$

$$-\mu + \Lambda_3^2 - 0.01125\Lambda = 0$$

From the first equation, we conclude that the bending mode has no contribution to static divergence. From the second and the third equations, we obtain the values of the static divergence for the torsion and chordwise modes, and we observe that they act individually. These results obtained in Ref. 29 coincide with those of Ref. 5 using the solution of the eigenvalue problem. Now, if we consider the damping effect, but omit the damping due to curvature, we will have to add to the system of Eq. (8.137) the following imaginary term:

$$[A_1] = 0.03125i(\Lambda\mu)^{\frac{1}{2}} \begin{bmatrix} 1 & 0 & 0 \\ 0 & 1 & 0 \\ 0 & 0 & 1 \end{bmatrix} \{q_0\} \tag{8.140}$$

Again, no flutter condition can take place because there is no aerodynamic coupling among the modes. Only static divergence can happen, and the effect of such damping when present alone is merely a frequency shift. Now, if the damping due to curvature is considered, the following imaginary term is further added to the equation of aeroelastic stability:

$$[A_2] = i(\Lambda\mu)^{\frac{1}{2}} \begin{bmatrix} 1 & 0.00339 & 0 \\ 0.00509 & 0 & 0.001974 \\ 0 & 0.0065 & 0 \end{bmatrix} \{q_0\} \tag{8.141}$$

Now we have aerodynamic coupling between modes 1 and 2 and modes 2 and 3. These are the types of flutter reported in Ref. 5 and can be explained only through the damping due to curvature.

For the first type of flutter (bending–torsion), this is a mild type of flutter, i.e., the damping curve crosses the zero line twice, or even decreases, then increases again without crossing the zero line, depending on the value of Λ_3 used in the analysis. This type of flutter is typical of secondary effects and can be attributed to damping due to curvature.

The second mode of flutter is a violent one due to the coupling between the torsion and chordwise modes. This type of flutter cannot be explained only due to the inclusion of the damping effect due to curvature. Now, if we examine the mode shapes of Ref. 5, we observe that the chordwise mode has been approximated by a mode with two nodal lines that run parallel to the leading edge. This was done to preserve orthogonality and approximate measured values. It is known that the first chordwise mode (two nodes in the chordwise direction) of a cantilever homogeneous square plate does not have such nodal lines. The nodal lines of this mode approach the leading and trailing edges at the root and leave these edges while moving spanwise. Furthermore, exact symmetry of nodal lines in relation to midchord position is preserved only if the plate is theoretically homogeneous. The measured values of the frequencies of Ref. 33 reveal that the plate was not homogeneous; its chordwise frequency is much less than that theoretically predicted for a square plate; it approaches the value of a plate with an aspect ratio of 1:2. To examine whether this mode is prone to flutter when coupling with the torsion mode, small disturbances in the aerodynamic stiffness matrix were made in Ref. 29. These disturbances were done by introducing to the aerodynamic stiffness matrix a value for the element (3,2) equal to a negative percentage of the element (2,3). The percentage used in Ref. 29 ranged from 1 to 20%. Notice that a 10% disturbance would be equivalent to moving the nodal lines only 1% in a forward chordwise position and introducing an assymmetry of 5% to the deflection of the trailing edge in relation to the leading edge. This disturbance has a much smaller effect on the frequency and mode shape than those revealed in the measurements of Ref. 33. The results of the analysis of Ref. 29 using these disturbances showed that the violent flutter type of that model was then evident even for a value of disturbance of 1% without the inclusion of any damping in the analysis.

This classical example has been analyzed in Ref. 29 in detail to show the importance in the accuracy in the mode shapes, especially if these are measured values, when used in flutter analyses, and to show the adequacy of the mode coalescence theory to predict the violent types of flutter when present. All the analyses of Ref. 29 were made using the p method and the direct method previously given in Section 8.5.1. The pioneering and now classical work of Ref. 33, made well before the advent of high computational devices, was performed using the classical k method of flutter analysis. In Ref. 31, the same example using the direct p method of analysis, including the damping effect, was reexamined. The main purpose of this reexamination was to show that the traditional V–g–ω plots using the k or p–k methods can miss some mild mode instabilities since the solution is made at discrete values of reduced frequencies or velocities. In Ref. 31, the analysis was made for a value of Λ_3 (the ratio of the chordwise to torsion frequency) equal to 1.833. From this analysis, it was shown that the problem presents two critical modes, the first

one being a mild bending–torsion flutter mode, while the second presents a violent torsion–chordwise flutter mode. The analysis of Ref. 31 shows that the first instability occurs for the mild mode at a value of the velocity parameter $U/b\omega_2 = 9.72$ and a flutter frequency ratio of $\omega/\omega_2 = 0.7058$. This mode becomes stable again at a value of $U/b\omega_2 = 12.92$ and a flutter frequency ratio of $\omega/\omega_2 = 0.643$. The second mode becomes unstable at a value of $U/b\omega_2 = 12.97$ and a flutter frequency ratio of $\omega/\omega_2 = 1.273$. The analysis of Ref. 33 made for discrete values of reduced frequency jumps the first instability and detects only the second one.

8.7 Optimization to Satisfy Flutter Requirements

Optimal design programs to satisfy strength requirements are now well developed and are commonly applied in the aerospace industry for preliminary structural design. Advances made during the last three decades in finite element structural dynamic analysis, nonstationary aerodynamics, and research provide useful and systematic optimization algorithms, provided the necessary means to apply the structural optimization process to satisfy flutter requirements. In this section, a brief account of the main achievements made in optimization techniques to satisfy flutter requirements are given.

The first reported results of aeroelastic optimization of lifting surfaces using variational methods were made by Turner,[34] and an application to a semi-infinite flat sandwich panel to satisfy supersonic flutter requirements subject to a minimum weight constraint was studied using the finite element method. In 1971, computerized preliminary design programs with flutter considerations were developed and reported in Refs. 35 and 36. Rudsill and Bhatia[37] developed search procedure techniques using gradient methods for flutter optimization. Later, they used the second partial derivatives of the eigenvalues of the flutter equation with respect to the structural parameter to develop expressions for the step size in a projected gradient search algorithm.[38] Applications were made to minimize the mass of a box beam that supports a lifting surface. Pierson[39] in 1972 presented a survey on optimal structural design under dynamic constraints. Weisshaar[40] presented a solution for a least weight skin thickness distribution of a one-dimensional flutter problem in supersonic flow. Simodynes[41] presented an optimization method by updating the gradient total weight of the structural components restrained to a fixed flutter speed. Gwin and Taylor[42] presented an optimization algorithm using the feasible directions method together with an efficient numerical procedure for the calculation of the gradient vectors for flutter optimization. Pines and Newman[43] used the finite element method and the quasistatic aerodynamic theory for the analysis part of a weight minimization variational method for flutter constraint velocity. Optimization applications to complex aeronautical structures to satisfy static, dynamic, and aeroelastic requirements were studied by Rao.[44] Numerous research papers and doctoral dissertations were generated during the 1970s at Stanford University in California under the supervision of Professor H. Ashley (see Refs. 45, 46, and 47) in the area of structural optimization with complex constraints such as flutter and dynamic response. A historical review on advances made in optimization for strength and aeroelastic requirements up to 1977 was given in Ref. 48. Librescu and Beiner[49] in 1986 presented a review paper on weight minimization of panels subjected to flutter speed constraints.

Optimal design of large-scale realistic stuctures with aeroelastic constraints are characterized by an increase in the analysis part requirements compared with static constraints. The methods proposed in Refs. 29 and 31 present an attempt to reduce the effort spent in the aeroelastic problem solution and can be used efficiently in aeroelastic optimal design programs.

References

[1] Scalan, R. H., and Rosenbaum, R., *Introduction to the Study of Aircraft Vibration and Flutter*, Macmillan, New York, 1951.

[2] Bisplinghoff, R. L., Ashley H., and Halfman, R. L., *Aeroelasticity*, Addison–Wesley, Reading, MA, 1955.

[3] Fung, Y. C., *An Introduction to the Theory of Aeroelasticity*, Wiley, New York, 1955.

[4] *Manual on Aeroelasticity*, AGARD, Vol. I–VII, NATO, first edited in 1959, edited by W. P. Jones, 1961, edited by R. Mazet, 1968, and continuously updated.

[5] Bisplinghoff, R. L., and Ashley, H., *Principles of Aeroelasticity*, Wiley, New York, 1962.

[6] Dowell, E. H., Curtis, H. C., Jr., Scalan, R. H., and Sisto, F., *A Modern Course in Aeroelasticity*, Sijthoff and Noordhoff, Alphen aan den Rijn, The Netherlands, 1978.

[7] Küssner, H. G., "Allgemeine Tragflachentheorie," *Luftfahrtforschung*, Vol. 17, No. 11–12, 1940, pp. 370–379.

[8] Landahl, M., "Kernel Function for Nonplanar Oscillating Surfaces in a Subsonic Flow," *AIAA Journal*, Vol. 5, No. 5, 1967, pp. 1045–1046.

[9] Albano, E., and Rodden, W., "A Doublet-Lattice Method for Calculating Lift Distribution on Oscillating Surfaces in Subsonic Flows," *AIAA Journal*, Vol. 7, No. 2, 1969, pp. 279–285.

[10] Watkins, C. E., Woolston, D. S., and Cunningham, H. L., "A Systematic Kernel Function Procedure for Determining Aerodynamic Forces on Oscillating or Steady Finite Wings at Subsonic Speeds," NASA TR-R-48, 1959.

[11] Laschka, B., "Zur Theorie der Harmonisch Schwingenden Tragenden Flache bei Unter-Schallanstromung," *Zeitschrift fur flugwissenschaften*, Vol. 11, No. 7, 1963, pp. 265–292.

[12] Vivian, H. T., and Andrew, L. V., "Unsteady Aerodynamics for Advanced Configurations," AFFDL-TTR-64-152, 1965.

[13] Rowe, W. S., Redman, M. C., Ehlers, F. E., and Sebastian, J. D., "Prediction of Unsteady Aerodynamic Loadings Caused by Leading and Trailing Edge Control Surface Motion in Subsonic Compressible Flow—Analysis and Results," NASA CR-2543, 1975.

[14] Cunningham, A. M., "A Rapid and Stable Collocation Method for Solving the Lifting-Surface Problems by Use of Quadratic Integration," AIAA/ASME 11th Structural Dynamics and Material Conference, Denver, CO, 1970.

[15] Cunningham, A. M., "Unsteady Collocation Method for Wings With and Without Control Surfaces," *Journal of Aircraft*, Vol. 9, No. 6, 1972, pp. 413–419.

[16] Dat, R., and Malfois, J. P., "Sur le Calcul du Noyau de l'Equation Integrale de la Surface Portante en Ecoulement Subsonique Instationaire," *La Recherche Aeroespatiale*, No. 5, 1970, pp. 251–259.

[17] Desmarais, R. N., "An Accurate and Efficient Method for Evaluating the Kernel of the Integral Equation Relating Pressure to Normalwash in Unsteady Potential Flow," AIAA paper 82-0687, 1982.

[18] Ueda, T., "Asymptotic Expansion of the Kernel Function in Subsonic Unsteady Lifting Surfaces Theory," *Journal of the Japan Society for Aeronautical Sciences*, Vol. 20, No. 326, 1981, pp. 169–174.

[19] Bismarck-Nasr, M. N., "Kernel Function Occurring in Subsonic Unsteady Potential Flow," *AIAA Journal*, Vol. 29, No. 6, 1991, pp. 878–879.

[20] Basset, A. B., *A Treatise on Hydrodynamics*, Vol. 2, Cambridge Univ. Press, Cambridge, England, UK, 1888.

[21] Nicholson, J. W., "Notes on Bessel Functions," *Quarterly Journal*, XLII, 1911, pp. 216–224.

[22] Gegenbauer, L., "Uber Einige Bestimmte Integrale," *Wiener Sitzungsberichte*, LXX (2), 1875, pp. 433–443.

[23] Watson, G. N., *A Treatise on the Theory of Bessel Functions*, 2nd ed., Macmillan, New York, 1945.

[24] *Handbook of Mathematical Functions with Formulas, Graphs and Mathematical Tables*, 8th ed., edited by M. Abramowitz and I. A. Stegnun, Dover, New York, 1972.

[25] Magnus, W., and Oberhettinger, F., *Formulas and Theorems for the Special Functions of Mathematical Physics*, Chelsea Publishing Co., New York, 1949.

[26] *Tables of Integral Transforms*, edited by A. Erdelyi, McGraw–Hill, New York, 1954.

[27] Watkins, C. E., and Berman, J. H., "On the Kernel Function of the Integral Equation Relating Lift and Downwash Distributions of Oscillating Wings in Supersonic Flow," NACA Rept. 1257, 1956.

[28] Bismarck-Nasr, M. N., "Kernel Function Occurring in Supersonic Unsteady Potential Flow," *AIAA Journal*, Vol. 29, No. 11, 1991, pp. 2006–2007.

[29] Bismarck-Nasr, M. N., "Coalescence of Aeroelastic Modes in Flutter Analysis," *Journal of Aircraft*, Vol. 29, No. 3, 1992, pp. 505–507.

[30] Pipes, L. A., *Applied Mathematics for Engineers and Physicists*, McGraw–Hill, New York, 1958.

[31] Bismarck-Nasr, M. N., "On a Direct Solution of the Aeroelastic Stability Equations," *Journal of Aircraft*, Vol. 31, No. 3, 1994, pp. 979–981.

[32] Yates, E. C., Jr., and Bennet, R. M., "Use of Aerodynamic Parameters from Nonlinear Theory in Modified-Strip-Analysis Flutter Calculations for Finite Span Wings at Supersonic Speeds," NASA TN D-1824, 1963.

[33] Dugundji, J., and Crisp, J. D. C., "On the Aeroelastic Characteristics of Low Aspect Ratio Wings with Chordwise Deformations," USAF Office of Scientific Research TN 59-787, 1959.

[34] Turner, M. J., "Optimization of Structures to Satisfy Flutter Requirements," *AIAA Journal*, Vol. 7, No. 5 , 1969, pp. 945–951.

[35] Stroud, W. J., Dexter, C. B., and Stein, M., "Automated Preliminary Design of Simplified Wing Structures to Satisfy Strength and Flight Requirements," NASA TN D-6534, 1971.

[36] Tripplet, W. E., and Ising, K. D., "Computer Aided Stability Design Including Aeroelastic Constraints," *Journal of Aircraft*, Vol. 8, No. 7, 1971, pp. 554–561.

[37] Rudsill, C. S., and Bhatia, K. G., "Optimization of Complex Structures to Satisfy Flutter Requirements," *AIAA Journal*, Vol. 9, No. 8, 1971, pp. 1487–1491.

[38] Rudsill, C. S., and Bhatia, K. G., "Derivatives of the Flutter Velocity and the Optimization of Aircraft Structures," *AIAA Journal*, Vol. 10, No. 12, 1972, pp. 1569–1572.

[39] Pierson, B. L., "A Survey of Optimal Structure Design Under Dynamic Constraints," *International Journal for Numerical Methods in Engineering*, Vol. 4, No. 4, 1972, pp. 491–499.

[40] Weisshaar, T. A., "Aeroelastic Optimization of a Panel in High Mach Number Supersonic Flow," *Journal of Aircraft*, Vol. 9, No. 9, 1972, pp. 611–617.

[41] Simodynes, E. E., "Gradient Optimization of Structural Weight for Specified Flutter Speed," *Journal of Aircraft*, Vol. 11, No. 4, 1974, pp. 143–147.

[42]Gwin, L. B., and Taylor, R. F., "A General Method for Flutter Optimization," *AIAA Journal,* Vol. 11, No. 12 , 1973, pp. 1613–1617.

[43]Pines, S., and Newman, M., "Constraint Structural Optimization for Aeroelastic Requirements," *Journal of Aircraft,* Vol. 11, No. 6, 1974, pp. 313–320.

[44]Rao, S. S., "Optimization of Complex Structures to Satisfy Static, Dynamic and Aeroelastic Requirements," *International Journal for Numerical Methods in Engineering,* Vol. 8, No. 2, 1973, pp. 249–269.

[45]Johnson, E. H., Rizzi, P., Ashley, H., and Segenreich, S. A., "Optimization of Continuous One-Dimensional Structures Under Steady Harmonic Excitation," *AIAA Journal,* Vol. 14, No. 12, 1976, pp. 1690–1698.

[46]Rizzi, P., "Optimization of Multi-Constrained Structures Based on Optimality Criteria," AIAA/ASME/SAE 17th Structures, Stuctural Dynamics, and Materials Conference, 1976, pp. 448–462.

[47]Segenreich, S. A., Johnson, E. H., and Rizzi, P., "Three Contributions to Minimum Weight Structural Optimization with Dynamic and Aeroelastic Constraints," SUDAAR No. 501, Stanford Univ., Dept. Aeron. and Astron., 1976.

[48]Lansing, W., Lerner, E., and Taylor, R. F., "Applications of Structural Optimization for Strength and Aeroelastic Requirements," AGARD Rept. No. 664, 1977.

[49]Librescu, L., and Beiner, L., "Recent Results on the Weight Minimization of Panels with a Flutter Speed Constraint," *Solid Mechanics Archives,* Vol. 11, No. 1, 1986, pp. 25–45.

9
Aeroelasticity of Plates and Shells

9.1 Introduction

The problem of aeroelasticity of plates and shells was recognized to be an important aspect of the design of high-speed vehicles when Jordan[1] observed that a number of the early V-2 rocket failures were due to flutter of their panels. Since then, extensive analytical and experimental research on the subject has been performed. In the 1970s, two books[2,3] devoted entirely to the subject were published. Several survey and review papers on the subject are available[4-8] in which the theoretical aspects and developments attained in the field were presented. Since the 1950s and until recently, current aeroelastic analyses have normally been made in a modal base, using measured frequencies and mode shapes, or based on approximate calculations of these. The finite element method can be used to predict more accurate calculations of frequencies and mode shapes needed for the aeroelasticity modal analysis. On the other hand, the method can be applied directly to some aeroelastic problems, avoiding thus the modal representation. One of the fields of aeroelasticity where this application can be performed directly is the aeroelasticity of plates and shells.

9.2 Flat Plates

Consider a thin isotropic rectangular flat plate of dimensions a and b and uniform thickness h mounted on rigid wall as shown in Fig. 9.1. The plate is subjected to an initial state of membrane direct and shear stresses as shown in Fig. 9.1.

The upper surface of the plate is exposed to a high supersonic airflow at zero angle of attack and parallel to its side edges. Beneath the plate, still air is present. In the presence of some disturbances, the plate can start to perform a perturbed motion with transverse deflection $w(x, y, t)$. We are interested in the study of the stability of the plate due to such motion. We further assume that initial in-plane stresses have not reached their critical buckling values, and we limit our analysis to the linear case. The theoretical formulation of the problem can be performed employing an energy approach using Hamilton's principle. The related principle for the problem at hand can be stated as

$$\int_{t_0}^{t_1} \delta(T - U - U_i)\, dt + \int_{t_0}^{t_1} \delta W\, dt = 0 \qquad (9.1)$$

where T is the kinetic energy, U is the bending strain energy due to small deformations, U_i is the strain energy due to prestress, W is the work done by the external aerodynamic load, t is the time, and δ is the variational operator. The
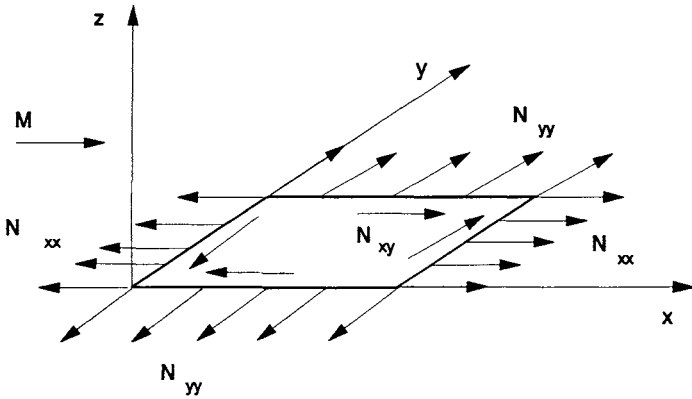
Fig. 9.1   Flat rectangular panel subjected to a state of initial membrane stresses in the presence of a supersonic flow.

kinetic energy T, neglecting in-plane and rotary inertia, reads

$$T = \frac{1}{2} \int_A \rho_m h \left(\frac{\partial w}{\partial t} \right)^2 dA \tag{9.2}$$

where ρ_m is the plate material density. The bending strain energy U, due to small deformations for isotropic thin plates, can be expressed as

$$U = \frac{D}{2} \int_A \left[\left(\frac{\partial^2 w}{\partial x^2} \right)^2 + \left(\frac{\partial^2 w}{\partial y^2} \right)^2 + 2\nu \frac{\partial^2 w}{\partial x^2} \frac{\partial^2 w}{\partial y^2} + 2(1 - \nu) \left(\frac{\partial^2 w}{\partial x \partial y} \right)^2 \right] dA \tag{9.3}$$

where $D = Eh^3/12(1 - \nu^2)$ is the plate flexural rigidity, ν is Poisson's ratio, and E is Young's modulus. The strain energy due to the initial membrane state of stress was treated in Chapter 4 Eq. (4.71) and reads

$$U_i = \frac{1}{2} \int_A \left[N_{xx} \left(\frac{\partial w}{\partial x} \right)^2 + N_{yy} \left(\frac{\partial w}{\partial y} \right)^2 + 2N_{xy} \frac{\partial w}{\partial x} \frac{\partial w}{\partial y} \right] dA \tag{9.4}$$

Using a first-order high Mach number approximation to the linear potential flow theory,[2,3] the work done by external aerodynamic forces reads

$$W = - \int_A \frac{2Q}{V\beta} \left(V \frac{\partial w}{\partial x} + \frac{M^2 - 2}{M^2 - 1} \frac{\partial w}{\partial t} \right) w \, dA \tag{9.5}$$

where $Q = \rho V^2/2$ and is the free stream dynamic pressure, $\beta = (M^2 - 1)^{1/2}$, V is the free stream velocity, M is the free stream Mach number, and ρ is the free stream air density. For sufficiently high Mach number, Eq. (9.5) can be approximated by

$$W = - \int_A \left(\frac{2Q}{M} \frac{\partial w}{\partial x} + \frac{2Q}{VM} \frac{\partial w}{\partial t} \right) w \, dA \tag{9.6}$$

The expression of the aerodynamic load given in Eq. (9.5) is known in the literature as the quasisteady case. Furthermore, if the aerodynamic damping, i.e., the term proportional to the velocity in Eq. (9.6) is neglected, we get the quasistatic Ackeret's expression

$$W = -\int_A \frac{2Q}{M}\left(\frac{\partial w}{\partial x}\right) w\, \mathrm{d}A \tag{9.7}$$

We notice that the loading in Eq. (9.7) is assumed to be that resulting from a flow over a stationary surface with the shape the same as that of the deflected plate at that instant of time. Substituting Eqs. (9.2), (9.3), and (9.7) into Hamilton's principle, integrating the kinetic energy by parts, applying the conditions of vanishing of the variations at $t = t_0$ and $t = t_1$, and minimizing with respect to the field variable w, we obtain the Euler–Lagrange equation governing the problem for the case of no initial stress and using the quasistatic aerodynamic theory as

$$D\left[\frac{\partial^4 w}{\partial x^4} + 2\frac{\partial^4 w}{\partial x^2 \partial y^2} + \frac{\partial^4 w}{\partial y^4}\right] + \rho_m h \frac{\partial^2 w}{\partial t^2} + \frac{2Q}{[M^2 - 1]^{\frac{1}{2}}}\frac{\partial w}{\partial x} = 0 \tag{9.8}$$

The variation operation gives the forced boundary conditions as

$$\begin{aligned}
w = 0 \qquad \frac{\partial w}{\partial x} = 0 \qquad \text{on } x = 0 \text{ and on } x = a \\
w = 0 \qquad \frac{\partial w}{\partial y} = 0 \qquad \text{on } y = 0 \text{ and on } y = b
\end{aligned} \tag{9.9}$$

and the natural or free boundary conditions as

$$D\left[\frac{\partial^3 w}{\partial x^3} + 2(1-v)\frac{\partial^3 w}{\partial x \partial y^2}\right] = Q_x = 0 \qquad D\left[\frac{\partial^2 w}{\partial x^2} + v\frac{\partial^2 w}{\partial y^2}\right] = M_x = 0$$

$$\text{on } x = 0 \text{ and on } x = a \tag{9.10a}$$

and

$$D\left[\frac{\partial^3 w}{\partial y^3} + 2(1-v)\frac{\partial^3 w}{\partial y \partial x^2}\right] = Q_y = 0 \qquad D\left[\frac{\partial^2 w}{\partial y^2} + v\frac{\partial^2 w}{\partial x^2}\right] = M_y = 0$$

$$\text{on } y = 0 \text{ and on } y = b \tag{9.10b}$$

For the four-edges simply supported case, a closed-form solution of the differential [Eq. (9.8)] can be obtained using the method of separation of variables and assuming solutions in the form of half-sine waves in the cross stream direction. Thus, write w as

$$w(x, y, t) = W(x)\sin[n\pi y/b]e^{\omega t} \tag{9.11}$$

and substituting Eq. (9.11) into Eq. (9.8), we obtain

$$D\left[\frac{\mathrm{d}^4 W}{\mathrm{d}x^4} - 2\left(\frac{n\pi}{b}\right)^2\frac{\mathrm{d}^2 W}{\mathrm{d}x^2} + \left(\frac{n\pi}{b}\right)^4 W\right] + \rho_m h\omega^2 W + \frac{2Q}{[M^2 - 1]^{\frac{1}{2}}}\frac{\mathrm{d}W}{\mathrm{d}x} = 0 \tag{9.12}$$

and the boundary conditions read

$$W(0) = W(a) = W(0) = W(a) = 0 \tag{9.13}$$

Equation (9.12) and the boundary conditions in Eq. (9.13) can be put in a nondimensionalized form through introduction of the variable $\xi = x/a$, and we obtain

$$\frac{d^4 W}{d\xi^4} + A \frac{d^2 W}{d\xi^2} + \lambda \frac{dW}{d\xi} + BW = 0 \tag{9.14}$$

and

$$W(0) = W(1) = W(0) = W(1) = 0 \tag{9.15}$$

where

$$A = -2n^2\pi^2[a/b]^2$$
$$B = k^2 + n^4\pi^4[a/b]^4$$
$$\lambda = 2Qa^3/D[M^2 - 1]^{\frac{1}{2}} \tag{9.16}$$
$$k^2 = \left[\rho_m h a^4/D\right]\omega^2$$

Equation (9.14) represents a parametric eigenvalue problem with B considered as the eigenvalue and λ being the parameter of the problem. Thus, writing solutions in the form

$$W(\xi) = W_0 e^{p\xi} \tag{9.17}$$

we obtain the characteristic equation of the problem as

$$p^4 + Ap^2 + \lambda p + B = 0 \tag{9.18}$$

Now, because λ is a real positive quantity and A is a real negative quantity, it can be shown that the roots of Eq. (9.18) can be written in the form

$$p_{1,2} = -\varepsilon \pm d \qquad p_{3,4} = \varepsilon \pm ic \tag{9.19}$$

where

$$d^2 = [\lambda/4\varepsilon] - [\varepsilon^2 + A/2]$$
$$c^2 = [\lambda/4\varepsilon] + [\varepsilon^2 + A/2] \tag{9.20}$$
$$B = -[\lambda/4\varepsilon]^2 + [2\varepsilon^2 + A/2]^2$$

Using the boundary conditions in Eq. (9.15), we obtain

$$\begin{bmatrix} 1 & 1 & 1 & 1 \\ p_1^2 & p_2^2 & p_3^2 & p_4^2 \\ e^{p_1} & e^{p_2} & e^{p_3} & e^{p_4} \\ p_1^2 e^{p_1} & p_2^2 e^{p_2} & p_3^2 e^{p_3} & p_4^2 e^{p_4} \end{bmatrix} \begin{Bmatrix} W_{01} \\ W_{02} \\ W_{03} \\ W_{04} \end{Bmatrix} = \begin{Bmatrix} 0 \\ 0 \\ 0 \\ 0 \end{Bmatrix} \tag{9.21}$$
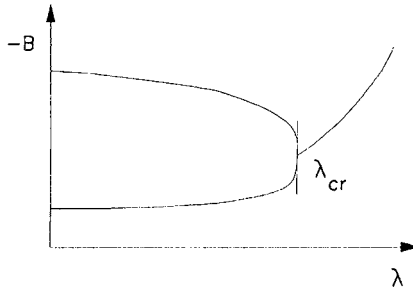
Fig. 9.2   Stability boundary.

For a nontrivial solution, the determinant in Eq. (9.21) must be equal to zero, and we get

$$[(c^2 + d^2) + 4\varepsilon^2(c^2 - d^2)] \sin c \sinh d - 8\varepsilon^2 cd [\cosh d \cos c - \cosh 2\varepsilon] = 0$$

$$(9.22)$$

The solution of the problem will proceed as follows: for given values of A and λ, we vary ε until Eq. (9.22) is satisfied; having obtained ε, the value of B is then determined from the third relation in Eq. (9.20). The results are drawn in the $\lambda - B$ plane as schematically shown in Fig. 9.2. When $\lambda = 0$, the values of B are proportional to the squares of the free vibration frequencies of the plate; with the increase of λ, the values of the frequencies change until reaching a value of λ_{cr} where two modes coalesce. Increasing further λ, a pair of complex conjugate eigenvalues is obtained, and in view of Eq. (9.11) an unstable motion is obtained. The value of λ_{cr} will thus determine the borderline of the stability. A plot of λ_{cr} vs $\underline{A} = A/\pi^2$ is shown in Fig. 9.3. For the case when the two side edges are simply supported and the trailing and leading edges have any other boundary conditions, an analytical solution can be obtained in a similar manner. Other boundary conditions do not have analytical solutions, and the problem must be solved using numerical methods.

### 9.2.1   Rayleigh–Ritz Solution

In the Rayleigh–Ritz method, we write approximate solutions in the form

$$W(x, y, t) = \phi_m(x, y)q_m(t) \qquad m = 1, 2, 3, \ldots \qquad (9.23)$$

where $\phi_m(x, y)$ are arbitrary functions that satisfy the geometric boundary conditions of the field variable w and $q_m(t)$ are the generalized coordinates.

Substituting the approximate solutions in Eq. (9.23) into Hamilton's principle and minimizing with respect to the generalized coordinates $q_m(t)$, we obtain the following matrix equation

$$[M]\{q''\} + [K]\{q\} + \lambda[A]\{q\} = \{0\} \qquad (9.24)$$
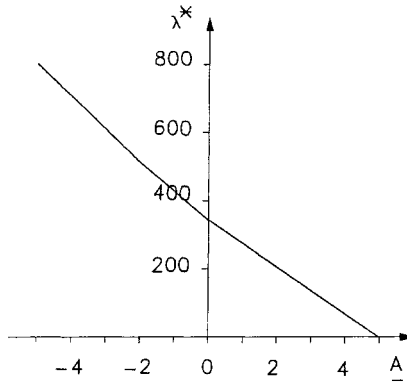
Fig. 9.3   Analytical exact solution of λ_{cr} for four-edges-simply-supported flat rectangular panels where $\underline{A} = A/\pi^2 = -2n^2[a/b]^2$, $\lambda^* = 2qa^3/D[M^2 - 1]^{1/2}$.

where the elements of the matrices in Eq. (9.24) are given by

$$M_{mn} = \int_A \rho_m h \phi_m \phi_n \, dx \, dy$$

$$K_{mn} = \int_A D \left[\frac{\partial^2 \phi_m}{\partial x^2} \frac{\partial^2 \phi_n}{\partial x^2} + \frac{\partial^2 \phi_m}{\partial y^2} \frac{\partial^2 \phi_n}{\partial y^2} + \nu \frac{\partial^2 \phi_m}{\partial x^2} \frac{\partial^2 \phi_n}{\partial y^2} \right.$$

$$\left. + \nu \frac{\partial^2 \phi_m}{\partial y^2} \frac{\partial^2 \phi_n}{\partial x^2} + 2(1 - \nu) \frac{\partial^2 \phi_m}{\partial x \partial y} \frac{\partial^2 \phi_n}{\partial x \partial y} \right] dx \, dy \qquad (9.25)$$

$$A_{mn} = \int_A \phi_m \frac{\partial \phi_n}{\partial x} \, dx \, dy$$

$$\lambda = \frac{2q}{[M^2 - 1]^{\frac{1}{2}}}$$

The matrices $[M]$, $[K]$, and $[A]$ are called the mass, the stiffness, and the aerodynamic matrices, respectively. Furthermore, as has been demonstrated in Chapter 3, the stiffness and mass matrices are diagonal matrices if the trial functions ϕ_m are taken as the natural mode shapes of free vibration. The system in Eq. (9.24) assumes solutions in the form

$$\{q\} = \{q_0\} e^{\omega t} \qquad (9.26)$$

Substituting Eq. (9.26) into Eq. (9.24), we obtain the following parametric eigenvalue problem

$$[[K + \lambda A] + \omega^2 [M]] \{q_0\} = \{0\} \qquad (9.27)$$

where ω^2 is the eigenvalue and λ is the parameter of the problem. When $\lambda = 0$, ω^2 are real negative values and correspond to the negative squares of the natural free vibration frequencies of the plate. With the increase of λ, some pairs of the eigenvalues coalesce and become complex conjugates. The first coalescence determines

the borderline of the stability as stated before. As an application, we consider the case of a four-edges-rectangular simply supported plate, and we assume solutions in the form

$$\phi_{mn} = \sin\frac{m\pi x}{a}\sin\frac{n\pi y}{b} \qquad m, n = 1, 2, 3, \ldots \qquad (9.28)$$

which satisfy the geometric boundary conditions. Furthermore, as shown in Chapter 3, they are the mode shapes of free vibration. Using these trial functions in Eq. (9.25), we obtain

$$\left[[K_{pq,rs}] + \lambda[A_{pq,rs}] + \omega^2[M_{pq,rs}]\right]\{q_{0rs}\} = \{0\} \qquad p, q, r, s = 1, 2, 3, \ldots \tag{9.29}$$

where

$$M_{pq,rs} = [\rho hab]/4 \qquad p = r \quad q = s$$

$$M_{pq,rs} = 0 \qquad p \neq r \quad q \neq s$$

$$K_{pq,rs} = \frac{D\pi^4}{a^4}\frac{ab}{4}\left[p^2 + q^2\left(\frac{a}{b}\right)^2\right]^2 \qquad p = r \quad q = s \tag{9.30}$$

$$K_{pq,rs} = 0 \qquad p \neq r \quad q \neq s$$

$$A_{pq,rs} = \frac{bpr}{[p^2 - r^2]} \qquad q = s \quad p + r \quad \text{odd}$$

$$A_{pq,rs} = 0 \qquad \text{otherwise}$$

Thus, we can write Eq. (9.29) as

$$\left[k^2\lceil I\rfloor + \lceil[p^2 + q^2(a/b)^2]^2\rfloor + \frac{4\lambda^*}{\pi^4}[\alpha] + \omega^2[M_{pq,rs}]\right]$$

$$\times \{q_{0rs}\} = \{0\} \qquad p, q, r, s = 1, 2, 3, \ldots \tag{9.31}$$

with

$$\alpha_{pq,rs} = pr/[p^2 + p^2] \qquad q = s \quad p + r \quad \text{odd}$$

$$= 0 \qquad \text{otherwise}$$

$$k^2 = [\rho_m h\omega^2 a^4]/[D\pi^4] \tag{9.32}$$

$$\lambda^* = 2qa^3/D[M^2 - 1]^{\frac{1}{2}}$$

As an application, we consider a two-mode approximation with $n = 1$ and $m = 1, 2$. Using Eq. (9.31), we obtain

$$\left[k^2\begin{bmatrix} 1 & 0 \\ 0 & 1 \end{bmatrix} + \begin{bmatrix} [1 + (a/b)^2]^2 & 0 \\ 0 & [4 + (a/b)^2]^2 \end{bmatrix}\right.$$

$$\left. + \frac{4\lambda^*}{\pi^4}\begin{bmatrix} 0 & -2/3 \\ 2/3 & 0 \end{bmatrix}\right]\begin{Bmatrix} q_{11} \\ q_{12} \end{Bmatrix} = \begin{Bmatrix} 0 \\ 0 \end{Bmatrix} \tag{9.33}$$

Expanding the determinant, we obtain

$$k^4 + (\alpha + \beta)k^2 + \alpha\beta + \frac{64}{9\pi^8}\lambda^{*2} = 0 \tag{9.34}$$

where

$$\alpha = [1 + (a/b)^2]^2 \qquad \beta = [4 + (a/b)^2]^2 \tag{9.35}$$

Solving Eq. (9.34), we get

$$k^2 = -\frac{[\alpha + \beta]}{2} \pm \sqrt{\left[\frac{[\alpha - \beta]}{2}\right]^2 - \frac{64\lambda^{*2}}{9\pi^8}} \tag{9.36}$$

Examining Eq. (9.36), we observe that, when $[\alpha - \beta]^2/4 > 64\lambda^{*2}/9\pi^8$, the motion is stable since the roots are negative real values; when $[\alpha - \beta]^2/4 < 64\lambda^{*2}/9\pi^8$, the motion is unstable because one of the roots will have a positive real exponential. On the borderline of stability, we have

$$\lambda^*_{\text{crit}} = \frac{9\pi^4}{16}\left[5 + 2\left[\frac{a}{b}\right]^2\right] \tag{9.37}$$

The results obtained using a two-mode approximation are given in Table 9.1 and are compared with the closed-form solution of the previous section. Taking now a four-mode approximation with $n = 1$ and $m = 1, 2, 3, 4$, we obtain

$$\left[k^2[I] + \begin{bmatrix} [1 + \mu]^2 & & & \\ & [4 + \mu]^2 & & \\ & & [9 + \mu]^2 & \\ & & & [25 + \mu]^2 \end{bmatrix}\right.$$

$$\left. + \frac{4\lambda^*}{\pi^4}\begin{bmatrix} 0 & -2/3 & 0 & -4/15 \\ 2/3 & 0 & -6/5 & 0 \\ 0 & 6/5 & 0 & -12/7 \\ 4/15 & 0 & 12/7 & 0 \end{bmatrix}\right]\begin{Bmatrix} q_{11} \\ q_{12} \\ q_{13} \\ q_{14} \end{Bmatrix} = \begin{Bmatrix} 0 \\ 0 \\ 0 \\ 0 \end{Bmatrix} \tag{9.38}$$

where $\mu = [a/b]^2$. The results obtained using a four-mode approximation are given in Table 9.1 and are compared with the previous solutions. From the results obtained, it can be concluded that the four-mode approximation is almost identical with the closed-form solution, showing the rapid convergence of the Rayleigh–Ritz solution for this kind of problem. Furthermore, it can be observed that the Rayleigh–Ritz solution is always less than the closed-form solution, i.e., the Rayleigh–Ritz solution is always less than the closed-form solution, i.e., the Rayleigh–Ritz solution is a conservative solution, and this can be always proven for this kind of problem, based on energy considerations.

9.2.2 Galerkin Solution

The Galerkin method is one of the weight residual techniques of obtaining approximate solutions of boundary value problems. In the Galerkin method, the

Table 9.1 λ_{cr}^* for simply supported rectangular plates

$2(a/b)^2$	Closed-form solution	Two-mode R-R solution	Four-mode R-R solution
0	343.34	273.96	340.00
1	426.01	328.76	421.40
2	512.65	383.55	505.10
3	603.06	438.34	591.60
4	697.10	493.13	680.25
5	794.59	547.93	770.80
6	895.42	602.72	862.69
7	999.48	657.51	955.59
8	1106.64	712.30	1049.18
9	1216.83	767.10	1143.16
10	1329.94	821.89	1237.29

weighting functions are taken as trial functions themselves. The advantage of the weight residual methods over the Rayleigh–Ritz variational method is that they work directly on the differential equations governing the problem without a need to find a variational principle. However, the admissible functions must satisfy all the boundary conditions, while in the variational methods only the forced boundary conditions need be satisfied. Taking solutions in the form

$$W(x, y, t) = \phi_m(x, y)q_m(t) \qquad m = 1, 2, 3, \ldots \qquad (9.39)$$

where $\phi_m(x, y)$ are arbitrary functions that satisfy all the boundary conditions of the differential equation governing the problem and $q_m(t)$ are the generalized co-ordinates. Substituting the approximate solutions to Eq. (9.39) into the differential [Eq. (9.12)], multiplying by the trial functions, and integrating over the domain, the following matrix equation is obtained

$$[M]\{q''\} + [K]\{q\} + \lambda[A]\{q\} = \{0\} \qquad (9.40)$$

where the elements of the matrices in Eq. (9.40) are given by

$$M_{mn} = \int_A \rho_m h \phi_m \phi_n \, dxdy$$

$$K_{mn} = \int_A D \left[\phi_m \left\{ \frac{\partial^4 \phi_n}{\partial x^4} + 2 \frac{\partial^4 \phi_n}{\partial x^2 \partial y^2} + \frac{\partial^4 \phi_n}{\partial y^4} \right\} \right] dxdy$$

$$A_{mn} = \int_A \phi_m \frac{\partial \phi_n}{\partial x} dxdy \qquad (9.41)$$

$$\lambda = \frac{2q}{[M^2 - 1]^{\frac{1}{2}}}$$

As an application, we consider again the case of a four-edges-rectangular simply supported plate, and we assume solutions in the form

$$\phi_{mn} = \sin\frac{m\pi x}{a}\sin\frac{n\pi y}{b} \qquad m, n = 1, 2, 3, \ldots \qquad (9.42)$$

which satisfy all the boundary conditions. Substituting the approximate solutions to Eq. (9.42) into the differential [Eq. (9.12)] and applying the Galerkin method, the same numerical results are obtained as in the Rayleigh–Ritz solution of the previous section. The solution of the stability problem proceeds in the same manner as previously given. It is to be observed that, once a variational principle exists and the same trial functions are used in both the Rayleigh–Ritz method and the Galerkin method, the same numerical solutions are obtained in both solutions.

9.2.3   Finite Element Method Solution

Dividing the plate into finite elements and writing within each element expressions for w in the form

$$w = [N]\{q^e\} \qquad (9.43)$$

where $\{q^e\}$ is the vector of the nodal degrees of freedom and $[N]$ is the matrix of the interpolation functions, substituting Eq. (9.43) into Hamilton's principle, and minimizing the functional, we obtain for each element the following matrix equation

$$[k^e]\{q^e\} + [m^e]\{q''^e\} + g\left[a_1^e\right]\{q'^e\} + \lambda\left[a_2^e\right]\{q^e\} = \{0\} \qquad (9.44)$$

where

$$g = 2Q(M^2 - 2)/V(M^2 - 1)^{\frac{3}{2}} \qquad (9.45)$$

which is called the aerodynamic damping parameter and

$$\lambda = 2Q/(M^2 - 1)^{\frac{1}{2}} \qquad (9.46)$$

which is the dynamic pressure parameter. In Eq. (9.44), $[k^e]$ and $[m^e]$ are the element stiffness and mass matrices, and $[a_1^e]$ and $[a_2^e]$ will be called the aerodynamic damping and the aerodynamic stiffness matrices, respectively, and are given by

$$\left[a_1^e\right] = \int_A [N]^T[N]\,dA \qquad (9.47)$$

and

$$\left[a_2^e\right] = \int_A [N]^T[N_{,x}]\,dA \qquad (9.48)$$

We notice that the aerodynamic damping matrix is proportional to the mass matrix and can be written as

$$\left[a_1^e\right] = [m^e]/\rho_m \qquad (9.49)$$

where ρ_m is the material mass density. Furthermore, the aerodynamic stiffness matrix $[a_2^e]$ is nonsymmetric due to the nonconservative nature of the aerodynamic

loading. For the entire structure, using the standard assembly technique of the finite element method and applying the appropriate boundary conditions, we can write for the whole structure the following matrix equation

$$[K]\{q\} + [M]\{q''\} + g[A_1]\{q'\} + \lambda[A_2]\{q\} = \{0\} \qquad (9.50)$$

where $[K]$, $[M]$, $[A_1]$, and $[A_2]$ are the system stiffness, mass, aerodynamic damping, and aerodynamic stiffness matrices and $\{q\}$ is the vector of the nodal degree of freedom of the system. The system in Eq. (9.50) assumes solutions in the form

$$\{q\} = e^{\omega t}\{q_0\} \qquad (9.51)$$

Substituting Eq. (9.51) into Eq. (9.50), we obtain

$$[[K] + \omega^2[M] + g\omega[A_1] + \lambda[A_2]]\{q_0\} = \{0\} \qquad (9.52)$$

Again, when $\lambda = 0$ and thus $g = 0$, ω^2 are real negative values and correspond to the squares of the natural free vibration frequencies of the plate. If the aerodynamic damping is neglected, we can write Eq. (9.52) as

$$[[K_1] - \alpha[M]]\{q_0\} = \{0\} \qquad (9.53)$$

where $[K_1] = [K] + \lambda[A_2]$ and $\alpha = -\omega^2$. The matrix $[K_1]$ is real but is no more symmetrical due to the aerodynamic contribution. With the increase of the dynamic pressure parameter λ, the values of the frequencies change until a value of λ_{cr} is reached where two modes coalesce. Increasing further λ, a pair of complex conjugate frequencies is obtained, and in view of Eq. (9.51) an unstable motion is obtained. The first attempt to apply the finite element method to the supersonic flutter of panels was made by Olson.[9] The investigation was made for two-dimensional plates, i.e., infinite span, using wide beam elements. Accurate results were obtained compared to the analytical solution,[2] as shown in Table 9.2.

Later, Olson[10] extended the application to three-dimensional plates (finite plates), using the 12-degree-of-freedom and 16-degree-of-freedom plate bending rectangular elements. Again, successful results were obtained (see Table 9.3). Explicit numerical values for the aerodynamic matrices were given for the two rectangular elements; however, for the 16-degree-of-freedom element, such matrices are more concisely written using the development of Ref. 11. This formulation is summarized below. For plate problems, using a finite element solution to have convergence, we must have C^1 continuity at the element interfaces. Rectangular elements possessing such properties can be derived using first-order Hermitian polynomials with the following degrees of freedom at the element corners: w, $w_{,x}$, $w_{,y}$, and $w_{,xy}$.

Table 9.2 Values of $\lambda_{cr}^* = \lambda_{cr} a^3/D$ for two-dimensional simply supported plates

	FEM[9]				Exact
λ_{cr}	454	399	341	342	343
No. of elem.	1	2	3	4	——

Table 9.3   Values of $\lambda_{cr}^* = \lambda_{cr} a^3/D$ for simply supported flat square plates; the exact analytical solution[2] is 512.22

Mesh	Rect. 12 DOF (Ref.10)	Rect. 16 DOF (Ref.10)	Parallelo- grammic (Ref.12)	Comp. Elem. (Ref. 13)	Rect. 16 DOF (Ref.14)
2×2	506	553	——	517.2	——
3×3	430	501	——	——	——
4×4	463	509	——	509.7	508
5×5	——	——	518.22	——	——
6×6	489	511.78	——	512.2	——

Thus, for a rectangular flat plate element, we can write for the field variable $w(x, y)$ an expression in the form

$$w(x, y) = \sum_{i=1}^{2} \sum_{j=1}^{2} H_{0i}(x)H_{0j}(y)w_{ij} + H_{1i}(x)H_{0j}(y)w_{.x_{ij}} + H_{0i}(x)H_{1j}(y)w_{.y_{ij}}$$

$$+ H_{1i}(x)H_{1j}(y)w_{.xy_{ij}} \qquad (9.54)$$

where the nodal points are designated by i, j as shown in Fig. 9.4. The first-order Hermitian polynomials $H_{ij}(x)$ are given by

$$H_{01}(\xi) = (2\xi^3 - 3\xi^2 + 1)$$

$$H_{02}(\xi) = (-2\xi^3 + 3\xi^2)$$

$$H_{11}(\xi) = a(\xi^3 - 2\xi^2 + \xi) \qquad (9.55)$$

$$H_{12}(\xi) = a(\xi^3 - \xi^2)$$

where $\xi = x/a$. The first-order Hermitian polynomials $H_{ij}(y)$ are obtained by replacing ξ by η and a by b in Eq. (9.55) with $\eta = y/b$. The plate dimensions are a and b as shown in Fig. 9.4. Substituting Eq. (9.54) into Hamilton's principle,
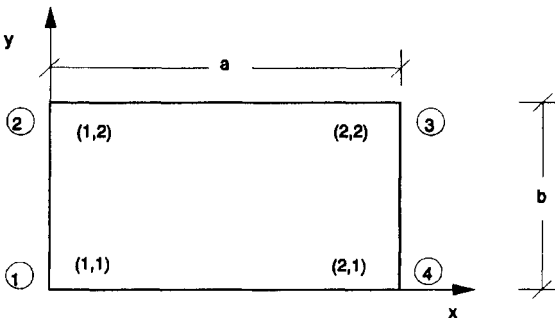
Fig. 9.4   Nodal points notation for the rectangular 16-degree-of-freedom plate bending element.

integrating, and maximizing, the elements of the stiffness matrix read

$$k_{ij} = D\left[k_{ij}^{(1)} + k_{ij}^{(2)} + \nu k_{ij}^{(3)} + 2(1-\nu)k_{ij}^{(4)}\right] \qquad (9.56)$$

where

$$k_{ij}^{(1)} = R1_a(n_i, n_j)R2_b(m_i, m_j)$$

$$k_{ij}^{(2)} = R2_a(n_i, n_j)R1_b(m_i, m_j)$$

$$k_{ij}^{(3)} = S1_a(n_i, n_j)S1_b(m_j, m_i) + S1_a(n_j, n_i)S1_b(m_i, m_j)$$

$$k_{ij}^{(4)} = R3_a(n_i, n_j)R3_b(m_i, m_j)$$

(9.57)

The $\{m\}$ and $\{n\}$ are index vectors and are given by

$$\{n\} = (1313; 1313; 2424; 2424)^{\mathrm{T}} \qquad \{m\} = (1133; 2244; 2244; 1133)^{\mathrm{T}} \qquad (9.58)$$

The matrices in Eq. (9.57) are (4×4) matrices and read

$$R1_a = \begin{bmatrix} \dfrac{12}{a^3} & -\dfrac{12}{a^3} & \dfrac{6}{a^2} & \dfrac{6}{a^2} \\ & \dfrac{12}{a^3} & -\dfrac{6}{a^2} & -\dfrac{6}{a^2} \\ & & \dfrac{4}{a} & \dfrac{2}{a} \\ \text{sym} & & & \dfrac{4}{a} \end{bmatrix}$$

$$R2_a = \begin{bmatrix} \dfrac{13a}{35} & \dfrac{9a}{70} & \dfrac{11a^2}{210} & -\dfrac{13a^2}{420} \\ & \dfrac{13a}{35} & \dfrac{13a^2}{420} & -\dfrac{11a^2}{210} \\ & & \dfrac{a^3}{105} & -\dfrac{a^3}{140} \\ \text{sym} & & & \dfrac{a^3}{105} \end{bmatrix}$$

(9.59)

$$R3_a = \begin{bmatrix} \dfrac{6}{5a} & -\dfrac{6}{5a} & \dfrac{1}{10} & \dfrac{1}{10} \\ & \dfrac{6}{5a} & -\dfrac{1}{10} & -\dfrac{1}{10} \\ & & \dfrac{2a}{15} & -\dfrac{a}{30} \\ \text{sym} & & & \dfrac{2a}{15} \end{bmatrix}$$

$$
S1_a = \begin{bmatrix}
-\dfrac{6}{5a} & \dfrac{6}{5a} & -\dfrac{1}{10} & -\dfrac{1}{10} \\[2mm]
\dfrac{6}{5a} & -\dfrac{6}{5a} & \dfrac{1}{10} & \dfrac{1}{10} \\[2mm]
-\dfrac{11}{10} & \dfrac{1}{10} & -\dfrac{2a}{15} & \dfrac{a}{30} \\[2mm]
-\dfrac{1}{10} & \dfrac{11}{10} & \dfrac{a}{30} & -\dfrac{2a}{15}
\end{bmatrix}
$$

To obtain the b matrices, a is replaced by b in the matrices given in Eq. (9.59). The elements of the mass matrix read

$$[m_{i,j}] = \rho t [R2_a(n_i, n_j)][R2_b(m_i, m_j)] \qquad i, j = 1, 2, \ldots, 16 \quad (9.60)$$

The elements of the aerodynamic matrices are given by

$$
\begin{aligned}
a_{1_{i,j}} &= R2_a(n_i, n_j) R2_b(m_i, m_j) \\
a_{2_{i,j}} &= S2_a(n_i, n_j) R2_b(m_i, m_j)
\end{aligned}
\quad (9.61)
$$

where $[S2]$ is given by

$$
[S2_a] = \begin{bmatrix}
-1/2 & -1/2 & -a/10 & a/10 \\
1/2 & 1/2 & a/10 & -a/10 \\
a/10 & -a/10 & 0 & a^2/60 \\
-a/10 & a/10 & -a^2/60 & 0
\end{bmatrix}
\quad (9.62)
$$

The standard assembly technique of the finite element method is then applied to obtain the system matrix equations. The stability problem is solved in the same way as previously mentioned. Several investigators analyzed the problem using various finite element formulations. Kari-Appa and Somashekar[15] used a 12-degree-of-freedom rectangular element and then extended their work to the case of skew panels[16] and included the effect of prestress and flow yawing[12] using parallelogrammic elements. Sander et al.[13] used a purely conforming compound quadrilateral element and considered the effect of initial prestress and the flow yawing in their analysis. Rosettos and Tong[17] used a hybrid rectangular element in the formulation of the problem; however, the flutter solution was made using the modal superposition technique. Ref. 14 treats the case of coupled plates using the finite element method. Some of the results obtained are reported in Table 9.3, for the case of simply supported square plates, using different finite element formulation in the analysis. The review paper of Ref. 8 contains more details on the application of the finite element method to the supersonic flutter of flat plates.

9.3 Effect of Prestress

We now proceed to study the effect of the initial prestress on the stability boundaries. The effect of in-plane stresses is particularly significant for the panels studied because they are in-plane, stress-resistant elements of aircraft or missiles. It will be assumed that the panel has reached a state of equilibrium due to the presence of

the initial stresses, and the stability of the system will be examined at this position. It is also assumed that the plate has not reached a buckled state. For the case at hand, the equation of motion [Eq. (9.8)] reads

$$D\left[\frac{\partial^4 w}{\partial x^4} + 2\frac{\partial^4 w}{\partial x^2 \partial y^2} + \frac{\partial^4 w}{\partial y^4}\right] + \rho_m h \frac{\partial^2 w}{\partial t^2} + \frac{2Q}{[M^2-1]^{\frac{1}{2}}}\frac{\partial w}{\partial x} - N_x \frac{\partial^2 w}{\partial x^2}$$

$$- N_y \frac{\partial^2 w}{\partial y^2} - 2N_{xy}\frac{\partial^2 w}{\partial x \partial y} = 0 \tag{9.63}$$

and the boundary conditions are the same as given in Eq. (9.9). In the absence of initial in-plane shearing loads and for simply supported end conditions, a closed-form solution of the equation of motion [Eq. (9.63)] can be obtained by writing a solution in the form

$$w(x, y, t) = W(x)\sin[n\pi y/b]e^{\omega t} \tag{9.64}$$

Substituting Eq. (9.64) into Eq. (9.63), we obtain

$$D\left[\frac{d^4 W}{dx^4} - 2\left(\frac{n\pi}{b}\right)^2 \frac{d^2 W}{dx^2} + \left(\frac{n\pi}{b}\right)^4 W\right] + \rho_m h \omega^2 W + \frac{2Q}{[M^2-1]^{\frac{1}{2}}}\frac{dW}{dx}$$

$$- N_x \frac{d^2 W}{dx^2} - N_y \left(\frac{n\pi}{b}\right)^2 W = 0 \tag{9.65}$$

and the boundary conditions read

$$W(0) = W(a) = W(0) = W(a) = 0 \tag{9.66}$$

Equation (9.65) and the boundary conditions in Eq. (9.66) can be put in a nondimensionalized form through the introduction of the variable $\xi = x/a$ and we obtain

$$\frac{d^4 W}{d\xi^4} + A\frac{d^2 W}{d\xi^2} + \lambda \frac{dW}{d\xi} + BW = 0 \tag{9.67}$$

and

$$W(0) = W(1) = W(0) = W(1) = 0 \tag{9.68}$$

where

$$A = -2n^2\pi^2[a/b]^2 - N_x a^2/D$$

$$B = k^2 + n^4\pi^4[a/b]^4 + n^2\pi^2[a/b]^2 N_y a^2/D$$

$$\lambda = 2Qa^3/D[M^2-1]^{\frac{1}{2}} \tag{9.69}$$

$$k^2 = [\rho_m h a^4/D]\omega^2$$

Comparing Eq. (9.67) with Eq. (9.14), we can make the following conclusions.
1) The solution of the problem will be obtained in exactly the same manner as previously given for the case of no initial prestress.

244   STRUCTURAL DYNAMICS IN AERONAUTICAL ENGINEERING

2) The cross stream, in-plane initial prestress N_y has no effect on the flutter boundary; in linear unbuckled flat plates, its only effect is a frequency shift, as can be observed from the parameter B in Eq. (9.69).

3) The same graph for λ_{cr} against A is obtained as given in Fig. 9.3; however, $\underline{A}$ is taken now as $\underline{A} = -2n^2(a/b)^2 - N_x a^2/D\pi^2$ and the stabilizing effect of N_x in tension and its destabilizing effect in compression is thus evident.

Other conclusions of the effect of the initial prestress on the flutter boundary will be discussed in the sequel, and we proceed now to obtain numerical solutions for the general case since the closed-form exact solution exists only for the simply supported case and in the absence of in-plane shear as stated before.

Again, in the Rayleigh–Ritz method, we write approximate solutions in the form

$$W(x, y, t) = \phi_m(x, y)q_m(t) \qquad m = 1, 2, 3, \ldots \qquad (9.70)$$

where $\phi_m(x, y)$ are arbitrary functions that satisfy the geometric boundary conditions of the field variable w and $q_m(t)$ are the generalized coordinates. Substituting the approximate solutions to Eq. (9.70) into Hamilton's principle and minimizing with respect to the generalized coordinates $q_m(t)$, we obtain the following matrix equation

$$[M]\{q''\} + [K + N_x K_{Nx} + N_y K_{Ny} + N_{xy} K_{Nxy}]\{q\} + \lambda[A]\{q\} = \{0\} \quad (9.71)$$

where $[M], [K], [A]$, and λ are as given in Eq. (9.25), and the elements of the initial stress matrices are given by

$$K_{Nx_{mn}} = \int_A \frac{\partial \phi_m}{\partial x} \frac{\partial \phi_n}{\partial x} \, dx dy$$

$$K_{Ny_{mn}} = \int_A \frac{\partial \phi_m}{\partial y} \frac{\partial \phi_n}{\partial y} \, dx dy \qquad (9.72)$$

$$K_{Nxy_{mn}} = \int_A \frac{\partial \phi_m}{\partial x} \frac{\partial \phi_n}{\partial y} + \frac{\partial \phi_m}{\partial y} \frac{\partial \phi_n}{\partial x} \, dx dy$$

As an application, we consider the case of a four-edges-rectangular simply supported plate, and we assume solutions in the form

$$\phi_{mn} = \sin \frac{m\pi x}{a} \sin \frac{n\pi y}{b} \qquad m, n = 1, 2, 3, \ldots \qquad (9.73)$$

which satisfy the geometric boundary conditions. Using these trial functions in Eqs. (9.71) and assuming exponential dependence of time of the field variable, we obtain

$$\left[[K + N_x K_{Nx} + N_y K_{Ny} + N_{xy} K_{Nxy}]_{pq,rs} + \lambda[A_{pq,rs}] \right.$$
$$\left. + \omega^2[M_{pq,rs}] \right] \{q_{0rs}\} = \{0\} \qquad p, q, r, s = 1, 2, 3, \ldots \qquad (9.74)$$

where $M_{pq,rs}$, $K_{pq,rs}$, and $A_{pq,rs}$ are given in Eq. (9.30), and the elements of the initial stress matrices read

$$K_{Nx_{pq,rs}} = \frac{ab}{4}\left[\frac{p\pi}{a}\right]^2 \qquad p = r \quad q = s$$

$$= 0 \qquad \text{otherwise}$$

$$K_{Ny_{pq,rs}} = \frac{ab}{4}\left[\frac{q\pi}{b}\right]^2 \qquad p = r \quad q = s$$

$$\tag{9.75}$$

$$= 0 \qquad \text{otherwise}$$

$$K_{Nxy_{pq,rs}} = \frac{8pqrs}{[p^2 - r^2][q^2 - s^2]} \qquad p + r \quad q + s \quad \text{odd}$$

$$= 0 \qquad \text{otherwise}$$

Thus, we can write Eq. (9.74) as

$$\left[k^2\lceil I\rfloor + \lceil[p^2 + q^2(a/b)^2]^2 + R_x p^2 + R_y q^2(a/b)^2]^2\rfloor + [\beta]\right.$$

$$\left. + \frac{4\lambda^*}{\pi^4}[\alpha] + \omega^2[M_{pq,rs}]\right]\{q_{0rs}\} = \{0\} \qquad p, q, r, s = 1, 2, 3, \ldots \tag{9.76}$$

where

$$\beta_{pq,rs} = \frac{32R_{xy}}{\pi^4}(a/b)\frac{pqrs}{[p^2 - r^2][q^2 - s^2]} \qquad q + s \quad p + r \quad \text{odd}$$

$$= 0 \qquad \text{otherwise} \tag{9.77}$$

$$R_x = \frac{N_x a^2}{D\pi^2} \qquad R_y = \frac{N_y a^2}{D\pi^2} \qquad R_{xy} = \frac{N_{xy} a^2}{D\pi^2}$$

We notice that $\lceil\beta\rfloor$ is not a diagonal matrix, stemming from the fact that the trial functions used are not the free vibration mode shapes in the presence of initial in-plane shear loads. Furthermore, if the trial solutions are taken with a single half-wave in the cross stream direction, i.e., $q = s = 1$, the elements of $\lceil\beta\rfloor$ are zero. Hence, the effect of in-plane prestress shear is transparent in such solutions. Inclusion of higher spanwise modes will induce nonzero elements in the $\lceil\beta\rfloor$ matrix. Leaving for the moment the effect of N_{xy} and considering as an

application a two-mode approximation with $n = 1$ and $m = 1, 2$, we obtain

$$
\begin{bmatrix}
k^2 + [1 + (a/b)^2]^2 + R_x + R_y(a/b)^2 & -\dfrac{8\lambda^*}{3\pi^4} \\[3mm]
\dfrac{8\lambda^*}{3\pi^4} & k^2 + [4 + (a/b)^2]^2 + 4R_x + R_y(a/b)^2
\end{bmatrix}
$$

$$
\times \begin{Bmatrix} q_{11} \\ q_{12} \end{Bmatrix} = \begin{Bmatrix} 0 \\ 0 \end{Bmatrix} \tag{9.78}
$$

Expanding the determinant, we obtain

$$
k^4 + (\alpha + \beta)k^2 + \alpha\beta + \frac{64}{9\pi^8}\lambda^{*2} = 0 \tag{9.79}
$$

where

$$
\alpha = [1 + (a/b)^2]^2 + R_x + R_y(a/b)^2]^2
$$
$$
\beta = [4 + (a/b)^2]^2 + 4R_x + R_y(a/b)^2]^2 \tag{9.80}
$$

Solving Eq. (9.79), we get

$$
k^2 = -\frac{[\alpha + \beta]}{2} \pm \sqrt{\left[\frac{[\alpha - \beta]}{2}\right]^2 - \frac{64\lambda^{*2}}{9\pi^8}} \tag{9.81}
$$

Examining Eq. (9.81), we observe that, when $[\alpha - \beta]^2/4 > 64\lambda^{*2}/9\pi^8$, the motion is stable because the roots are negative real values; when $[\alpha - \beta]^2/4 < 64\lambda^{*2}/9\pi^8$, the motion is unstable because one of the roots will have a positive real exponential. On the borderline of stability, we have

$$
\lambda^*_{\mathrm{crit}} = \frac{9\pi^4}{16}\left[5 + 2\left[\frac{a}{b}\right]^2 + R_x\right] \tag{9.82}
$$

again showing that the critical value of λ^* does not depend on R_y and this has only a shift effect on the frequencies as can be concluded from Eq. (9.81). Furthermore, the stabilizing effect of the initial prestress tension and the destabilizing effect of the initial prestress compression are readily observed from Eq. (9.82).

In Ref. 18 the Galerkin method, which as stated before leads to the same numerical results for the case at hand when using the same interpolation functions in either formulation, has been used for plates with combined effect of in-plane shear and axial prestress loads. The analysis of in-plane shear alone showed that convergence in the solution was attained when a 16-term trigonometric trial function approximation, with $p, q, r, s = 1, 2, 3,$ and 4, was used for the solution. Furthermore, it was observed that the initial in-plane shear had a destabilizing effect on the critical flutter value λ^*. Now, writing Eq. (9.71) as

$$
[[\underline{K}] + \omega^2[M]]\{q_0\} = \{0\} \tag{9.83}
$$

where $[\underline{K}] = [K] + [K_G] + \lambda[A]$, it can be observed that the airstream has a stabilizing effect on the static stability. For $\lambda = 0$, at the prestress buckling load, $[\underline{K}]$ is singular. For a postbuckling load and $\lambda \neq 0$, the system still has positive
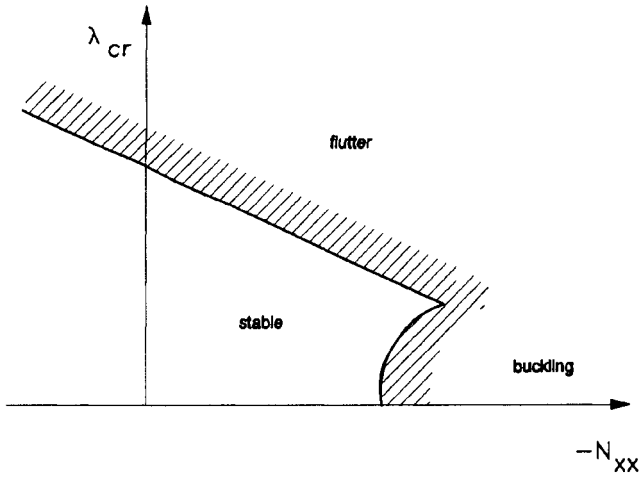
Fig. 9.5 Stability boundaries with the effect of prestress.

values of ω^2. With the increase of λ, we will reach a point on the borderline of static stability where again $[\underline{K}]$ is singular, thus giving an in-plane buckling load higher than the in vacuo value. For further increase of λ, the system will be statically and dynamically stable until reaching a higher value of λ at which an eigenvalue coalescence takes place, thus defining λ_{cr} for the dynamic stability. This is schematically shown in Fig. 9.5.

9.4 Curved Panels

Flutter characteristic determination of curved plates is of prime importance in supersonic aircraft and launch vehicle designs. The first analytical research on supersonic flutter of thin cylindrically curved panels was made by Voss,[19] using Reissner's shallow shell equations,[20] quasistatic aerodynamic theory, and the Galerkin method for the solution of the freely supported ends boundary conditions. Nonlinear panel flutter analysis of cylindrically curved panels was investigated by Dowell[21,22] using the quasistatic aerodynamic theory and the Galerkin method for the solution of the aeroelastic equations. Dowell's investigations showed that the in-plane edge restraints had a great influence on the flutter boundaries of the cylindrically curved panels, and the reason was attributed to the frequency spectrum of the shells analyzed. In Refs. 23 and 24, a finite element formulation based on Reissner's two field variable variational principle for the solution of the supersonic flutter of cylindrically curved panels was presented. In the following, the analysis presented in Refs. 23 and 24 is summarized, and the main conclusions obtained in these references are reported. Consider the cylindrically curved shallow shell shown in Fig. 9.6. The variational equation for the problem at hand, neglecting in-plane inertias and considering the work done by the external nonstationary aerodynamic load and the effect of the initial membrane prestresses shown in
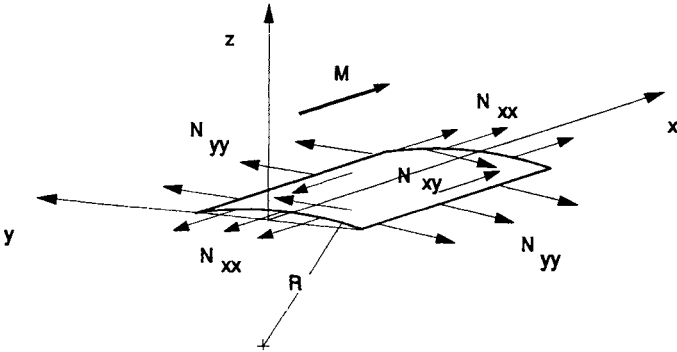
Fig. 9.6   Cylindrically curved thin shell panel subjected to an initial state of prestress membrane loads in the presence of a supersonic external flow.

Fig. 9.6, can be expressed as[24]

$$
\delta\pi^* = \delta \int_{t_1}^{t_2} \left[\left\{ \frac{1}{2} \int_A \rho h w_{,t}^2 \, dA - \frac{D}{2} \int_A \left[w_{,xx}^2 + w_{,yy}^2 + 2\nu w_{,xx} w_{,yy} \right. \right. \right.
$$

$$
+ 2(1 - \nu) w_{,xy}^2 \right] dA + \frac{1}{2Eh} \int_A \left[F_{,xx}^2 + F_{,yy}^2 - 2\nu F_{,xx} F_{,yy} \right.
$$

$$
+ 2(1 + \nu) F_{,xy}^2 \right] dA - \int_A \frac{w}{R} F_{,xx} \, dA - \frac{1}{2} \int_A \left[N_{xx} w_{,x}^2 + N_{yy} w_{,y}^2 \right.
$$

$$
\left. + 2N_{xy} w_{,x} w_{,y} \right] dA - \int_A w \Delta p \, dA \right\} \right] dt = 0 \tag{9.84}
$$

The functions subjected to variation in Eq. (9.84) are the transverse displacement w and the Airy stress function F. In Eq. (9.84), $D = Eh^3/12(1 - \nu^2)$ is the shell flexural rigidity; ν is Poisson's ratio; E is Young's modulus; R is the shell radius; h is the shell thickness; ρ is the material mass density per unit area; and N_{xx}, N_{yy}, and N_{xy} are the initial membrane stresses. In Eq. (9.84), Δp is the nonstationary aerodynamic pressure difference. Now, using the quasistatic aerodynamic theory, the relationship between Δp and w can be written as

$$
\Delta p = -\frac{2Q}{\sqrt{M^2 - 1}} \left[\cos \Lambda \frac{\partial w}{\partial x} + \sin \Lambda \frac{\partial w}{\partial y} \right] \tag{9.85}
$$

where $Q = \rho V^2/2$ is the dynamic pressure, M is the free stream Mach number, V is the free stream velocity of the external flow, and Λ is the angle between the free stream direction and the x direction. Performing the variational operation, grouping terms, and applying Green's theorem and the minimization operation,

we obtain the Euler–Lagrange equations governing the problem as[24]

$$D\nabla^4 w + \frac{1}{R} F_{,xx} - \frac{2Q}{\sqrt{M^2 - 1}}[\cos \Lambda w_{,x} + \sin \Lambda w_{,y}] - N_{xx} w_{,xx}$$

$$- N_{yy} w_{,yy} - 2N_{xy} w_{,xy} = 0 \tag{9.86}$$

$$\nabla^4 F - \frac{Eh}{R} w_{,xx} = 0$$

and the boundary conditions are as given in Ref. 24 and, on an edge, $\nu = $ const is given by
  1) Clamped edges: $w = w_{,\nu} = 0$ and at a corner $F_{,\mu\nu} = 0$.
  2) Free edges: $F = F_{,\nu} = 0$ and at a corner $M_{,\mu\nu} = 0$ (i.e., $w_{,\mu\nu} = 0$).
  3) Simply supported edges: $w = 0$ and at a corner $F_{,\mu\nu} = 0$.
  4) Freely supported edges: $w = F = 0$.
  A finite element method for the solution of the problem at hand can be performed using rectangular elements that preserve C^1 continuity by writing for the functions w and F interpolation functions in terms of the nodal parameter as

$$z(x, y) = \sum_{i=1}^{2} \sum_{j=1}^{2} \left[H_{0i}(x)H_{0j}(y)z_{ij} + H_{1i}(x)H_{0j}(y)z_{,x_{ij}} \right.$$

$$\left. + H_{0i}(x)H_{1j}(y)z_{,y_{ij}} + H_{1i}(x)H_{1j}(y)z_{,xy_{ij}} \right] \tag{9.87}$$

where z stands for w or F and H_{mn} are first-order Hermitian polynomials previously discussed in the derivation of the 16-degree-of-freedom plate bending element. Using the standard finite element technique, we obtain for each element a set of two equations cast in the form

$$[k_{ww}]\{w\} + [k_{wF}]\{F\} + \left[N_{xx}\left[k_{G_{Nxx}}\right] + N_{yy}\left[k_{G_{Nyy}}\right] + N_{xy}\left[k_{G_{Nxy}}\right] \right]\{w\}$$

$$+ \lambda[a]\{w\} + [m]\{w''\} = 0 \tag{9.88}$$

$$[k_{Fw}]\{w\} + [k_{FF}]\{F\} = 0$$

The element matrices have all been considered before. Using now the standard finite element assembly technique and applying the boundary conditions, we obtain for the whole structure the following two matrix equations

$$[M]\{w''\} + \lambda[A] + [K_{ww}]\{w\} + [K_{wF}]\{F\} + \left[N_{xx}\left[K_{G_{Nxx}}\right] \right.$$

$$\left. + N_{yy}\left[K_{G_{Nyy}}\right] + N_{xy}\left[K_{G_{Nxy}}\right] \right]\{w\} = 0 \tag{9.89}$$

$$[K_{Fw}]\{w\} + [K_{FF}]\{F\} = 0$$

We observe that the degree of freedom $\{F\}$ can be eliminated using the compatibility equation of the system of equations, i.e., the second equation of the system
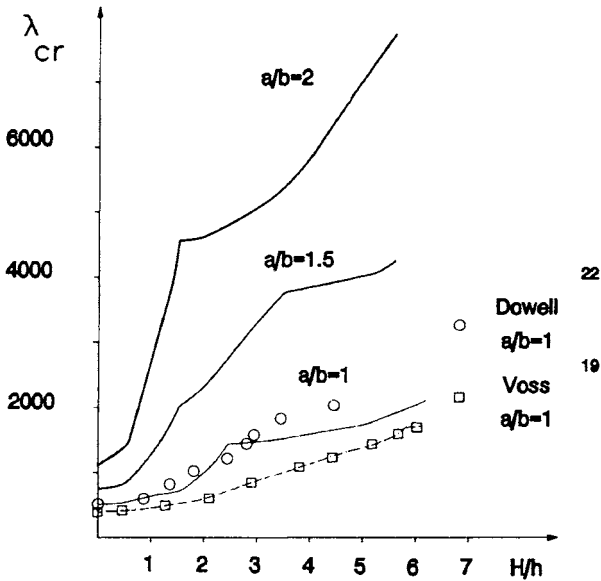
Fig. 9.7   Flutter dynamic pressure parameter vs shell rise for flow in the x direction and all edges freely supported.

[Eq. (9.89)], to obtain

$$[K_{eq}]\{w\} + [M]\{w''\} + \lambda[A]\{w\} + \left[N_{xx}\left[K_{G_{Nxx}}\right] + N_{yy}\left[K_{G_{Nyy}}\right]\right.$$

$$\left. + N_{xy}\left[K_{G_{Nxy}}\right]\right]\{w\} = 0 \tag{9.90}$$

where

$$[K_{eq}] = [K_{ww}] - [K_{wF}][K_{FF}]^{-1}[K_{Fw}] \tag{9.91}$$

An examination of Eq. (9.90) reveals that the computational effort required for the solution of the aeroelastic stability problem when the present formulation is used is equivalent to that of a flat plate. Furthermore, the in-plane boundary conditions are applied on F, $F_{,x}$, $F_{,y}$, and $F_{,xy}$ and are all nodal degrees of freedom of the finite element model. Figures 9.7–9.9 present some of the results obtained using the present formulation. Figure 9.7 presents the critical flutter parameter λ_{cr} vs the shell rise H/h, where H is the maximum shell height and h is the shell thickness for different values of the panel aspect ratio a/b for rectangular freely supported panels on all edges. The results are compared with the two-mode Galerkin solution of Voss[19] and Dowell's solution.[22]

Dowell's solution is a six-chordwise-mode Galerkin approximation with a half-sine wave in the cross stream direction. Dowell's solution practically coincides
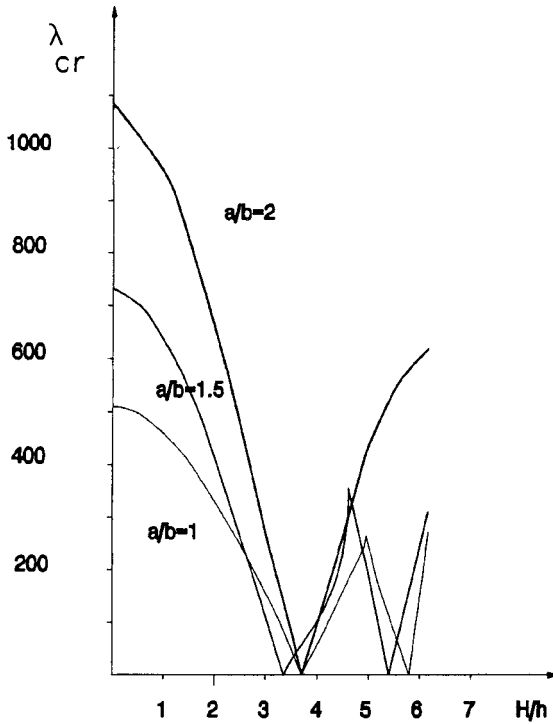
Fig. 9.8   Flutter dynamic pressure parameter vs shell rise for flow in the y direction and all edges freely supported.

with the present finite element formulation for the part of the curve where $n = 1$ are the critical modes for instability. Voss's two-mode solution, despite being conservative, shows the same trend as the finite element solution.

Figure 9.8 presents the results of freely supported panels with flow in the y direction and for different aspect ratios of the panels. Figure 9.9 presents the results for four-edge clamped panels with flow in the x direction.

Observing the results of Figs. 9.7–9.9, the following conclusions can be made:

1) When the curvature parameter is very small and therefore the panel approaches the flat plate behavior and for flows in the x direction, the critical modes for flutter are for $n = 1$ and are the first spanwise modes. In this region, the curvature effect is stabilizing in the sense that the critical dynamic pressure increases with the increase of the curvature. With further increase in the curvature, the panel passes through a transition region characterized from a flat plate behavior to a deep shell behavior. This region is characterized by the dips, knees, and cups observed in the dynamic pressure parameter vs curvature effect and is explained by the coalescence of successive higher modes to produce the first critical flutter condition. After this transition region, with further increase in the curvature, the panel behaves as a deep shell, and the critical flutter modes are those with an elevated number of waves in
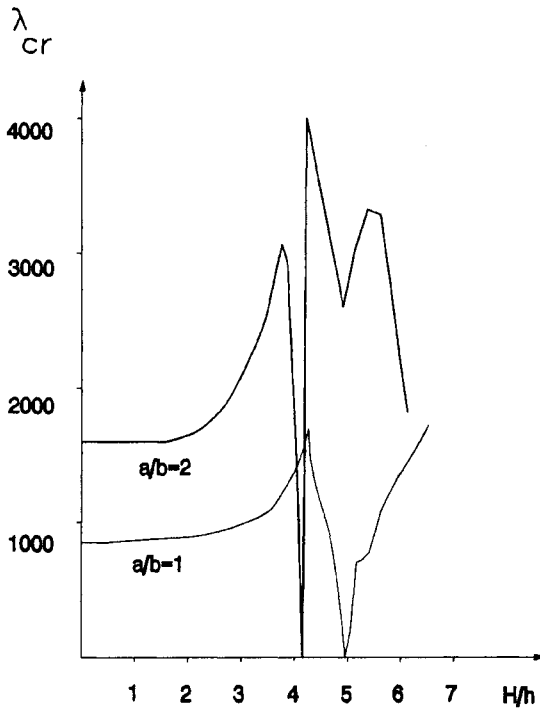
Fig. 9.9   Flutter dynamic pressure parameter vs shell rise for flow in the x direction and all edges clamped.

the cross stream direction and the first streamwise modes. In this part, the shallow shell theory is no longer adequate and deep shell theory should be used in the analysis. The present shallow shell theory is therefore limited to the flat plate and the transition part behavior of the curved panels.

2) For flow parallel to the y direction, the curvature effect is destabilizing, a decrease of the flutter dynamic pressure with the increase of the curvature. Again, this is explained by the frequency spectrum of the panel. In the transition region, the panel is characterized by the same behavior demonstrated in the x direction flow case, and coalescence of successive values of n_{cr} occurs.

3) For the clarity of the exposition, no damping effect, whether of structural or aerodynamic nature, has been incorporated to the analysis. If a constant viscous-type structural damping and/or aerodynamic damping term of the potential flow theory is used in the analysis, it can be shown that the effect is always stabilizing,[8] an increase of the critical dynamic pressure. The effect of such damping is small in the flat plate and deep shell regions. In the transition region, such damping has a greater influence on the panel stability and removes the sharp minimums or dips observed in the critical dynamic pressure parameter, which are due to coalescence of modes with nearly identical frequencies and small aerodynamic coupling.

9.5   Laminated Fiber-Reinforced Shallow Shells

Laminated fiber-reinforced composite materials are being utilized increasingly in the design of exposed skin construction of supersonic and reentry vehicles. In general, such panels have greater strength-to-weight ratio than the conventional isotropic panels and thus provide considerable weight savings. However, their use in the design of aerospace vehicles introduces several complication factors that are not present in the conventional isotropic panels. Such complications are mainly due to the fiber orientation, which introduces a twisting–bending coupling, and due to the number of layers and their stacking sequence, which introduces a material stretching–bending coupling. A further complication is introduced by the geometric stretching–bending coupling due to the shell curvature. All these factors interact in a complicated manner on the free vibration frequency spectrum of the shells and therefore affect their borderline of dynamic stability. An efficient use of these modern material constructions needs therefore a good understanding of their structural dynamic stability behavior under various loadings and boundary conditions.

Since the earlier works on panel flutter, the complications introduced to the design due to the use of composite materials were addressed by several investigators.[25–28] These pioneering works mainly concentrated on flat orthotropic panels and used the Rayleigh–Ritz and the Galerkin methods for the problem solution. With the advent of high-speed computation devices and the efficient use of the finite element method in structural dynamic stability problems, much research on the aeroelasticity of fiber-reinforced composite material panels, using the finite element method, was published.[29–33] In all these references, the total potential energy functional was used for the finite element formulation of the problem. Alternatively, the problem can be formulated using a two-field variable modified functional with the transverse displacement w and Airy stress function F as the field variables of the problem. Such formulation was proposed in Ref. 34, where a C^1 continuity rectangular finite element was used for the problem solution. In the following, the problem of fiber-reinforced doubly curved shallow shells subjected to external nonconservative aerodynamic loads will be analyzed in detail starting from the functional formulation. It is shown that the functional presented has no explicit material bending–extension coupling terms.

These effects appear only in the equivalent material bending stiffness constitutive constants. The solution of the problem is then made using a C^1 continuity finite element method. It is shown that the computational effort, when the present formulation is used, is equivalent to the effort required for an isotropic flat plate solution. Numerical results are given, and the results obtained are discussed and are compared with previous solutions, whenever available. The effect of material extension–bending coupling, i.e., the number of layers and their stacking sequence; the effect of the twisting–bending coupling, i.e., the fiber orientation; and the effect of geometric extension–bending coupling, i.e., the shell curvature, on the borderline of the aeroelastic stability is examined in a detailed and conclusive manner. For the clarity of the exposition, no damping effect, whether of structural or aerodynamic nature, has been incorporated to the analysis. The damping effect on the panel aeroelastic stability[8] is the same whether the shell is isotropic or of fiber-reinforced composite material.

9.5.1 Problem Formulation

In this section, the classical laminated fiber-reinforced theory[35-37] is used to obtain material global constitutive relations. Some of these relationships, available in the literature, are repeated in this section for completeness of the presentation and for giving a formulation that completely avoids the factors 2 or 1/2 that are commonly used in this classical laminated fiber-reinforced theory[36,37] and present an apparent asymmetry in material constitutive relations. The stress–strain relations for a thin orthotropic lamina, lying in the x–y plane with major principal material coordinates in the 1–1 direction, can be written as[37]

$$
\begin{Bmatrix} \sigma_1 \\ \sigma_2 \\ \tau_{12} \end{Bmatrix} = [Q] \begin{Bmatrix} \varepsilon_1 \\ \varepsilon_2 \\ \gamma_{12} \end{Bmatrix} = \begin{bmatrix} \dfrac{E_{11}}{1 - \nu_{12}\nu_{21}} & \dfrac{\nu_{21}E_{11}}{1 - \nu_{12}\nu_{21}} & 0 \\ \dfrac{\nu_{12}E_{22}}{1 - \nu_{12}\nu_{21}} & \dfrac{E_{22}}{1 - \nu_{12}\nu_{21}} & 0 \\ 0 & 0 & G_{12} \end{bmatrix} \begin{Bmatrix} \varepsilon_1 \\ \varepsilon_2 \\ \gamma_{12} \end{Bmatrix} \quad (9.92)
$$

where, in Eq. (9.92), the engineering contracted notation commonly used in the laminated fiber-reinforced composite material literature[36,37] has been used. According to this notation, the engineering strain γ_{12} is twice the shear strain component ε_{12} of the strain tensor, i.e., $\gamma_{12} = 2\varepsilon_{12}$. The stress and strain components can be written in terms of the reference coordinate system x–y using the law of tensor coordinate transformation and read

$$
\begin{Bmatrix} \sigma_x \\ \sigma_y \\ \tau_{xy} \end{Bmatrix} = [T] \begin{Bmatrix} \sigma_1 \\ \sigma_2 \\ \tau_{12} \end{Bmatrix}
$$

$$
= \begin{bmatrix} \cos^2\theta & \sin^2\theta & -2\sin\theta\cos\theta \\ \sin^2\theta & \cos^2\theta & 2\sin\theta\cos\theta \\ \sin\theta\cos\theta & -\sin\theta\cos\theta & \cos^2\theta - \sin^2\theta \end{bmatrix} \begin{Bmatrix} \sigma_1 \\ \sigma_2 \\ \tau_{12} \end{Bmatrix} \quad (9.93)
$$

and

$$
\begin{Bmatrix} \varepsilon_x \\ \varepsilon_y \\ \dfrac{\gamma_{xy}}{2} \end{Bmatrix} = \begin{Bmatrix} \varepsilon_{xx} \\ \varepsilon_{yy} \\ \varepsilon_{xy} \end{Bmatrix} = [T] \begin{Bmatrix} \varepsilon_{11} \\ \varepsilon_{22} \\ \varepsilon_{12} \end{Bmatrix} = [T] \begin{Bmatrix} \varepsilon_1 \\ \varepsilon_2 \\ \dfrac{\gamma_{12}}{2} \end{Bmatrix} \quad (9.94)
$$

where $[T]$ is the tensorial transformation matrix for tensors of the second kind and θ is the angle of the fiber orientation of the lamina measured from the x direction to the major material principal direction. Using Eqs. (9.92–9.94) we can write the stress–strain relations in the material reference coordinates x–y as

$$
\begin{Bmatrix} \sigma_x \\ \sigma_y \\ \tau_{xy} \end{Bmatrix} = [Q^*] \begin{Bmatrix} \varepsilon_x \\ \varepsilon_y \\ \gamma_{xy} \end{Bmatrix} \quad (9.95)
$$

where Q^* is the constitutive material matrix of the lamina and is a symmetric matrix with elements given by

$$Q_{11}^* = l^4 Q_{11} + 2l^2 m^2 (Q_{12} + 2Q_{33}) + m^4 Q_{22}$$

$$Q_{22}^* = m^4 Q_{11} + 2l^2 m^2 (Q_{12} + 2Q_{33}) + l^4 Q_{22}$$

$$Q_{12}^* = l^2 m^2 (Q_{11} + Q_{12} - 4Q_{33}) + (l^4 + m^4) Q_{12}$$

$$Q_{13}^* = l^3 m (Q_{11} - Q_{12} - 2Q_{33}) + lm^3 (Q_{12} - Q_{22} + 2Q_{33})$$

$$Q_{23}^* = lm^3 (Q_{11} - Q_{12} - 2Q_{33}) + l^3 m (Q_{12} - Q_{22} + 2Q_{33})$$

$$Q_{33}^* = l^2 m^2 (Q_{11} + Q_{22} - 2Q_{12} - 2Q_{33}) + (l^4 + m^4) Q_{33}$$

(9.96)

where Q_{ij} are obtained from Eq. 9.92, $l = \cos\theta$ and $m = \sin\theta$. Consider now a laminated fiber-reinforced composite material composed of n laminas, under the assumption of Kirchhoff–Love hypothesis for thin plates and shells. We can write the strains in the laminate in terms of the middle surface strains and curvatures as

$$\begin{Bmatrix} \varepsilon_x \\ \varepsilon_y \\ \gamma_{xy} \end{Bmatrix} = \begin{Bmatrix} \varepsilon_x^0 \\ \varepsilon_y^0 \\ \gamma_{xy}^0 \end{Bmatrix} + z \begin{Bmatrix} \kappa_x \\ \kappa_y \\ \kappa_{xy} \end{Bmatrix}$$

(9.97)

where z is measured from the middle surface of the laminate. Defining the internal stress and moment resultants as

$$\begin{Bmatrix} N_x \\ N_y \\ N_{xy} \end{Bmatrix} = \int_{-h/2}^{h/2} \begin{Bmatrix} \sigma_x \\ \sigma_y \\ \tau_{xy} \end{Bmatrix} dz \qquad \begin{Bmatrix} M_x \\ M_y \\ M_{xy} \end{Bmatrix} = \int_{-h/2}^{h/2} \begin{Bmatrix} \sigma_x \\ \sigma_y \\ \tau_{xy} \end{Bmatrix} z\, dz$$

(9.98)

and using Eqs. (9.95–9.98), we can write an expression for the stress and moment resultants in terms of the middle surface strains and curvature as

$$\begin{Bmatrix} \{N\} \\ \{M\} \end{Bmatrix} = \begin{bmatrix} [A] & [B] \\ [B] & [D] \end{bmatrix} \begin{Bmatrix} \{\varepsilon^0\} \\ \{\kappa\} \end{Bmatrix}$$

(9.99)

The global constitutive relationships $[A]$, $[B]$, and $[D]$ of the laminated fiber-reinforced composite material are obtained from the laminas's properties as[36,37]

$$A_{ij} = \sum_{k=1}^{n} Q_{ij_k}^* (h_k - h_{k-1})$$

$$B_{ij} = \frac{1}{2} \sum_{k=1}^{n} Q_{ij_k}^* \left(h_k^2 - h_{k-1}^2\right)$$

(9.100)

$$D_{ij} = \frac{1}{3} \sum_{k=1}^{n} Q_{ij_k}^* \left(h_k^3 - h_{k-1}^3\right)$$

where h is the vectorial distance from the middle surface of the laminated composite material to the upper surface of the lamina k and n is the total number of the laminas. Inverting the first relation of Eq. (9.99), we obtain

$$\left\{ \begin{array}{c} \{\varepsilon^0\} \\ \{M\} \end{array} \right\} = \left[\begin{array}{cc} [A^*] & [-A^{-1}B] \\ [BA^{-1}] & [D^*] \end{array} \right] \left\{ \begin{array}{c} \{N\} \\ \{\kappa\} \end{array} \right\} \tag{9.101}$$

where $[A^*] = [A]^{-1}$ and $[D^*] = [D] - [B][A]^{-1}[B]$. Defining an Airy stress function F as

$$N_{xx} = \frac{\partial^2 F}{\partial y^2} \qquad N_{yy} = \frac{\partial^2 F}{\partial x^2} \qquad N_{xy} = -\frac{\partial^2 F}{\partial x \partial y} \tag{9.102}$$

and neglecting the in-plane inertia terms, we can write the variational equation of doubly curved shallow shells of laminated fiber-reinforced composite material, considering the effect of the work done by external incremental nonstationary airloads applied to the upper surface as

$$\delta(\Pi^*) = \delta \int_{t_1}^{t_2} \left[\frac{1}{2} \int_A \rho h w_{,t}^2 \, dA - \int_A w \left\{ \frac{F_{,xx}}{R_x} + \frac{F_{,yy}}{R_y} \right\} dA \right.$$

$$- \frac{1}{2} \int_A \left[D_{11}^* w_{,xx}^2 + D_{22}^* w_{,yy}^2 + 2D_{12}^* w_{,xx} w_{,yy} + 4D_{33}^* w_{,xy}^2 \right.$$

$$+ 4D_{13}^* w_{,xx} w_{,xy} + 4D_{23}^* w_{,yy} w_{,xy} \right] dA + \frac{1}{2} \int_A \left[A_{22}^* F_{,xx}^2 + A_{11}^* F_{,yy}^2 \right.$$

$$+ 2A_{12}^* F_{,xx} F_{,yy} + 4A_{33}^* F_{,xy}^2 - 2A_{23}^* F_{,xx} F_{,xy} - 2A_{13}^* F_{,yy} F_{,xy} \right] dA$$

$$\left. + \int_A w \Delta p \, dA \right] dt = 0 \tag{9.103}$$

where the functions subjected to variation are the transverse displacement w and the Airy stress function F. Notice the simplicity of the present formulation where we do not have explicit material bending–in-plane coupling terms; their effect appears only in the equivalent constitutive elements D_{ij}^*. Using Eq. (9.103), the Euler–Lagrange equations governing the problem are obtained and read

$$D_{11}^* w_{,xxxx} + D_{22}^* w_{,yyyy} + 2(D_{12}^* + 2D_{33}^*) w_{,xxyy} + 4D_{13}^* w_{,xxxy}$$

$$+ 4D_{23}^* w_{,xyyy} + \frac{F_{,xx}}{R_x} + \frac{F_{,yy}}{R_y} + \rho h w_{,tt} + \Delta p = 0$$

$$A_{22}^* F_{,xxxx} + A_{11}^* F_{,yyyy} + (A_{12}^* + A_{33}^*) F_{,xxyy} - 2A_{23}^* F_{,xxxy} \tag{9.104}$$

$$- 2A_{13}^* F_{,xyyy} - \frac{w_{,xx}}{R_x} - \frac{w_{,yy}}{R_y} = 0$$

The boundary conditions are obtained as follows:

1) On x = const: w is prescribed or $M_{x,x} + 2M_{xy,y} = 0$, $w_{,x}$ is prescribed or $M_x = 0$, F is prescribed or $u_{,yy} = 0$, and $F_{,x}$ is prescribed or $v_{,y} = 0$.

2) On y = const: w is prescribed or $M_{y,y} + 2M_{xy,x} = 0$, $w_{,y}$ is prescribed or $M_y = 0$, F is prescribed or $v_{,xx} = 0$, and $F_{,y}$ is prescribed or $u_{,x} = 0$.

3) At a corner (discontinuity in C): $M_{xy} = 0$ (equivalent to $w_{,xy} = 0$), if w is not prescribed, and $F_{,xy} = 0$, if F is not prescribed.

The first conditions are the forced or geometrical conditions, and the second ones are the free or natural conditions. When using a variational formulation for a boundary value problem, the admissible functions should satisfy only the forced boundary conditions. Therefore, using the above conditions, we can write the classical boundary conditions on an edge μ = const, where μ stands for x or y and η is taken as the normal direction to μ as follows:

Clamped edge: $w = w_{,\mu} = 0$ and at a corner $F_{,\mu\eta} = 0$

Free edge: $F = F_{,\mu} = 0$ and at a corner $M_{,\mu\eta} = 0$ (i.e., $w_{,\mu\eta} = 0$)

Simply supported edge: $w = 0$ and at a corner $F_{,\mu\eta} = 0$
$$(9.105)$$

Freely supported edge: $w = F = 0$

Using the quasistatic aerodynamic theory, the relationship between the incremental nonstationary aerodynamic pressure Δp and the transverse displacement w can be written as

$$\Delta p = -\frac{2Q}{(M^2 - 1)^{\frac{1}{2}}} \frac{\partial w}{\partial x} \qquad (9.106)$$

where $Q = \rho V^2/2$ is the dynamic pressure and M and V are the free stream Mach number and velocity, respectively. Now, a finite element solution for the problem at hand can be performed using rectangular elements preserving C^1 continuity, based on the functional given in Eq. (9.103). Thus, we can write

$$\zeta(x, y) = \sum_{i=1}^{2} \sum_{j=1}^{2} \left[H_{0i}(x)H_{0j}(y)\zeta_{ij} + H_{1i}(x)H_{0j}(y)\zeta_{,x_{ij}} \right.$$

$$\left. + H_{0i}(x)H_{1j}(y)\zeta_{,y_{ij}} + H_{1i}(x)H_{1j}(y)\zeta_{,xy_{ij}} \right] \qquad (9.107)$$

where ζ stands for w or F and H_{mn} are first-order Hermitian polynomials. Using the standard finite element technique, we obtain for each element a set of two equations cast in the form below

$$[k_{ww}]\{w\} + [k_{wF}]\{F\} + [m]\{\ddot{w}\} + \lambda[a]\{w\} = \{0\} \qquad (9.108)$$

and

$$[k_{Fw}]\{w\} + [k_{FF}]\{F\} = \{0\} \qquad (9.109)$$

The element stiffness matrix $[k_{ww}]$, the compatibility matrix $[k_{FF}]$, the coupling matrix $[k_{wF}]$, and its transposed $[k_{Fw}]$ read

$$[k_{ww}] = D_{11}^*[k^{(1)}] + D_{22}^*[k^{(2)}] + D_{12}^*[k^{(3)}] + 4D_{33}^*[k^{(4)}]$$
$$+ 2D_{13}^*[k^{(5)}] + 2D_{23}^*[k^{(6)}] \tag{9.110a}$$

$$[k_{FF}] = A_{22}^*[k^{(1)}] + A_{11}^*[k^{(2)}] + A_{12}^*[k^{(3)}] + A_{33}^*[k^{(4)}]$$
$$- A_{23}^*[k^{(5)}] - A_{13}^*[k^{(6)}] \tag{9.110b}$$

$$[k_{wF}] = \frac{1}{R_x}[k^{(7)}] + \frac{1}{R_y}[k^{(8)}] \tag{9.110c}$$

The elements of the matrices $[k^{(i)}]$ for $i = 1-4$ have been treated in the previous sections. The remaining matrices, using the same concise notation of Refs. 11 and 24, read

$$k_{ij}^{(5)} = S3_a(n_i, n_j)S2_b(m_i, m_j) + S3_a(n_j, n_i)S2_b(m_j, m_i) \tag{9.111a}$$

$$k_{ij}^{(6)} = S3_b(m_i, m_j)S2_a(n_i, n_j) + S3_b(m_j, m_i)S2_a(n_j, n_i) \tag{9.111b}$$

$$k_{ij}^{(7)} = S1_a(n_j, n_i)R2_b(m_i, m_j) \tag{9.111c}$$

$$k_{ij}^{(8)} = S1_b(m_j, m_i)R2_a(n_i, n_j) \tag{9.111d}$$

and

$$[S3_a] = \begin{bmatrix} 0 & 0 & 1/a & -1/a \\ 0 & 0 & -1/a & 1/a \\ -1/a & 1/a & -1/2 & -1/2 \\ 1/a & -1/a & 1/2 & 1/2 \end{bmatrix} \tag{9.112}$$

where the same notation of Refs. 11 and 24 has been used and the remaining sub-matrices, the mass matrix and the aerodynamic, are the same as given in previous sections. Using the finite element standard assembly technique and applying the appropriate boundary conditions, the matrix equations for the whole structure read

$$[K_{ww}]\{w\} + [K_{wF}]\{F\} + [M]\{\ddot{w}\} + \lambda[A]\{w\} = \{0\} \tag{9.113}$$

and

$$[K_{Fw}]\{w\} + [K_{FF}]\{F\} = \{0\} \tag{9.114}$$

Now, the degrees of freedom $\{F\}$ can be eliminated using the compatibility Eq. (9.114), and the solution of the problem is reduced to

$$[K_{eq}]\{w\} + \lambda[A]\{w\} + [M]\{\ddot{w}\} = \{0\} \tag{9.115}$$

where

$$[K_{eq}] = [K_{ww}] - [K_{wF}][K_{FF}]^{-1}[K_{Fw}] \tag{9.116}$$

An examination of Eq. (9.116) reveals that the computational effort required for the solution of the stability problem is equivalent to that of a flat plate problem when

the present formulation is used. Furthermore, the in-plane boundary conditions are applied for F, $F_{,x}$, $F_{,y}$, and $F_{,xy}$ and are all nodal degrees of freedom. It is to be observed that the boundary conditions on F and its partial derivatives are performed on Eq. (9.114) before the application of the static condensation procedure.

9.5.2 Numerical Results

The problem of vibration and flutter of doubly curved laminated fiber-reinforcement composite material shells presents several complication factors. The fiber orientation, the number of layers, and their stacking sequence introduce extension–bending, twisting–bending, and extension–shear couplings. The shell geometric curvature presents a further extension–bending interaction effect. The transverse and in-plane boundary condition affect the natural vibration frequency spectrum and therefore the borderline of the flutter stability of the shell. To study the effect and the trend of these parameters on the stability of the shell in a systematic and organized manner, several examples are presented in this section. These examples address one or more parameters at a time to determine their effect on the borderline of the flutter stability of the shell. The results obtained in this section are discussed and compared with alternative solutions available in the literature, whenever possible, to show the efficiency and validity of the present formulation.

The first examples presented are flutter solutions of flat single-layer orthotropic rectangular panels with the four edges clamped or simply supported. This problem was addressed by several investigators; one can mention the earlier works of Calligeros and Dugundgi,[25,26] Ketter,[27] and Sawyer[28] who used the Rayleigh–Ritz and the Galerkin methods for the solution of the problem and the finite element method solutions of Pidaparti and Yang,[32] Gray and Mei,[33] and Lin et al.[30] The present numerical calculations were performed for $a = 400$ in., $h = 2$ in., $E_1 = 13.5 \times 10^6$ psi, $E_2 = 2.7 \times 10^6$ psi, $\nu = 0.3$, $G_{12} = 0.945 \times 10^6$ psi, and $\rho = 0.192 \times 10^{-3}$ lb·s^2/in.^{4} These dimensions and material properties have been used to compare the present analysis with the results available in the literature where the same properties have been used. For these material and geometrical properties, we observe that there is no material bending–extension coupling since only one layer is considered ($B_{ij} = 0$) and no geometric bending–extension coupling since the panel is flat. The only coupling present is that due to twisting–bending when the fiber orientation angle is not aligned with the plate reference axis. The results of the present analysis for a square planform using a finite element mesh of 4×4 elements are shown in Fig. 9.10 and are plotted for a nondimensional critical pressure parameter $\lambda_{cr}^* = \lambda_{cr} a^3 / E_2 h^3$ against the variation of the fiber orientation angle θ and are compared with the results of Refs. 30 and 32. Both references (30 and 32) use the finite element method for the problem solution. Reference 32 uses compatible displacement rectangular shell finite element with 48 degrees of freedom that reduces to a 16-degree-of-freedom element for the case of a single-layer flat plate, and Ref. 30 uses a compatible flat 18-degree-of-freedom triangular element. It can be seen from the results of Fig. 9.10 that the present finite element solution coincides with the solutions of Refs. 30 and 32. From the results presented, it can be seen that the clamped boundary condition presents higher flutter dynamic pressure compared to the simply supported case. Furthermore, for the case analyzed, a square planform, the maximum dynamic pressure parameter is
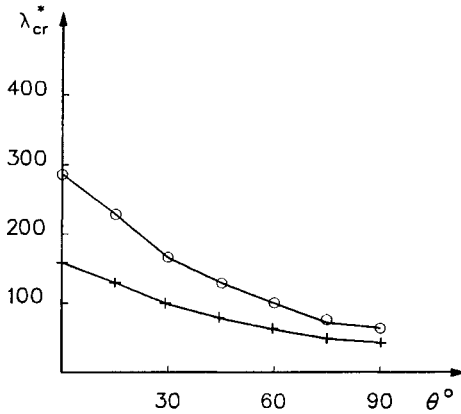
Fig. 9.10   Nondimensional aerodynamic critical pressure parameter $\lambda_{cr}^* = \lambda_{cr} a^3 / E_2 h^3$ **vs variation of the fiber orientation angle** θ **degrees for a single-layer flat orthotropic plate** $a/b = 1$, **and** $E_2 = 2.7 \times 10^6$ **psi,** $E_1/E_2 = 5$, $G_{12} = 0.35\, E_2$, $\nu_{12} = 0.3$, **and** $\rho = 0.192 \times 10^{-3}$ **lb·s²/in.⁴ Present analysis (O clamped and + simply supported) compared with the results of Refs. 30 and 32.**

attained when the orthotropicity angle is zero, i.e., when the 1-axis of the material coincides with reference x-axis of the plate, which in turn coincides with the flow direction, and reaches a minimum value when $\theta = 90$ deg. However, this fact is only for a square planform; it has been demonstrated in earlier works on flutter of orthotropic plates[25,26,27] that, for plates with aspect ratios, different from one, a local maximum for the dynamic pressure parameter is reached at an orthotropicity angle between 0 and 90 deg. This fact is evidenced in the results shown in Fig. 9.11, where the same calculations were repeated for $a/b = 3$. From the results of Fig. 9.11, it can be observed that the maximum dynamic pressure parameter value is reached at a fiber orientation angle in the vicinity of 30 deg for both simply supported and clamped boundary conditions. These first series of calculations aimed to study the effect of the bending–twisting parameter (i.e., the fiber orientation angle), the panel aspect ratio effect, and the general trend of the influence of the transverse boundary condition on the flutter behavior of fiber-reinforced composite material panels.

In the sequel, the effect of the number of layers and their stacking sequence on the borderline of the flutter stability of laminated fiber-reinforced composite panels is examined. Two examples are presented and are a flutter analysis of laminated fiber-reinforced boron-epoxy square plates clamped on all edges. In the first case, the plate is composed of eight symmetrically disposed layers $[0/90]_{2s}$. The dimensions used in the analysis are 400×400 in. and a thickness of 8 in. The material properties considered in the analysis are $E_1 = 31 \times 10^6$ psi, $E_2 = 2.7 \times 10^6$ psi, $G_{12} = 0.75 \times 10^6$ psi, $\nu_{12} = 0.28$, and $\rho = 0.192 \times 10^{-3}$ lb·s²/in.⁴ Again, these dimensions and material properties have been used to compare the present analysis with the results available in the literature where the same properties have been used. It is to be observed that, in the present example, there is no material or geometric
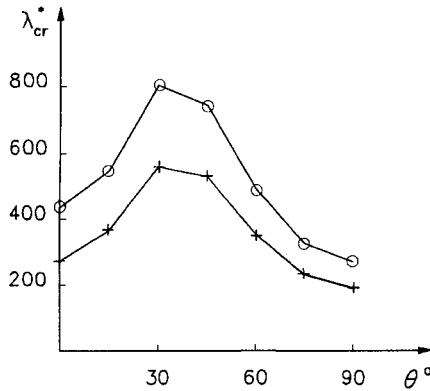
Fig. 9.11   Nondimensional aerodynamic critical pressure parameter $\lambda_{cr}^* = \lambda_{cr} a^3 / E_2 h^3$ vs variation of the fiber orientation angle θ degrees for a single-layer flat orthotropic plate $a/b = 3$, and $E_2 = 2.7 \times 10^6$ psi, $E_1/E_2 = 5$, $G_{12} = 0.35 E_2$, $\nu_{12} = 0.3$, and $\rho = 0.192 \times 10^{-3}$ lb·s²/in.⁴ Present analysis (O clamped and + simply supported).

bending–stretching coupling nor bending–twisting coupling, i.e., only the effect of orthotropicity is evidenced.

Table 9.4 shows the results obtained using the present formulation and the comparison with the results of the same problem using different methods of solution available in the literature. In the second example, the same material properties and geometry as in the first example are used except for the number of layers of their disposition about the plate middle surface. In this second example, the laminate has two layers stacked as [0/90]. In this case, a bending–stretching coupling exists due to the asymmetric disposition of the layers. The results of the analysis are given in Table 9.5 and are compared with other methods of solution available in the literature.

From the results shown in Tables 9.4 and 9.5, it can be observed that favorable agreement exists between the different methods of analysis. Furthermore, comparing the results of Tables 9.4 and 9.5, it can be observed that the material

Table 9.4   Flutter boundary, $\lambda_{cr}^* = \lambda_{cr} a^3 / E_2 h^3$ and $\omega_{cr}^* = \omega_{cr} (a^2/h)(E/\rho)^{1/2}$, for a squared laminated boron-epoxy composite with eight layers symmetrically arranged $[0/90]_{2s}$, clamped-on-all-edges flat plate, $a = b = 400$ in., $h = 8$ in., $E_1 = 31 \times 10^6$ psi, $E_2 = 2.7 \times 10^6$ psi, $G_{12} = 0.75 \times 10^6$ psi, $\nu_{12} = 0.28$, and $\rho = 0.192 \times 10^{-3}$ lb·s²/in.⁴

Source	λ_{cr}^*	ω_{cr}^*
Finite elements triangular (mesh 8 × 8) (Ref. 31)	471.00	46.89
Finite elements rectangular (mesh 6 × 6) (Ref. 32)	472.00	46.80
Series solution (Ref. 29)	474.60	47.19
Integral equations method (Ref. 29)	446.36	46.09
Finite elements present (mesh 4 × 4)	452.54	46.09

Table 9.5   Flutter boundary, $\lambda_{cr}^* = \lambda_{cr} a^3 / E_2 h^3$ and $\omega_{cr}^* = \omega_{cr} (a^2/h)(E/\rho)^{1/2}$, for a squared laminated boron-epoxy composite material with two layers [0/90], clamped-on-all-edges flat plate, $a = b = 400$ in., $h = 8$ in., $E_1 = 31 \times 10^6$ psi, $E_2 = 2.7 \times 10^6$ psi, $G_{12} = 0.75 \times 10^6$ psi, $\nu_{12} = 0.28$, and $\rho = 0.192 \times 10^{-3}$ lb·s²/in.⁴

Source	λ_{cr}^*	ω_{cr}^*
Finite elements rectangular (mesh 6 × 6) (Ref. 32)	194.00	31.46
Series solution (Ref. 29)	173.31	29.79
Integral equations method (Ref. 29)	163.23	28.99
Finite elements present (mesh 4 × 4)		
First flutter point	168.29	21.48
Second flutter point	201.00	30.42

bending–stretching coupling has a big influence on the flutter boundary and is destabilizing. The flutter dynamic pressure parameter for the symmetric stacking arrangement is more than twice the value for the asymmetric arrangement. Furthermore, comparing the present results with those of Ref. 32, it can be observed the solution given in Ref. 32 coincides with the present formulation for the second flutter point, while Ref. 32 misses the first flutter point.

In the previous examples, the effects of the bending–twisting coupling (fiber orientation) and the material bending–stretching coupling (number of layers and their disposition) on the borderline of the flutter stability of laminated fiber-reinforced composite materials have been examined. In the sequel, the effect of the bending–stretching coupling due to the geometric curvature on the borderline of flutter stability will be studied in detail. First, a series of free vibration results are given and compared with previous solutions available in the literature; aeroelastic results are then presented. The first case considered in this series of calculations is a free vibration analysis of cross-ply [0/90] shallow spherically and cylindrically curved shells. The numerical calculations were performed for $a = b = 10$ in., $h = 0.1$ in., $E_1 = 21 \times 10^6$ psi, $E_2 = 1.4 \times 10^6$ psi, $\nu = 0.3$, $G_{12} = 0.6 \times 10^6$ psi, and $\rho = 0.1475 \times 10^{-3}$ lb·s²/in.⁴ For this example, there is no bending–twisting material coupling since $D_{13}^* = D_{23}^* = 0$; however, a high degree of material extension–bending coupling is present together with a geometric extension–bending coupling due to the shell curvature. The present analyses were performed using a 4 × 4 finite element mesh for different R/a values and for clamped boundary conditions on all edges. The results of the analyses for the fundamental natural frequency are shown in Table 9.6 and compared with the finite element results obtained in Ref. 38, which used a 20-degree-of-freedom rectangular element. The results obtained using the present formulation agree favorably with the results of Ref. 38. Furthermore, the effect of the curvature coupling is shown to increase the fundamental frequency. However, the geometric curvature, as will be shown in the sequel, interacts in a complicated manner on the frequency spectrum and mode shapes of the shell and therefore has a complicated effect on the flutter boundaries of the shell. The next example presented is again a free vibration problem of shallow spherically curved fiber-reinforced composite material with four layers

Table 9.6   Fundamental natural frequency of clamped spherical
and cylindrical cross-ply [0/90] shells; $a = b = 10$ in., $h = 0.1$ in.,
$E_1 = 21 \times 10^6$ psi, $E_2 = 1.4 \times 10^6$ psi, $\nu = 0.3$, $G_{12} = 0.6 \times 10^6$
psi, and $\rho = 0.1475 \times 10^{-3}$ lb·s²/in.⁴

| | Fundamental natural frequency f, Hz | | | |
| | Clamped spherical shell | | Clamped cylindrical shell | |
R/a	Ref. 38	Present	Ref. 38	Present
20	380.27	380.00	331.54	328.59
40	303.84	303.67	289.74	288.31
50	293.29	293.13	284.19	283.04
∞ (plate)	273.48	273.35	273.48	273.35

disposed in a symmetric arrangement [0,90,90,0]. The numerical calculations were performed for $a = b = 100$ in., $h = 1$ in., $E_1 = 21 \times 10^6$ psi, $E_2 = 0.84 \times 10^6$ psi, $G_{12} = 0.42 \times 10^6$ psi, $\nu_{12} = 0.25$, and $\rho = 1$ lb·s²/in.⁴ The analysis was performed for a finite element mesh of 4×4 elements and for freely supported boundary conditions on the four edges of the shell. For this example, there is no material bending–extension coupling since the disposition of the layers is symmetric. The only coupling present is due to the shell geometric curvature. The results of the analyses are shown in Table 9.7 for the fundamental natural frequency and for different shell curvature. The present results are compared with the previously mentioned finite element solution of Ref. 38 and the closed-form analytical solution of Ref. 39. The results show good agreement among the various methods of solution, and again the effect of the curvature coupling is shown to increase the fundamental frequency.

The final series of calculations presented are flutter solutions of doubly curved laminated fiber-reinforced composite material shallow shells. The material

Table 9.7   Comparison of the fundamental nondimensional
natural frequency, $\omega^* = \omega a^3 (\rho/E_2 h)^{1/2}$, of freely supported
spherical four-layer [0/90/90/0] shells; $a = b = 100$ in.,
$h = 1$ in., $E_1 = 21 \times 10^6$ psi, $E_2 = 0.84 \times 10^6$ psi,
$G_{12} = 0.42 \times 10^6$ psi, $\nu_{12} = 0.25$, and $\rho = 1$ lb·s²/in.⁴

R/a	Ref. 38	Ref. 39	Present
2	68.498	68.294	69.87
3	47.553	47.415	47.94
4	37.184	37.082	37.34
5	31.159	31.079	31.24
10	20.417	20.380	20.44
∞ (plate)	15.195	15.184	15.23
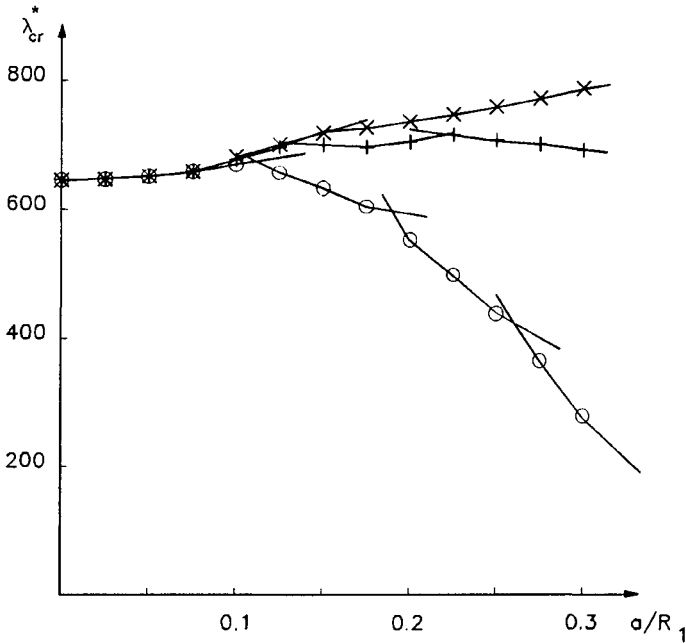
Fig. 9.12 Nondimensional aerodynamic critical pressure parameter $\lambda_{cr}^* = \lambda_{cr} a^3 / E_2 h^3$ vs variation of cross stream curvature parameter a/R_1 for spherical shells O, paraboloidal shells +, and cylindrical shells x, of fiber-reinforced laminated composite material, having square planform and freely supported boundary conditions on the four edges.

properties common to all these calculations are $E_1 = 21 \times 10^6$ psi, $E_2 = 0.84 \times 10^6$ psi, $G_{12} = 0.42 \times 10^6$ psi, $\nu_{12} = 0.25$, and four-layer [0/90/90/0].

The shells analyzed are all square planforms of dimensions 100×100 in. and a thickness of 1 in. The calculations were performed for cylindrical, paraboloidal, and spherical shells. The boundary conditions considered are freely supported boundary conditions on the four edges. All the analyses were performed using a finite element mesh of 4×4 elements. The results of the analyses are summarized in Fig. 9.12. The results presented are plotted for the variation of the critical dynamic pressure parameter $\lambda_{cr}^* = \lambda_{cr} a^3 / E_2 h^3$ vs a variation of a curvature parameter a/R_1. In these calculations, R_1 was considered as the radius of curvature in the cross stream direction and is common for all the types of shells analyzed. In the streamwise direction, R_2 is infinity for the cylindrical shells, $R_2 = R_1$ for the spherical shells, and R_2 was taken as $2R_1$ for the paraboloidal shells. For these shells analyzed, there is no material extension–bending coupling since the stacking disposition of the material laminate is symmetric. Therefore, the only extension–bending coupling considered is due to the geometric curvature. From the results of the analyses, it can be concluded that the streamwise curvature is destabilizing, i.e., for the same cross stream curvature the cylindrical shell is more stable than the paraboloidal shell, and this is more stable than the spherical shell. The effect of

cross stream curvature is similar to the case of isotropic shallow shells previously analyzed in Refs. 23 and 24. For very small curvature, the critical flutter modes are the first modes, and λ_{cr}^* is practically the same as for a flat panel. With the increase of curvature, higher modes coalesce first, and the coalescence is characterized by the decrease or increase in the critical dynamic pressure parameter. In the region of the flat plate behavior, the curvature effect is stabilizing. With the increase of curvature, the shell passes through a transition region, characterized by successive waves of successive higher modes's coalescence. After this transition region, the panel behaves as a deep shell, and λ_{cr}^* is for an elevated number of waves in the cross stream direction and for the first spanwise modes.

9.6 Shells of Revolution

In this section, the aeroelasticity of axisymmetric shells of revolution is studied. Namely, we will be concerned with the solution of the problem of aeroelasticity of circular cylindrical and conical shells. General shells of revolution will be briefly discussed.

9.6.1 Circular Cylindrical Shells

The Hamilton principle for the problem at hand can be written as

$$\int_{t_1}^{t_2} \delta(T - U_1 - U_i)\, \mathrm{d}t + \int_{t_1}^{t_2} \delta W\, \mathrm{d}t = 0 \tag{9.117}$$

where the functional T, U_1, and U_i are given in Section 4.4.1 and W is the work done by the external aerodynamic load and reads

$$W = \int_0^{L/R} \int_0^{2\pi} \Delta p w R^2\, \mathrm{d}\theta\, \mathrm{d}s \tag{9.118}$$

where Δp is the aerodynamic pressure. In the following, a first-order high Mach number approximation will be used for the representation of the aerodynamic pressure term, which can be written as[2,40]

$$\Delta p = -\frac{2Q}{(M^2 - 1)^{\frac{1}{2}}} \left[\frac{\partial w}{R \partial s} + \frac{(M^2 - 2)}{V(M^2 - 1)} \frac{\partial w}{\partial t} - \frac{w}{2R(M^2 - 1)^{\frac{1}{2}}} \right] \tag{9.119}$$

Substituting Eq. (9.119) into Eq. (9.118), we obtain

$$W = -\frac{2QR}{(M^2 - 1)^{\frac{1}{2}}} \int_0^{L/R} \int_0^{2\pi} w \left[\frac{\partial w}{\partial s} + \frac{R(M^2 - 2)}{V(M^2 - 1)} \frac{\partial w}{\partial t} - \frac{w}{2(M^2 - 1)^{\frac{1}{2}}} \right] \mathrm{d}s\, \mathrm{d}\theta \tag{9.120}$$

where $Q = \rho_a V^2/2$ is the dynamic free stream pressure, ρ_a is the free stream density, V is the free stream velocity, M is the free stream Mach number, and other notations are as defined previously. Through application of Hamilton's principle, the following Euler–Lagrange equations are obtained

$$[[L_0] + k[L_1]]\{q\} = \{0\} \tag{9.121}$$

where $[L_0]$ is the differential operator according to Donnell–Mushtari's theory, $[L_1]$ is the differential operator incorporated according to the modified shell theory used, and $\{q\} = [u \ v \ w]^T$. The Donnell–Mushtari operator for the case at hand reads

$$L_{0_{11}} = \frac{\partial^2}{\partial s^2} + \frac{1-\nu}{2}\frac{\partial^2}{\partial \theta^2} - \rho\frac{1-\nu^2}{E}R^2\frac{\partial^2}{\partial t^2} - \frac{1-\nu^2}{4Eh}\left(N_{xx}^0 + N_{\theta\theta}^0\right)\frac{\partial^2}{\partial \theta^2}$$

$$L_{0_{12}} = \frac{1+\nu}{2}\frac{\partial^2}{\partial s\partial\theta} - \frac{1-\nu^2}{4Eh}\left(N_{xx}^0 + N_{\theta\theta}^0\right)\frac{\partial^2}{\partial\theta\partial s}$$

$$L_{0_{13}} = \nu\frac{\partial}{\partial s}$$

$$L_{0_{22}} = \frac{(1-\nu)}{2}\frac{\partial^2}{\partial s^2} + \frac{\partial^2}{\partial\theta^2} - \rho\frac{1-\nu^2}{E}R^2\frac{\partial^2}{\partial t^2} - \frac{1-\nu^2}{4Eh}$$

$$\times\left[N_{\theta\theta}^0 - \frac{1}{4}\left(N_{xx}^0 + N_{\theta\theta}^0\right)\frac{\partial^2}{\partial s^2}\right]$$

$$L_{0_{23}} = \frac{\partial}{\partial\theta} - \frac{1-\nu^2}{Eh}N_{\theta\theta}^0\frac{\partial}{\partial\theta} \tag{9.122}$$

$$L_{0_{33}} = 1 - k\nabla^4 + \rho\frac{1-\nu^2}{E}R^2\frac{\partial^2}{\partial t^2} + \frac{1-\nu^2}{Eh}R\frac{2Q}{(M^2-1)^{\frac{1}{2}}}$$

$$\times\left[\frac{\partial}{\partial s} + \frac{R(M^2-2)}{V(M^2-1)}\frac{\partial}{\partial t} - \frac{1}{2(M^2-1)^{\frac{1}{2}}}\right]$$

$$+ \frac{(1-\nu^2)}{Eh}\left[-N_{\theta\theta}^0\frac{\partial^2}{\partial s^2} - N_{\theta\theta}^0\frac{\partial^2}{\partial\theta^2}\right]$$

$$L_{0_{ij}} = L_{0_{ji}} \qquad i,j = 1,2,3$$

The modified oprator $[L_1]$, according to the various modified shell theories, is as given before in Section 4.4.1.

Now, if the analysis is limited to the Donnell–Mushtari theory, the in-plane inertia terms and initial in-plane stress terms in u and v are neglected. It can be shown (see for example Ref. 41) that the problem is governed by a single differential equation in w and can be written as

$$\left[D\nabla^8 + EhR^2\frac{\partial}{\partial s^4} + R^2\nabla^4\left\{\left(-N_{\theta\theta}^0\frac{\partial^2}{\partial s^2} - N_{\theta\theta}^0\frac{\partial^2}{\partial\theta^2}\right) + \rho h\frac{\partial^2}{\partial t^2}\right.\right.$$

$$\left.\left. + \frac{2QR}{(M^2-1)^{\frac{1}{2}}}\left[\frac{\partial}{\partial s} + \frac{R(M^2-2)}{U(M^2-1)}\frac{\partial}{\partial t} - \frac{1}{2(M^2-1)^{\frac{1}{2}}}\right]\right\}\right]w = 0 \tag{9.123}$$

Most of the aeroelastic stability analyses of circular cylindrical shells have been solved using the simplified differential equation of motion [Eq. (9.123)] coupled with the classical Galerkin method for the case of freely supported end conditions.

In the following, the main contributions to the problem's solution are briefly discussed. The first attempts to obtain a solution of the problem were made by Leonard and Hedgepeth[42] and Miles,[43] who treated the problem of infinitely long cylinders and assumed the solution in the form of traveling waves. The solution of finite length cylinder was then presented by Holt and Strack[44] using Goldenweizer shell theory and applying the Laplace transformation to obtain the generalized aerodynamic forces. Voss[19] used the Goldenweizer shell theory with in-plane inertias retained and quasisteady aerodynamic theory for expressing aerodynamic loads. The problem was solved using the Galerkin method. The effect of initial prestress was included in the analysis. However, there were missing terms in the formulation compared to the derivation exposed above for initial prestress and included unsymmetric terms. The numerical calculations performed in his analysis did not include prestress cases and, for the typical shell geometry used, showed that there were two values for λ_{cr}, one with a large number of nodes in the axial direction and zero nodes in the circumferential direction and the other with many circumferential nodes (of the order of 18 for the shell considered) and with $m = 1$ in the axial direction. Kobayashi[45] used the simplified Donnell–Mushtari equations and the quasisteady aerodynamic theory coupled with a Galerkin solution. For a two-mode Galerkin solution, he obtained a simple expression for the solution as

$$\lambda_{cr}^* = \frac{3}{16}\left\{\left[(4+k)^2 - (1+k)^2 + \frac{16\alpha}{(4+k)^2} - \frac{\alpha}{(1+k)^2} + 3q_x\right]^2\right.$$

$$\left. + 2\gamma_c^2\left[(4+k)^2 + (1+k)^2 + \frac{16\alpha}{(4+k)^2} + \frac{\alpha}{(1+k)^2} + 5q_x^2 + 2kq_y\right]\right\}^{\frac{1}{2}}$$

(9.124)

where

$$\lambda_{cr}^* = \frac{2QL^3}{D\pi^4(M^2 - 1)^{\frac{1}{2}}} \qquad k = \left[\frac{nL}{\pi R}\right]^2$$

$$\alpha = [12(1 - v^2)/\pi^4][L^2/n^2R^2]$$

$$q_x = N_{xx}^0 L^2/\pi^2 D \qquad q_y = N_{\theta\theta}^0 L^2/\pi^2 D$$

$$\gamma_c = \frac{M^2 - 2}{M^2 - 1}\left[\frac{\rho_a L\lambda_{cr}^*}{\rho h(M^2 - 1)^{\frac{1}{2}}}\right]^{\frac{1}{2}}$$

Notice that γ_c is the effect of the aerodynamic damping. Thus, the solution to Eq. (9.124) is made iteratively if such damping is included in the analysis. Furthermore, n is a parameter of the problem, and the minimum value of λ_{cr}^* must be determined while varying n. Notice further that, if the aerodynamic damping is neglected, the solution is independent of $N_{\theta\theta}$, i.e., the internal pressure has no effect in such a solution. In 1966, Dowell and Widnall[46] presented a method for calculating the generalized aerodynamic forces based on the linearized potential flow theory. Johns[47] examined the case of large n, using Donnell's equations, piston theory, and a two-mode Galerkin solution, obtaining simple expressions for n_{cr}

and Q_{cr} given by

$$n_{cr} = \left[5\pi^2 \left(\frac{R}{L} \right)^2 (1 - \nu^2) \frac{12R^2}{h^2} \right]^{\frac{1}{6}} \qquad (9.125)$$

and

$$Q_{cr} = \left[0.91 \left(n_{cr}^2 \frac{R}{h} \right)^{\frac{1}{3}} \frac{R}{h} \right]^3 (M^2 - 1)^{\frac{1}{2}} E \qquad (9.126)$$

Olson and Fung[48] presented a linear and a nonlinear analysis for the problem at hand. For the linear case, they used Donnell's equation and a Galerkin solution. The aerodynamic part was made using the piston theory and a linearized potential theory. The results were compared with experimental findings. For no axial forces, it was shown that both theories presented discrepancies compared to the experimental values as functions of the internal pressure. Typical results obtained in their investigations are shown in Fig. 9.13. Carter and Stearman[49] presented a nonlinear analysis using Donnell's equation and a first-order high Mach number approximation to the linear potential flow theory. The numerical results obtained showed the same trends as those of Olson and Fung.[48] In an attempt to explain the discrepancies between theory and experiments, Barr and Stearman[50] included the effect of initial imperfections in the analysis in the form of streamwise sinusoidal imperfections. Donnell's equation was used, coupled with a Galerkin solution. The stability was studied from the initial imperfections state of deformation. The analysis with imperfections correlated better with experimental values (see Fig. 9.13).
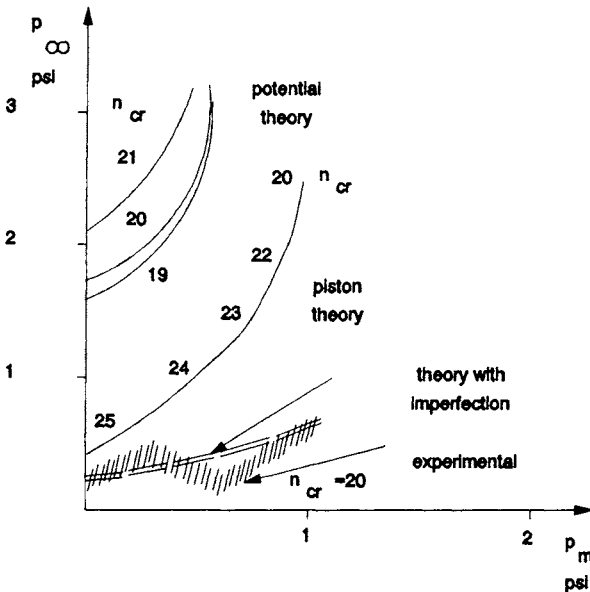
Fig. 9.13   Flutter boundary of cylindrical shells.

Table 9.8   Values of α as functions of L/R for use in Eqs. (9.127) and (9.128)

L/R	0	0.75	1	2	4	6	10
α	347.7	1408	1190	40.41	4.063	1.844	0.723

Librescu and Malaiu[51] treated the orthotropic cylinder using the Galerkin solution. In Ref. 52, Dixon and Hudson made various numerical calculations using Donnell's equation, no initial prestress, quasisteady aerodynamic theory, and up to a 24-mode Galerkin solution. Parametric studies were made for various R/h and L/R, and an empirical formula was obtained by fitting the results to get a quick prediction of the flutter condition of unstressed freely supported cylinders. The formula was deduced to obtain a better estimation than that given in Eq. (9.124) using a two-mode solution. The semiempirical formula reads

$$\lambda_{cr} = \alpha(1 - \nu^2)(R/h)^x \qquad \text{for } L/R \geq 1 \qquad (9.127)$$

and

$$\lambda_{cr} = \alpha(1 - \nu^2)(R/H)^x(R/L)^3 \qquad \text{for } L/R < 1 \qquad (9.128)$$

where $x = \tan h(L/2R)$ and α is a parameter depending on L/R and is furnished in Table 9.8.

In Ref. 53, the problem of shells of revolution in general, but with a slight deviation from the cylinder, was studied. The aerodynamic theory used was a full linearized potential flow theory, and the problem was solved by applying the Galerkin method to both the equations of motion and the aerodynamic equation using expressions that satisfy exactly the boundary conditions of the flow and the equations of motion. The in-plane inertia was conserved in the analysis. Numerical calculations were performed for an elliptic shell of revolution, where it was shown that the curvature has a stabilizing effect on the stability boundary and n_{cr} decreases with the increase of the curvature. For the limiting case of the cylinder, the results approached those of Olson and Fung[48] and Carter and Stearman.[49] It was shown that a curvature parameter of $H/R_{\max} > 0.05$ completely stabilizes the shell (see Fig. 9.14). Dowell and Voss in Ref. 54 give a review of the problem, and Parthan and Johns in Ref. 55 compare various aerodynamic theories used, coupled with the Galerkin method of solution.

In Ref. 56, a finite element solution was presented for the solution of the problem. In-plane inertia was retained, and the effects of internal pressure and axial loads were included in a consistent formulation using Eq. (9.122). The element used was the conical frustum element specialized for the case of circular cylinders. The element stiffness, mass, initial stiffness, and aerodynamic matrices are given in Ref. 56. Various numerical results were performed and the results obtained agree well with those of other investigators.

9.6.2   Conical Shells

Thin conical shells have been used extensively as adapter sections in rockets, supersonic aircraft, and reentry vehicles. Thus, a knowledge of their aeroelastic
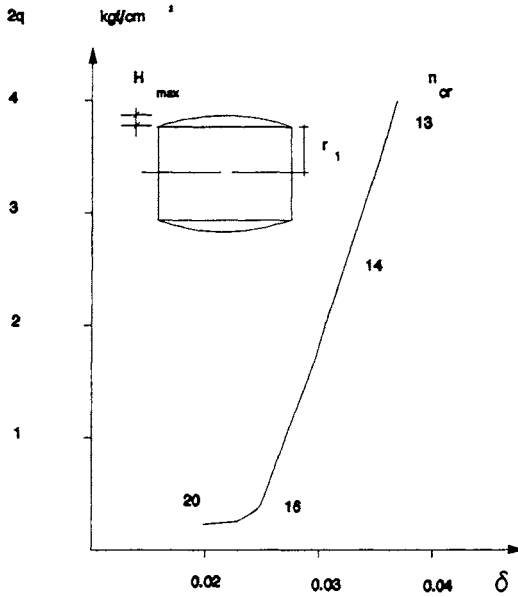
Fig. 9.14   Stability boundary of an elliptic shell of revolution $\delta = H_{max}/r$.

behavior is required. In this section, the problem formulation will be based on Novozhilov's theory of thin shells,[57] here specialized for the case of a frustum of a cone as shown in Fig. 9.15. The analysis will be limited to the use of the first-order high Mach number approximation to the linear potential flow theory for expressing the aerodynamic pressure. The effects of internal pressure and axial loads are discussed. Hamilton's principle for the problem at hand can be expressed as

$$\int_{t_0}^{t_1} \delta(T - U - U_i)\, dt + \int_{t_0}^{t_1} \delta W\, dt = 0 \qquad (9.129)$$

where the functionals U, T, and U_i have been treated in Chapter 4. The work done by the aerodynamic load reads

$$W = \int_0^{2\pi} \int_{s_1}^{s_2} \Delta p w r\, d\theta ds \qquad (9.130)$$

where Δp is the aerodynamic pressure. Using a first-order high Mach number approximation to the linear potential flow theory and including the effect of the curvature term, we can write

$$\Delta p = -\frac{2Q}{(M^2-1)^{\frac{1}{2}}}\left[\frac{\partial w}{\partial s} + \frac{(M^2-2)}{V(M^2-1)}\frac{\partial w}{\partial t} - \frac{w}{2r(M^2-1)^{\frac{1}{2}}}\right] \qquad (9.131)$$

where M is the local Mach number.

If the in-plane inertia terms are neglected, the analysis is limited to Donnell's simplified theory; the terms in u and v in the initial stress energy functional are
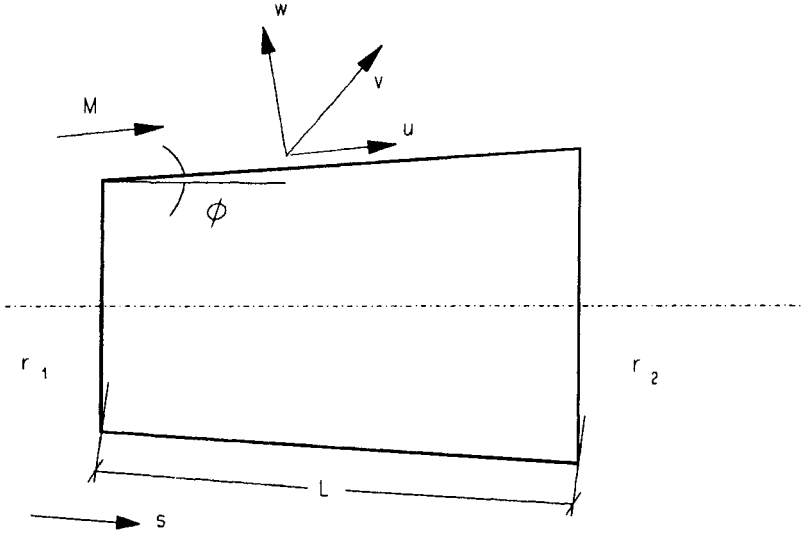
Fig. 9.15   Conical shell notations.

neglected, and defining an Airy stress function F as

$$N_{ss} = \frac{1}{s^2 \sin^2 \phi} \frac{\partial^2 F}{\partial \theta^2} + \frac{1}{s} \frac{\partial F}{\partial s} \qquad N_{\theta\theta} = \frac{\partial^2 F}{\partial s^2}$$

$$N_{s\theta} = N_{\theta s} = \frac{1}{s \sin \phi} \left[\frac{1}{s} \frac{\partial F}{\partial \theta} - \frac{\partial^2 F}{\partial \theta \partial s} \right]$$

(9.132)

it can be shown that the differential equation governing the problem reduces to

$$D \nabla^4 w + \nabla_R^2 F = -\rho h \frac{\partial^2 w}{\partial t^2} + N_{ss}^0 \frac{\partial^2 w}{\partial s^2} + N_{\theta\theta} \left[\frac{1}{s^2 \sin^2 \phi} \frac{\partial^2 w}{\partial \theta^2} + \frac{1}{s} \frac{\partial w}{\partial s} \right]$$

$$- \frac{2Q}{(M^2 - 1)^{\frac{1}{2}}} \left[\frac{\partial w}{\partial s} + \frac{(M^2 - 2)}{V(M^2 - 1)} \frac{\partial w}{\partial t} - \frac{w}{2r(M^2 - 1)^{\frac{1}{2}}} \right]$$

(9.133)

$$\nabla^4 F - Eh \nabla_R^2 w = 0$$

where $D = Eh^3/12(1 - \nu^2)$ and

$$\nabla^2 = \frac{\partial^2}{\partial s^2} + \frac{1}{s} \frac{\partial w}{\partial s} + \frac{1}{s^2 \sin^2 \phi} \frac{\partial^2}{\partial \theta^2}$$

(9.134)

$$\nabla_R^2 = \frac{1}{s \tan \phi} \frac{\partial^2}{\partial s^2}$$

Table 9.9   Dynamic pressure parameter
$\lambda_{cr} = 2qr_1^3/D(M^2 - 1)^{1/2}$ **for a conical shell**

Source	λ_{cr}	n_{cr}
Galerkin		
Two terms (Ref. 3)	448	5
Four terms (Ref. 58)	669	6
Eight terms (Ref. 58)	558	5
Twelve Terms (Ref. 58)	590	5
FEM solution (Ref. 60)		
A_1	670	6
A_2	662	6
A_3	702	6
FEM solution (Ref. 61)		
Ten elements	700	6
Twenty elements	609	5

The initial prestress loads are related to the internal pressure p_m and the external applied axial load p_x (positive for traction) through the relations

$$N_{ss}^0 = \sigma_{ss}h = \frac{p_x}{2\pi r \sin\phi \cos\phi} + \frac{p_m}{2}s\tan\phi$$

$$N_{\theta\theta}^0 = \sigma_{\theta\theta}h = s\tan\phi p_m$$

(9.135)

We notice that the first part of Eq. (9.133) is an equation of motion in the radial direction, while the second equation is an equation of compatibility. Most available analytical solutions of the problem were made using Eq. (9.133) coupled with the Galerkin method of solution. In Ref. 58, the approximate Galerkin modes were put in the second part of Eq. (9.133) to obtain F in terms of the assumed modes, and this in turn was substituted in the first part of Eq. (9.133), and the Galerkin method was then applied. In Ref. 3, the Galerkin method was applied directly to both parts of Eq. (9.133). In Refs. 59 and 60, a finite element method formulation for the problem was presented using Novozhilov's theory of thin shell. The formulation of the element aerodynamic matrices follows the same procedure as was made for the case of circular cylindrical shells and is given in Ref. 60. In the formulation of such matrices of the conical frustum element, numerical integration is preferable; otherwise, we will be faced with a huge amount of analytical formulas that are difficult to manipulate and verify.

In Refs. 61 and 62, finite element formulation for the problem at hand was made using Donnell–Mushtari thin shell theory. Some of the results obtained in these analyses are shown in Table 9.9 and are compared with other analytical solutions. The following parameters were used in the calculations: Young's modulus $E = 6.5 \times 10^6$ lb/in.^{2}, Poisson's ratio $\nu = 0.29$, material density $\rho = 8.33 \times 10^{-4}$ lb·s^2/in.^{4}, shell thickness $h = 0.051$ in., cone semivertex $\phi = 5$ deg, $M_\infty = 3$, $T_\infty = 288.15$ K, $p_{a\infty} = 14.696$ lb/in.^{2}, $r_1/h = 148$, and $L/r_1 = 8.13$. The finite element results of Refs. 59 and 60 were made using a mesh of 10 elements. In these

analyses, three sets of computations were performed and are labeled A_1, A_2, and A_3 in Table 9.9. The calculations labeled A_1 were done neglecting the damping and effect of curvature in the formulation of aerodynamic loads. The calculations labeled A_2 were performed with the inclusion of the curvature term. The third case, labeled A_3, includes both damping and curvature effects. From these limited results, it can be shown that, for the case treated here, the curvature effect has a small effect on the stability boundary, while the damping effect has a greater influence and is stabilizing. In these analyses, Novozhilov's theory of thin shell was used, and the in-plane inertia terms were retained in the analysis. The analytical solution of Table 9.9 and the finite element solution of Ref. 61 use the simplified Donnell–Mushtari theory. Furthermore, the finite element solution of Ref. 62 uses the static condensation technique in the flutter solution and neglects the in-plane inertia terms. The static condensation technique for the complicated problem treated here is not recommended because it relies on intuition (see Ref. 63).

9.7 Damping in Aeroelasticity of Plates and Shells

In this section, an attempt is made to assess and discuss the effect of damping in panel flutter analysis. The sources of damping in aeroelasticity of plates and shells are of aerodynamic and structural nature. The aerodynamic damping enters in the formulation through the term proportional to the velocity in the aerodynamic surface loading expression. If a first-order high Mach number approximation to the linear potential flow theory is used as has been exposed in the previous sections, the aerodynamic damping is a mass proportional type and has always a stabilizing effect, i.e., the critical dynamic pressure parameter with aerodynamic damping considered is greater than the critical dynamic pressure parameter when damping is not considered. In general, for the practical range of the parameters inolved in the aerodynamic damping estimation, its effect on the stability boundary is small. Exceptions to this general rule are cases when the critical flutter modes present nearly identical natural frequencies associated with weak aerodynamic coupling. Examples of these situations are stressed flat panels with aspect ratios greater than one[64] and circular cylindrical shells with large length-to-radius ratios where the critical modes are higher axial modes with a low circumferential number of nodes.[45,51,65] Extreme cases are when pairs of natural frequencies coincide or at a buckling prestress of the panel; in such cases a zero critical dynamic pressure is observed with no inclusion of aerodynamic damping. The aerodynamic damping effect in such cases has a greater influence on the stability of the panels and removes the sharp minimums or dips observed in curves of critical dynamic pressure parameter vs prestress loads when damping is not considered. The second source of damping is of a structural nature. Ellen[66] provides a useful classification of the different types of damping by representing their effect in the equations of motion by terms written in the form

$$g \frac{\partial^{n+1} w}{\partial t \, \partial x^n} \tag{9.136}$$

where g is a structural damping coefficient and x is any spatial coordinate on the surface. When g is a constant, the structural damping is a viscous-type damping. Furthermore, when n is zero, the viscous damping is of the same type of the

aerodynamic damping previously considered and its effect is cumulative and always conservative in the sense previously discussed. This type of viscous damping is extensively used in the literature. When n is different from zero, a viscoelastic damping type is considered, which is strain dependent (and thus stress dependent) in general. The effect of such damping when considered alone can be stabilizing or destabilizing depending on the way of interaction with the structure, i.e., if it dissipates or supplies energy to the system. In fact, a viscous damping proportional to the restoring membrane stress but in phase with the velocity is destabilizing to the membrane flutter.[66,67] Another type of structural damping that has been considered in the aeroelasticity of plate and shell analysis is a hysteretic-type damping. This can be incorporated by writing in the equations of motion a damping term in the form,[66]

$$\frac{g}{\omega}\frac{\partial^{n+1}w}{\partial t \partial x^n} \qquad (9.137)$$

where ω is the modulus of the complex frequency response and g is a constant. Again, for n different from zero, the incorporation of such damping alone can stabilize or destabilize the system. A formulation well adapted for aeroelastic discrete system equations (e.g., finite element, Rayleigh–Ritz, Galerkin methods, etc.) for the incorporation of a constant viscous damping effect in the analysis was proposed in Refs. 68 and 69. The various methods proposed in these two references reconstruct a viscous damping matrix $[c]$, knowing the modal damping ratio ξ_i (measured or assumed) of a number of natural modes of vibration. A similar method to those proposed in Refs. 68 and 69 to reconstruct a viscous damping matrix $[c]$ from the knowledge or the assumption of the modal damping ratio ξ_i of a number of natural modes can be written as

$$[c] = \left[[\phi] \left[\frac{1}{\beta_i} \right] [\phi]^T \right]^{-1} \qquad (9.138)$$

where $[\phi]_{nm}$ is the mode shape matrix of the m modes considered with damping, n is the total number of degrees of freedom of the dynamic system, and $[\beta_i]$ is a diagonal matrix with $\beta_i = 2\xi_i\omega_i\mu_i$, where ω_i and μ_i are the natural frequency and the generalized mass of the mode in consideration. This formulation, despite leading to a full matrix $[c]$, has the advantage of attributing different modal damping ratio values to an individual number of modes and can be used in a parametric way to study the effect of variation of damping for one or more modes on the system stability. Finally, it should be emphasized that structural damping is a complex physical problem and simple mathematical models to represent it must be validated by experimental evidence.

9.8   Nonlinear Models

The material presented in this section is based on Ref. 70.

9.8.1   Flat Plate Models

In this section, we will use the von Kármán nonlinear plate theory for the problem formulation, which is a subset of the general nonlinear theory of elasticity.

For more details on the theory, the reader is referred to the classic textbooks on the subject, e.g., Refs. 71–74. The derivation assumes large displacements, but the rotations and strains are assumed to be small compared to unity, so that the changes in the geometry in the definition of the stresses and the integrations are neglected. Furthermore, use is made of Kirchoff's assumption, i.e., planes normal to the undeformed middle surface remain plane and normal to the deformed middle surface. Under such assumptions, the strain displacement relations can be written as

$$\varepsilon_{xx} = \frac{\partial u}{\partial x} + \frac{1}{2}\left[\frac{\partial w}{\partial x}\right]^2 - z\frac{\partial^2 w}{\partial x^2}$$

$$\varepsilon_{yy} = \frac{\partial v}{\partial y} + \frac{1}{2}\left[\frac{\partial w}{\partial y}\right]^2 - z\frac{\partial^2 w}{\partial y^2}$$

$$\varepsilon_{zx} = \varepsilon_{zy} = 0 \qquad (9.139)$$

$$\varepsilon_{xy} = \frac{1}{2}\left[\frac{\partial u}{\partial y} + \frac{\partial v}{\partial x} - 2z\frac{\partial^2 w}{\partial x \partial y}\right] + \frac{1}{2}\frac{\partial w}{\partial x}\frac{\partial w}{\partial y}$$

$$\varepsilon_{zz} = \frac{1}{2}\left[\frac{\partial w}{\partial x}\right]^2 + \frac{1}{2}\left[\frac{\partial w}{\partial y}\right]^2$$

where we have neglected the transverse shear deformations and Cartesian coordinates have been used; with x–y being the plate midplane, u and v are the displacements of the middle surface in the x–y directions, w is the transverse displacement in the z direction, and ε is the strain tensor. The stress–strain relations are given by

$$\sigma_{xx} = \frac{E}{(1-\nu^2)}[\varepsilon_{xx} + \nu\,\varepsilon_{yy}]$$

$$\sigma_{yy} = \frac{E}{(1-\nu^2)}[\varepsilon_{yy} + \nu\,\varepsilon_{xx}] \qquad (9.140)$$

$$\sigma_{xy} = 2G\varepsilon_{xy} \qquad \sigma_{yz} = 2G\varepsilon_{yz} = 0 \qquad \sigma_{xz} = 2G\varepsilon_{xz} = 0 \qquad \sigma_{zz} = 0$$

where we have assumed that the plate is thin ($\sigma_{zz} = 0$) and isotropic with E, G, and ν being Young's modulus, shear modulus ($= E/2[1+\nu]$), and Poisson's ratio, respectively. The strain energy of small deformations reads

$$U = \frac{1}{2}\int_V [\sigma_{xx}\varepsilon_{xx} + \sigma_{yy}\varepsilon_{yy} + \sigma_{xy}\varepsilon_{xy}]\,\mathrm{d}x\,\mathrm{d}y\,\mathrm{d}z = U(u, v, w) \quad (9.141)$$

where the quantities subjected to variation are the displacements u, v, and w and Eqs. (9.139) and (9.140) are to be used in Eq. (9.141). Now, defining the in-plane stress resultants as

$$N_{xx} = \int_{-h/2}^{h/2} \sigma_{xx}\,\mathrm{d}z \qquad N_{yy} = \int_{-h/2}^{h/2} \sigma_{yy}\,\mathrm{d}z \qquad N_{xy} = \int_{-h/2}^{h/2} \sigma_{xy}\,\mathrm{d}z \quad (9.142)$$

where h is the plate thickness and introducing an Airy stress function F, which satisfies the in-plane equilibrium and is related to the in-plane stress resultants as

$$N_{xx} = \frac{\partial^2 F}{\partial y^2} \qquad N_{yy} = \frac{\partial^2 F}{\partial x^2} \qquad N_{xy} = -\frac{\partial^2 F}{\partial x \partial y} \qquad (9.143)$$

it can then be shown that Eq. (9.141) can be written as

$$U^* = -\frac{1}{2Eh} \int_A \left[\left(\frac{\partial^2 F}{\partial x^2} \right)^2 + \left(\frac{\partial^2 F}{\partial y^2} \right)^2 - 2\nu \frac{\partial^2 F}{\partial x^2} \frac{\partial^2 F}{\partial y^2} \right.$$

$$+ 2(1+\nu) \left(\frac{\partial^2 F}{\partial x \partial y} \right)^2 \right] dA + \frac{D}{2} \int_A \left[\left(\frac{\partial^2 w}{\partial x^2} \right)^2 + \left(\frac{\partial^2 w}{\partial y^2} \right)^2 \right.$$

$$+ 2\nu \frac{\partial^2 w}{\partial x^2} \frac{\partial^2 w}{\partial y^2} + 2(1-\nu) \left(\frac{\partial^2 w}{\partial x \partial y} \right)^2 \right] dA$$

$$+ \frac{1}{2} \int_A \left[\left(\frac{\partial^2 w}{\partial x^2} \right)^2 \frac{\partial^2 F}{\partial y^2} + \left(\frac{\partial^2 w}{\partial y^2} \right)^2 \frac{\partial^2 F}{\partial x^2} - 2 \frac{\partial w}{\partial x} \frac{\partial w}{\partial y} \frac{\partial^2 F}{\partial x \partial y} \right] dA \qquad (9.144)$$

where $D = Eh^3/12(1-\nu^2)$. The quantities subject to variation in Eq. (9.144) are F and w and have been reduced to two due to the introduction of the Airy stress function and the in-plane equilibrium is automatically satisfied. Note further that the thickness h has been assumed constant in the functional of Eq. (9.144). Moreover, the functional in Eq. (9.144) contains lower order terms compared to the functional in Eq. (9.141) and possesses similarity in F and w, a fact that facilitates the problem formulation when using numerical methods for the problem solution. If the in-plane and rotary inertias are neglected, the kinetic energy expression reads

$$T = \frac{1}{2} \int_A \rho_m h \left[\frac{\partial w}{\partial t} \right]^2 dA \qquad (9.145)$$

where ρ_m is the plate density. Using now the simple Ackeret's expression to relate the aerodynamic external pressure to the plate motion, we can write the work done by the aerodynamic load as

$$W = \int_A \Delta p w \, dA \qquad (9.146)$$

where

$$\Delta p = -\frac{2q}{\sqrt{M^2 - 1}} \frac{\partial w}{\partial x} \qquad (9.147)$$

where $q = \rho V^2/2$ is the free stream dynamic pressure, V is the free stream velocity, and M is the free stream Mach number. The flow is assumed to act only on the upper surface and to be in the x direction. Assuming further that the plate is subjected to a prestress state of in-plane stress resultants, N_{xx}^0, N_{yy}^0, and N_{xy}^0, the strain energy due to prestress reads

$$U_i = \frac{1}{2} \int_A \left[N_{xx}^0 \left(\frac{\partial w}{\partial x} \right)^2 + N_{yy}^0 \left(\frac{\partial w}{\partial y} \right)^2 + 2N_{xy}^0 \frac{\partial w}{\partial x} \frac{\partial w}{\partial y} \right] dA \qquad (9.148)$$

Hamilton's principle for the problem at hand can be written as

$$\int_{t_0}^{t_1} \delta(T - U - U_i)\, dt + \int_{t_0}^{t_1} \delta W\, dt = 0 \qquad (9.149)$$

where Eqs. (9.141), (9.145), (9.146), and (9.148) are to be used in Eq. (9.149) and the quantities subjected to variation are u, v, and w. Applying the variational operation, Eq. (9.149) will furnish one equation of motion in w and two equations of equilibrium in u and v as the Euler–Lagrange equations governing the problem together with the boundary conditions. Alternatively the problem can be formulated using the functional in Eq. (9.144) to obtain a modified variational principle written as

$$\int_{t_0}^{t_1} \delta(T - U^* - U_i)\, dt + \int_{t_0}^{t_1} \delta W\, dt = 0 \qquad (9.150)$$

where the quantities subjected to variation are w and F. Applying the variational operation, Eq. (9.150) will furnish one equation of motion in w and an equation of compatibility in F as the Euler–Lagrange equations governing the problem together with the boundary conditions. It can be easily shown that the related equations for this case are

$$D\nabla^4 w = \frac{\partial^2 F}{\partial x^2}\frac{\partial^2 w}{\partial y^2} + \frac{\partial^2 F}{\partial y^2}\frac{\partial^2 w}{\partial x^2} - \frac{\partial^2 F}{\partial x \partial y}\frac{\partial^2 w}{\partial x \partial y} + N_{xx}^0 \frac{\partial^2 w}{\partial x^2} + N_{yy}^0 \frac{\partial^2 w}{\partial y^2}$$

$$+ 2N_{xy}^0 \frac{\partial^2 w}{\partial x \partial y} - \rho_m h \frac{\partial^2 w}{\partial t^2} - \frac{2q}{\sqrt{M^2 - 1}}\frac{\partial w}{\partial x} \qquad (9.151)$$

and

$$\frac{1}{Eh}\nabla^4 F = \left(\frac{\partial^2 w}{\partial x \partial y}\right)^2 - \frac{\partial^2 w}{\partial x^2}\frac{\partial^2 w}{\partial y^2} \qquad (9.152)$$

It is to be observed that, when the inertia and the aerodynamic terms are neglected in Eq. (9.151), Eqs. (9.151) and (9.152) reduce to the celebrated nonlinear von Kármán equations. Furthermore, the variational operation leads to the following boundary conditions:

$$\left[\frac{1}{Eh}\left\{\frac{\partial^2 F}{\partial n^2} - \nu\frac{\partial^2 F}{\partial s^2}\right\} - \frac{1}{2}\left(\frac{\partial w}{\partial s}\right)^2\right]\delta\left(\frac{\partial F}{\partial n}\right) = 0$$

$$\left[-\frac{1}{Eh}\left\{\frac{\partial^3 F}{\partial n^3} + (2+\nu)\frac{\partial^3 F}{\partial n \partial s^2}\right\} - \frac{\partial w}{\partial n}\frac{\partial^2 w}{\partial s^2}\right]\delta F = 0$$

$$\qquad (9.153)$$

$$\left[D\left\{\frac{\partial^2 w}{\partial n^2} + \nu\frac{\partial^2 w}{\partial s^2}\right\}\right]\delta\left(\frac{\partial w}{\partial n}\right) = 0$$

$$\left[D\left\{\frac{\partial^3 w}{\partial n^3} + (2-\nu)\frac{\partial^3 w}{\partial n \partial s^2}\right\} - \frac{\partial w}{\partial n}\frac{\partial^2 F}{\partial s^2} + \frac{\partial w}{\partial s}\frac{\partial^2 F}{\partial n \partial s}\right]\delta w = 0$$

where, in Eq. (9.153), n and s denote the normal and the tangential directions, respectively, on the boundary.

Problem Solution. Almost all the analytical solutions of the nonlinear aero-elastic problems of plates have been made using the von Kármán equations coupled with the Galerkin approximate method of solution since no exact solutions of differential Eqs. (9.151) and (9.152) exist. Such solutions lead to a set of nonlinear ordinary differential equations whose solution is made using various techniques. In the following, these methods are presented and their relative merits are discussed. A Rayleigh–Ritz solution can be made using the modified variational principle in Eq. (9.150) with the admissible functions satisfying the forced boundary conditions or a Galerkin solution can be formulated with the admissible functions satisfying all the boundary conditions of the problem. In both cases, the solution is made by writing for the field variables w and F, expressions in the form

$$w(x, y, t) = \sum_m \psi_m(x, y) q_m(t) \tag{9.154}$$

and

$$F(x, y, t) = \sum_r \phi_r(x, y) a_r(t) \tag{9.155}$$

The trial functions ψ_m and ϕ_r must satisfy only the geometric boundary conditions in the Rayleigh–Ritz solution or all the boundary conditions in the Galerkin solution. The substitution of Eqs. (9.154) and (9.155) in the related variational principle or in the von Kármán equations and the application of the minimization process will lead to the following set of ordinary nonlinear differential equations

$$[M]\{q''\} + [[k] + \lambda[A]]\{q\} = \{c_1\} \tag{9.156}$$

and

$$[H]\{a\} = \{c_2\} \tag{9.157}$$

In Eqs. (9.156) and (9.157), the matrices $[M]$, $[k]$, $[A]$, and $[H]$ are the linear mass, stiffness, aerodynamic, and compatibility matrices, respectively, and $\{c_1\}$ and $\{c_2\}$ are the nonlinear contributions and are given by

$$\{c_1\} = a_1[L_1]\{q\} + a_2[L_2]\{q\} + \cdots + a_r[L_r]\{q\} = \left[\sum_{i=1}^r a_i[L_i]\{q\}\right] \tag{9.158}$$

and

$$\{c_{2_i}\} = \left[\{q\}^T[B_i]\{q\}\right] \tag{9.159}$$

The matrices $[L_i]$ and $[B_i]$ are linear matrices obtained from the integrations of the trial functions over the domain. It is to be observed that Eq. (9.159) is an algebraic equation, so that the vector $\{a\}$ can be written as

$$\{a\} = [H]^{-1}\{c_2\} \tag{9.160}$$

Substitution of Eq. (9.160) into Eq. (9.158) gives

$$[M]\{q''\} + [[k] + \lambda[A]]\{q\} = \{c\} \tag{9.161}$$

The vector $\{c\}$ is the nonlinear contribution with elements given by

$$c_i = \sum_{r=1}^{m} \sum_{s=1}^{m} \sum_{t=1}^{m} c_{i\,rst} q_r q_s q_t \tag{9.162}$$

where c_{irst} are constants. Equation (9.161) represents a set of nonlinear ordinary differential equations where $\{c\}$ contributes to the nonlinear part. When $\{c\} = \{0\}$, the problem is reduced to the linear aeroelasticity problem. Furthermore, we notice that the contribution of an aerodynamic damping or a structural damping in the problem formulation will lead to an augmented term function of the velocity, i.e., $[G]\{q'\}$ in the right-hand side. Thus the general procedure of the solution will be the same. Moreover, the matrix $[k]$ includes both the linear stiffness matrix and the initial stiffness matrix due to prestress. The solution of Eq. (9.161) has been made by various authors using various techniques and these are discussed in the following.

Dowell[75,76] uses the direct numerical integration technique for the solution of Eq. (9.161). Because only the steady-state solution is of interest, the solution can be started from any initial condition, $\{q_0\}$ and $\{q_0'\}$. Thus, the solution proceeds as follows. Given a value $\lambda > \lambda_c$, where λ_c is the linear critical dynamic pressure, and fixing a value for the amplitude level, $(w/h)_{max}$, the equations of motion are numerically integrated and the permanent state solution is obtained as a function of time. If this solution is stable, i.e., decaying with time, the value of $(w/h)_{max}$ is augmented until a limit cycle is obtained, from which the frequency of vibration and the amplitude are calculated for the predefined value of λ. The whole process is then repeated for another λ, to obtain a graph of $(w/h)_{max}$ vs λ. Dowell[75,76] did not discuss the stability of the plate when the limit cycle is reached. Small perturbations about the limit cycle oscillations were discussed by Eastep and McIntosh[77] and Evenson and Olson[78] to study the stability of the solution when the limit cycle is obtained. In these references, the method used for the numerical integration was not given. However, any stable algorithm, e.g., the Newmark method with limitation on the time interval Δt can be used. Furthermore, enhancement of the accuracy and a reduction in the time spent in the numerical integration methods can be achieved, using the method of Ref. 79.

Morino[80] used the perturbation techniques for solving the nonlinear aeroelastic problem. For details of the perturbation methods of solution of the autonomous ordinary nonlinear differential equations, the reader is referred to textbooks on the subject (see for instance Ref. 81). In the following, the method proposed by Morino[80] is given without proof. For the solution of Eq. (9.161) at a value $\lambda > \lambda_c$, we write

$$\lambda = \lambda_c + \varepsilon^2 \lambda_c + O(\varepsilon^4) \tag{9.163}$$

and

$$\{q\} = \varepsilon\{q^{(1)}\} + \varepsilon^3\{q^{(3)}\} + O(\varepsilon^5) \tag{9.164}$$

For the values of λ and q and for the frequency, we write

$$\omega = \omega_c + \varepsilon^2 \omega_c + O(\varepsilon^4) \tag{9.165}$$

and we define

$$\tau = \omega t = (\omega_c + \varepsilon^2 \omega_c)t = \omega_c t + \varepsilon^2 \omega_c t = \tau_0 + \tau_2 \qquad (9.166)$$

so that

$$\frac{\mathrm{d}}{\mathrm{d}\tau} = \frac{\partial}{\partial \tau_0} + \frac{\partial}{\partial \tau_2}$$

where ε is a small quantity. Substituting Eqs. (9.163–9.166) into the equation of motion [Eq. (9.161)] and applying the perturbation technique, i.e., balancing terms of equal power of ε, Morino[80] obtained for the terms ε and ε^3 the following equations

$$[M]\left\{\frac{\partial^2 q^1}{\partial \tau_0^2}\right\} + [K]\{q^1\} + \lambda_c[A]\{q^1\} = \{0\} \qquad (9.167)$$

and

$$[M]\left\{\frac{\partial^2 q^3}{\partial \tau_0^2}\right\} + [K]\{q^3\} + \lambda_c[A]\{q^3\}$$

$$= \left[2[M]\frac{\partial^2}{\partial \tau_0 \partial \tau_2} + [A]\right]\{q^1\} - \sum_{n=1}^{m}\sum_{p=1}^{m}\sum_{q=1}^{m} c_{inpq} q_n^1 q_p^1 q_q^1 \qquad (9.168)$$

Equation (9.167) represents the linear solution from which the values of λ_c and ω_c can be determined. The linear solution vector can be written as

$$\{q^1\} = \text{Real } S\{u\}\, e^{i\tau_0} \qquad (9.169)$$

where S is in general complex and corresponds to the amplitude at the fluttering condition ω_c and $\{u\}$ is the eigenvector of the linear eigenvalue problem. Substituting Eq. (9.169) into Eq. (9.168), we obtain

$$[M]\left\{\frac{\partial^2 q^3}{\partial \tau_0^2}\right\} + [K]\{q^3\} + \lambda_c[A]\{q^3\} = -\{Z^1\}e^{i\omega_c \tau_0} + \{Z^3\}e^{3i\omega_c \tau_0} \qquad (9.170)$$

where

$$\{Z^1\} = S\,[i\omega_c[M] + [A]]\,\{u\}$$

$$+ \sum_{n=1}^{m}\sum_{p=1}^{m}\sum_{q=1}^{m} c_{inpq}(u_n u_p u_q^* + u_n u_p^* u_q + u_n^* u_p u_q)S^2 S^* \qquad (9.171)$$

and

$$\{Z^3\} = \sum_{n=1}^{m}\sum_{p=1}^{m}\sum_{q=1}^{m} c_{inpq} u_n u_p u_q S^3 \qquad (9.172)$$

In Eq. (9.171), the values denoted with asterisks are the conjugates of the corresponding variables. We notice that the solution $\{q^3\}$ is not needed if the analysis is limited to the terms $O(\varepsilon^3)$. Now, because $\{u\}$ is a solution of the homogeneous

Eq. (9.170), then to avoid the secular terms in the solution, using the perturbation methods, $\{Z^1\}$ must be orthogonal to $\{u^L\}$, where $\{u^L\}$ is the left eigenvector of the linear solution. Thus, we can write

$$\{u^L\}\{Z^1\} = 0 \qquad (9.173)$$

Morino[80] obtained this condition as

$$\frac{\partial S}{\partial \tau_2} + \beta S + \gamma S^2 S^* = 0 \qquad (9.174)$$

where

$$\beta = \frac{1}{\alpha}\{u^L\}^T[A]\{u\} \qquad (9.175)$$

and

$$\gamma = \frac{1}{\alpha}\{u^L\}^T \cdot \left\{ \sum_{n=1}^{m} \sum_{p=1}^{m} \sum_{q=1}^{m} c_{inpq}(u_n u_p u_q^* + u_n u_p^* u_q + u_n^* u_p u_q) \right\} \qquad (9.176)$$

where $\alpha = i\omega_c\{u^L\}^T[M]\{u\}$. The stability of the limit cycle is determined from the sign of the real part of γ, i.e., the solution is stable for values of $\gamma_R > 0$. The amplitude and the frequency of the limit cycle are obtained for $\tau \to \infty$ and read

$$\left| \frac{w}{h}(x, y, t) \right|_{\tau \to \infty} = 2(\lambda - \lambda_c)^{\frac{1}{2}} \left(-\frac{\beta_R}{\gamma_R} \right)^{\frac{1}{2}} \left| \sum_{n=1}^{N} u_n \phi_n(x, y) \right| \qquad (9.177)$$

and

$$\omega_{\tau \to \infty} = \omega_c - (\lambda - \lambda_c)\left(\beta_I - \frac{\beta_R}{\gamma_R}\gamma_I \right) \qquad (9.178)$$

The solution of the problem will proceed as follows: λ_c, ω_c, $\{u\}$, and $\{u^L\}$ are determined from the linear solution of Eq. (9.167). These are used in Eqs. (9.175) and (9.176) to obtain the values of β and γ, and these in turn are used to determine the amplitude and the frequency for a given value of $\lambda > \lambda_c$. The reduction in the computational time is thus evident compared to the direct numerical integration.

Wind-tunnel experiments[2] and results of direct numerical integration methods showed that periodic vibrations exist once the critical dynamic pressure is exceeded. This led some authors to use the harmonic balance technique to solve the nonlinear flutter problem. This was first made by Fung[82] and Kobayashi[83] using the two-mode Galerkin solution and was then generalized by Morino[80] for n Galerkin terms. The solution of Eq. (9.161) proceeds as follows: we write $\{q\}$ as

$$\{q\} = \{a_n\}\sin \omega t + \{b_n\}\cos \omega t \qquad (9.179)$$

where ω is the frequency of vibration for $\lambda > \lambda_c$. Substituting Eq. (9.179) into Eq. (9.161) and separating the terms in $\sin \omega t$ and $\cos \omega t$, since the solution is valid for any ωt, we obtain a set of $2N$ equations for the $2N$ unknowns $\{a_1 b_1 \ldots a_n b_n\}$. Two of these variables are fixed for a given value of w/h, i.e., fixing the amplitude level, and are replaced as unknowns by λ and ω; the solution then proceeds to obtain the $2N$ unknowns, namely, $\{\omega \lambda a_2 b_2 \ldots a_n b_n\}$, using any suitable method for the

solution of a set of nonlinear algebraic equations. The stability of the solution can be made by making small perturbations about the solution obtained.

A further method for the solution of the nonlinear flutter problem is the Lyapunov stability criteria. Such a method has been discussed by Bolotin,[84] Librescu,[3] and Parks.[85] However, the difficulty of the Lyapunov method in the nonlinear case is to find a Lyapunov functional for the stability criteria; more details on the Lyapunov method are given in Ref. 81.

Limit cycle amplitude two-dimensional panel flutter using the finite element method was studied by Mei and Rogers,[86] Mei,[87] and Rao and Rao.[88] Finite element solutions of the three-dimensional nonlinear panel flutter were investigated by Mei and Weidman,[89] Han and Yang,[90] and Mei and Wang.[91] Large amplitude two-[92] and three-dimensional hypersonic panel flutter[33] were studied using the finite element method. Structural nonlinearity using the finite element method for composite materials was analyzed in Refs. 32, 93, and 94.

In all of these finite element solutions, the nonlinear part was solved using the direct numerical integration method or the energy balance technique. The structural part of the problem was formulated using the von Kármán large deflection plate theory with u, v, and w taken as the field variables. In addition to the structure nonlinearity, Ref. 33 considers also aerodynamic nonlinearity using a third-order hypersonic piston theory where it is shown that the effect of the aerodynamic nonlinearity was very small on the stability boundaries for the cases analyzed. The finite element method has been applied to the problem of nonlinear supersonic flutter suppresion using adaptive materials actuators in Refs. 95 and 96.

9.8.2 Curved Panel Models

In this section, the aeroelastic problem of large deformations of curved panels is considered. Again, the von Kármán large deformation theory is used for the problem formulation. The analysis is limited to cylindrically curved plates and to Kirchoff's assumption. Consider a cylindrically curved plate with a rectangular base and a curvature in the y direction. The strain-displacement relationships can be written as

$$\varepsilon_{xx} = \frac{\partial u}{\partial x} + \frac{1}{2}\left[\frac{\partial w}{\partial x}\right]^2 - z\frac{\partial^2 w}{\partial x^2}$$

$$\varepsilon_{yy} = \frac{\partial v}{\partial y} - \frac{w}{R} + \frac{1}{2}\left[\frac{\partial w}{\partial y}\right]^2 - z\frac{\partial^2 w}{\partial y^2}$$

$$\varepsilon_{xy} = \frac{1}{2}\left[\frac{\partial u}{\partial y} + \frac{\partial v}{\partial x} - 2z\frac{\partial^2 w}{\partial x \partial y}\right] + \frac{1}{2}\frac{\partial w}{\partial x}\frac{\partial w}{\partial y}$$

$$\varepsilon_{zz} = \frac{1}{2}\left[\frac{\partial w}{\partial x}\right]^2 + \frac{1}{2}\left[\frac{\partial w}{\partial y}\right]^2 \qquad \varepsilon_{zx} = \varepsilon_{zy} = 0$$

(9.180)

The stress–strain relationships are the same as given by Eq. (9.140) and the strain energy of deformation reads

$$U = \frac{1}{2} \int_V [\sigma_{xx}\varepsilon_{xx} + \sigma_{yy}\varepsilon_{yy} + \sigma_{xy}\varepsilon_{xy}] \, dx \, dy \, dz = U(u, v, w) \quad (9.181)$$

Now, introducing an Airy stress function as was made in the previous section, which satisfies the in-plane equilibrium, we obtain the following modified functional

$$U^* = -\frac{1}{2Eh} \int_A \left[\left(\frac{\partial^2 F}{\partial x^2} \right)^2 + \left(\frac{\partial^2 F}{\partial y^2} \right)^2 - 2\nu \frac{\partial^2 F}{\partial x^2} \frac{\partial^2 F}{\partial y^2} \right.$$

$$\left. + 2(1 + \nu) \left(\frac{\partial^2 F}{\partial x \partial y} \right)^2 \right] dA + \frac{D}{2} \int_A \left[\left(\frac{\partial^2 w}{\partial x^2} \right)^2 + \left(\frac{\partial^2 w}{\partial y^2} \right)^2 \right.$$

$$\left. + 2\nu \frac{\partial^2 w}{\partial x^2} \frac{\partial^2 w}{\partial y^2} + 2(1 - \nu) \left(\frac{\partial^2 w}{\partial x \partial y} \right)^2 \right] dA$$

$$+ \frac{1}{2} \int_A \left[\left(\frac{\partial^2 w}{\partial x^2} \right)^2 \frac{\partial^2 F}{\partial y^2} + \left(\frac{\partial^2 w}{\partial y^2} \right)^2 \frac{\partial^2 F}{\partial x^2} - 2 \frac{\partial w}{\partial x} \frac{\partial w}{\partial y} \frac{\partial^2 F}{\partial x \partial y} - \frac{2w}{R} \frac{\partial^2 F}{\partial x^2} \right] dA$$

$$(9.182)$$

where the same notation has been used as in the previous section. The kinetic energy functional, the strain energy functional due to prestress, and the work done by the external aerodynamic loads are the same as given by Eqs. (9.145), (9.148), and (9.146), respectively. Using these functionals, a modified variational principle is obtained and reads

$$\int_{t_0}^{t_1} \delta(T - U^* - U_i) \, dt + \int_{t_0}^{t_1} \delta W \, dt = 0 \quad (9.183)$$

where the quantities subjected to variation are w and F. Performing the variational operation, the Euler–Lagrange equations governing the problem are obtained as

$$D\nabla^4 w = \frac{\partial^2 F}{\partial x^2} \left[\frac{1}{R} + \frac{\partial^2 w}{\partial y^2} \right] + \frac{\partial^2 F}{\partial y^2} \frac{\partial^2 w}{\partial x^2} - \frac{\partial^2 F}{\partial x \partial y} \frac{\partial^2 w}{\partial x \partial y}$$

$$+ N_{xx}^0 \frac{\partial^2 w}{\partial x^2} + N_{yy}^0 \frac{\partial^2 w}{\partial y^2} + 2N_{xy}^0 \frac{\partial^2 w}{\partial x \partial y} - \rho_m h \frac{\partial^2 w}{\partial t^2} - \frac{2q}{\sqrt{M^2 - 1}} \frac{\partial w}{\partial x} \quad (9.184)$$

and

$$\frac{1}{Eh} \nabla^4 F = \left(\frac{\partial^2 w}{\partial x \partial y} \right)^2 - \frac{\partial^2 w}{\partial x^2} \left[\frac{\partial^2 w}{\partial y^2} + \frac{1}{R} \right] \quad (9.185)$$

Again, Eq. (9.184) is an equation of motion in the normal direction and Eq. (9.185) is a compatibility equation. Furthermore, the variational operation leads to the following boundary conditions:

$$\left[\frac{1}{Eh} \left\{ \frac{\partial^2 F}{\partial n^2} - v \frac{\partial^2 F}{\partial s^2} \right\} - \frac{1}{2} \left(\frac{\partial w}{\partial s} \right)^2 \right] \delta \left(\frac{\partial F}{\partial n} \right) = 0$$

$$\left[-\frac{1}{Eh} \left\{ \frac{\partial^3 F}{\partial n^3} + (2 + v) \frac{\partial^3 F}{\partial n \partial s^2} \right\} - \frac{\partial w}{\partial n} \frac{\partial^2 w}{\partial s^2} \right] \delta F = 0$$

$$\left[D \left\{ \frac{\partial^2 w}{\partial n^2} + v \frac{\partial^2 w}{\partial s^2} \right\} \right] \delta \left(\frac{\partial w}{\partial n} \right) = 0$$

$$\left[D \left\{ \frac{\partial^3 w}{\partial n^3} + (2 - v) \frac{\partial^3 w}{\partial n \partial s^2} \right\} - \frac{\partial w}{\partial n} \frac{\partial^2 F}{\partial s^2} + \frac{\partial w}{\partial s} \frac{\partial^2 F}{\partial n \partial s} \right] \delta w = 0$$

$$(9.186)$$

where the geometric conditions are given by the variational terms and the free boundary conditions are given by the expressions between brackets, respectively.

Problem Solution. The same procedures of solution as discussed for the flat plate problem can be applied for the present case. The problem of nonlinear flutter of curved panels, freely supported on all edges, has been treated by Dowell[21,22] using Eqs. (9.184) and (9.185) coupled with the Galerkin method of solution. The limit cycle amplitude problem has been solved using the numerical integration process. Further, cylindrical curvature in the streamwise direction was also treated. Dowell's investigations showed that the in-plane edge restraints had a great influence on the flutter boundaries and this was attributed to the frequency spectrum of the shells analyzed.

Linear models have been analyzed in Refs. 23 and 24 using the finite element method and the two field variable variational principle given by Eq. (9.183). The two field variable variational principle with the transverse displacement and Airy stress function taken as the field variables represents an efficient alternative for the treatment of shallow shell problems. In spite of the simplifications it introduces, Reissner's principle is scarcely used in the finite element formulation. The main reason is attributed to the difficulties encountered when applying the boundary conditions on Airy stress function. In Ref. 97, starting from Reissner's variational equation for the free vibration of cylindrically curved panels, the Euler–Lagrange equations and the boundary conditions of the problem were deduced. It was shown that the boundary conditions on the Airy stress function are as simple and direct to apply as on the transverse displacements. The variational principle was used to derive C^1 continuity rectangular finite elements using the concise formulation of Ref. 11. The formulation was then extended to the buckling analysis of cylindrically curved panels,[98] supersonic panel flutter,[23,24] the problem of stability of cylindrically curved panels in the presence of nonconservative follower forces,[99] and free vibration[100] and aeroelasticity[34] of composite material doubly curved shallow shells. The results of these investigations showed that the in-plane boundary conditions have an important effect on the stability boundaries of the shells, principally in the transition region as the curvature increases and the shell departs

from the flat plate behavior to a deep shell behavior. Extending the formulation to nonlinearity using modern materials, optimization to satisfy flutter requirements using the direct methods of stability of Refs. 101 and 102 and the problem of nonlinear supersonic panel flutter suppression using adaptive materials actuators are directly applicable.

References

[1] Jordan, P. F., "The Physical Nature of Panel Flutter," *Aero Digest*, Feb., 1956, pp. 34–38.

[2] Dowell, E. H., *Aeroelasticity of Plates and Shells*, Noordhoff International, Leyden, The Netherlands, 1975.

[3] Librescu, L., *Elastostatics and Kinetics of Anisotropic and Heterogeneous Shell-Type Structures*, Noordhoff International, Leyden, The Netherlands, 1975.

[4] Fung, Y. C., *A Summary of the Theories and Experiments on Panel Flutter*, AGARD Manual on Aeroelasticity, Part III, Chap. 7, 1961.

[5] Johns, D. J., *A Survey of Panel Flutter*, AGARD Advisory Rept. 1, Nov., 1965.

[6] Johns, D. J., *A Panel Flutter Review*, AGARD Manual on Aeroelasticity, Part III, Chap. 7, 1969.

[7] Dowell, E. H., "Panel Flutter: A Review of the Aeroelastic Stability of Plates and Shells," *AIAA Journal*, Vol. 8, No. 3, 1970, pp. 385–399.

[8] Bismarck-Nasr, M. N., "Finite Element Analysis of Aeroelasticity of Plates and Shells," *Applied Mechanics Reviews*, Vol. 45, No. 12, Part 1, 1992, pp. 461–482.

[9] Olson, M. D., "Finite Elements Applied to Panel Flutter," *AIAA Journal*, Vol. 5, No. 12, 1967, pp. 2267–2270.

[10] Olson, M. D., "Some Flutter Solution Using Finite Elements," *AIAA Journal*, Vol. 8, No. 4, 1970, pp. 747–752.

[11] Bismarck-Nasr, M. N., "On the Sixteen Degree of Freedom Rectangular Plate Element," *International Journal of Computers and Structures*, Vol. 40, No. 4, 1991, pp. 1059–1060.

[12] Kari-Appa, V., Somashekar, B. R., and Shah, C. G., "Discrete Element Approach to the Flutter of Skew Panels with Inplane Forces Under Yawed Supersonic Flow," *AIAA Journal*, Vol. 8, No. 11, 1970, pp. 2017–2022.

[13] Sander, G., Bon, C., and Geradin, M., "Finite Element Analysis of Supersonic Panel Flutter," *International Journal for Numerical Methods in Engineering*, Vol. 7, No. 3, 1973, pp. 379–394.

[14] Bismarck-Nasr, M. N., "Finite Element Method Applied to the Flutter of Two Parallel Elastically Coupled Flat Plates," *International Journal for Numerical Methods in Engineering*, Vol. 11, No. 7, 1977, pp. 1188–1193.

[15] Kari-Appa, V., and Somashekar, B. R., "Application of the Matrix Displacement Methods in the Study of Panel Flutter," *AIAA Journal*, Vol. 7, No. 1, 1969, pp. 50–53.

[16] Kari-Appa, V., and Somashekar, B. R., "Flutter of Skew Panels by the Matrix Displacement Approach," *Aeronautical Journal*, Vol. 74, No. 716, 1970, pp. 672–675.

[17] Rosettos, J. N., and Tong, P., "Finite Element Analysis of Vibration and Flutter of Cantilever Anistropic Plates," *Journal of Applied Mechanics, Trans ASME*, Vol. 41(E), 1974, pp. 1075–1080.

[18] Eisley, J. G., and Luessen, G., "Flutter of Thin Plates Under Combined Shear and Normal Edge Forces," *AIAA Journal*, Vol. 1, No. 6, 1963, pp. 620–626.

[19] Voss, H. M., "The Effect of an External Supersonic Flow on the Vibration Characteristics of Thin Cylindrical Shells," *Journal of Aero/Space Science*, Vol. 28, No. 12, 1961, pp. 945–956.

[20]Reissner, E., "On Transverse Vibration of Thin, Shallow Elastic Shells," *Quarterly of Applied Mathematics*, Vol. 13, No. 2, 1955, pp. 169–176.

[21]Dowell, E. H., "Nonlinear Flutter of Curved Plates," *AIAA Journal*, Vol. 7, No. 3, 1969, pp. 424–431.

[22]Dowell, E. H., "Nonlinear Flutter of Curved Plates II," *AIAA Journal*, Vol. 8, No. 2, 1970, pp. 259–261.

[23]Bismarck-Nasr, M. N., "Supersonic Panel Flutter Analysis of Shallow Shells," *AIAA Journal*, Vol. 31, No. 7, 1993, pp. 1349–1351.

[24]Bismarck-Nasr, M. N., "Analysis of Cylindrically Curved Panels Based on a Two Field Variable Variational Principle," *Applied Mechanics Reviews*, Vol. 46, No. 11, Part 2, 1993, pp. S71–S78.

[25]Calligeros, J. M., and Dugundji, J., "Supersonic Flutter of Rectangular Orthotropic Panels with Arbitrary Orientation of Orthotropicity," AFOSR Rept. No. 5328, 1963.

[26]Calligeros, J. M., and Dugundji, J., "Effect of Orthotropicity Orientation on Supersonic Panel Flutter," *AIAA Journal*, Vol. 1, No. 9, 1963, pp. 2180–2182.

[27]Ketter, D. J., "Flutter of Flat, Rectangular, Orthotropic Panels," *AIAA Journal*, Vol. 5, No. 1, 1967, pp. 116–124.

[28]Sawyer, J. W., "Flutter and Buckling of General Laminated Plates," *Journal of Aircraft*, Vol. 14, No. 4, 1977, pp. 387–393.

[29]Srinivasan, R. S., and Babu, B. J., "Free Vibration and Flutter of Laminated Quadrilateral Plates," *Computers and Structures*, Vol. 27, No. 2, 1987, pp. 297–304.

[30]Lin, K. J., Lu, P. J., and Tarn, J. Q., "Flutter Analysis of Composite Panels Using High Precision Finite Elements," *Computers and Structures*, Vol. 33, No. 2, 1989, pp. 561–574.

[31]Lee, I. N., and Cho, M. H., "Flutter Analysis of Composite Panels in Supersonic Flow," *Proceedings of the AIAA/ASME/ASCE/AHS/ASC 31st Structures, Structural Dynamics, and Materials Conference*, Long Beach, CA, 1990 (AIAA Paper 90-1180).

[32]Pidaparti, R. M. V., and Yang, H. T. Y., "Supersonic Flutter Analysis of Composite Plates and Shells," *AIAA Journal*, Vol. 31, No. 6, 1993, pp. 1109–1117.

[33]Gray, C. E., and Mei, C., "Large Amplitude Finite Element Flutter Analysis of Composite Panels in Hypersonic Flow," *AIAA Journal*, Vol. 31, No. 6, 1993, pp. 1090–1099.

[34]Bismarck-Nasr, M. N., "Aeroelasticity of Laminated Fibre-Reinforced Doubly Curved Shallow Shells," *AIAA Journal*, Vol. 36, No. 4, 1998, pp. 661–663.

[35]Reissner, E., and Stavsky, Y., "Bending and Stretching of Certain Types of Heterogeneous Aleotropic Elastic Plates," *Journal of Applied Mechanics*, Vol. 26, No. 9, 1961, pp. 402–408.

[36]Visson, J. R., and Chou, T. W., *Composite Materials and Their Use in Structures*, Material Science Series, Applied Science Publishers, Ltd., London, 1975.

[37]Jones, R. M., *Mechanics of Composite Materials*, McGraw–Hill, Tokyo, 1975.

[38]Chandrashekhara, R., "Free Vibrations of Anisotropic Laminated Doubly Curved Shells," *Computers and Structures*, Vol. 33, No. 2, 1989, pp. 435–440.

[39]Reddy, J. N., "Exact Solution of Moderately Thick Laminated Shells," *Journal of the Engineering Mechanics Division, ASCE*, Vol. 110, 1984, pp. 794–809.

[40]Krumhaar, H., "The Accuracy of Linear Piston Theory When Applied to Cylindrical Shells," *AIAA Journal*, Vol. 1, No. 6, 1963, pp. 1448–1449.

[41]Bisplinghoff, R. H., and Ashley, H., *Principles of Aeroelasticity*, Wiley, New York, 1962.

[42]Leonard, R. W., and Hedgepeth, J. M., "On Panel Flutter and Divergence of Infinitely Long Unstiffened and Ring-Stiffened Thin Walled Circular Cylinders," NACA TN 3638, 1956.

[43] Miles, J. W., "Supersonic Flutter of Cylindrical Shell," *Journal of Aeronautical Science*, Vol. 24, No. 3, 1957, pp. 107–118.

[44] Holt, M., and Strack, S. L., "Supersonic Panel Flutter of a Cylindrical Shell of Finite Length," *Journal of Aero/Space Science*, Vol. 28, No. 3, 1961, pp. 197–208.

[45] Kobayashi, S., "Supersonic Panel Flutter of Unstiffened Circular Cylindrical Shells Having Simply Supported Ends," *Transactions of the Japan Society of Aeronautical and Space Sciences*, Vol. 6, No. 9, 1963, pp. 27–35.

[46] Dowell, E. H., and Widnall, S. E., "Generalized Aerodynamic Forces on an Oscillating Cylindrical Shell," *Quarterly of Applied Mechanics*, Vol. 24, No. 1, 1966, pp. 1–17.

[47] Johns, D. J., "Cylindrical Shell Flutter—Theory and Experiment," *Journal of Royal Aeronautical Society*, Vol. 70, No. 664, 1966, p. 533.

[48] Olson, M. D., and Fung, Y. C., "On Comparing Theory and Experiment for the Supersonic Flutter of Circular Cylindrical Shells," *AIAA Journal*, Vol. 5, No. 10, 1967, pp. 1849–1856.

[49] Carter, L. L., and Stearman, R. O., "Some Aspects of Cylindrical Shell Panel Flutter," *AIAA Journal*, Vol. 6, No. 1, 1968, pp. 37–43.

[50] Barr, G. W., and Stearman, R. O., "Aeroelastic Stability Characteristics of Cylindrical Shells Considering Imperfections and Edge Restraint," *AIAA Journal*, Vol. 7, No. 5, 1969, pp. 912–919.

[51] Librescu, L., and Malaiu, E., "Supersonic Flutter of Circular Cylindrical Heterogeneous Orthotropic Thin Panels of Finite Length," *Journal of Sound and Vibrations*, Vol. 8, No. 3, 1968, pp. 494–512.

[52] Dixon, S. C., and Hudson, M. L., "Flutter Boundary for Simply Supported Unstiffened Cylinders," *AIAA Journal*, Vol. 7, No. 7, 1969, pp. 1390–1391.

[53] Bismarck-Nasr, M. N., *Stabilité Aaeroelastique d'une Coque de Revolution Mince, Voisine d'un Cylindre dans un Écoulement Supersonique*, Thesis D. ès Sc., No 604, Univ. Paris, Orsay, 1970.

[54] Dowell, E. H., and Voss, H. M., "Experimental and Theoretical Panel Flutter Studies in the Mach Range 1.0 to 5.0," *AIAA Journal*, Vol. 3 , No. 12, 1965, pp. 2292–2304.

[55] Parthan, S., and Johns, D. J., "Aerodynamic Generalized Forces for Supersonic Shell Flutter," *AIAA Journal*, Vol. 10, No. 10, 1971, pp. 1369–1371.

[56] Bismarck-Nasr, M. N., "Finite Element Method Applied to the Supersonic Flutter of Circular Cylindrical Shells," *International Journal for Numerical Methods in Engineering*, Vol. 10, No. 2, 1976, pp. 423–435.

[57] Novozhilov, V. V., *The Theory of Thin Elastic Shells*, Noordhoff International, Leyden, The Netherlands, 1964.

[58] Dixon, S. C., and Hudson, M. L., "Flutter, Vibration and Buckling of Truncated Orthotropic Conical Shells with Generalized Edge Restraint," NASA TND-5759, 1970.

[59] Savio, H. R. C., *Aplicação do Método de Elementos Finitos ao Problema Aeroelastico de Cascas Cônicas*, M.Sc. Thesis, Instituto Tecnológico de Aeronáutica, São José dos Campos, São Paulo, 1978.

[60] Bismarck-Nasr, M. N., and Savio, H. R. C., "Finite Element Solution of the Supersonic Flutter of Conical Shells," *AIAA Journal*, Vol. 17, No. 10, 1979, pp. 1148–1150.

[61] Ueda, T., and Kobayashi, S., "Supersonic Flutter of Truncated Conical Shells," *Transactions of the Japan Society of Aeronautical and Space Sciences*, Vol. 20, No. 47, 1977, pp. 13–30.

[62] Ueda, T., "Nonlinear Analysis of the Supersonic Flutter of Truncated Conical Shells Using the Finite Element Method," *Transactions of the Japan Society of Aeronautical and Space Sciences*, Vol. 20, No. 50, 1978, pp. 225–240.

288   STRUCTURAL DYNAMICS IN AERONAUTICAL ENGINEERING

[63]Bismarck-Nasr, M. N., and Savio, H. R. C., Reply to Comment on "Finite Element Solution of the Supersonic Flutter of Conical Shells," *AIAA Journal*, Vol. 19, No. 2, 1981, pp. 256.

[64]Shore, P. C., "Effects of Structural Damping on Flutter of Stressed Panels," NASA TN D-4990, 1969.

[65]Voss, H. M., and Dowell, E., "Effect of Aerodynamic Damping on Flutter of Thin Panels," *AIAA Journal*, Vol. 2, No. 1, 1964, pp. 119–120.

[66]Ellen, C. H., "Influence of Structural Damping on Panel Flutter," *AIAA Journal*, Vol. 6, No. 11, 1968, pp. 2169–2174.

[67]Houbolt, J. C., *A Study of Several Aerothermoelastic Problems of Aircraft Structures in High-Speed Flight*, Mitteilung aus dem Institut für Flugzeugstatik und Leichtbau, Verlag Leeman, Zürich, 1958.

[68]Bathe, K. J., and Wilson, E. L., *Numerical Methods in Finite Element Analysis*, Prentice–Hall, Englewood Cliffs, NJ, 1976.

[69]Wilson, E. L., and Penzien, J., "Evaluation of Orthogonal Damping Matrices," *International Journal for Numerical Methods in Engineering*, Vol. 4, No. 1, 1972, pp. 5–10.

[70]Bismarck-Nasr, M. N., "Finite Element in Aeroelasticity of Plates and Shells," *Applied Mechanics Reviews*, Vol. 49, No. 10, Part 2, 1996, pp. 17–24.

[71]Dym, C. L., and Shames, I. H., *Solid Mechanics: A Variational Approach*, McGraw–Hill, New York, 1973.

[72]Fung, Y. C., *Foundation of Solid Mechanics*, Prentice–Hall, Englewood Cliffs, NJ, 1965.

[73]Novozhilov, V. V., *Foundations of the Nonlinear Theory of Elasticity*, Graylock, Rochester, NY, 1953.

[74]Washizu, K., *Variational Method in Elasticity and Plasticity*, 2nd ed., Pergamon Oxford, England, UK, 1974.

[75]Dowell, E. H., "Nonlinear Oscillations of a Fluttering Plate," *AIAA Journal*, Vol. 4, No. 7, 1966, pp. 1267–1275.

[76]Dowell, E. H., "Nonlinear Oscillations of a Fluttering Plate II," *AIAA Journal*, Vol. 5, No. 10, 1967, pp. 1856–1862.

[77]Eastep, F. E., and McIntosh, S. C., "The Analysis of Nonlinear Panel Flutter and Response Under Random Excitation or Nonlinear Aerodynamic Loadings," *AIAA/ASME 11th Structures, Structural Dynamics, and Materials Conference*, Denver, CO, 1970, pp. 36–47.

[78]Evenson, D. A., and Olson, M. D., *Nonlinear Flutter of a Circular Cylindrical Shell in Supersonic Flow*, NASA TND-4265, 1967.

[79]Bismarck-Nasr, M. N., and de Oliveira, A. M., "On Enhancement of the Accuracy in Direct Integration Dynamic Response Problems," *Earthquake Engineering & Structural Dynamics*, Vol. 20, No. 7, 1991, pp. 699–703.

[80]Morino, L., "A Perturbation Method for Treating Nonlinear Panel Flutter Problems," *AIAA Journal*, Vol. 7, No. 3, 1969, pp. 405–411.

[81]Meirovitch, L., *Elements of Vibration Analysis*, McGraw–Hill, New York, 1975.

[82]Fung, Y. C., "Two-Dimensional Panel Flutter," *Journal of Aero/Space Science*, Vol. 25, No. 3, 1958, pp. 145–159.

[83]Kobayashi, S., "Flutter of Simply Supported Rectangular Panels in a Supersonic Flow; Two-Dimensional Panel Flutter I, Simply Supported Panels II, Clamped Panels," *Transactions of the Japan Society of Aeronautical and Space Sciences*, Vol. 5, No. 1, 1962, pp. 79–118.

[84]Bolotin, V. V., *Nonconservative Problems in the Theory of Elastic Stability*, Macmillan, New York, 1963.

[85]Parks, P. C., "A Stability Criterion for Panel Flutter via the Second Method of Liupanov," *AIAA Journal*, Vol. 4, No. 1, 1966, pp. 175–178.

[86]Mei, C., and Rogers, J. L., Jr., *Application of Nastran to Large Deflection Supersonic Flutter of Panels*, NASA TM X-3428, 1976, pp. 67–97.

[87]Mei, C., "A Finite Element Approach for Nonlinear Panel Flutter," *AIAA Journal*, Vol. 15, No. 8, 1997, pp. 1107–1110.

[88]Rao, K. S., and Rao, G. V., "Large Amplitude Supersonic Flutter of Panels with Ends Elastically Restrained Against Rotation," *Computers and Structures*, Vol. 11, No. 3, 1980, pp. 197–201.

[89]Mei, C., and Weidman, D. J., "Nonlinear Panel Flutter—A Finite Element Approach," *Computational Methods for Fluid-Structure Interaction Problems*, edited by T. Belytschko and T. L. Geers, AMR-Vol. 26, American Society of Mechanical Engineers, 1977, pp. 139–165.

[90]Han, A. D., and Yang, T. Y., "Nonlinear Panel Flutter Using High Order Triangular Finite Elements," *AIAA Journal*, Vol. 21, No. 10, 1983, pp. 1453–1461.

[91]Mei, C., and Wang, H. C., "Finite Elements Analysis of Large Amplitude Supersonic Flutter of Panels," *Proceedings of the International Conference on Finite Element Methods*, Shanghai, China, Gordon and Breach, New York, 1982, pp. 944–951.

[92]Gray, C. E., Jr., Mei, C., and Shore, C. P., "Finite Element Method for Large Amplitude Two-Dimensional Panel Flutter at Hypersonic Speeds," *AIAA Journal*, Vol. 29, No. 2, 1991, pp. 290–298.

[93]Xue, D. Y., and Mei, C., "Finite Element Nonlinear Flutter with Arbitrary Temperatures in Supersonic Flow," *AIAA Journal*, Vol. 31, No. 1, 1993, pp. 154–162.

[94]Zhou, R. C., Xue, D. Y., and Mei, C., "Finite Element Time Domain—Model Formulation for Nonlinear Flutter of Composite Panels," *AIAA Journal*, Vol. 32, No. 10, 1994, pp. 2044–2059.

[95]Scott, R. C., and Weisshaar, T. A., "Panel Flutter Suppression Using Adaptive Material Actuators," *Journal of Aircraft*, Vol. 31, No. 1, 1994, pp. 213–222.

[96]Zhou, R. C., Lai, Z., Xue, D. Y., Huang, J. K., and Mei, C., "Supresion of Nonlinear Panel Flutter with Piezoelectric Actuators Using Finite Element Method," *AIAA Journal*, Vol. 33, No. 6, 1995, pp. 1098–1105.

[97]Bismarck-Nasr, M. N., "On Vibrations of Thin Cylindrically Curved Panels," *Proceedings of the Third Pan American Congress of Applied Mechanics, PACAM III*, São Paulo, Brazil, 1993, pp. 696–699.

[98]Bismarck-Nasr, M. N., "Buckling Analysis of Cylindrically Curved Panels Based on a Two Field Variational Principle," *International Journal of Computers and Structures*, Vol. 51, No. 4, 1994, pp. 453–457.

[99]Bismarck-Nasr, M. N., "Dynamic Stability of Shallow Shells Subjected to Follower Forces," *AIAA Journal*, Vol. 33, No. 2, 1995, pp. 355–360.

[100]Bismarck-Nasr, M. N., and Silva, D. H. A., "Vibration of Laminated Doubly Curved Shallow Shells," *Proceedings of the Fourth Pan American Congress of Applied Mechanics, PACAM IV*, Buenos Aires, Argentina, Vol. 1, 1995, pp. 337–342.

[101]Bismarck-Nasr, M. N., "On Coalescence of Aeroelastic Modes in Flutter Analysis," *Journal of Aircraft*, Vol. 29, No. 3, 1992, pp. 505–507.

[102]Bismarck-Nasr, M. N., "On a Direct Solution of the Aeroelastic Stability Equations," *Journal of Aircraft*, Vol. 31, No. 4, 1994, pp. 979–981.

This page intentionally left blank

Index